京都大学化学研究所
国際共同利用・共同研究拠点

化学関連分野の深化・連携を基軸とする
先端・学際グローバル研究拠点

令和５年度
成果報告書

まえがき

京都大学化学研究所は、平成２２年度から「化学関連分野の深化・連携を基軸とする先端・学際研究拠点」（平成２８年度から第二期）として国内外の共同利用・共同研究を推し進め、それを新たな糧としてより多様でグローバルな化学研究の展開と若手研究者の育成・輩出を図って参りました。特にこの拠点活動では、化学関連コミュニティの研究者の皆様からの要請を踏まえながら、化学研究所の研究分野の広がりと深さに加えて、これまでの様々な連携実績を活かし、国内外の研究機関の相互協力を担保するハブ環境も提供してきました。先端・学際的分野深耕にあたっては、関連コミュニティの研究者の皆様と化学研究所の教員が推進する分野選択型、課題提案型、施設・機器利用型、連携・融合促進型等の多彩な共同研究と、拠点として主催・共催する各種国際会議、シンポジウム、研究会等を通じて、多様性と先進性を担保し、さらに、国際的視点に基づいて次代の化学関連分野を担う若手研究者の育成にも注力しました。また、拠点運営では、所外、学外の関連分野有識者と化学研究所の教員を委員とする共同研究委員会および運営評議会を核として、共同研究課題の公募・採択などを戦略的に遂行してきました。

このようなグローバルな拠点活動が評価され、化学研究所は、平成３０年１１月１３日文部科学大臣から国際共同利用・共同研究拠点に認定され、「化学関連分野の深化・連携を基軸とする先端・学際グローバル研究拠点」として発展的な活動を強化しています。国際共同利用・共同研究拠点活動第二期２年目にあたる令和５年度には、化学研究所教員が一丸となって、２２３件の応募の中から採択された１４７件の共同研究を遂行しました。そのうち、グローバルな化学研究の展開と人材育成のため、国際共同研究枠を採択数の４８％に当たる７１件（若手国際枠３件を含む）を遂行しました。令和２年度から始まった世界的な新型コロナウイルス感染症拡大による国際・国内共同研究の対面交流の制限がようやく解除され、従前に近い共同研究活動がようやく再開されました。一方で、この災禍を機に拠点活動支援として整備したリモート実験環境やハイブリッド会議システムなど、新たな研究・教育環境も引き続き有効に活用しています。今後とも、国際的ハブ機能を活用し、国際共同利用・共同研究の一層の促進、国際学術ネットワークの充実、国際的・先進的視野をもつ若手研究者の育成に取り組むことで、化学を中心とする研究分野の深化と境界学術分野の新規開拓を一層推進して参ります。皆様にはさらなるご支援・ご協力のほどよろしくお願い申し上げます。

本報告書は、令和５年度の本拠点における研究成果をとりまとめたものです。本報告書をご一読頂き、今後の本拠点の目指すべき方向や活動の推進方法などに関する忌憚のないご意見・ご提案などをお聞かせ下されば幸甚に存じます。

化学研究所
所長 島川 祐一

令和5年度 共同利用・共同研究報告書 目次

1. 共同研究成果報告

分野選択型共同研究

ビーム科学分野

元素科学分野

※ 国際共同利用・共同研究

※ 国際共同利用・共同研究

※ 国際共同利用・共同研究

※ 国際共同利用・共同研究

※ 国際共同利用・共同研究

※ 国際共同利用・共同研究

※ 国際共同利用・共同研究

※ 国際共同利用・共同研究

施設・機器利用型共同研究

※ 国際共同利用・共同研究

２．国際学会、シンポジウム・研究報告会

３．成果発表論文

（令和 6 年 3 月までに刊行された論文で、平成 22－令和 4 年度の成果報告書に掲載されていないもの）

紙数の都合により、*を付けた論文のみについて、別刷りを本報告書に記載する。

1)* Mirusviruses link herpesviruses to giant viruses, *Nature*, 616, 783–789 (2023).

2)* Unusual nuclear exchange within a germanium-containing aromatic ring that results in germanium atom transfer, *Nat. Commun.*, 14, 4519 (2023).

3) Inkjet-Based Intracellular Delivery System that Effectively Utilizes Cell-Penetrating Peptides for Cytosolic Introduction of Biomacromolecules through the Cell Membrane, *ACS Appl. Mater. Interfaces*, 15, 47855–47865 (2023).

4) An Unsymmetrical 5,15-Disubstituted Tetrabenzoporphyrin: Effect of Molecular Symmetry on the Packing Structure and Charge Transporting Property, *Org. Lett.*, 25, 7354–7358 (2023).

5) Bar Coating Process of Two-Dimensional Lead Iodide Perovskite Solar Cells: Effects of Vertical Orientation, Anisotropic Photoconductivity, and Conversion Time, *ACS Appl. Energy Mater.*, 6, 9381–9389 (2023).

6) DIENELACTONE HYDROLASE LIKE PROTEIN1 negatively regulates the KAI2-ligand pathway in Marchantia polymorpha, *Curr. Biol.*, 33, 3505-3513 (2023).

7) Effect of helium irradiation on the hydrogen isotope retention in tungsten by in situ TEM and STEM-EELS analysis, *Nucl. Mater. Energy*, 36, 101484 (2023).

8) Intense absorption of azulene realized by molecular orbital inversion, *Chem. Commun.*, 59, 10604-10607 (2023).

9) Torsion Angle Analysis of a Thermally Activated Delayed Fluorescence Emitter in an Amorphous State Using Dynamic Nuclear Polarization Enhanced Solid-State NMR, *J. Am. Chem. Soc.*, 145, 16324–16329 (2023).

10) iAMPCN: a deep-learning approach for identifying antimicrobial peptides and their functional activities, *Brief. Bioinformatics*, 24, bbad240 (2023).

11) Competitive Double Friedel-Crafts 2,5-and 1′ ,2-Diacylation of Monophosphaferrocenes, *Organometallics*, 42, 1667–1673 (2023).

12) Fertilization controls tiller numbers via transcriptional regulation of a MAX1-like gene in rice cultivation, *Nat. Commun.*, 14, 3191 (2023).

13) Asymmetric Metathesis Dimerization/Kinetic Resolution of Racemic Planar-Chiral Vinylphosphaferrocenes, *Organometallics*, 42, 1629–1638 (2023).

14) Development of Bronze Phase Titanium Dioxide Nanorods for Use as Fast-Charging Anode Materials in Lithium-Ion Batteries, *ACS Omega*, 8, 15360–15370 (2023).

15) Nonlinear shear rheology of concentrated poly(vinyl alcohol)/borax aqueous solution: Nonlinearity of sticky Rouse relaxation, *J. Non-Newton. Fluid Mech.*, 316, 105012 (2023).

16) Effect of the internal pressure of helium bubbles on the morphology and mobility of beryllium, *Fusion Eng. Des.*, 191, 113720 (2023).

17) Rouse Analysis of Nonlinear Rheology of Unentangled Polymer Melts under Fast Shear: Viscoelastic Response to Superposed Oscillatory Strain, *Macromolecules*, 56, 2930–2938 (2023).

18) Redundant function of the Arabidopsis phosphatidylinositol 4-phosphate 5-kinase genes PIP5K4-6 is essential for pollen germination, *Plant J.*, 117, 212-225 (2023).

19) Synthesis, Characterization, and Catalytic Activity of a Cubic [Mo3S4Pd] Cluster Bearing Bulky Cyclopentadienyl Ligands, *Eur. J. Inorg. Chem.*, 26, e202300399 (2023).

20) A rapid genome-wide analysis of isolated giant viruses using MinION sequencing, *Environ. Microbiol.*, 25, 2621-2635 (2023).

21) CH_3CN@open-C_{60}: An Effective Inner-Space Modification and Isotope Effect Inside a Nano-Sized Flask, *Chem. Eur. J.*, 29, e202301161 (2023).

22) Tin Halide Perovskite Solar Cells with Open-Circuit Voltages Approaching the Shockley-Queisser Limit, *ACS Appl. Mater. Interfaces*, 15, 32487–32495 (2023).

23) Thermal properties and phase transition behaviors of possible caloric materials $Bi_{0.95}Ln_{0.05}NiO_3$, *J. Mater. Chem. A*, 11, 15389-15393 (2023).

24) Construction of a 21-Membered-Ring Orifice on [60]Fullerene, *ChemPlusChem*, 88, e202300225 (2023).

25) Bilateral π-extension of an open-[60]fullerene in a helical manner, *Chem. Commun.*, 59, 6560-6563 (2023).

26) Synthesis of open-[70]fullerenes bearing huge orifices, *Chem. Commun.*, 59, 7387-7390 (2023).

27) Open-[60]fullerene-aniline conjugates with near-infrared absorption, *RSC Adv.*, 13, 14575-14579 (2023).

28) Cascade Charge Transitions of Unusually High and Mixed Valence $Fe^{3.5+}$in the A-Site Layer-Ordered Double Perovskite $SmBaFe_2O_6$, *J. Am. Chem. Soc.*, 145, 10756–10762 (2023).

29) π -Extended Open-[70]Fullerenes with a Fused Azaacene, *Org. Lett.*, 25, 2815–2819 (2023).

30) Effects of electron-accepting substituents on the fluorescence of oxygen-bridged triarylamine, *Dyes Pigm.*, 215, 111281 (2023).

31) Synthesis of Hydrogen-Bonded Open-[60]Fullerenol Dimers, *ChemPlusChem*, 88, e202300136 (2023).

32) Electron microscopy of carbides in annealed 28 wt% Cr-1 wt% (Mo/W) cast irons, *Mater. Charact.*, 198, 112723 (2023).

33) Giant caloric effects in charge-spin-lattice coupled transition-metal oxides, *J. Mater. Chem. A*, 11, 12695-12702 (2023).

34) Dual Catalysis of Gold Nanoclusters: Photocatalytic Cross-Dehydrogenative Coupling by Cooperation of Superatomic Core and Molecularly Modified Staples, *Angew. Chem. Int. Ed.*, 63, e202312135 (2024).

35) Identification of a Self-Assembling Small-Molecule Cancer Vaccine Adjuvant with an Improved Toxicity Profile, *J. Med. Chem.*, 66, 13266–13279 (2023).

36) Radical Caging Strategy for Cholinergic Optopharmacology, *J. Am. Chem. Soc.*, 145, 10651–1065 (2023).

37) Macropinoscope: Real-Time Simultaneous Tracking of pH and Cathepsin B Activity in Individual Macropinosomes, *Anal. Chem.*, 95, 11410–11419 (2023).

38) Structural Dissection of Epsin-1 N-Terminal Helical Peptide: The Role of Hydrophobic Residues in Modulating Membrane Curvature, *Chem. Eur. J.*, 29, e202300129 (2023).

39) Bulk Rashba-Type Spin Splitting in Non-Centrosymmetric Artificial Superlattices, *Adv. Sci.*, 10, 2206800 (2023).

40) A Fast and Easy Method to Co-extract DNA and RNA from an Environmental Microbial Sample, *Microbes. Environ.*, 38, ME22102 (2023).

41) Bilayer Indium Tin Oxide Electrodes for Deformation-Free Ultrathin Flexible Perovskite Solar Cells, *Sol. RRL*, 7, 2300221 (2023).

42) Multiple Stimuli-Responsive Supramolecular Organic Framework under Concomitant Emission Color Changes, *J. Phys. Chem. C*, 127, 20459–20465 (2023).

43) Dynamic nuclear polarization - nuclear magnetic resonance for analyzing surface functional groups on carbonaceous materials, *Carbon*, 206, 84-93 (2023).

44) Biosynthesis of gibberellin-related compounds modulates far-red light responses in the liverwort Marchantia polymorpha, *Plant. Cell.*, 35, 4111–4132 (2023).

45) Synthesis of inter-[60]fullerene conjugates with inherent chirality, *Nat. Commun.*, 15, 514 (2024).

46) Structural and Magnetic Properties of the B-Site-Ordered Double Perovskites Ln_2NiTiO_6 (Ln = La, Pr, and Nd), *Bull. Chem. Soc. Jpn.*, 96, 1269–1273 (2023).

47) Small molecule activation based on novel heavier group 13/15 interelement compounds, λ3,λ3-phosphanylalumanes, *Bull. Chem. Soc. Jpn.*, 97, bcsj.20230186 (2024).

48) SMG: self-supervised masked graph learning for cancer gene identification, *Brief. Bioinformatics*, 24, bbad406 (2023).

49) Multicomponent Approach for Stable Methylammonium-Free Tin-Lead Perovskite Solar Cells, *ACS Energy Lett.*, 9, 432–441 (2024).

50) Mixed-Ligand Approach to Palladium-Catalyzed Direct Arylation of Heteroarenes with Aryl Chlorides: Controlling Reactivity of Catalytic Intermediates via Dynamic Ligand Exchange, *Organometallics*, 42, 3454–3465 (2023).

51) Crystal-Like Atomic Arrangement and Optical Properties of $25La_2O_3$-$75MoO_3$ Binary Glasses Composed of Isolated MoO_4^{2-}, *Inorg. Chem.*, 63, 5701–5708 (2024).

52) Cobalt-Functionalized Open-[60]Fullerenes, *Organometallics*, 43, 227–232 (2024).

53) An open-cage bis[60]fulleroid as an electron transport material for tin halide perovskite solar cells, *Chem. Commun.*, 60, 2172-2175 (2024).

54) Recent progress in the chemistry of heavy aromatics, *Proc. Jpn. Acad., Ser. B, Phys. Biol. Sci.*, 99, 480-512 (2023).

54) Synthesis and Luminescence Properties of Self-Assembled Lanthanide Complexes with an EDTA-Type Chelating Ligand in Aqueous Ethanol Solution, *Bull. Chem. Soc. Jpn.*, 96, 538–544 (2023).

55) The Reduction of Metallabenzenes: Different Scenarios Highly Dependent on the Central Group 14 Elements, Si vs. Ge, *Chem. Asian J.*, 19, e202300945 (2024).

56) Potassium 2-germanaphthalenide: an isolable polycyclic system of germanium-incorporated anionic benzenoid, *Inorg. Chem. Front.*, 11, 400-408 (2024).

57) Synthesis and characterization of novel hydrodigermenide and digermyne radical anion, *Polyhedron*, 244, 116614 (2023).

58) Disruption of p-coumaroyl-CoA:monolignol transferases in rice drastically alters lignin composition, *Plant Physiology*, 194, 832–848 (2024).

59) Anthriscus *sylvestris* Deoxypodophyllotoxin Synthase Involved in the Podophyllotoxin Biosynthesis, *Plant Cell Physiol.*, 64, 1436–1448 (2023).

60) Simultaneous suppression of lignin, tricin and wall-bound phenolic biosynthesis via the expression of monolignol 4-O-methyltransferases in rice, *Plant Biotechnol. J.*, 22, 330-346 (2024).

61) SciPROP-R: An Effective Bisphosphine Ligand for the Chemo-Selective Iron-Catalyzed Suzuki-Miyaura Coupling of Alkyl Chlorides, *Bull. Chem. Soc. Jpn.*, 96, 1298–1309 (2023).

62) Biological evaluation of a phosphate ester prodrug of 10-methyl-aplog-1, a simplified analog of aplysiatoxin, as a possible latency-reversing agent for HIV reactivation, *Biosci. Biotechnol. Biochem.*, 87, 1453–1461 (2023).

４．参考資料

1. 共同研究成果報告

Radiolysis of concentrated native proteins by accelerated electrons

Quentin Raffy　Institut Plurisdisciplinaire Hubert Curien

We conduct basic researches on radiolysis, especially in a context of radiotherapy. Our aim is to better describe and understand the physico-chemical mechanisms of radiolysis of water and biomolecules. In the present project, radiolysis of concentrated proteins by accelerated electrons was studied. The aim was to compare the results with data obtained with accelerated ions at HIMAC, Japan, ACACIA, France, and with quasi continuous electron beams at Aerial, France. Experiments took place February 7, 8 ant 9th at Kyoto University, with Ryo Ogawara and Satoshi Kodaria and Tamn Kusumoto, from QST team.

The experiments were performed in a lab-made remote-controlled irradiation cell built by IPHC. Protein radiolysis was followed on-line by UV-Visible and infrared spectroscopies, using portable spectrometers. Three proteins were irradiated, chosen for their secondary structures and which have all been also studied under ion irradiation. They were irradiated in form of thin (20 µm) protein gels in D_2O. We were able to reconstruct evolution of the secondary structure of the proteins with irradiation dose. For myoglobin, similar results were obtained compared with lower dose-rate electron irradiations. Compared to accelerated ions, the evolution is much more drastic with dose, showing a possible difference in the radiolysis mechanisms involved. Data with other proteins are currently being analyzed.

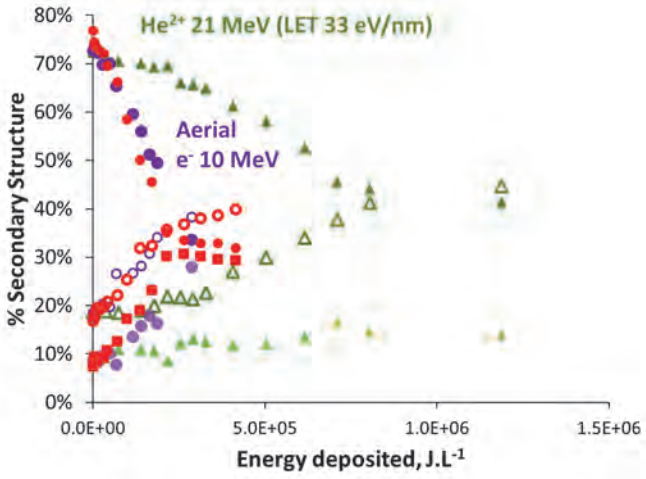

Figure: Evolution of the secondary structure of myoglobin with deposited energy. Red symbols, irradiations with 12 MeV e^-, Kyoto Univ. (circles: beta structures, discs: alpha and random structures). Violet symbols, irradiations with 10 MeV e^-, Aerial (Circles: beta structures, discs: alpha and random structures). Green symbols, Irradiations with 21 MeV He^{2+} ions, HIMAC (empty triangles: beta structures, full triangles: alpha and random structures).

Development of energy sensitive muon spin rotation (muSR) spectrometer

Yue Ma RIKEN

Research Purpose

Muon spin rotation (muSR) method is a widely used experimental technique to study the magnetic properties of materials. In a muSR experiment, a beam of positive muons is implanted into a sample and the muons' spin precession in the local magnetic field is measured by employing the alignment between muon spin and positron emission angle This alignment depends on the energy of the positron: a higher-energy positron exhibits a more precise alignment with the direction of the muon spin. However, current muSR spectrometers are not able to detect the energy of positrons. We, therefore, propose to develop a new type of muSR spectrometer that can measure the positron energy and improve the precision of the muSR method. To fully understand the capabilities and limitations of our proposed energy-sensitive muSR spectrometer, it is important to investigate the actual energy resolution in the range of 10 to 50 MeV covering the decayed positron energy.

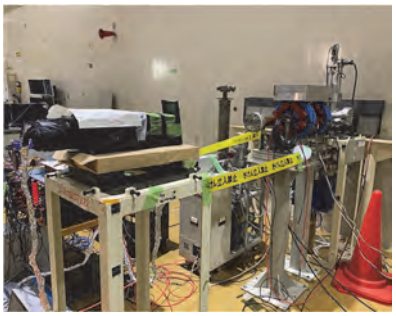

Figure 1, Experiment setup. Electron beam comes from the right side and hit on the lead glass crystal installed on the left.

Experiment method

The experiment setup is shown in Figure 1. We prepared a lead glass crystal with dimension of 12cm×12cm×34cm to investigate its energy resolution with 30, 40 and 50 MeV electron beam. We used a flash Analog-to-Digital converter to record the full waveform information of the photomultiplier signal, which enables us to effectively select the true physical events. Two configurations are used to compare the energy resoltion. In the beginning, we shoot the electron beam along the longitudinal direction; after that, we rotate the crystal by 90 degree to bombard electron from the side direction. The data taking was carried out during December 11th~15th, 2023 at KAKEN.

Experiment result

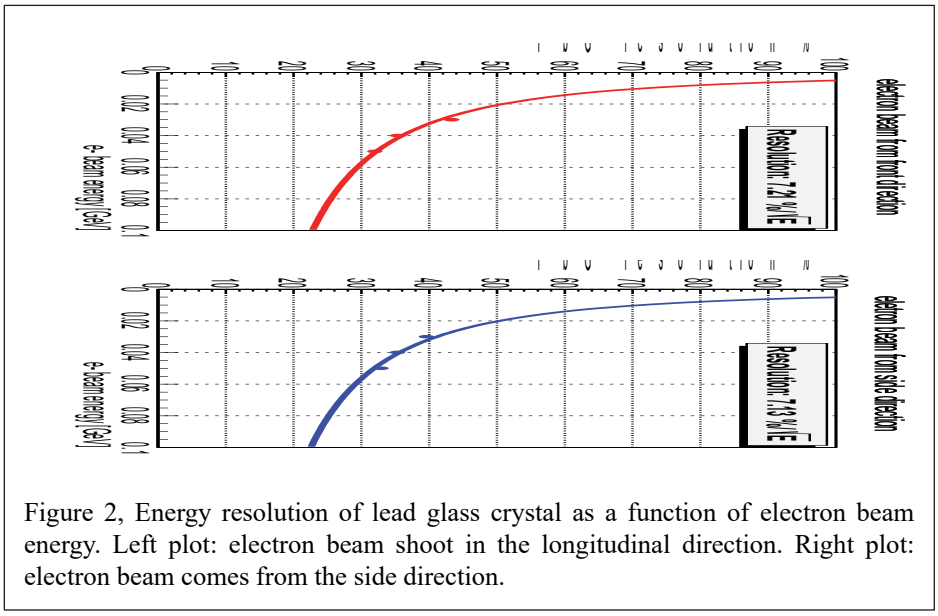

Figure 2, Energy resolution of lead glass crystal as a function of electron beam energy. Left plot: electron beam shoot in the longitudinal direction. Right plot: electron beam comes from the side direction.

The results for the lead glass crystal energy resolution as a function of the electron beam energy is given in Figure 2. Both data sets are fitted by $y = R/\sqrt{E}$, where R is the energy resolution we are interested, and E is electron beam energy in the unit of GeV. To our best knowledge, this is the first direct demonstration that the electromagnetic calorimeter holds the $R/\sqrt{E}$ type of energy resolution even with electron energy well below 100 MeV. This encouraging discovery allows us to proceed to estimate the performance of the proposed energy sensitive muSR spectrometer. Specifically, the derived ~7% energy resolution is among the top-class performance for a similar setup, which can improve the muSR precision by ~1.5 times according to our simulation.

Summary

With the fruitful collaboration with KAKEN, we have successfully measured the energy resoltuion for the lead glass crystal at 30, 40 and 50 MeV electron beam energy. The derived energy resolution provides a solid ground for the further development of our innovative muSR spectrometer.

Development of new nano-structure target for ISOL

Tetsuya Ohnishi　RIKEN

[Objective] In the Isotope-online-separator (ISOL) method, which is one of the production methods of radioactive isotopes (RI), the production target is irradiated with high-energy particles, and unstable nuclei produced in the target are extracted by heating the target to a high temperature around 2,000 degrees. For this reason, carbides with low vapor pressure at high temperature and high melting points are often used as production targets. However, previous studies show that the life time of the carbide target is about one week. This is because the carbides are sintered in a high-temperature environment, resulting in smaller gaps inside the production target and the un-appearance of unstable nuclei. Although carbides with carbon nanotubes are proposed, they are easily combustible due to its nano structure, and dedicated equipment is required for handling. The objective of this study is to develop easy-to-handle production target for ISOL using new carbides with nanostructures such as carbon nanotubes and graphene.

[Methods] First step: Using compounds of the objective elements (oxides etc) and carbon materials, disks with 1 mm of thickness and about 20 mm of diameter are made pressing high pressure, around 8 MPa. Second step: Produced disks are converted to the carbides heating to a high temperature, about 1,300 degrees, in the vacuum chamber. Third step: produced carbide disks are examined their nano structure using electron microscope, and they are also examined their life time and RI-production efficiency through the production rate of unstable nuclei.

This year, based on previous experience, we reviewed mainly how to safely perform target-handling operations, particularly those using the carbonization equipment.

[Results] At the start of the use of the carbonization equipment, uranium target is stable as an oxide. After the carbonization, uranium carbide target is highly combustible and quickly heat up in air, revert to oxides, and crumble easily. Therefore, it is a key issue how to safely extract uranium carbide targets from the equipment. To meet such a requirement, we decided to add a glove port chamber (left figure in Figure 1) to the existing carbonization equipment. This year, we prepared the target port chamber (right figure in Figure 1), which is a part of the glove port chamber.

[Consideration] This fiscal year, due to budget constraints, we were only able to improve a portion of the planned glove port chamber, but next fiscal year we plan to take budgetary action, improve the glove port chamber, and perform the carbonization. We would like to make improvements based on the results, and also plan to improve the handling of irradiated carbonized targets.

[Reports] None in particular.

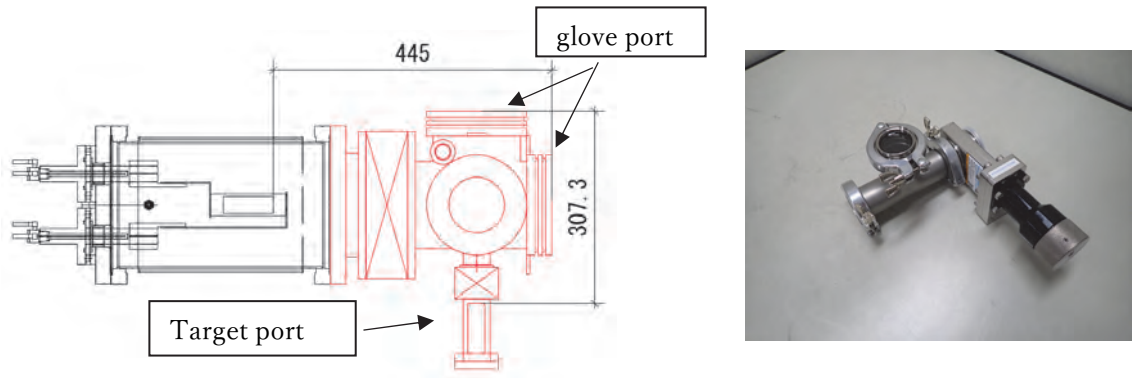

Fig. 1 Left) Systematic figure of the glove port chamber, Red-colored parts are new items to be manufactured. Right) Photograph of the target port chamber.

On the mechanism of proton reduction catalyzed by cubic [Mo_3S_4Pd] clusters: a computational study

W. M. C. Sameera　University of Colombo

Transition metal complexes and clusters can be used as homogeneous catalysis to perform N_2 reduction and catalytic H_2 evolution under mild conditions. Quantitative mechanistic details are very important for experimental researchers to understand atomic scale chemical events. In this direction, quantum chemical calculations, employing Density functional theory (DFT), are essential.

Objectives: The Ohki group at the ICR developed a [$Cp^{SiEt3}{}_3Mo_3S_4Pd$]Cl cluster that can perform hydrogen evolution in the presence of $HOCH_2CF_3$. A detailed computational study was performed to rationalize the mechanisms of the full catalytic cycle.

Computational methods: The possible spin states [$Cp^{SiEt3}{}_3Mo_3S_4Pd$]Cl cluster and the mechanism of the hydrogen evolution and catalytic reduction of CO_2 to CO were calculated using DFT.

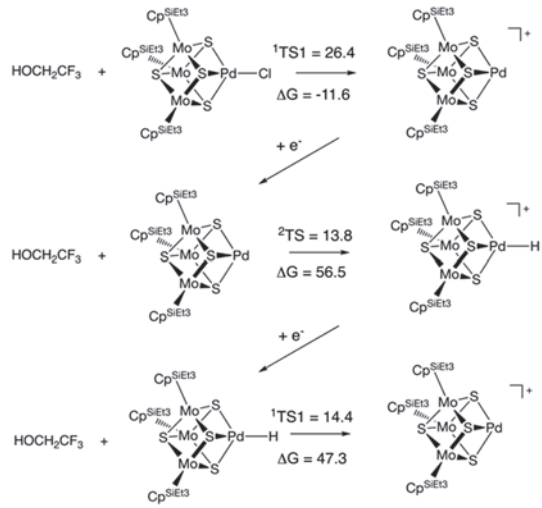

Results and discussions: The ground state of the [$Cp^{SiEt3}{}_3Mo_3S_4Pd$]Cl is the closed-shell singlet, $S = 0$. Starting from this, the active intermediate, [$Cp^{XL}Mo_3S_4Pd$], can be formed through a free energy barrier of 26.4 kcal/mol. After that, subsequent protonation and one election reduction steps occur through relatively low energy barriers to produce H_2. This study gave important electronic structural and mechanistic implications to develop novel transition metal clusters for catalytic H_2 evolution under mild conditions. The mechanism of the catalytic reduction of CO_2 to CO is under investigation.

Joint Publication on This Work: H. Izu, D. G. Bhave, Y. Matsuoka, W. M. C. Sameera, K. Tanifuji, Y. Ohki, *Eur. J. Inorg. Chem.* 2023, 26, e202300399.

Representative Presentation: W. M. C. Sameera, Quantum chemical modeling of excited states and properties, Kwansei Gakuin University, Japan. (Invited)

Development and device evaluation of new D-A emitters based on rigidified planar triarylborone acceptors

Todd B. Marder　Julius-Maximilians-Universität Würzburg

Thermally activated delayed fluorescence (TADF) materials have become popular as next generation fluorescent emitters in organic light-emitting diodes (OLEDs). For TADF applications in OLEDs, it is critical to accelerate reverse intersystem crossing (RISC) because slow RISC leads to a decline in device performance. For fast RISC, enhancing spin-orbit coupling by mediating a locally excited triplet state (^{3}LE) in RISC is an effective method. In this work, we dealt with triarylborane TADF emitters, **Phox-^{Me}π**, **Phox-^{MeO}π**, and **^{MeO3}Ph-^{FMe}π** prepared by our group [1]. **Phox-^{MeO}π** and **^{MeO3}Ph-^{FMe}π** were designed to locate the ^{3}LE$_\pi$ (^{3}LE$_\pi$: LE confined on π-bridge) close in energy to the charge transfer triplet state (^{3}CT) to be involved in RISC by changing the substituents (MeO, CF_3) on the π-bridge (**Figure 1**). Therefore, we can expect fast RISC for **Phox-^{MeO}π** and **^{MeO3}Ph-^{FMe}π**.

With the Kaji group, we fabricated doped films of **Phox-^{Me}π**, **Phox-^{MeO}π**, and **^{MeO3}Ph-^{FMe}π** with 5 wt% in mCBP for photophysical experiments. Device fabrications were conducted for **Phox-^{Me}π** and **Phox-^{MeO}π** by a solution process. The device structure was ITO (50 nm)/PEDOT:PSS (45 nm)/PVK (15 nm)/5 wt% emitter: mCBP (40 nm)/PPF (10nm)/TPBi (45 nm)/Liq (1 nm)/Al (80 nm). In these devices, ITO and Al act as the anode and cathode, respectively. PEDOT:PSS was used for the hole injection layer, PVK for the hole blocking layer, mCBP for the host material of the emitter layer, PPF for the electron blocking layer, TPBi for the electron transport layer, and Liq for the electron injection layer.

Transient photoluminescence (PL) measurements showed that the lifetimes of delayed fluorescence (τ_{DF}s) were 1.4, 0.9, and 2.2 μs for **Phox-^{Me}π**, **Phox-^{MeO}π**, and **^{MeO3}Ph-^{FMe}π**, respectively, suggesting fast RISC. We obtained large rate constants of RISC (k_{RISC}s) exceeding 10^6 s^{-1} for **Phox-^{MeO}π** and **^{MeO3}Ph-^{FMe}π** as we expected, which indicates the effectiveness of ^{3}LE mediation in RISC. **Phox-^{Me}π** and **Phox-^{MeO}π**-based OLEDs exhibited maximum external quantum efficiencies (EQE_{max}) of 10.0% and 6.7%, respectively. Moreover, **Phox-^{Me}π**-based OLED rendered a smaller efficiency-roll off than **Phox-^{MeO}π**-based OLED. This is because of the smaller k_{ISC}/k_{RISC} value of **Phox-^{Me}π**. From these experiments, we found that mediating ^{3}LE in RISC is effective in facilitating a RISC and a small k_{ISC}/k_{RISC} value leads to suppressing efficiency roll-off.

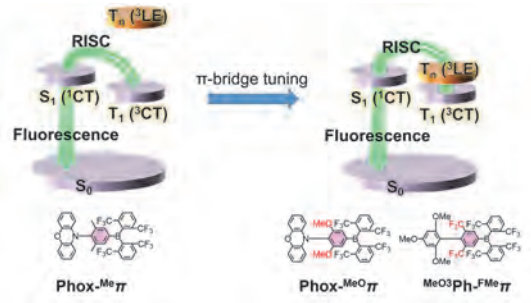

Figure 1. Schematic illustration of molecular design.

[1] A. K. Narsaria, J. Nitsch, F. M. Bickelhaupt, T. B. Marder *et al.*, *Adv. Funct. Mater*. **30**, 2002064 (2020).

Design and Tailoring Advanced Functional Materials: Symmetry Operation and High Pressure Synthesis

Wei-Tin Chen　National Taiwan University

[Introduction] It is essential in modern condensed matter sciences to explore and realise novel functional materials with fascinating physical and chemical properties, not only to understand their fundamental mechanism and also their potential applications. Within various advance crystalline sample preparation methods, high pressure high temperature (HPHT) synthesis techniques are one of most effective approaches to explore such novel materials and to tailor their functionalities. In this project, it is aimed to design and to realise metalstable oxide materials which exhibit exotic phase transitions that are owing to the lattice/charge/orbital/spin degree of freedom. The ultra high pressure and temperature conditions were carried out with the collaboration with Advanced Solid State Chemistry Laboratory (Prof. Shimakawa), and further high resolution synchrotron x-ray diffraction (SXRD) were conducted at Taiwan Photon Source (TPS) for structure analysis.

[Results and discussion] In order to study the magnetic interaction with extended pathway, recently we successfully stablised Mn^{2+} (d^5) and Te^{6+} (d^{10}) B-site ordered double perovskite with calcium and mercury into the A site. Ca_2MnTeO_6 (CMTO) adapts $P2_1/n$ monoclinic structure, while Hg_2MnTeO_6 (HMTO) crystallised in a R-3 rhombohedral lattice. Both CMTO and HMTO exhibit antiferromagnetic behavior at low temperature with T_N ~10 K. The ionic radii of calcium and mercury are rather similar, yet CMTO and HMTO crystallised in very different space group with distinct symmetry operation such as octahedral rotation and tilting. The magnetic structures of CMTO and HMTO were with the same manner when ordered below the T_N, yet a novel incommensurate magnetic ordering possibly originated from a helical structure was revealed in HMTO at base temperature. To further understand the structure transition in between CMTO and HMTO, a series of $(Ca_xHg_{1-x})_2MnTeO_6$ solid solution was prepared with HPHT synthesis techniques. The series are successfully prepared indicating by x-ray diffraction (Fig. 1). Further magnetic and physical property measurements will be carried out and examined.

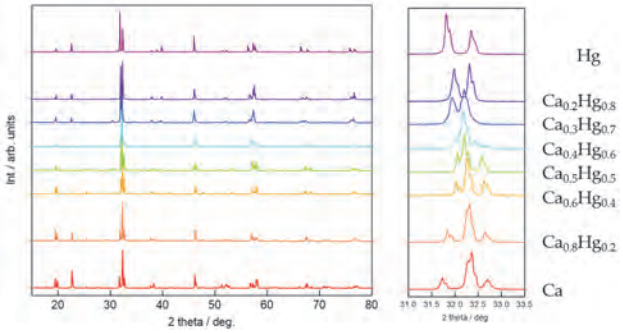

Fig. 1 XRD patterns of $(Ca_xHg_{1-x})_2MnTeO_6$ perovskite series.

High-performance materials for energy storage electrochemical devices

Susana García-Martín　Complutense University of Madrid

Objectives:

Synthesis and structural characterization of Fe-oxides with perovskite related structure with electrocatalytic properties for cathodes of solid oxide fuel cells (SOFCs). Determination of the electronic structure of Fe-perovskites.

Experimental Methods:

Synthesis: The compounds have been prepared by solid state reaction at air. Some of the oxides have been followed a thermal treatment under ozone atmosphere with the aim of increasing the Fe-oxidation state by increasing the oxygen content. Progress of the reactions were inspected by powder X-ray diffraction.

The oxygen content of the compounds was determined by thermo-gravimetric analysis. Besides, the average oxidation state of Fe was determined by Mössbauer spectroscopy.

Crystal structure characterization has been carried out by means of synchrotron X-ray diffraction (SXRD) and Mössbauer spectroscopy.

DFT calculations of the electronic structure of some of the compounds were carried out using the WIEN2k program.

Results:

We have prepared different oxides with stoichiometry $AA'Fe_2O_{5+\delta}$ (A = Y or lanthanide element, A' = Ba, Ca) with different oxygen contents. Mössbauer spectroscopy confirmed that the oxidation state of the Fe in the oxides with low δ value is 3+. However higher oxidation states for Fe have been found in the compounds after oxidation in ozone. Coordination polyhedra around the Fe atoms were evaluated by Mössbauer spectroscopy that in addition to SXRD data, allowed us to determine the crystal structure. We have found complex orderings of the A and A' cations in combination with the ordering of the oxygen-polyhedra around the Fe atoms. During heating, the Y-compounds show valence changes from Fe^{4+} to Fe^{3+} through an intermediate $Fe^{3+\delta}$ in such a way that a charge ordering model is being proposed.

Publications: These results are going to be presented in the next Gordon Conference on Solid State Chemistry (July-2024).

High-pressure synthesis and Li conducting study of Li-Al-Cl compounds as solid electrolytes in batteries

KOEDTRUAD Anucha　Chinese Academy of Science

Objectives: we aim to introduce the metastable Li ions at tetrahedral sites of ternary $LiAlCl_4$ by preparing the compounds with nominal composition Li_2AlCl_5 and Li_3AlCl_6 via mechanochemical synthesis and high pressure synthesis

Experiment: The materials were initially prepared via mechanochemical synthesis using a ball milling machine. Starting materials, LiCl and $AlCl_3$ were roughly mixed and grinded using a mortar and a pestle in a glovebox. The mixture was then loaded in a sealed ZrO_2 grinding pot and milled through the machine with the milling speed 300-500 rpm for 3 hrs. The obtained materials were then characterized by a conventional XRD.

Results and discussion: Figure 1 shows XRD patterns of the Li_3AlCl_6 prepared under different grinding speed. At grinding speed of 400 rpm, the pattern shows new peaks indicating new phase formation. With increasing the speed to 500 rpm, the peaks become broad and less intense which indicate low crystallinity due to decomposition. Therefore, the speed of 400 rpm was chosen for further synthesis of other compositions. The patterns of all compositions, $LiAlCl_4$,Li_2AlCl_5 and Li_3AlCl_6, indicate mixed phases. To improve the quality of samples, longer milling time may be required. Furthermore, using a high pressure synthesis technique may also provide better quality samples. Unfortunately, the proposed high pressure experiment in ICR could not been conducted due to some reasons and the results shown here are only based on the typical mechanosynthesis.

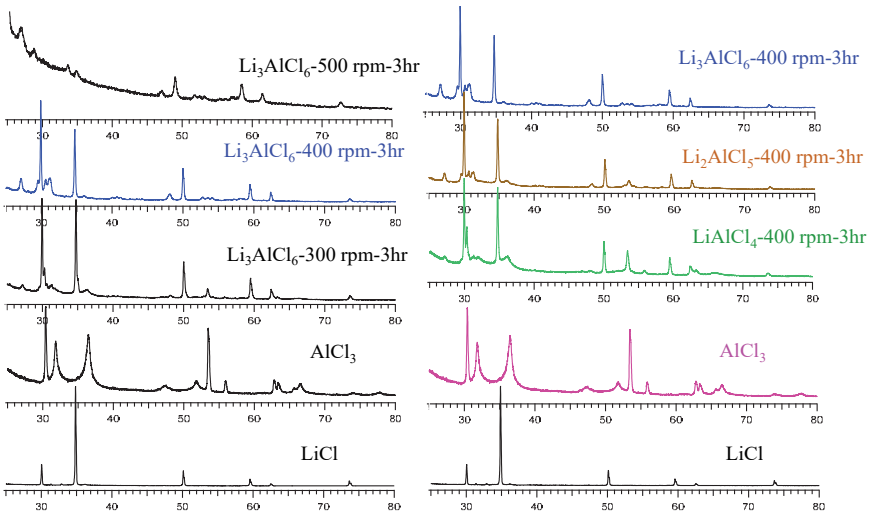

Figure 1. XRD patterns of the Li_3AlCl_6 prepared at different grinding speed (left) and of the $LiAlCl_4$, Li_2AlCl_5 and Li_3AlCl_6 prepared at grinding speed of 400 rpm (right)

Crystal structures and oxygen conduction properties research of metal oxides at high temperature

Haichuan Guo　Chinese Academy of Sciences

Introduction

Metal oxides are important class of materials in energy-related technology fields. They are used, for example, as cathodes in solid oxide fuel cells and as ceramic membranes separating oxygen from air. In our former joint research, we found that in perovskite oxides, the oxygen contents at high temperature were highly affected by the degree of the *A*-site ions order.[1] Here, *A*-site layer ordered and disordered $LaCa_2Fe_3O_9$ (LCFO) with unusually high valence $Fe^{3.67+}$ were synthesized using high-pressure and high-temperature method. Their crystal structures at high temperature were investigated using neutron powder diffraction (NPD) method.

Experiments and results

LCFO were obtained by oxidizing the oxygen deficient $LaCa_2Fe_3O_8$ precursor at 4 GPa using cubic-anvil high-pressure equipment in ICR. The degree of the *A*-site ions order was determined by the oxidizing temperature. Reaction at 500°C kept the *A*-site layered structure while the temperature of 1500°C made the *A*-site cations disordered. NPD measurements was performed on the two species with the same chemical composition at Multi-Physics Instrument of CSNS. The low angle bank diffraction patterns of *A*-site ordered and disordered LCFO at 727°C are shown in Fig.1. The high temperature patterns are very similar, however, the superlattice diffraction peak at approximately 13.5 Å of the *A*-site ordered LCFO indicates that the *A*-site layered structure maintained at this temperature. On the other hand, the generation of *A*-site layered structure is not observed in the disordered LCFO during the measurement. Further analysis of NPD data and oxygen conduction properties research of LCFO are planned.

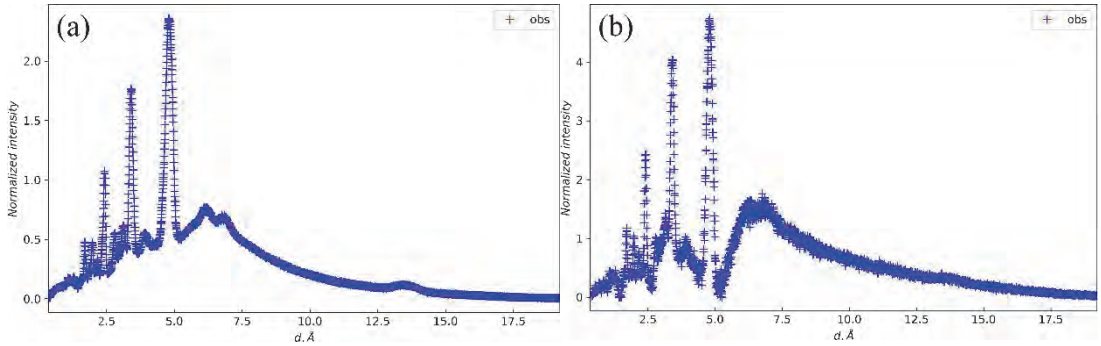

Fig.1 NPD patterns of (a) *A*-site ordered and (b) disordered LCFO at 727°C

[1] *Chemistry of Materials*, 2022.01, 34(1), 345-350

Photocatalytic C-H Bond Functionalization

Alakananda Hajra　Visva-Bharati University

ICR partner researcher's name: Prof. Masaharu NAKAMURA

Objective: Development of C-H bond forming reactions using earth-abundant non-toxic Fe-catalysis under visible light photo-catalysis.

Visible-light photocatalysis has become an impressive tool in organic synthesis. In this realm, the merger of transition metal catalysis and visible light photoredox catalysis offers an exciting opportunity to perform the organic transformations in mild conditions. Oxazolines are naturally occurring and show potential bioactivity. We planned a photocatalytic hydrofunctionalization reaction of some unsaturated amides to construct an oxazoline-containing ring. The excited photocatalyst participates in SET with allylic amide to generate cation radical which undergoes 5-*exo-trig* cyclization to form alkyl radical.

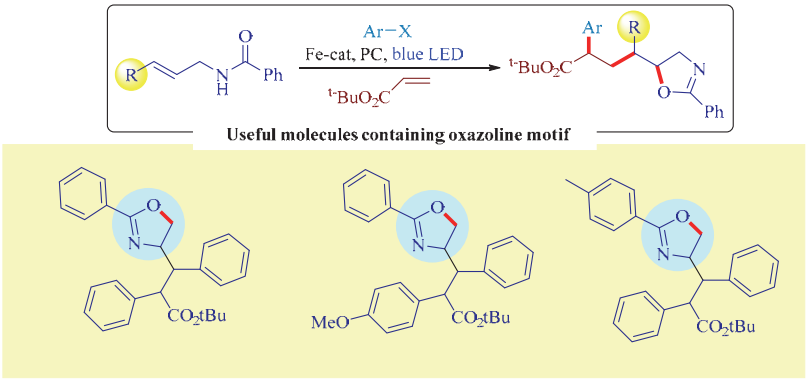

Presently we are focusing on the precise role of Fe-catalyst and visible light, and late stage modification of the compound.

A review has been communicated which is supported by grant # 2023-10.

[A review is already published which is supported by the International Collaborative Research Program of Institute for Chemical Research, Kyoto University (grant # 2022-7). https://doi.org/10.1039/D3OB00230F]

Development of Transformation of Lignin–based Aromatic Building Blocks Using Organocatalyst

Toru Hashimoto　Sanyo-Onoda City University

Objectives:

As environmental issues are growing concern, finding efficient, atom-economical and step-economical strategies for directly transformation using alcohols is a major challenge in organic chemistry. In this research project, we are challenging the development of a highly efficient and environmentally friendly synthetic process using alcohols mediated by the organosilicom compounds.

Outcomes:

Recently, we found that Ph_3SiH works the Lewis acid catalyst for the ring-opening reaction of di- and tri-substituted epoxides to afford the β-alkoxy alcohols in high regioselectivity.[1] Based on the our study, we forced on the Lewis acidity of organosilicom compounds and examined the cross-etherification reaction of the alcohols. As a result, alkoxysilane is found to be an effective mediator for the cross-etherification reaction between two distinct alcohols, namely, a secondary benzyl alcohol and an aliphatic alcohol, providing the unsymmetrical dialkyl ethers in good-to-high yields.[2] Mechanistic studies suggested that the carbocation derived from benzyl alcohol was formed, and subsequently aliphatic alcohol attacked the in situ formed carbocation to afford the desired products.

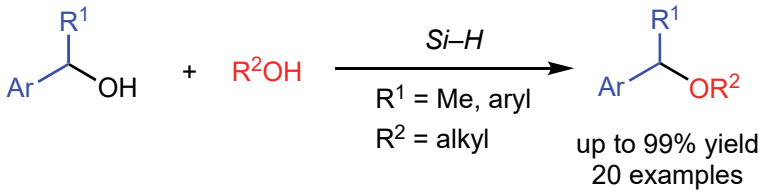

Publications:

1) Hashimoto, T.; Nishikimura, K.; Hojo, M. *ChemistrySelect* **2023**, *8*, e202303292.
2) Hashimoto, T.; Matsunaga, Y.; Okamura, Y.; Takao, S.; Hojo, M. *under preparation for submission*.

Development of Unsymmetrical π-Electron Systems of Heavier Main Group Elements and Elucidation of Their Property

Takeaki Iwamoto　Tohoku University

Objectives: We have aimed at developing unsymmetrical π-electron systems containing a double bond between group-14 and group-13 elements. These remain scarce compared to other heavier π-electron systems but are expected as prospects for advanced materials and reagents for small molecule activation.

Experimental Methods: Preparation of aluminum iodide adducts of a cyclic dialkylsilylene, (2,2,5,5-tetrakis(3,5-di-*tert*-butyl-4-methoxyphenyl)silacyclopentane-1,1-diyl) (**1**, Chart 1) and its reactions.

Outcomes: Silylene **1** reacted with AlI_3 in benzene to provide the corresponding silylene-AlI_3 complex **2** in good yield. NMR spectra of **2** indicate that the two-coordinate silicon atom of **1** simply coordinates to the Al atom of the AlI_3 moiety. Though it was difficult to obtain **2** in a pure form, **2** was isolated as a diethyl ether adduct **2**·(Et_2O). The structure of **2**·(Et_2O) was determined by single-crystal XRD analysis. In the solid state, diethyl ether in **2**·(Et_2O) coordinates to the aluminum center and one iodine atom was substituted on the silicon center. Compound **2** further reacted with TMPLi (TMP = 2,2,6,6-tetramethylpiperidyl) to provide TMP adduct **3** which was characterized by NMR spectroscopy. Product **3** should be a good precursor for the Si=Al bonded species. As a related species, unsaturated borasilacycles **4** was synthesized and characterized by single-crystal XRD analysis.

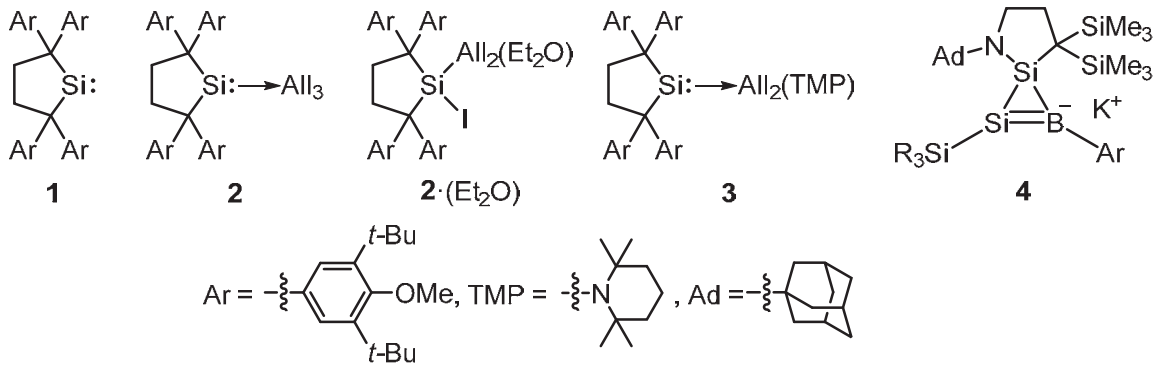

This project was done with Professors Yoshiyuki Mizuhata (ICR Partner Researcher) and Shigeyoshi Inoue (International Collaborating Researcher, Technical University of München, Germany).

Creation of Effective Oxidation Scavenger for Efficient Perovskite-based Solar Cells

Takahiro Sasamori　University of Tsukuba

The goal of our collaborative research with Prof. Dr. Atsushi Wakamiya (ICR, Kyoto University) is development of an organic oxidation scavenger for the creation of efficient lead-free perovskite-based solar cells, and pioneering research achievements on the basis of the fusion of elemental science and functional physical chemistry. Challenges for lead-free efficient perovskite-based solar cells such as Sn(II)-based ones compared with their Pb counterparts predominantly include the facile oxidation of divalent Sn(II) into Sn(IV) which leads to the increased nonradiative charge recombination in the perovskite films. Thus, we have focused our research targets on the creation of low-coordinated main group element species as effective oxidation scavengers, which exhibit redox-active property and considerable solubility in organic solvents.

Silylenes (R_2Si:) are attractive intrinsically extremely reactive species, which would exhibit possible ability of working as effecting oxidation scavengers. Isolable silylenes remain scarce, and in most hitherto reported examples, the silylene center is stabilized by electron-donating substituents (e.g., heteroatoms such as nitrogen), which results in electronic perturbation. We have been interested in the chemistry of redox-active silylenes with carbon-based substituents such as ferrocenyl groups. Furthermore, we have designed a ferrocene-based phosphenium ion with “reversible” intramolecular donor coordination, $Fc^P{}_2Si$: (**1**, Fc^P = 1’-dicyclohexylphosphino-1-ferrocenyl). The Fc^P group ascribes both stability and reactivity for the silylene center with its “switchable” donor coordination caused by the rotation of the cyclopentadienyl moiety Accordingly, the possible precursor for the silylene such as $Fc^P{}_2SiBr_2$ (**2**) and $Fc^P{}_2Si(SiMe_3)_2$ (**3**) were synthesized. The attempted synthesis of the corresponding silylene **1** by the reduction of **2** or the photochemical reaction of **3** is currently investigated. We are grateful to Prof. Wakamiya (ICR, Kyoto Univ.) for the support on the research, and fruitful discussions.

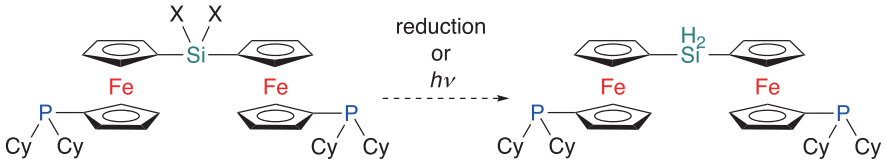

2: X = Br
3: $Si(CH_3)_3$

1

ホスフィンで保護された鉄クラスター群の合成と磁性の評価

志賀拓也　筑波大学

【緒言】

我々は、Fe や Mn を基盤とする多核金属錯体を創製し、複数の金属中心に由来する柔軟な電子状態を利用した反応性や機能性の発現に成功している。特に多核金属錯体の磁性について、複数原子間の複雑な相互作用を緻密にモデル化することで、構造・機能相関性を明らかにしてきた。本研究では、化学研究所の檜垣達也助教と共同し、低配位 Fe(II)アミド錯体である[Fe{N(SiMe$_3$)$_2$}$_2$]とホウ素試薬及びホスフィン類を混合する one-pot 型反応により新規鉄クラスターを合成した。合成したクラスターについて、ヒステリシスおよび磁化率を測定し、磁性を評価することで、鉄クラスターの新規磁性材料としての可能性について検証した。

【結果と考察】

本研究では、嵩高いホスフィンである P^{t}Bu$_3$ を配位子として合成に用いた。不活性雰囲気下でホウ素試薬および[Fe{N(SiMe$_3$)$_2$}$_2$]と反応させたところ、鉄 55 核クラスター錯体が鉄 6 核クラスターとのイオン対として再現性良く得られた。得られたクラスター錯体は、石英管にサンプリングし、MPMS-5XL にて磁化率測定を行った。まず極低温でヒステリシス測定を行ったところ、2 T 付近で磁化が飽和する様子が確認された。飽和した磁化の値は不対電子の数で約 150 個に相当し、非常に大きな値が観測された。またヒステリシス曲線はほとんど閉じているものの、小さいながらも保磁力が観測された。同様な測定を室温下で行ったところ、5 T においても磁化の飽和は観測されなかった。また MH 曲線に直線性は見られず、磁化が飽和している成分の存在が示唆された。

また同様な合成反応を Ni(II)錯体に対して行ったところ、ニッケル 4 核クラスター錯体が再現良く得られた。得られたクラスターに対し、磁化率測定を行ったところ想定よりも小さな磁化率が観測された。これはホスフィン配位子の強い配位子場により、スピン量子数のより小さい状態が安定化されるためと考えられる。

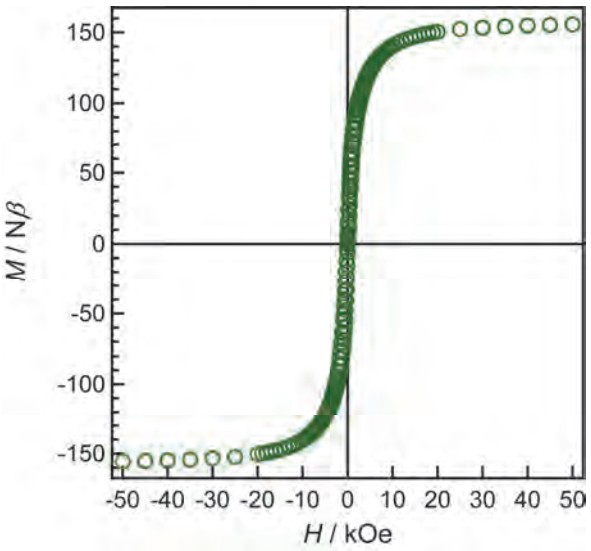

Fig. 1. Magnetization versus field plot of the Fe cluster complex at 1.8 K.

【成果報告】 田中 奏多，大石 峻也，川本 晃希，高畑 遼，志賀 拓也，山添 誠司，Zihan Zhang，唯 美津木，吉川 聡一，寺西 利治，二瓶 雅之，Karsten Meyer，檜垣 達也，大木 靖弘　日本化学会第 104 春季年会、日本大学船橋キャンパス、2024.

Catalytic Activation of Silicon-Oxygen Bond via Nucleophilic Activation of Silane

Hajime Kameo　Osaka Metropolitan University

Purpose

Silicon is one of the most abundant elements in the earth's crust, and its compounds generally have low toxicity and environmental impact. In addition, electropositive silicon forms very strong chemical bonds with electronegative oxygen and this property has led to the development of a variety of silicon materials with excellent heat resistance, durability, and weather resistance. On the other hand, it is difficult to break the silicon–oxygen bond under mild conditions due to its high stability. In this study, we will establish an intellectual foundation for catalytic conversion of silicon–oxygen bonds in order to establish a fundamental technology for freely converting silicon–oxygen bonds. Based on this knowledge, we will develop efficient synthetic methods for silicon compounds, directly synthesize silicon materials from naturally occurring silicon dioxide, and recycle silicon materials, which has hardly been realized.

Experimental Methods and Results

Previously, the first coupling reaction using fluorosilanes has bee developed (Figure 1). The cleavage of the silicon–fluoro bond, which is the key to the catalysis, likely proceeded via the reaction of a Lewis acid with an fluorosilane nucleophilically activated by the M→Si–F interaction. Based on this knowledge, this research was expanded to the development of alkoxysilane conversion reactions. The Pd-catalyzed arylation of alkoxysilane $ArSiMe_2(OMe)$ (**1**: Ar = $(Ph_2P)C_6H_4$-) was found to be realized under a condition that $ZnPh_2$ and MgI_2 were employed as arylation reagent and Lewis acid, respectively. The arylation worked well with the aryl reagents bearing a functional group (OMe, Cl, F etc.). Furthermore, the use of relatively higher nucleophilic reagent ($MgBr[Zn(CH_2CH_2Ph)_3]$) enabled the alkylation of $ArSiMe(OMe)_2$ (**2**: Ar = $(Ph_2P)C_6H_4$-). To the best of our knowledge, the result described here is the first example of catalytic arylation and alkylation of alkoxysilanes. Manuscript is in preparation for reporting the results described here.

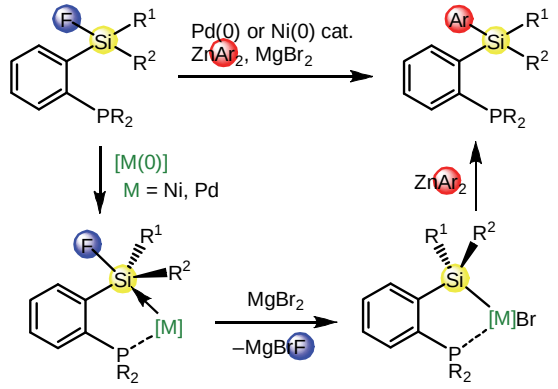

J. Am. Chem. Soc. **2020**, *142*, 14039 (*Cover Art*).

Figure 1　Negishi-Coupling of Fluorosilane

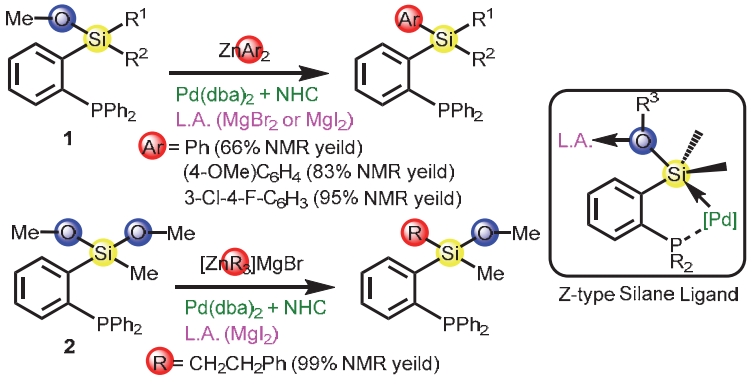

Figure 2　Silicon-Oxygen Bond Activtion (This work)

Asymmetric synthesis of planar-chiral metallocenes by plane-to-plane chirality transfer

Masamichi Ogasawara　Tokushima University

Ferrocene undergoes the double Friedel-Crafts (FC) acylation, in which the two acyl substituents are distributed between the two Cp moieties forming the corresponding 1,1'-diacylferrocene predominantly. Acetylation of 1,1'-diphosphaferrocene is similar to that of ferrocene, and 2,2'-diacetyl products were obtained as a mixture of *meso*- and *chiral*-isomers. On the other hand, the reactions of monophosphaferrocenes with acyl electrophiles are different from the above. The double FC acylation of 3,4-dimethylphosphaferrocene (**1a**) was reported to be unattainable;[1] after the first FC acetylation of **1a** giving **2ax**, the reaction of **2ax** with excess AcCl/$AlCl_3$ led to the $AlCl_3$-induced decomposition. Against these reports, we have found out that the double Friedel-Crafts diacylations of monophosphaferrocenes **1** were operated under the optimized conditions.[2]

Treatment of **1a** with an equimolar mixture of AcCl and $AlCl_3$ provided a complex mixture, which contained the 2-acetylphosphaferrocene (**2ax**; 28%) and a small amount of the two diacetylphosphaferrocene species, **3axx** (11%) and **4axx** (6%). Both **3axx** and **4axx** were stable under argon, and their hitherto unavailability was ascribed to the lack of proper synthetic methods. A rationale for the earlier failure of introducing the second acetyl group on **2ax** was postulated to be the competitive $AlCl_3$-induced decomposition. We envisioned that the exclusion of extra $AlCl_3$ from the attempted FC acetylation of **2ax** might avoid the undesirable decomposition and provide **3axx** and/or **4axx** in better yields. Based on this hypothesis, the acetylation of **2ax** was examined using the electrophile generated from AcCl and a deficient amount of $AlCl_3$ (with respect to AcCl). As we expected the reaction was clean giving a mixture of **3axx**, and **4axx**.

For the success of the double acylation of **1**, the stepwise introduction of the two acyl groups was a key issue. The two acyl groups in **3** and **4** are not necessarily the same. By choosing a proper carboxylic anhydride and an acyl chloride, preparation of various 2,5- and 1',2-diacylphosphaferrocenes could be realized (**Table 1**). In all the cases examined, the double acylation took place cleanly to provide **3** and **4** in >80% combined isolated yields. The 2,5- and 1',2-diacylations are competing in the second FC acylation, and the former is the dominant reaction path. This is a clear contrast to the double FC acetylation of ferrocene and of 1,1'-diphosphaferrocene in which the first and the second acetylations take place on different Cp rings.

Through the joint project with Prof. Ohki, we published two research papers this year.[2,3]

Table 1. Stepwise Double Friedel-Crafts Acylation of Monophosphaferrocenes **1**

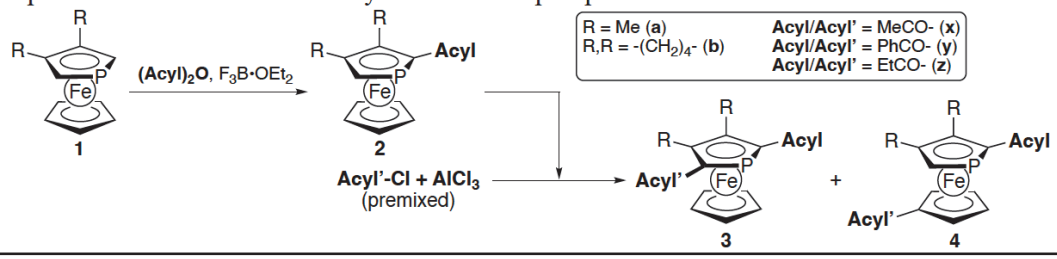

entry	substrate	$(Acyl)_2O$	yield of **2**[a]	Acyl'-Cl[b]	**3**/**4**	yield of **3**[a]	yield of **4**[a]
1	**1a**	$(MeCO)_2O$	>99 % (**2ax**)	MeCOCl (3.0/2.6)	82/18	71% (**3axx**)	16% (**4axx**)
2	**1a**			PhCOCl (12.0/10.4)	90/10	84% (**3axy**)	10% (**4axy**)
3	**1a**			EtCOCl (3.0/2.6)	71/29	56% (**3axz**)	24% (**4axz**)
4	**1a**	$(PhCO)_2O$	>99 % (**2ay**)	MeCOCl (6.0/5.2)	82/18	76% (**3ayx**)	12% (**4ayx**)
5	**1a**			PhCOCl (12.0/10.4)	93/7	78% (**3ayy**)	4% (**4ayy**)
6	**1b**	$(MeCO)_2O$	>99 % (**2bx**)	MeCOCl (3.0/2.6)	85/15	82% (**3bxx**)	15% (**4bxx**)

[a] The isolated yields by silica gel column chromatography. [b] Numbers in parentheses are the molar ratios of acyl chloride and $AlCl_3$ relative to **2**.

References.

[1] Mathey, F. *J. Organomet. Chem.* **1977**, *139*, 77.
[2] Masaoka, K.; Taue, H.; Higaki, T.; Ohki, Y.; Ogasawara, M. *Organometallics* **2023**, *42*, 1667.
[3] Masaoka, K.; Taue, H.; Wakioka, M.; Ohki, Y.; Ogasawara, M. *Organometallics* **2023**, *42*, 1629.

Cu ヒドリド錯体と官能基化シリカの組み合わせによる CO_2 還元触媒の開発

中島隆行　奈良女子大学

[背景と目的]

電力駆動により二酸化炭素（CO_2）から燃料を直接かつ効率的に生成する技術は注目を集めており、特に Cu 電極を用いたエチレン合成を皮切りに関連報告が相次いでいる。Cu は CO_2 を還元する第一段階に当たる CO 生成に高い活性を示す一方で、電子豊富であるために金属に結合する原子を多くできず、複数の Cu 原子を用いなければ C-C 結合の形成反応を実現できない。現在の研究では Cu ナノ粒子が触媒として用いられているが、より反応性が高く、隣接の Cu 原子間での協奏的な反応に期待できる Cu-クラスター錯体を分子触媒として用いれば、CO_2 還元生成物の炭素鎖伸長が実現できる。

そこで本研究では、(i)Cu-クラスター錯体を均一系 CO_2 電解還元触媒へと展開することで Cu ナノ粒子に代わる新たな触媒材料を見出し、さらに(ii)それらをシリカ系担体に担持し基質などの物質拡散を制御する機構を取り入れることで、高活性な電解 CO_2 還元による燃料生成を目指す。

[研究成果]

まず本研究では、Cu-クラスター錯体を CO_2 電解還元触媒へと展開するために、図 1 に示す 2 種類の Cu-2 核錯体に着目し、それらの酸化還元挙動の調査を行なった。

Cu_2-^{t}BuNC のサイクリックボルタンメトリー（CV）測定を行ったところ、3 つの不可逆な還元波が観測された（図 2-a）。スキャンレートを変えて調査を行ったところ、比較的遅いスキャンレートでは周回ごとでの還元電位・電流に変化は観測されず、**Cu_2-^{t}BuNC** は還元に対して十分な安定性を有することがわかった。対して比較的速いスキャンレートでは、周回ごとに還元に伴う電流値が減少し、生成した還元種の高い安定性が示唆された。多段階な還元過程及び還元への安定性より、**Cu_2-^{t}BuNC** は CO_2 還元触媒に適した性質を有することが明らかとなった。

同様に **Cu_2H-PPh_3** の CV 測定を行ったところ、1 つの不可逆な還元波が観測され、その還元挙動はスキャンレートに依存しなかった（図 2-b）。このことから、**Cu_2H-PPh_3** は還元に対して安定であり、CO_2 に対して迅速な電子輸送が可能なことが示唆された。

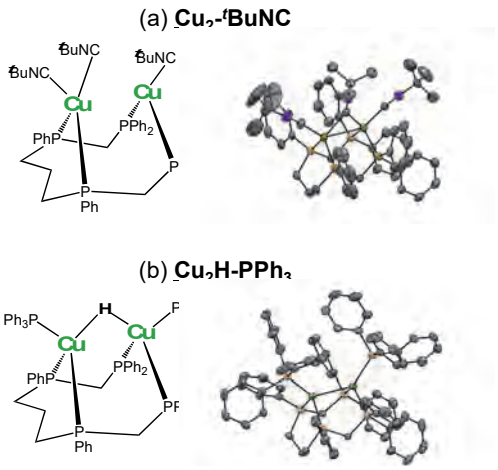

図 1.　本研究で用いた Cu-クラスター錯体の構造.

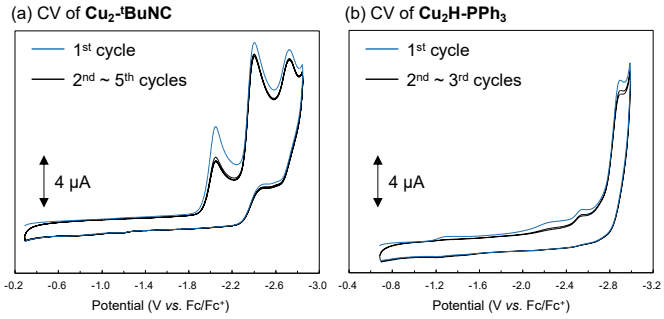

図 2.（a）Cu_2-^{t}BuNC 及び（b）Cu_2H-PPh_3 のサイクリックボルタモグラム.（scan rate: 100 mV/s）

電子移動制御を利用したナノ金属クラスター触媒の高活性化

近藤美欧　大阪大学

[背景と目的]

二酸化炭素（CO_2）は気候変動の主要因となる温室効果ガスであり、削減と同時にその有効利用によるカーボンニュートラルな人間活動の達成が期待されている。CO_2 を電気化学的に還元し、燃料となりうる炭化水素分子や化成品原料を合成できれば、この目標を実現する大きな足がかりとなる。そこで本研究では、多電子移動能を有するナノ金属クラスターに対して電化伝達サイトを導入した電極触媒材料を開発し、電気エネルギーを用いた CO_2 から炭化水素への高効率な直接変換を目指す。

[研究成果]

ポリ(ピラゾリル)メタンを金属への配位部位、カルバゾールを重合起点ならびに電化伝達サイトとして機能する新規配位子を合成し、それをナノ金属クラスター[Mo_3S_4]と反応させることで、新規配位子を有する[Mo_3S_4]クラスターの合成を行なった。得られたクラスターに対してジクロロメタン中で酸化電位を印加したところ、カルバゾールの 2 量化を起点とする重合反応が進行し、ナノ金属クラスターが固定化された修飾電極が得られた。この修飾電極を用いて還元側の酸化還元能を調査したところ、[Mo_3S_4]由来のピークが観測され、ナノ金属クラスターが分解せずに電極上に担持されたことを確認した。さらに電極上に担持された[Mo_3S_4]に対して Fe イオン（反応点として機能）を導入することで、酸化還元挙動の変化が観測され Fe イオンの導入に成功した。

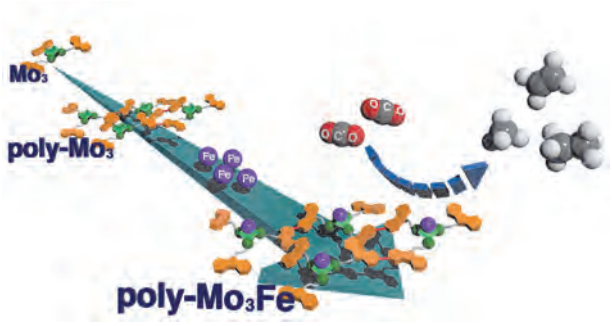

図 1. 本研究の研究成果概要

[Mo_3S_4Fe]を担持した修飾電極を用いて CO_2 還元能を評価したところ、2%ほどのファラデー効率で炭化水素（メタン、エチレン、エタン）を生成していることが明らかとなった。また、[Mo_3S_4]のみを担持した修飾電極では炭化水素の生成は確認されなかった。このことから、CO_2 を電気化学的に還元し炭化水素を生成可能な触媒材料の開発に成功した（図 1）。

[成果報告]

~学会発表~

渡部 凜, 伊豆 仁, 谷藤 一樹, 近藤 美欧, 正岡 重行, 大木 靖弘, “[Mo_3S_4]クラスター部位を有する修飾電極の創出”, 日本化学会 第 104 春季年会, 2024 年 3 月.

~特許出願~

ナノ金属クラスターが担持された修飾電極の作成手法に関して特許出願準備中（3/1 に申請予定）

A Caging Strategy for Cholinergic Optopharmacology

Satoshi Arai Kanazawa University

A photocaged method creates a concentration jump of the target bioactive molecule with high temporal and spatial resolution by light illumination. The method enables us to investigate a role of the bioactive molecule at the signaling pathway of interest in living cells. In particular, for decades, several caged neurotransmitters for glutamate, dopamine, and noradrenaline have been developed for studies on central and peripheral nervous systems in the research field of neuroscience. However, even though it is the earliest found neurotransmitter, photocaged acetylcholine has not been reported yet due to the difficulty of synthetic approach. To overcome the problem, we synthesized photocaged acetylcholine through the novel chemical synthetic methodology using photocleavable carbon–boron bond.[1] This photocaged compound could release acetylcholine efficiently in the presence of glutathione upon UV light. Using a confocal microscope, we visualized the photo-triggered release of acetylcholine at the target place in HEK cells expressing biosensor of acetylcholine on the surface. It was found that release of Ach from the caged compound induced an increment of acetylcholine concentration only at the target cell. We further demonstrated the usability of the compound in Ca^{2+} imaging of C2C12 myotube and Drosophila brain. After inducing a concentration jump of acetylcholine, the elevation of intracellular Ca^{2+} level was observed in these biospecimens through the stimulation of acetylcholine receptors on the cellular surface.

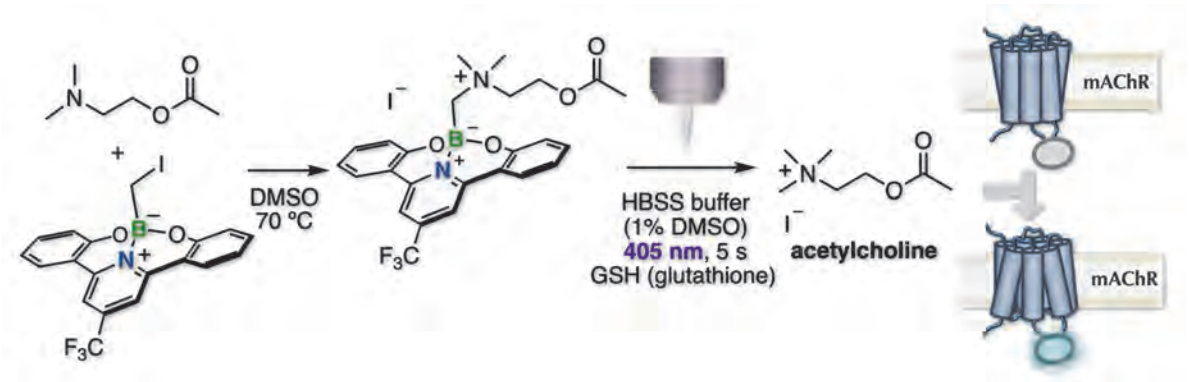

Publication

(1) Nakamura, R.; Yamazaki, T.; Kondo, Y.; Tsukada, M.; Miyamoto, Y.; Arakawa, N.; Sumida, Y.; Kiya, T.; Arai, S.; Ohmiya, H. Radical Caging Strategy for Cholinergic Optopharmacology, *J. Am. Chem. Soc.* **145**, 10651–10658 (2023).

振動強結合を用いた発光特性の制御

平井健二　北海道大学

２枚の光反射ミラーが向かいあった光共振器の中では、共振条件を満たす光のエネルギー準位が共振器モードとして規定される。この光共振器の中では、分子が光の吸収と放出を可逆に繰り返す強結合と呼ばれる状態になる。特に、分子の振動モードとの強結合は振動強結合とよばれる。振動強結合と呼ばれる量子光学的現象は 2015 年に観測されて以降、化学反応の制御方法として発展してきた。本研究では、集積型金属錯体の振動を振動強結合によって変調させることで、発光特性の制御を行う。これまで量子光学の分野で発展してきた振動強結合の概念を錯体化学の分野に導入することで、新たな融合領域の開拓を試みた。

本研究では発光性金属錯体である$(PPh_4)_2[ReN(CN)_4](ethanol)$（**1**）を用いた。**1** は約 400nm の光を吸収すると電子遷移が起こり、約 500nm の発光を示す。**1** を polyethylene glycol（PEG）フィルムの中に分散させて光共振器の中に導入し、ミラー間の距離を調整することで共振器モードのエネルギー準位を調整した。

共振器モードを $1100cm^{-1}$ 付近に調整すると **1** の Re≡N 伸縮振動/PEG の C-O 振動結合が観測された。振動ポラリトンが形成され、上枝ポラリトン（P+）と下枝ポラリトン（P-）に分裂するラビ分裂が観測された。振動強結合の状態で発光測定を行い、発光強度の向上と発光寿命の増加を確認した（**図**）。通常、**1** の発光寿命は 1.1μs であるが、振動強結合の状態では 2.3μs と算定され、振動強結合よって発行寿命が変化している可能性が示唆された。

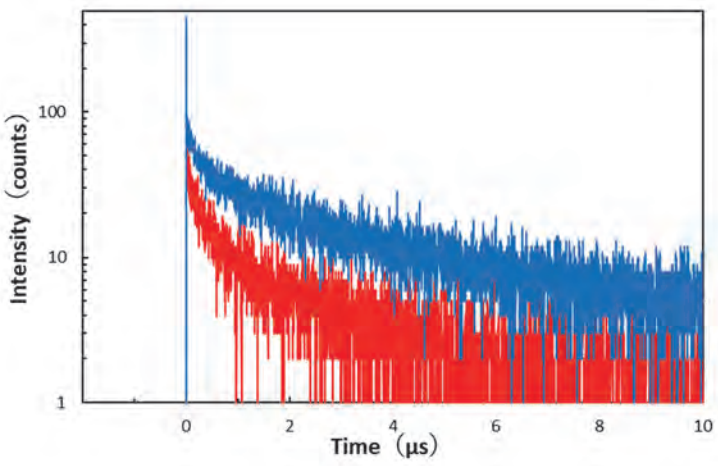

図. 発光寿命測定. 青: 振動強結合の状態, 赤: 振動強結合ではない状態. 緑帯: Re≡N の分子振動. Re≡N と共振器モードが $1105cm^{-1}$ で一致すると振動強結合が起こる.

半導体光学冷却に向けたドットインクリスタル型ペロブスカイトの光物性の解明

山田泰裕　千葉大学

強い電子-フォノン相互作用をもつ半導体では、入射光よりも高エネルギーの光が放出される現象（＝アンチストークス発光）が観測される。アンチストークス発光の外部発光量子効率が 100%近い場合には、継続的な光照射によって半導体はエネルギーを失う。すなわち、アンチストークス発光を介した固体レーザー冷却が期待できる。本研究では、このようなアンチストークス光学冷却に向けた基礎物理の解明を目指して研究を行った。高い発光効率と強い電子-フォノン相互作用を兼ね備えたハロゲン化金属ペロブスカイトのナノ構造に着目し、特に量子ドットが安定なホスト結晶内に埋め込まれた「ドット・イン・クリスタル」と呼ばれる構造を対象とした。具体的には $CsPbBr_3$ 量子ドットが Cs_4PbBr_6 ホスト結晶に閉じ込められた複合材料（以下、$CsPbBr_3/Cs_4PbBr_6$）を用いた。この材料では 100%近い高発光効率が報告されており、さらに従来のペロブスカイト半導体で問題となってきた光劣化に対する耐久性の面でも優れた性質をもつ。

研究代表者らは、試料作製とアンチストークス発光特性の評価を行った。発光励起分光の結果から、発光量子効率に対する $CsPbBr_3/Cs_4PbBr_6$ の光学冷却ゲインスペクトルを決定し、光学冷却の実現には 97%以上の発光量子効率が必要であることを見出した。さらに、化学研究所で共同研究者らとともに時間分解発光分光による励起状態ダイナミクスの測定を行った。高密度励起下では、量子ドット内に閉じ込められた光キャリア間の多体相互作用に由来した量子化オージェ再結合が観測された。差分化法による解析で３および２励起子状態のオージェ再結合寿命を決定した。オージェ再結合は無輻射再結合過程であって、高密度励起下で発光量子効率を低下させ、光学冷却を阻害する要因となる。そこで、発光ダイナミクスの結果をもとに連続光励起下での光学冷却ゲインの励起光強度依存性を計算した。弱励起下では冷却ゲインは励起光強度に対して線形に増大するが、オージェ再結合が顕著になる高密度励起下では無輻射再結合レートの増大に伴って冷却ゲインは減少し、ある強度以上では光加熱が生じることが分かった。すなわち、光学冷却の実現には、励起光強度が強ければ強いほど良いわけではなく、最大の冷却ゲインを与える最適な光強度があることを見出した。

今後は、本研究で得られた知見を基に半導体光学冷却に挑戦する予定である。本研究で用いた材料に対して積分球を用いた発光量子効率測定を行ったところ、最大でも 80%程度の量子効率であった。この発光効率では光学冷却の実現には至らないが、発光効率の高い微結晶を選択的に励起するなどの工夫を施して実験を行う。これに並行して高発光効率試料の開発も進める。本研究成果の一部は、第 84 回応用物理学会秋季学術講演会における招待講演で発表したほか[1]、現在投稿論文を準備中である。

［1］山田 泰裕“電子・フォノン・イオンの相互作用がもたらすペロブスカイト半導体の光物性”［20a-A307-2］　第 84 回応用物理学会秋季学術講演会　2023 年 9 月 19－23 日（招待講演）

Quantum properties of lead perovskite solar cells by two-dimensional optical Fourier transform spectroscopy

Yoshihiro Ogawa　Joetsu Univiersity of Education

Lead perovskite solar cells are a promising new solar cell material due to their excellent energy conversion efficiency. To understand the electrical and optical properties of lead perovskite solar cells, it is important to understand the photocarrier dynamics in the medium [1]. In this study, we attempt to characterize the time evolution and electronic correlations of photocarriers in lead perovskite solar cells by using two-dimensional optical Fourier spectroscopy measurements.

We used $CH_3NH_3PbBr_3$ single crystals as the sample. The supercontinuum (SC) light was obtained by introducing a mode-locked Ti:Sapphire laser into a photonic crystal fiber, and four excitation pulse sequences were generated by a nested Mach-Zehnder interferometer. The photocurrent was measured by irradiating the sample with these pulses. Each pulse was frequency-labeled with an acousto-optic modulator to obtain the required four-wave mixing signal. The two-dimensional Fourier spectra were obtained by Fourier transforming the two-dimensional interferogram acquired by scanning the time interval of the pulse sequences.

The two-dimensional Fourier spectra of $CH_3NH_3PbBr_3$ single crystals measured at 8 K are shown in the figure. The vertical axis represents the absorption energy, and the horizontal axis represents the emission energy. It is found that the peak x originates from exciton absorption. The inhomogeneous broadening is given by the width in the direction of the diagonal component of the peak, and the homogeneous width can be measured as the component perpendicular to it, allowing us to evaluate the spectrum without the effect of exciton inhomogeneity. Peaks (α, α') were observed on the 20 meV higher energy side of the exciton energy, that is consistent with the LO phonon energy of $CH_3NH_3PbBr_3$ (20.1 meV). Thus, the peaks α and α' are considered to be a phonon sideband. By scanning the waiting time, we can determine the interstate dephasing time of the phonon sidebands and obtain information about the exciton-phonon interaction. The investigation of the interstate dephasing time of the phonon sideband will be conducted in the future. Furthermore, we will analyze the origin of the peaks β and β' by studying their temperature and polarization dependences.

[1] Y. Ogawa, H. Tahara, N. Igarashi, Y. Yamada, and Y. Kanemitsu, PRB **103**, L081201 (2021).

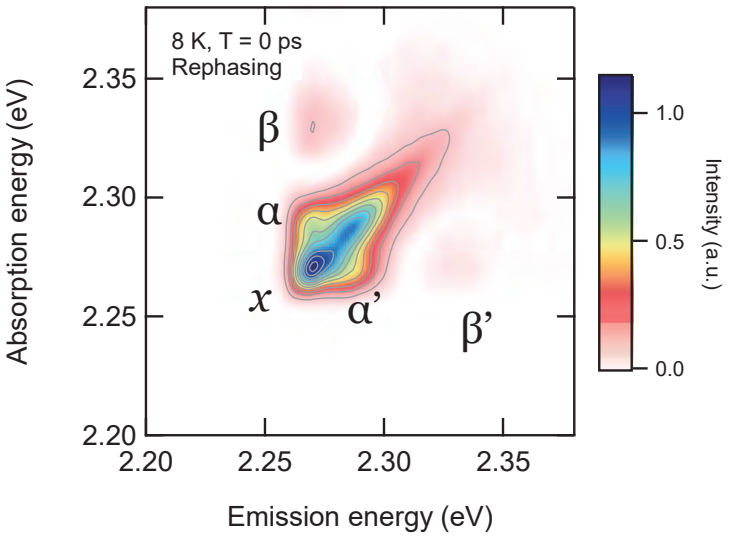

Figure: 2D Fourier spectra of $CH_3NH_3PbBr_3$ single crystal measured at 8 K. Waiting time is 0 ps.

低温強磁場対応 THz-STM の開発と評価

立崎武弘　東海大学

物性やデバイスの機能を担う電気伝導や光電変換，磁性による情報の保持などは主に電子（キャリア）が担っている。固体における非平衡な電子ダイナミクスは現代物性物理学における最先端の関心であり、関わる実験手法の確立は重要な課題である。電子の時空間的挙動を正確に把握して理解することは応用科学の端緒となる。また、定常状態におけるキャリアの振る舞いも、その運動開始からフェムト秒程度の超短時間におけるダイナミクスが決定づける。フェムト秒時間でキャリアはナノメートル程度運動するため、フェムト秒時間・アトミックスケールの分解能でキャリアの運動を追跡して把握できる計測技術の確立が求められている。

本研究では、フェムト秒時間分解能とアトミックススケールの空間分解能を両立させる、テラヘルツ（THz）パルスをトンネルバイアスに利用した走査トンネル顕微鏡（STM）である THz-STM を研究開発している。本申請では、トポロジカル物質などの量子物質への応用を見据えて、低温強磁場対応 THz-STM の開発を進めてきた。試料・探針処理用の超高真空チャンバを冷凍機と統合して装置として完成させ、低温超高真空の冷凍機内にある探針先端に THz パルスを集光することによって発生するトンネル電流の定量評価を目的としている。

超電導マグネットを備えた液体ヘリウム溜め込み式の冷凍機に設けたビューポートより、長さ ~700 mm、内径 14 mm のパイプを通して THz ビームを STM ヘッドへ導入した。パイプを抜けた THz ビームは、新しく開発した STM ヘッドに備えられた焦点距離 50 mm の放物面鏡によって探針先端へ集光される。本研究では、冷却時の熱収縮に起因して変形する光学系の影響を被らずに探針先端へ THz パルスを集光できるように設計した。この装置を用い、繰り返し周波数 1 MHz の超短光パルスレーザーを光源としてパルス面傾斜法によって発生させた単極性 THz パルスを、真空中 STM ヘッドの PtIr 探針と高配向性熱分解グラファイト HOPG の間に作ったトンネルジャンクションに集光した。結果、THz パルス起因の瞬時トンネル電流を 6 pA 程度得られることを確認した（図 1）。THz パルスに 407 Hz の振幅変調をかけ、DC バイアスがゼロの状態で流れる THz 起因のトンネル電流だけをロックインアンプで計測した。このような電流計測は、今後行う時間分解計測と全く同じであり、本装置を使って時間分解 STM 計測ができることを示している。原子分解 STM 計測に必要な清浄表面・清浄探針を得るために、電子ビーム加熱装置やロードロック、試料劈開機構を備えた超高真空チャンバを構築した。これにより探針と試料を高真空内で一括して処理・準備し、低温 STM へ搬送して測定することが可能となった。この設備を用いれば、電荷密度波物質や超伝導体物質、トポロジカル絶縁体物質への計測を進めている。

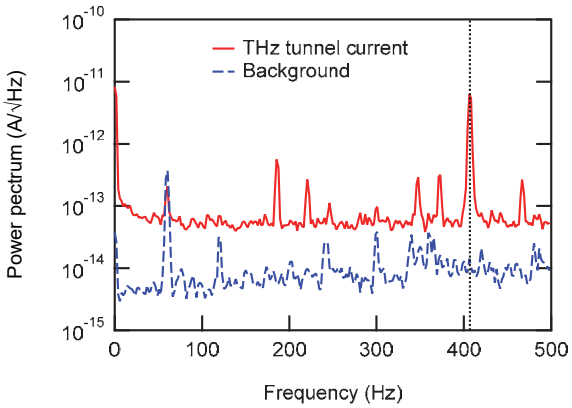

図 1 観測した THz パルス誘起のトンネル電流（赤実線）。黒点線が 407 Hz で変調した THz 電流成分。青破線が背景ノイズ。

非エルミート・トポロジカルエッジ状態によるテラヘルツレーザー

小布施秀明　北海道大学

テラヘルツ波は、高速無線通信、生化学センシング、非破壊検査などの分野において広く利用されています。このため、より小型、より効率のよいテラヘルツ波の新規生成デバイス開発は、上記応用利用のさらなる浸透、また新たな利用機会の創出につながるため、よりよい社会基盤の構築が可能となります。しかし、小型デバイスでは、製造過程で生じる欠陥・不整合により、動作の不安定化や吸収損失による効率の低下が避けられないため、テラヘルツ波の発生を高度に制御することが課題となっています。本研究では、近年、電子物性物理学の分野で飛躍的な理論・実験研究の発展を遂げたトポロジカル絶縁体と非エルミート系の知見を活かすことにより、上記問題を克服するテラヘルツ波生成が可能であることを理論的に明らかにします。さらに、基礎動作原理検証のための実験系や将来的な応用デバイスのデザインの提案を理論的に行うことを目的として研究を行いました。

電子物性分野で研究が行われているトポロジカル絶縁体には、系の端に強く局在するエッジ状態と呼ばれる特殊な状態が存在します。系の大域的な性質を表すトポロジーに起因し現れるエッジ状態は、系の局所的な欠陥・不純物があっても、エネルギー的・空間的に極めて安定であり、存在しつづけます。トポロジカル絶縁体は電子に対する性質ですが、同様の特殊な状態はフォトニック結晶を用いることにより光･電磁波の固有モードとして現れることがすでに分かっております。本研究の第一段階として、テラヘルツ波に対し、近軸近似とスカラー波近似を用いることにより，簡単な 1 次元鎖モデルに置き換え，このモデルの固有値問題を理論的に調べ、トポロジカルなエッジ状態が生成可能であることを明らかにしました。これにより、1 次元鎖の端に、エッジ状態が現れる基本構造を同定しました。

さらに、このモデルに対し、ゲイン物質による光の増幅効果や光の損失効果を取り入れることにより、上記モデルを開放系を記述する非エルミート系に拡張したうえで、例外点を発生可能であることを明らかにしました。これにより、光の増幅効果を高度に制御することが可能であることが分かりました。光の増幅・減衰量を制御し、エッジ状態（固有モード）が例外点の近傍にあるように系をデザインすることで、エッジ状態に閉じ込められたテラヘルツ波の増幅・減衰効果を制御することが可能であることが分かりました。

今後、上記性質をより詳しく調べることによりレーザー発振の条件を明確にすることができます。さらに今回の研究成果を踏まえ、今後はより現実に即した電磁波に対するマクスウェル方程式を，有限要素法を用いた数値計算を行うことにより、実験可能なパラメーターを同定します。そのうえで、実験により基礎動作原理の検証を行い、本研究成果を論文にまとめ成果発表を行う予定です。

酸化物における水素スピルオーバー制御

細川三郎　京都工芸繊維大学

水素社会の実現に向けて、水素の制御を可能にする現象の理解や材料の開発が重要となっている。酸化物に担持された金属触媒上において生成した活性水素（原子状の水素）が酸化物表面上へと拡散する現象である水素スピルオーバーは、1964 年に発見されて以来、様々な反応や物質開発に利用されきた。しかしながら、水素はその軽さゆえに実験的に観測が難しいこともあり、水素スピルオーバーに関連する現象に対する理解は定性的である。そのため、活性水素の拡散距離やその支配因子など、いまだ理解されていない点が多く残されてる。申請者らは、酸素欠損型ペロブスカイト鉄酸化物エピタキシャル薄膜をモデル触媒担体として水素スピルオーバーが触媒担体に与える影響を調べ、活性水素の表面拡散がサブミリメートルにも及ぶことを見出した[T. Kamada, D. Kan et al., J. Am. Chem. Soc. (2023)]。また理論計算から、表面拡散距離は酸化物中における価数不安定性と相関していることも示唆された。そこで、本課題では、酸化物中の価数不安定性をチューニングすることで、これまで難しいとされてきた水素スピルオーバーの制御を試みた。

本課題では、$SrFeO_x$ に $SrCoO_x$ を固溶させた $Sr(Fe,Co)O_x$ に着目した。まず、$Sr(Fe,Co)O_x$ における Fe と Co とで価数の安定性が異なることを調べるために、$SrFeO_x$ および $SrCoO_x$ にプロトン注入した際における Fe と Co の価数変化を X 線吸収測定によって調べた。図 1 に示すのは、パルスレーザー堆積法で作製した $SrFeO_x$ および $SrCoO_x$ エピタキシャル薄膜試料における、プロトン挿入前後での吸収スペクトルの変化である。吸収スペクトルは SPring-8 における BL01B1 ビームラインで室温において測定した。プロトン注入に伴って、$SrFeO_x$ の Fe-K 端吸収スペクトルはほとんど変化しないのに対して、$SrCoO_x$ の Co-K 端吸収スペクトルにおいては Co の価数低下に伴うスペクトル変化が観測された。これらの結果は、$SrCoO_x$ における Co 価数が不安定であり、プロトンと相互作用しやすいのに対して、$SrFeO_x$ では Fe 価数が安定であり、プロトンと相互作用しにくいことを示唆する結果である。またこの価数安定性の違いは、$SrFeO_x$ 表面における水素スピルオーバーの距離が非常に長いことと合致しており、Co 置換とともに、スピルオーバー距離が短くなることを示唆するものである。今後、得られれた知見をともに、$Sr(Fe,Co)O_x$ エピタキシャル薄膜をモデル触媒担体として、水素スピルオーバーの距離の計測を行う予定である。

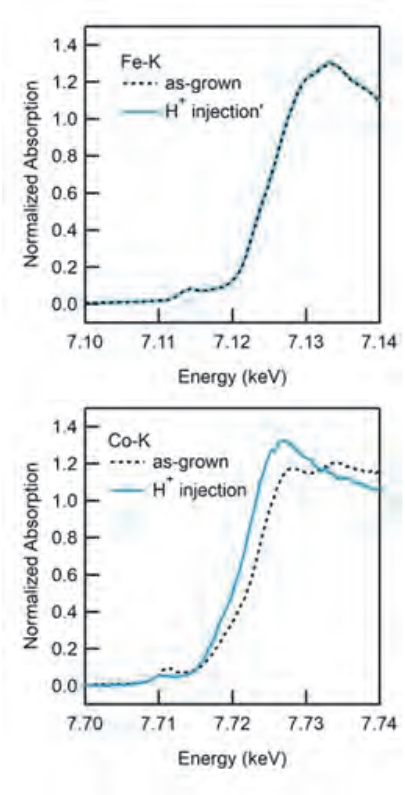

図 1：プロトン注入前後における（上）$SrFeO_x$ 薄膜試料の吸収スペクトルおよび（下）$SrCoO_x$ 薄膜試料における Co-K 端吸収スペクトル。

Regioselective C–H Activation Enabled by Substrate Recognition

Laurean ILIES　RIKEN

Direct functionalization of organic substrates is of much interest for streamlining the synthesis of complex molecules. However, the greatest challenge for these reactions is the control of site selectivity, the differentiation between the multiple C–H bonds in a molecule. Strategies to address this problem include the reaction of an activated substrate, or utilization of a substrate possessing a specialized directing group, but these strategies based on substrate control do not provide a general solution for site-selective functionalization. Inspired by Nature, where the protein pocket of an enzyme catalyst recognizes a reaction site in a fixed conformation, we proposed a general strategy based on catalyst control for selective activation of a variety of organic molecules, where a precisely designed catalyst will activate a substrate through molecular recognition.

In order to achieve the catalyst control strategy, we designed a SpiroBipyridine (**SpiroBpy**) molecule that provide a framework for placing substrate recognition groups at a remote position from the reaction center, and we demonstrated this concept by placing a “steric roof” group that recognizes molecular shape though remote steric interactions and enables *meta*-selective borylation of monosubstituted arenes (*Science* **2022**, *375*, 658). During FY2023, we found that **SpiroBpy** can also act as an efficient ligand for iridium-catalyzed C–H borylation, which we rationalized through an attractive noncovalent interaction between the C–H bond of the ligand backbone and the π electrons of the arene substrate. This interaction was probed through DFT calculation, and also experimentally through an unprecedented ligand kinetic isotope effect, which showed that a deuterated **SpiroBpy** ligand reacted faster, probably because of entropic reasons. This work was submitted (manuscript under revision), and also presented at several national and international conferences. Very recently, we found that a **SpiroBpy** ligand that bears a hydroxyl (OH) group recognizes pyridine and quinoline substrates for iridium-catalyzed C–H borylation (manuscript in preparation, oral presentation at the 2024 Annual Meeting of CSJ). The hydrogen bonding interaction controls regioselectivity in a modular fashion, and also accelerates the reaction in a manner reminiscent of enzymatic catalysis.

On June 2, 2023, I visited The Institute for Chemical Research, and I gave a talk on “Catalyst Design for Selective and Efficient Reactions” (hosted by Prof. Masaharu Nakamura). After the seminar, we discussed about ligand design, and possible expansion of the use of **SpiroBpy** ligands for Earth-abundant metal catalysis such as iron catalysis. Based on advice from Prof. Nakamura, we are investigating such reactions at the moment.

Development of co-facial-type dinuclear complexes

Yoshitaka Yamaguchi　Yokohama National University

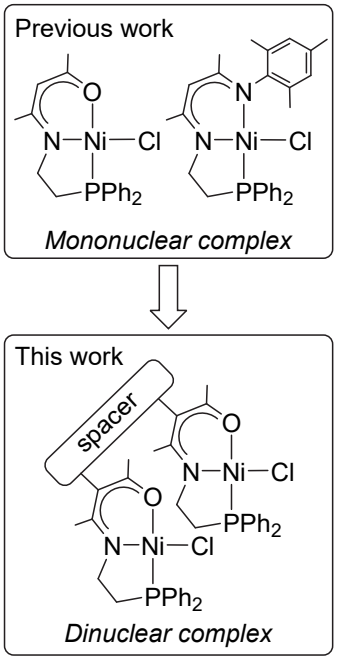

Dinuclear complexes have generated significant interest in recent years because such complexes containing two metal centers in proximity would exhibit a bimetallic cooperative effect in catalytic transformations. Therefore, dinuclear complexes can activate inert chemical bonds in various organic molecules. On the other hand, extensive attention has been focused on the development of tridentate pincer-type complexes because the pincer-type ligand stabilizes a metal complex, and its properties can be tuned to achieve the best reactivity of the complex. We have already reported a series of acetylacetonato-based pincer-type nickel(II) complexes, which utilize a combination of β-aminoketonato or β-diketiminato frameworks with a third donor such as a phosphino or amino group. Our study on these nickel(II) complexes revealed that the modification of the ligand framework has a significant influence on the catalytic performance in biaryl cross-coupling reactions (*Dalton Trans*. **2018**, *47*, 8003.; *Eur. J. Inorg. Chem*. **2019**, 126.). Furthermore, we have recently demonstrated that the *O,N,P*-type nickel(II) complex serves as a catalyst in a highly Markovnikov-selective hydroboration of vinylarenes with bis(pinacolato)diboron (B_2Pin_2) (*Org. Lett.* **2020**, *22*, 4033.) and a hydrosilylation of styrenes using 1,1,3,3-tetramethyldisiloxane as a surrogate for Me_2SiH_2, leading to Markovnikov products (*Eur. J. Org. Chem.* **2021**, 5449.). We have shown that the *O,N,P*-type nickel(II) complex acts as an effective catalyst for the transformation of organic molecules. Therefore, we considered that a dinuclear complex utilizing the highly active pincer-type nickel complex, in which two metal centers are located in close proximity to each other, would serve as an effective catalyst for the activation of inert chemical bonds. We intended to synthesize a dinuclear catalyst system constructed by two sets of the *O,N,P*-type nickel-pincer complex in a co-facial arrangement using an appropriate spacer molecule.

9,9-Dimethylxanthene (**1**) was selected as a spacer for the desired dinuclear complex. 4,5-Diformyl-9,9-dimethylxanthene (**2**) was prepared by the reaction of **1** with *n*-BuLi/tetramethylethylenediamine (TMEDA) and then treatment of dimethylformamide (DMF). Bis(acetylacetone) derivative **3** was prepared by the reaction of **2** with 2,2,2-trimethoxy-4,5-dimethyl-1,3-dioxaphospholene. Next, we examined the preparation of the ligand precursor **4** by the reaction of **3** with 2-(diphenylphosphino)ethylamine under various conditions, whereas the desired product **4** was not obtained. Under these reaction conditions, decomposition of the xanthene framework was observed. We are now investigating another framework as a spacer molecule.

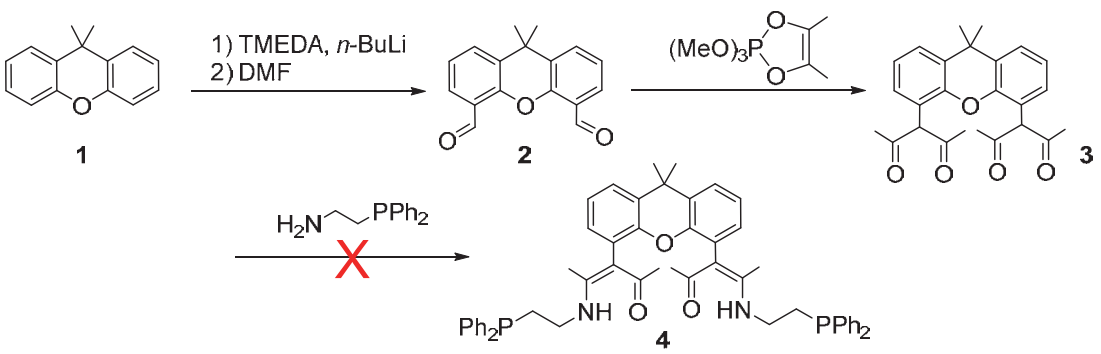

Development of defective nickel oxide catalysts for highly selective functionalization

Ayako TAKETOSHI Yokohama National University

Nickel oxide is an oxygen-excess metal oxide that intrinsically forms Ni vacancy (cation defect) sites. We conceived that defective nickel oxide would be a catalyst capable of simultaneously activating different substrates due to the Ni^{3+} and Ni^{2+} coexisting on its surface. We chose hydroboration of styrenes with bis(pinacolato)diboron (**2**) as a model reaction, which gives organoboron compounds useful synthetic intermediates. Nickel oxide supported on various metal oxides was used as a catalyst. All reactions afforded the corresponding Markovnikov-selective hydroboration products **3**. Among them, nickel oxide supported on niobium oxide (NiO/Nb_2O_5) showed the highest catalytic activity and selectivity.

The acidity of the NiO catalysts was estimated from the NH_3-TPD measurement. Figure 1a plots the yield of **3** versus the density of acid sites, which is the amount of desorbed NH_3 divided by the specific surface area of the catalyst. Higher acid densities appear to be more catalytically active. XPS analysis was also performed to obtain the electronic state of Ni. The ratio of Ni^{3+} and Ni^{2+} on the surface varied depending on the support. As shown in Figure 1b, the more Ni^{3+} there is, the higher the catalytic activity is. The NH_3-TPD and XPS analyses suggest that acid sites of niobium oxide as a support and the oxidation state of the nickel of the catalyst affect this reaction.

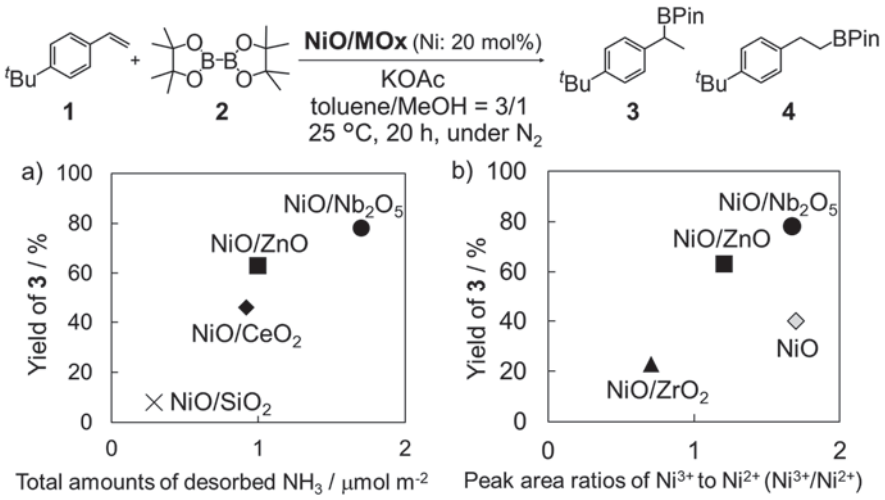

Fig.1 Relationship between catalytic activity in the hydroboration of **1** and a) density of acid sites, b) amount of Ni^{3+} sites.

Academic Meeting (domestic)

1. Oral: Markovnikov-selective hydroboration of styrenes catalyzed by supported nickel oxide
   Ayako Taketoshi, Eiji Hirano, Yusei Kimura, Toru Murayama, Yoshitaka Yamaguchi
   132nd The Catalysis Society of Japan (CATSJ) Meeting, 2E05, Hokkaido University (September, 2023)
2. Poster: Development of supported nickel oxide catalysts for Markovnikov-selective hydroboration of styrenes
   Ayako Taketoshi, Eiji Hirano, Yusei Kimura, Toru Murayama, Yoshitaka Yamaguchi
   2023 Summer Symposium of the Japanese Society for Process Chemistry, 2P24, Tower Hall Funabori (August, 2023)
3. Oral: Markovnikov-selective hydroboration of styrenes by supported nickel oxide catalysts
   Ayako Taketoshi, Eiji Hirano, Toru Murayama, Yoshitaka Yamaguchi
   84th Symposium of the Society of Synthetic Organic Chemistry, Japan (Kanto branch), C13, Tokyo University of Agriculture and Technology (May, 2023)

ジフルオロボリル基またはスルホニル基を有するπ共役系分子の効率合成とその物性

光藤耕一　岡山大学

N,O-二座配位ジフルオロボロン誘導体は Stokes シフトが大きく、溶液状態と固体状態の双方で優れた蛍光特性を有する化合物群である[1-2]。*N,O*-二座配位ジフルオロボロン誘導体の一般的な合成法は、*o*-位に*N*-ヘテロ芳香環を持つフェノール類に対し、Et_3N などの塩基存在下、BF_3•OEt_2 を作用させる手法である(Scheme 1a)。しかし、ヒドロキシヘテロアリールが比較的不安定なため、発光特性の面から興味がもたれるヘテロアリール部位の導入は困難である。例えば、ベンゾチオフェン部位を有する *N,O*-二座配位ジフルオロボロン誘導体の合成は一例のみで、その収率も中程度にとどまる（Scheme 1b)[3]。

Scheme 1. 従来の合成法

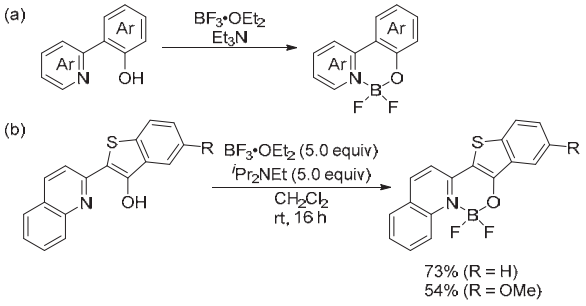

Scheme 2. 本研究

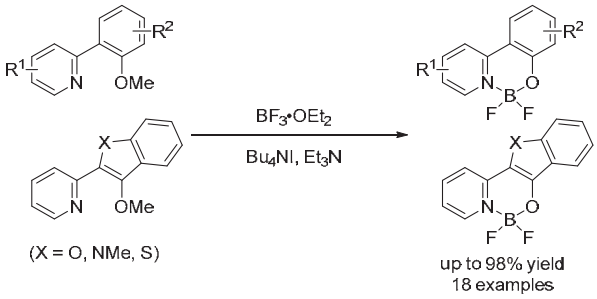

ところで当研究室では最近、安定な基質からの脱メチル化を経るチオフェン環やフラン環を有する 1,2-オキサボリンの合成法を報告している[4]。今回我々はこの手法に着想を得て、安定な前駆体からの脱メチル化を経る *N,O*-二座配位ジフルオロボロン誘導体の合成法を確立した(Scheme 2)。Bu_4NI, Et_3N 存在下、メトキシ基を有するピリジルアレーンに BF_3•OEt_2 を作用させると脱メチル化を経て、*N,O*-二座配位ジフルオロボロン誘導体が得られた。本法を用いると、ベンゾチオフェン部位を有する *N,O*-二座配位ジフルオロボロン誘導体も高収率で得られた。

得られた一連の *N,O*-二座配位ジフルオロボロン誘導体の光学特性の評価を行ったところ、$CHCl_3$ 中にて UV–vis 測定を行ったところ 326–411 nm 付近に強い吸収が観測されたのに対し、蛍光測定においては、401–496 nm に強い発光が観測された。全ての誘導体の Stokes シフトは 3944–10514 cm^{-1} と高い値を示した。また、溶液および固体状態での蛍光量子収率の測定を行ったところ、π 拡張した一部の誘導体では固体状態での蛍光量子収率が低かったが、そのほかの誘導体は溶液状態と固体状態で同等の蛍光量子収率を示すことが明らかとなった。

[文献]

(1) Santra, M.; Moon, H.; Park, M.; Lee, T. Kim, Y. K.; Ahn, K. H. *Chem. Eur. J.* **2012**, *18*, 9886–9893.
(2) Frath, D.; Azizi, S.; Ulrich, G.; Retailleau, P.; Ziessel, R. *Org. Lett.* **2011**, *13*, 3414–3417.
(3) Wang, D.; Xiao, F.; Zhang, F.; Deng, G. *Chin. J. Chem.* **2021**, *39*, 2483–2488.
(4) Shigemori, K.; Watanabe, M.; Kong, J.; Mitsudo, K.; Wakamiya, A.; Mandai, H.; Suga, S. *Org. Lett.* **2019**, *21*, 2171–2175.

Developing machine learning approaches for prediction of protein stability changes upon missense mutations

Jiangning Song　Monash University

Objective. It is known that even a single missense mutation of an amino acid can change protein's structure and stability. Hence, prediction of the stability of a protein against mutations is significantly important. Existing studies show that missense mutations can be harmful to health and disease-related by causing changes in the stability of a protein. Accordingly, the accurate estimation of protein stability change (ΔΔG) measured as Gibb's free energy change is crucial. Although many methods have been developed, the resulting accuracies are not yet satisfactory. Therefore, we will develop novel machine learning methods for this problem, by combining state-of-the-art machine learning techniques and various types of informative protein sequence and structural features. Our team has been successfully developing various methods/tools for analyzing protein sequence data, which include PROSPER, iLearn, iProt-Sub, Cascleave and PROSPERous. Based on these successful collaborations, we will continue and extend our development for prediction of protein stability change and related bioinformatics problems.

Results. Although development of methods for prediction of protein stability is still ongoing, we have obtained results on related topics. We have developed a novel deep learning-based method for prediction of Dicer cleavage sites in miRNAs by utilizing predicted secondary structure data [1]. We also developed a novel deep learning-based framework for cancer gene identification, termed self-supervised masked graph learning (SMG), which comprises SMG reconstruction and task-specific fine-tuning [2]. In addition, we developed a deep learning-based method for identifying antimicrobial peptides and their related 22 functional activities [3].

Publications

[1] Mu, L., Song, J., Akutsu, T., Mori, T.: DiCleave: a deep learning model for predicting human Dicer cleavage sites. BMC Bioinformatics. 25(1):1, 2024.

[2] Cui, Y., …, Akutsu, T., ..., Song, J. SMG: self-supervised masked graph learning for cancer gene identification, Brief Bioinform. 24(6):bbad406, 2023.

[3] Xu, J.,…, Akutsu, T., Song, J.: iAMPCN: a deep-learning approach for identifying antimicrobial peptides and their functional activities. Brief Bioinform. 24(4):bbad240, 2023.

Integrating Omics Data and Module-based Network with Deep Learning to Develop Cancer Type Predictive Models

Jinn-Moon Yang　National Yang Ming Chiao Tung University

Objective. Accurate classification and prediction of cancer subtypes have been an important research topic both in biomedicine and bioinformatics. To tackle this important issue, various machine learning methods have been developed. However, many of existing studies focus on specific cancer types, and thus it is needed to explore mechanisms across multiple cancer types. For understanding of such mechanisms, it is crucial to analyze the topology of biological networks and biochemical progress in cells. To this end, integrated analysis of omics data and biological networks is required. Although many such studies have recently been done, currently available approaches are not satisfactory. In this project, we will continue our collaboration to extend our previous approaches (e.g., deep learning-based methods for integrated analysis of gene expression and evolutionary information, graph theoretic approach to analysis of protein structure data) to include other kinds of omics data, such as genetic and metabolic networks as well as protein-protein interactions.

Results. In order to extend our previous method (graph theoretic approach to identification of hot spots in proteins) to prediction of protein-drug interactions, three students visited Prof. Akutsu's laboratory for about three weeks. We discussed tentative approaches for this issue using drug side-effect prediction, drug target identification, and large language models for drug discovery. We hope that based on these discussions, we can develop some novel method for predicting protein-drug interactions in FY 2024.

We also tried to develop methods for prediction of cell-cell communications. We designed a method for predicting gene regulatory relations between different types of cells using single cell gene expression data by combing regression models and graph matching methods. We implemented a preliminary version of the method and evaluated it using simulation data. The results suggest that the proposed method can identify some interactions. However, we need to confirm the effectiveness of the method using actual gene expression data. Therefore, we plan to apply the method to single cell gene expression data on bone mallow cells and to improve it based on the analysis of predicted regulatory relations.

Ecology and evolution of large and giant DNA viruses

Tom O. Delmont CNRS

Background:

Recent studies suggest that large DNA viruses of eukaryotes are the major drivers of the ecosystem and evolution, but much remain to be elucidated in terms of their diversity, genomic and ecological functions, impacts on the early and recent cellular evolution as well as their mysterious origins and possible links to the emergence of other viral lineages. Viruses of phyla *Nucleocytoviricota* (realm *Varidnaviria*) and *Mirusviricota* (realm *Duplodnaviria*) represent these large DNA viruses, present in diverse environments. Since 2019, we embarked on a journey to investigate and tackle these issues by leveraging the *Tara* Oceans project, an international research project on the global ocean ecosystem that combines ecology, systems biology, and oceanography, in collaboration with the ICR partners.

Objectives:

(1) Automated method for building metagenome assembled genomes (MAGs) for large DNA viruses (data generation); (2) Robust phylogenies of viruses and cellular organisms (evolutionary frameworks); (3) Quantitative assessment of gene exchanges among viruses and cellular organisms (origin of the genome giantism); (4) Characterization of niche specific viral functions (adaptation); (5) Characterization of the emerging viral lineages (a new window of diversity).

Results:

Objective (1) was achieved by developing a dedicated bioinformatics pipeline for MAG screening (manuscript in preparation). Objective (2) and (3) was in part achieved for the virus tree, but the tree for cellular organisms remains as a future work. The viral tree was used for evolutionary reconstruction of viral genes (doi: https://doi.org/10.1101/2023.09.26.559659). We also performed an extensive phylogenetic analyses of viral aminoacyl-tRNA synthetases (doi: https://doi.org/10.1101/2023.12.10.570958), which strongly suggested that ancestral nucleocytoviruses at the epoque of proto-eukaryotes had already complex genomes. Objective (4) was carried out for the polar adaptation of giant viruses (doi: 10.1038/s41467-023-41910-6). Objective (5) was in part addressed through an analysis of eukaryotic genomes for the trace of mirusvirus infection (doi: https://doi.org/10.1101/2024.01.18.576163). These results were obtained in a tight and intensive collaboration the PI's group and ICR's group including graduate students.

Application of metagenomics and a temperature-driven mathematical model to estimate the global distribution of Micromonas viruses

David Demory　CNRS

Objectives

The genus *Micromonas* is a significant component of photosynthetic picoeukaryotes in the ocean. It is proposed that the *Micromonas* virus (MpV) is an important regulator of the community compositions of *Micromonas* spp. I have revealed that the infection activity of MpV changed significantly with seawater temperature. However, the relationship between temperature and the distribution of MpV is not well understood at global ocean scales. In this study, we aimed to reconstruct the phylogeny of MpV using the *Tara* Oceans global metagenomic data to assess the diversity and distribution of MpV at the clade and sub-clade levels. Also, we developed a mechanistic model describing temperature-driven pole-to-pole distribution of MpV.

Methods

Taxonomic classification of MpV was conducted using EPA-ng, which is based on the evolutionary placement algorithm. The maximum likelihood tree of MpVs, which is used as a reference tree, was generated from the PolB sequences of MpV isolates and selected environmental PolB sequences obtained from the Ocean Microbial Reference Gene Catalog version 2 (OM-RGC.v2). By using the taxonomic information, an abundance profile of MpVs was made from the Nucleocytoviricota frequency matrix (Endo et al., 2020, 10.1038/s41559-020-01288-w). Modeling analyses were performed using an epidemiological modeling as described in Demory et al. (2021, 10.1111/ele.13722).

Results

We recruited in total 122 PolB sequences affiliated with MpV from the Tara Oceans metagenomic dataset. By examining the dataset, we revealed that temperature is the key descriptor of the distribution of MpVs at the global ocean scale. Also, temperature-driven infection model could reproduce the population dynamics of the *in-situ* MpV distribution. These results contribute to the mechanistic understanding of the MpV and their hosts, which are sentinel organisms for monitoring the impacts of climate change on marine ecosystems.

Publications

The corresponding manuscript co-authored by PI and Partner Researcher is in preparation.

A Study on Statistical Machine Learning for Efficient Graph Structured Data Analysis

Masayuki Karasuyama　Nagoya Institute of Technology

In this study, we focus on developing methodologies for machine-learning-based knowledge extraction from scientific data represented by a graph. In recent data science, graph-based representations are widely used for capturing structured relations that are often difficult to be handled by the standard numerical table-type datasets. For example, a chemical composition is typically represented as a graph in which a node indicates an atom and an edge indicates a bond. Graph-based models such as graph neural networks (GNNs) and graph kernels have been widely studied in the machine learning community. However, achieving an interpretable model with high predictive performance remains a challenging issue. Our previous approach [1], which is based on a sparse modeling with graph mining, identifies important subgraphs inside a machine learning prediction model, but it cannot deal with a graph having continuous attributes on its nodes or edges. For example, a graph node of a chemical composition can have numerical information derived from the three-dimensional position or chemical properties of each atom.

We propose an interpretable graph-based prediction model for “attributed” graph data [2,3], which learns importance weights for small attributed subgraphs, called attributed graphlets, while simultaneously optimizing their attribute vectors. This enables us to obtain a combination of subgraph structures and their attribute vectors that strongly contributes to the prediction. Our approach regards all the subgraph structures in the training dataset as candidate important structures. This can investigate all the potentially important subgraphs, but obviously, a naive implementation requires prohibitive amount of computations. To avoid this computational difficulty, we introduce an efficient pruning strategy by combining the proximal gradient descent and a graph mining tree search. This strategy guarantees that we can obtain the same results compared with the exhaustive computation without the pruning. We experimentally verified our approach actually identifies a small number of important attributed graphlets while achieving similar prediction performance to other well-known approaches such as GNNs.

[1] T. Yoshida, I. Takeuchi and M. Karasuyama, Distance Metric Learning for Graph Structured Data, *Machine Learning*, vol.110, no.7, 1765-1811, 2021.

[2] S. Tajima, R. Sugihara, R. Kitahara and M. Karasuyama, Learning Attributed Graphlets: Predictive Graph Mining by Graphlets with Trainable Attribute, *arXiv*:2402.06932, 2024.

[3] R. Sugihara, S. Tajima, R. Kitahara and M. Karasuyama, Predictive Graph Mining for Attributed Graph Data through Proximal Gradient Pruning, IEICE technical report, vol.123, no.91, IBISML2023-16, 98-105, 2023 (in Japanese).

テンソル分解を用いた教師なし学習による変数選択法を用いた MetNet Comp Database の予測評価

田口善弘　中央大学

１．目的

田村 武幸准教授が開発公開している MetNet Comp Database は遺伝子を部分的にノックアウトすることで代謝ネットワークの生成物を最大化することを理論的に予測したものである。その結果を複数の生物種に対して複数の代謝物に対してどの遺伝子をノックアウトすれば最大化が果たされるかのリストが網羅的に公開されている。しかし、現実にこの遺伝子の組をノックアウトし、代謝物の生成量を実験的に調べることは困難がある。これをテンソル分解を用いた教師なし学習による変数選択法を用いて新たな実験を行わずに既存のデータセットの解析だけで予測することが目的である。

２．理論の構成

テンソル分解を用いた教師なし学習による変数選択法は遺伝子発現プロファイルを解析し、条件によって変動する遺伝子を選択する汎用的な方法である。同手法を用いれば、単一の遺伝子をノックアウトした場合の遺伝子発現プロファイルを組み合わせることで、複数の遺伝子を同時にノックアウトした場合に影響を受ける遺伝子を推定することができる。この変動遺伝子を代謝ネットワークにマッピングすれば、現実の生物で MetNet Comp Database の予測通りに代謝ネットワークが活性化／抑止されるかを推定できることが期待された。

３．理論の結果

GEO を中心としたデータベースで単一遺伝子をノックアウトした場合の遺伝子発現プロファイルを探索した。意外なことに、一部の MetNet Comp Database 対象種においては全体の８割程度が網羅的にノックアウトされた場合の遺伝子発現プロファイルがある場合があったにも関わらず、MetNet Comp Database の組み合わせに合致する代謝物は１つもなかった。MetNet Comp Database では最小たった２個の遺伝子をノックアウトする場合も含まれていたのにこのたった２個がノックアウトされている組み合わせさえ見つからなかった

４．考察

１つの可能性として、MetNet Comp Database に含まれている遺伝子が必ずリーサルなものを含んでしまっている可能性がある。その場合、MetNet Comp Database の予言通りのノックアウトはそもそもできない。この点を確認するため予算の残額を RNA-seq に充ててノックアウト実験を行う予定である。

５．成果報告

上記のような状態なので成果は得られなかった。

Control and Analysis of Complex Networks via Probabilistic Minimum Dominating Sets

Jose Nacher　Toho University

Objective. In cells and organisms, various types of molecules interact with each other to carry out life activities. Thus it is important to analyze networks formed by these interactions to understand life. To this end, we have been conducting studies on controllability of various biological networks such as protein-protein interaction networks, metabolic networks, and ncRNA-protein networks. In recent years, we have been focusing on controllability studies based on the minimum dominating set (MDS), which is a well-known graph theoretic concept. In particular, we developed methods to classify nodes into critical, intermittent, and redundant based on occurrence of nodes in MDS solutions. In this year, we extend this framework by further classifying intermittent nodes by considering the number of occurrences in MDS solutions.

Results. We proposed the concept of the criticality for evaluating the importance of each intermittent node using (MDS)-based control model. Next we developed an efficient heuristic algorithm based on integer linear programming and the Hamming distance for computing the criticality of intermittent nodes. The performance of the algorithm was evaluated using artificially generated scale-free networks. The computational experiments demonstrated the appropriateness of the solution of the proposed heuristic algorithm as well as the improvements obtained in the computational time. Then we applied the proposed criticality algorithm to three biological networks and systems: the human RTK signal transduction pathway, the human cytokine-cytokine interaction network and the connectome of the nematode Caenorhadbitis elegans. The results unveiled that the intermittent nodes play a more important role than previously assumed. For example, our findings show that the set of high criticality proteins in the human RTK signaling pathway are associated with phosphorylation and cancer [1].

Publication

[1] W. Someya, T. Akutsu, J. M. Schwartz, J. C. Nacher: Measuring criticality in control of complex biological networks, NPJ Systems Biology and Applications, 10(1):9, 2024.

巨大ウイルス感染アメーバのトランスクリプトーム解析による宿主・巨大ウイルス相互作用の解明

武村政春　東京理科大学

【目的】研究代表者と共同研究者である京都大学化学研究所・緒方博之教授らのグループが 2019 年に分離したメドゥーサウイルスは、Phylum *Nucleocytoviricota*（核細胞質ウイルス門）、Family *Mamonoviridae*（魔物ウイルス科）に分類される二本鎖 DNA ウイルスで、真核生物と同じくヒストンを５種すべてコードし、細胞核で DNA を複製するという、巨大ウイルスの中では特異な表現型を有する。本研究では、メドゥーサウイルスヒストンのうち役割の不明なリンカーヒストン H1（medusa H1）遺伝子を強制的に安定発現させたアメーバ株を樹立し、その表現型をトランスクリプトミクスにより解析することを主として、メドゥーサウイルス・宿主相互作用の解明を目指した。

【実験方法】まず、AlphaFold2 などを用いた medusa H1 の立体構造予測を行った。次に、medusa H1 遺伝子を pGAPDH-EGFP-Neo ベクター（慶北大学・Yeonchul Hong 博士より供与）に挿入した pGAPDH-EGFP-H1 を用いて強制安定発現アメーバを樹立した。次に、野生株アメーバと共に total RNA を抽出し、RNA-seq を行い、これらのトランスクリプトーム解析を行った。また、medusa H1 安定発現株を用いて medusa H1 と相互作用するタンパク質を免疫沈降法により探索した。

【実験結果・考察】立体構造ならびにドメイン予測の結果、medusa H1 は、N 末端側に真核生物 H1 がもつ H1 ドメインを、C 末端側に機能未知のドメインを保有していた。H1 ドメインに DNA 結合部位が予測されたため、DNA と結合能を有することが示唆された。

トランスクリプトーム解析により、medusa H1 安定発現株では RNA 成熟や細胞分裂に関する遺伝子が優位に発現促進されていることがわかった。また、medusa H1 安定発現株では、EGFP-H1 のシグナルが細胞核に集積し、さらにその細胞動態解析により、野生株と比較して細胞核が大きくなっていることがわかった。これらのことから、medusa H1 安定発現株では、細胞核で転写が起こりやすい環境になっていることが示唆された。

Medusa H1 安定発現株からの、抗 EGFP 抗体を用いた共免疫沈降実験により、medusa H1 と相互作用する 33 kDa のタンパク質が見つかった。medusa H1 は、細胞核においてこの 33 kDa タンパク質と相互作用し、何らかの機能を遂行することが示唆された。

これらの結果ならびに先行研究から、medusa H1 は、真核生物 H1 のリンカーヒストンとしての役割とは異なる機能をもつ可能性があり、今後、相互作用する 33 kDa タンパク質の同定などを通じて、medusa H1 の機能を明らかにしていく予定である。

【成果報告（論文、学会発表等）】

1. 山本果奈、武村政春. Medusavirus ヒストン H1 の強制発現による宿主細胞核や感染サイクルへの影響. 日本微生物生態学会第 36 回大会、浜松、2023.11.28.-30.
2. 山本果奈、武村政春. Medusavirus histone H1 の発現によって誘導される宿主の細胞核や感染サイクルへの影響. 第 46 回日本分子生物学会年会、神戸、2023.12.6.-8.

ウイルスダークマターの解明に向けたウイルスゲノム情報基盤の構築

西村陽介　海洋研究開発機構

【研究目的】地球に生息する全ての生物はウイルスに感染すると考えられており、地球上に存在するウイルスの粒子数は 10^{31} 個と推定されている。ウイルスは生物の主要な死因となると共に、様々な生物と共生関係を築き上げることで、その進化と多様性に影響を与え、地球上の生命活動に広く関与している。近年ではメタゲノム解析により環境中に存在する多様なウイルスを解析することが可能になり、公共 DB にはメタゲノムデータが蓄積されているものの、そこに含まれるウイルス配列に関する膨大なデータの効果的な利用がなされていない。本研究は、メタゲノムビッグデータを統一的に再解析してウイルスゲノムを大規模に探索し、得られたウイルスゲノムやウイルス系統、生息環境、機能遺伝子を統合した新しいデータベースを構築するとともに、ビッグデータ解析に必要なツール群を開発することで、生命科学や医療の発展に貢献する。

【手法と結果】NCBI SRA から 10,000 メタゲノムサンプルに由来する配列データ（約 100 兆塩基対）を入手した。MEGAHIT を用いて配列アセンブリを行い、VirSorter2 によってウイルスに由来するゲノム配列を同定した。その結果様々な環境に由来する、71,000 の完全長ゲノムを含む、1600 万のウイルスゲノム断片が得られた。また、収集したメタゲノムデータはすべて出版済みの文献に紐付けられており、文献に記載された情報を用いてメタゲノムの由来となる環境情報の収集とその整備を約 5,000 サンプルに関して完了した。同定されたウイルスゲノムを対象に、自作の解析パイプライン GANA を用いて KEGG KO の相同遺伝子や、Pfam などの機能ドメインを探索することで、これらのウイルスが持つ遺伝子機能を情報化した。また、新たにウイルスや微生物の比較ゲノム解析ツールである DiGAlign の開発を行い、GenomeNet にて公開した（成果 1）。DiGAlign は、比較ゲノム解析における可視化手法であり、ゲノム間の類似性を分かりやすく示す「シンテニーマップ」を作成するウェブツールであり、これまでのツールでは困難な、最大 300 ゲノムの大規模な比較ゲノム解析が可能である。独自の機能として、類似性をもとに構築されるゲノム系統樹である「ガイドツリー」によって、類似性の高いゲノム間の比較図を迅速に表示できる上に、遺伝子の同定とその機能予測も可能である。DiGAlign は以上の機能により、ウイルスデータを解釈するための仮説を持たない場合でもデータ駆動でゲノムデータの理解を促進し、大量のゲノム情報を入手可能な現代におけるゲノム解析のスピードを加速する。

【成果報告】原著論文

（1） Yosuke Nishimura, Kohei Yamada, Yusuke Okazaki, and Hiroyuki Ogata. ‘DiGAlign: versatile and interactive visualization of sequence alignment for comparative genomics’ Microbes and Environments (Accepted).

効果的な生体分子解析方法の開発と医学・農学への応用

茅野光範　帯広畜産大学

本研究では、機械学習と統計学を融合させた統計的機械学習の観点から、効果的な生体分子解析法を提案し、それを用いて医学・農学における問題を解決する。分子レベルとして、ゲノム・遺伝子・代謝に焦点を当て、遺伝子ネットワークや代謝ネットワーク（代謝パスウェイ）の推定や、それらのネットワークへのゲノムの影響、実験条件（健常者と患者等）による違い等を検証するための解析方法を提案する。

我々は、これまで、図 1 に示した分子発現の相関構造の変化を捉える解析手法を提案し、これを改良した提案手法の数値実験による評価、公共の遺伝子発現データ（Gene Expression Omnibus；GEO から入手した延べ約 100 万個の遺伝子群）に提案手法を適用し、生物学的に意義のある遺伝子群が検出出来ることを確認した。また、先行研究で報告されている、相関ネットワークが変化する遺伝子群の具体例を集めた。さらに、これまでの提案手法をさらに発展させ、グラフネットワーク理論、計算機統計学、アルゴリズムやマイニング理論を駆使した機械学習・統計学的な分子ネットワーク解析法の提案へ向けて検討を重ねている。

今年度は、これらの解析法の医学分野（特に加齢研究）および農学分野（特に農作物）における具体的な生命科学現象への応用を検討し、医学分野として、ヒトと動物の加齢および加齢関連疾患研究、また、農学分野として、農作物のオミックス解析研究を進めている。

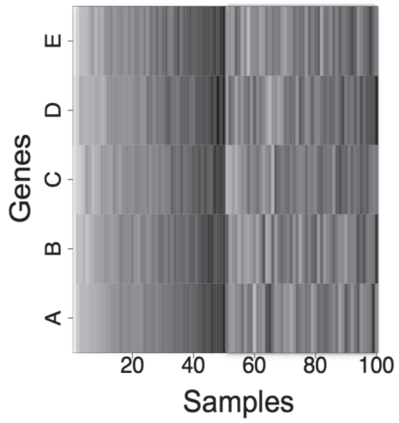

図 1. 2 つの群間（サンプル 1〜50 および 51〜100）で相関構造が変化する 5 つの遺伝子 A, B, C, D, E のヒートマップ表示（濃いほど発現量が高い）。遺伝子 A-E の中から任意の対をとると、サンプル 1 から 50 の群では相関を持つが、サンプル 51-100 の群では相関構造が崩れる［Kayano M., Shiga M. and Mamitsuka H., IEEE/ACM Trans. Comp. Biol. Bioinform., 11(1): 154-167, 2014 より転載］

Investigations into cofactor biosynthesis of N_2-reducing enzyme via semi-synthetic approach

Markus W. Ribbe　University of California, Irvine

[Objectives]

FeMoco ([(*R*-homocitrate)$MoFe_7S_9C$]) is the metal-sulfur cofactor of Mo-nitrogenase that reduces atmospheric dinitrogen into ammonia. Biosynthesis of FeMoco starts from two cubic [Fe_4S_4] clusters (K-cluster) to give an Fe-only analog of FeMoco ([Fe_8S_9C], L-cluster) with concurrent C- and S-atom insertions (Fig. 1). Previous research have revealed that the C atom originates from a CH_3 group of *S*-adenosylmethionine (SAM); however, the reaction pathway to the "naked" C atom remains mostly elusive. This research aims to gain insights into its mechanistic details.

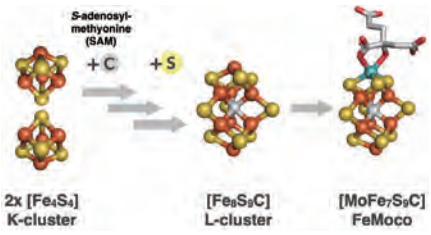

Fig. 1. Biosynthetic pathway of FeMoco, the cofactor of the N_2-reducing enzyme (nitrogenase).

[Methods]

NifB is the enzyme that houses the K-cluster and mediates the C- and S-atom insertion processes. As we have developed a methodology to incorporate [Fe_4Se_4] clusters into proteins using a synthetic [Fe_4Se_4] cluster ([$Fe_4Se_4(SCH_2CH_2OH)_4]^{2-}$), a similar approach was applied to NifB. The mentioned CH_3 group of SAM is transferred onto a S atom of the K-cluster at the initial step, followed by an H-atom abstraction that proposedly leads to the formation of $\bullet CH_2$ species. The S-to-Se substitution should thus alter the reactivity of the unidentified $\bullet CH_2$ species and potentially terminate the insertion process in the middle.

[Results and Discussion]

NifB protein reconstituted with [$Fe_4\underline{Se}_4$] cluster displayed SAM cleavage activity that is comparable to the one with [$Fe_4\underline{S}_4$] cluster (Fig. 2). The SAM cleavage reaction produced *S*-adenosylhomocysteine (SAH) as the CH_3 transfer product and 5'-deoxyadenosine (5'-dAH) as the clue of the radical formation. However, electron paramagnetic resonance (EPR) spectroscopy showed no sign of the formation of the L-cluster, which is determined as an isotropic signal observed around g = 1.92, and exhibited novel signals that may be resolved into multiple species. Given the results, we think that the new signals can be assigned to intermediates of the C-atom insertion process or their closely related states. Further investigations into these species will be conducted.

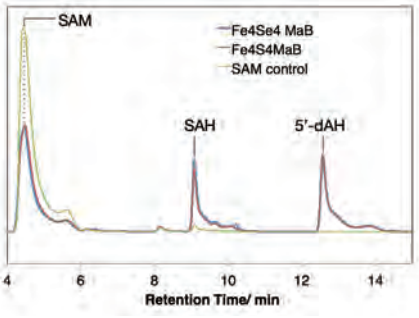

Fig. 2. HPLC-elution profiles SAM (green), SAM treated with NifB containing [Fe_4Se_4] clusters (blue) or [Fe_4S_4] clusters (red).

Radical-polar crossover catalysis for synthesis of complex natural products

Sunkyu Han　Korea Advanced Institute of Science & Technology

The field of total synthesis of natural products has shown dramatic progress over the last century. Through collective efforts of the synthetic community, complex targets have been synthesized using inventive solutions, and those solutions have formed the basis for the development of new drugs and materials. With increasing expectations imposed on synthetic organic chemists, the role of total synthesis (i) as a driving force for the discovery of novel synthetic strategies, (ii) as a platform to discover novel reactions that enable unprecedented bond formations, (iii) as a tool to enhance the understanding of biosynthetic machineries, and (iv) as a means for generating chemicals of extraordinary biological significance in substantial quantities will continue to grow. With these goals in mind, this project seeks to develop the synthesis of complex natural products. This work focuses on exploration of the discovery of novel transformations and bond forming strategies based on radical-polar crossover catalysis developed by Ohmiya group. The pursuit of convergent and flexible synthetic approaches should enable access to not only a single target but various natural products with structural and biosynthetic relevance, or unnatural products with higher biological potency.

In the course of examining the above joint research, we synthesized suffranidine B from biosynthetically relevant precursors, the kojic acid-derived vinylogous ketoaldehyde and 2,3-dehydroallosecurinine, in two steps, both involving acidic conditions. To minimize the population of the detrimental monoprotonated iminium ion intermediate, meticulous selections of acids were carried out based on the mechanistic analyses of each step. A mild and heterogeneous acidic alumina was identified to be optimal for the heterotrimerization step, and a high hydronium ion concentration at an elevated temperature was essential for the stereocontrolled desymmetrizing cyclization step. This work highlights the power of biosynthetic considerations during the synthetic planning of complex natural products and the intricacies involved in the actual execution of the biomimetic synthesis.

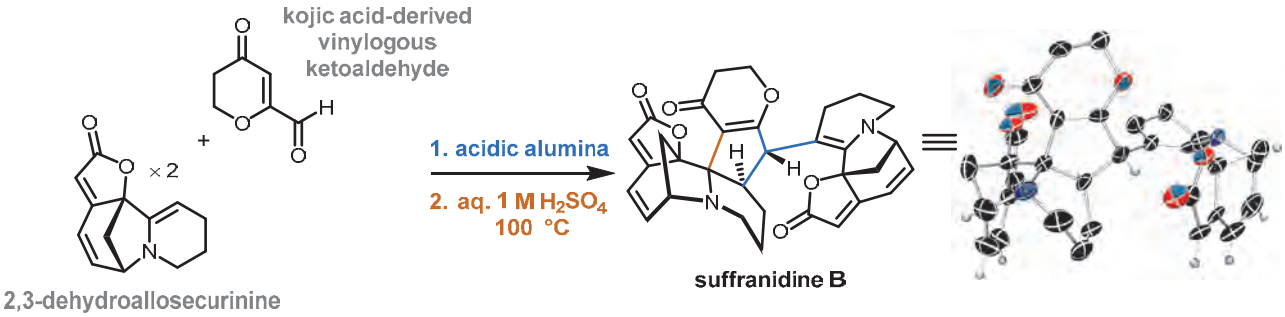

Development of multi-resonant TADF emitters with short delayed lifetimes and their use in long lifetime OLEDs

Eli Zysman-Colman　University of St Andrews

We have reported three collaborative studies between the Zysman-Colman and Kaji labs involving multiresonant thermally activated delayed fluorescence (TADF) molecular design and their use in OLEDs.

We developed derivatives of **SpAC-tBuDOBNA** (TDBA-SAF)[1] containing donor dendrons, **SpAC-tBuDOBNA-DCZ** and **SpAC-tBuDOBNA-DCz** (Figure **1**). The 10 wt% doped films of **SpAC-tBuDOBNA**, **SpAC-DOBNA-DCz** and **SpAC-tBuDOBNA-DCz** in DPEPO emit at λ_{PL} of 456, 466 and 475 nm with Φ_{PL} of 90, 65 and 59%, respectively. All three emitters showed TADF behaviour with τ_p of 31, 40 and 44 ns and τ_d of 1.34, 1.44 and 1.10 μs, respectively. The solution-processed OLED devices with **SpAC-tBuDOBNA**, **SpAC-DOBNA-DCz** and **SpAC-tBuDOBNA-DCz** exhibited promising EQE_{max} values of 17.8, 17.2 and 13.1% at CIE coordinates of (0.15, 0.12), (0.16, 0.26) and (0.14, 0.19), respectively. However, due to the high turn-on voltages and high efficiency roll-off for all devices further investigations regarding the device architecture are necessary.

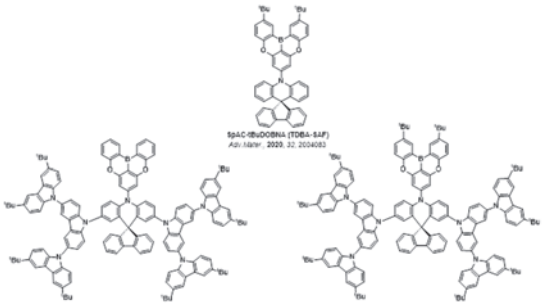

Figure 1. Chemical structures of **SpAc-tBuDOBNA**, **SpAc-DOBNA-DCz** and **SpAc-tBuDOBNA-DCz**.

In another collaborative research project, a new MR-TADF emitter **2,7-tBuCzNB** (Figure **2**) has been developed for solution-processed OLEDs. The second-generation carbazole donor dendron promotes an increased intermolecular distance and reduces the aggregation-caused quenching. **2,7-tBuCzNB** emits at 498 nm with a narrow FWHM of 47 nm and has a ΔE_{ST} of 0.15 eV, Φ_{PL} of 86%, a τ_p of 9.9 ns and a τ_d of 1.89 ms in 5 wt% doped film in a mCP/OXD-7(30 wt%) host matrix. We are now evaluating this compound in solution-processed OLEDs.

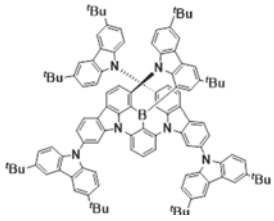

Figure 2. Chemical structure of **2,7-tBuCzNB**.

A third collaborative research project involved the design, synthesis, and analysis of a D-A typed TADF emitter, **tMCzSe** (Figure **3**). Selenium, the "heavy" atom, has been strategically integrated into the acceptor moiety to enhance SOC leading to an acceleration of the RISC process. **tMCzSe** emits at λ_{PL} of 504 and 509 nm, and has Φ_{PL} of 22 and 57%, respectively, in dilute toluene solution and 10 wt% doped films in PMMA. The emitter has a small ΔE_{ST} of 0.02 eV. **tMCzSe** exhibits short τ_d of 621 ns in toluene and 2.3 μs in 10 wt% doped films in PMMA; the τ_p has not been determined yet due to the detection limit. The HOMO and LUMO energies for **tMCzSe** are -5.62 and -2.91 eV. We are presently evaluating this compound as an emitter in OLEDs.

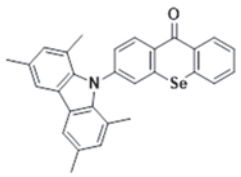

Figure 3. Chemical structure of **tMCzSe**.

References.

(1) Lim, H.; Cheon, H. J.; Woo, S. J.; Kwon, S. K.; Kim, Y. H.; Kim, J. J. Highly Efficient Deep-Blue OLEDs using a TADF Emitter with a Narrow Emission Spectrum and High Horizontal Emitting Dipole Ratio. *Adv. Mater.* **2020**, *32* (47), e2004083.

Design and synthesis of linear molecules for improving outcoupling efficiency of solution-possessed OLEDs

P. Rajamalli　Indian Institute of Science

Project Outcome Report

Objectives: Design and synthesis of heavy atom induced TADF materials. Photophysical investigation of the TADF emitters with screening of potential emitters for device fabrication. Followed by, device architecture will be optimized to realize the high efficacy OLEDs.

Theoretical Analysis: As per the objective, the designed furan and thiophene based molecules were subjected for the TD-DFT calculations, which results both the designed emitters are TADF in nature.

Experimental Methods and Discussions: Based on the TD-DFT results, we have synthesized both the emitters using two step reactions and characterized well with spectroscopic techniques. Subsequently, photophysical studies reveals that the molecules fall in the cyan blue region (λ_{max} = 478 nm and 482 nm), also increasing the solvent polarity the emission wavelengths shifted to red region, shows strong ICT character. The singlet-triplet energy gap found to be calculated ΔE_{ST} = 0.10 and 0.11 eV and enhanced PLQY in the thin film state. Also, the experimentally calculated kinetic parameters also further confirm the TADF property of the compounds.

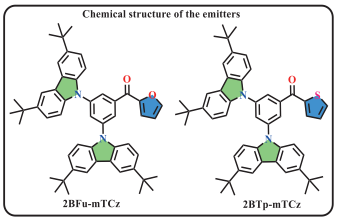

Electroluminescent Properties: To explore the electroluminescence (EL) properties, multilayer OLED devices were fabricated using synthesized emitter with help of our collaborator *Prof. Hironori Kaji* from Kyoto University. These emitters showed the EQE maximum of 9.6% (**2BFu-mTCz**) and 9.0% (**2BTp-mTCz**) with sky-blue emission (λ_{em} = 487 and 489 nm). The transition dipole orientation of the emitters (**2BFu-mTCz** and **2BTp-mTCz**) in the doped film (7 vol% emitter: 80 nm thick PPF host) was measured using angle-dependent p-polarized photoluminescence (PL) spectra to simulate the efficiency of out-coupling. The measured transition dipole orientation is Θ = 74% in both the emitters. From the molecular orientations and PLQYs in the doped films, EQE_{maxs} were predicted to be 7.0–10.4% for **2BFu-mTCz** and 8.1–12.0% for **2BTp-mTCz** assuming 100% charge recombination, in good agreement with the experimental values. This work was published in the *ACS Applied Optical Materials.*

This work could guide subsequent designing ideas by weak A-π-D-D systems; this could serve as a step towards enhancing the RISC process along with shorter lifetimes and it may open up a new pathway to design and development of new TADF materials for OLED applications.

1. T. Viswanathan, Y. Kusakabe, A. Upasha, **H. Kaji**, and **P. Rajamalli**, Benzoylfuran and Thiophene-Based Thermally Activated Delayed Fluorescence Emitters for Organic Light-Emitting Diodes, *ACS Applied Optical Materials,* **2024**. (doi.org/10.1021/acsaom.3c00475).

Precise synthesis and controlling higher-order structure of tadpole-like Janus cellulose nanocrystal

Atsushi GOTO　Nanyang Technological University

Objectives – Cellulose nanocrystal (CNC) is a rod-like particle which obtained by hydrolysis of cellulose microfibril. We expected that the CNC derivative with polymer brushes of different molecular weight (long chain at reducing end and short chain at the other surface) (asymmetrically polymer-brush-modified CNC: aPB-CNC) could form a new higher order structure. In this study, we have developed a synthetic path for aPB-CNC (Scheme 1) and assessed the interparticle interactions of a monolayer on the water surface.

Scheme1. Synthetic route for asymmetrically polymer-brush-modified CNC.

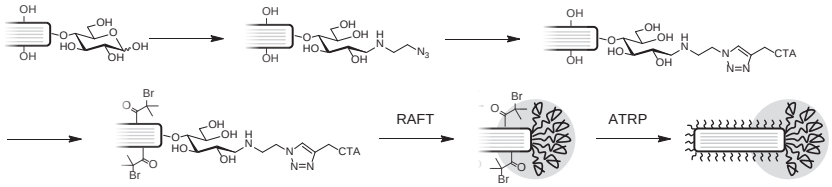

Results and Discussion – CNC derivative with an initiator for reversible addition fragmentation chain transfer (RAFT) polymerization were synthesized introducing an azido group by reductive amination reaction and click reaction with RAFT agent. An atom transfer radical (ATRP) initiator was then introduced to the other surface of the CNC derivative to yield a multi-functional CNC initiator regioselectivity modified with two kinds of initiators for controlled radical polymerization. Bicinchoninic acid assay, infrared absorption spectrometry and elemental analysis revealed that the sufficient amount of initiators for RAFT polymerization and ATRP were introduced to CNC for the later modification with dense polymer brush. Subsequently, RAFT polymerization and ATRP were sequentially and successfully conducted to obtain the target CNC derivative, aPB-CNC. The surface pressure-area isotherm of aPB-CNC on a water surface indicated that transition from anisotropic to isotropic phases occurred when the surface pressure exceeded a critical point. Additionally, the comparison of the isotherm with a CNC derivative with polymer brushes introduced uniformly suggested that the high-molecular-weight polymer brush at the reducing end of aPB-CNC affected the interparticle interactions.

Development of lead free metal halide perovskite

Yasuhiro Tachibana　RMIT University

Introduction

Metal halide perovskite has recently attracted considerable attention as one of promising materials to be applied for solar cells, owing to their low cost preparation process, attractive optical properties including a band gap tunability, and choice of a variety of morphologies from 0D quantum dots to 2D nanoplatelets. However, these applications have been investigated by employing toxic lead halide materials, since lead halide perovskites have so far shown the highest performance, and no alternative metal has not been identified to replace lead halide perovskite.

In this project, we aim at developing Sn based perovskite structures including multi-crystalline films and nanocrystals with high PLQY. So far Sn(2+) based perovskite is known to be unstable under ambient condition. We will therefore synthesize/stabilize films/nanocrystals with novel capping reagents. We will also conduct transient absorption studies to understand charge carrier dynamics inside lead based perovskite films. We have conducted this project with Professors Teranishi and Wakamiya at the ICR.

Experimental

(1) Preparation of Sn based perovskite structures, and control of their surface structure

We have already established methods to synthesize Sn(2+) and Sn(4+) halide perovskite films and nanocrystals. But to control their surface, we will replace common ligands to be used for nanocrystal synthesis with hydrophobic ligand to stabilize their surface. We mainly employed 4 different types of fluorobenzene phosphoric acid.

(2) Excitation power dependence on electron-hole recombination in lead based perovskite films

Picosecond to microsecond TAS studies were conducted by a picosecond transient absorption spectrometer (UNISOKU Co., Ltd., RIPT Pico-TAS, time-resolution: 70 ps). The details of the spectrometer will be published elsewhere. Briefly, the sample was excited by a diode pumped picosecond Nd:YAG laser (EKSPLA, PL2210A-1K-TH) and an optical parametric generator (OPG, EKSPLA, PG403, ~25 ps pulse duration). Transient absorption signal was probed by a mode locked white light supercontinuum pulse laser (YSL Photonics Co., Ltd., SC-Pro-M-20, ~100 ps pulse duration). Transient data were collected with 570 nm excitation with a wide variety of excitation intensity from 0.18 to 127 μJ cm^{-2} with a repetition rate of 1 kHz at 22 °C.

Results and Discussion

(1) Emissive $CsSnI_3$ nanocrystals will were obtained. These nanocrystals were stable under anhydrous condition over a few weeks. However, we found that the nanocrystals were oxidized within several tens of minutes as soon as the nanocrystal solution was exposed to ambient condition.

(2) With low excitation intensity (<2 μJ cm^{-2}), the charge recombination decay is comfortably fitted with the 1st order reaction rate equation, while with the higher excitation intensity (>2 μJ cm^{-2}), the fit requires addition of the 2nd order rate law. By comparing the half lifetimes of the 1st order reactions, trap states with at least 3 different potential levels are identified. By comparing the 1st and the 2nd order reactions, the charge trap state density was estimated to be 1 x 10^{17} cm^{-3} in this perovskite film.[1]

We also identified the relationship of spin-coating temperature with lead-based perovskite film morphology and solar cell performance.[2]

Outcomes

[1] **A. Wakamiya**, **Y. Tachibana** and co-workers, *J. Photopolym. Sci. Technol.*, **in press** (2023).
[2] **A. Wakamiya**, **Y. Tachibana** and co-workers, *submitted*.

Synthesis of Graphene Nanoribbons Containing Non-Hexagonal Rings Optoelectronic Materials with Open-cage C60 Derivatives as Building Blocks

Chaolumen　Inner Mongolia University

Exploring efficient synthesis and novel properties of polycyclic aromatics with pentagons are significantly important for developing new optoelectronic materials. During the Ph D study at ICR, the applicant found 5,11-diphenyltetracene can smoothly proceed double oxidative cyclization at the Scholl condition to give tetrabenzo-fused pyracylene (TBP).

After Joining IMU, the research interest of the applicant focused on synthesis and properties of novel molecular nanocarbons containing non-hexagonal rings, particularly pentagons and research outcomes as below.

(1) Synthesis of a dichlorotetracene and its related derivatives. By a multi-chlorination followed by dechlorination strategy, we successfully synthesized a unprecedented dichlorotetracene derivative, which might be an excellent p-type semiconducting material according to the previously reported dichlorotetracene derivative. This method can produce this dichlorotetracene with excellent yield without any column chromatography step. This dichlorotetracene can proceed Suzuki-Miyaura coupling with various arylboronic acids to give a wide range of diaryltetracene which are hardly synthesized by the reported methods.

(2) Bis-tetracene derivatives. By a concise and efficient method, we have successfully synthesized a bis-tetracene derivative and its structure is unambiguously determined by single-crystal X-ray diffraction. Compared to the reported bis-tetracene derivative and its heteroatom containing analogue by Mullen and co-workers, the compound we synthesized exhibited excellent photo stability, reversible redox behaviors, pure NIR absorption and unique twist chirality. The detailed properties of this molecule are still under investigation in our lab.

In this research, all of X-ray crystallographic analysis were performed by Dr. Hashikawa, who is current assistant professor at Murata lab.

Optoelectronic Materials with Open-cage C60 Derivatives as Building Blocks

Sheng ZHANG　Henan University

Objectives

Fullerenes have yet to serve as π-units for synthesizing π-conjugated polymers, primarily due to the inherent challenge of transforming sp^2 hybridized carbon atoms into sp^3 hybridized ones upon surface derivatization. This project aims to address this limitation by constructing a fullerene-based π-conjugated polymer utilizing open-cage fullerene derivatives as building blocks. These derivatives can be bonded to a conjugated scaffold using sp^2 hybridized elements such as carbon and nitrogen.

Experimental Methods

Commercial solvents used in reactions were first dried over NaH, and subsequently distilled prior to utilization. All oxygen and water-sensitive reactions were conducted under an argon atmosphere employing the standard Schlenk technique. ^{1}H NMR spectra were acquired at either 400 MHz or 500 MHz using a mixed solvent of CS_2/$CDCl_3$ (*v*/*v* 2:1). DFT calculations were carried out at the B3LYP/6-31G* level of theory using the Gaussian 16 program.

Outcomes

The open-[60]fullerene monomer (**BrOF**) was synthesized following established protocols as reported by the collaborative researchers of the current project (*Science* **2011**, *333*, 613; *Chem. Commun.* **2023**, *59*, 6560). Subsequently, polymerization with **SnBT** was carried out via Stille coupling to yield polymer **pOFBT** (as shown in figure). Preliminary characterization utilizing ^{1}H NMR and TLC confirmed the product as a polymer. DFT calculations revealed that the HOMO and LUMO of the repeat unit predominantly localize at the thiophene and fullerene-cage moieties, respectively.

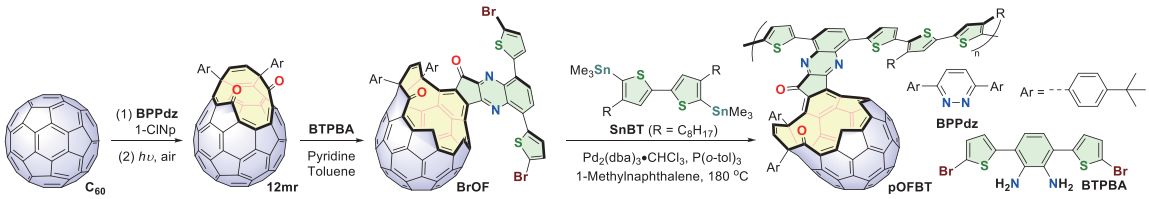

Analysis

Polymerization employing **BrOF** proceeded at a higher temperature (180°C) compared to typical reactions (110°C) due to residual O_2 inside the cage, which could potentially poison the catalyst. The orthogonal distribution of orbitals facilitates intramolecular charge transfer, imparting potential for electronic material applications.

The Reactivity of Guanidino-Isatins in Prato Cycloaddition Reaction

Davor Margetic　Rudjer Boskovic Institute

Objectives

Synthesis of novel guanidinium isatin reagents and investigation of their reactivity for fullerene derivatization by cycloadditions with partner ICR researcher Professor Murata Yasujiro.

Experimental results. Synthesis of guanidine functionalized isatins **1** with solubilizing *n*-hexane substituent was carried out. The cycloaddition properties of isatins **1** were established by their participation in the Prato reaction with fullerene C_{60}. Fullerene reacted with **1**, providing pyrrolidine functional derivatives of **2** (Scheme 1). Detailed study and optimization of reaction conditions have revealed that the best conditions for preparation of products **4-6** were solid-state mechanochemical ball-milling at room temperature (i.e. for less soluble products). Synthesis of **7** and **8** (better soluble products) better proceeded in thermal solution conditions (toluene/ethanol).

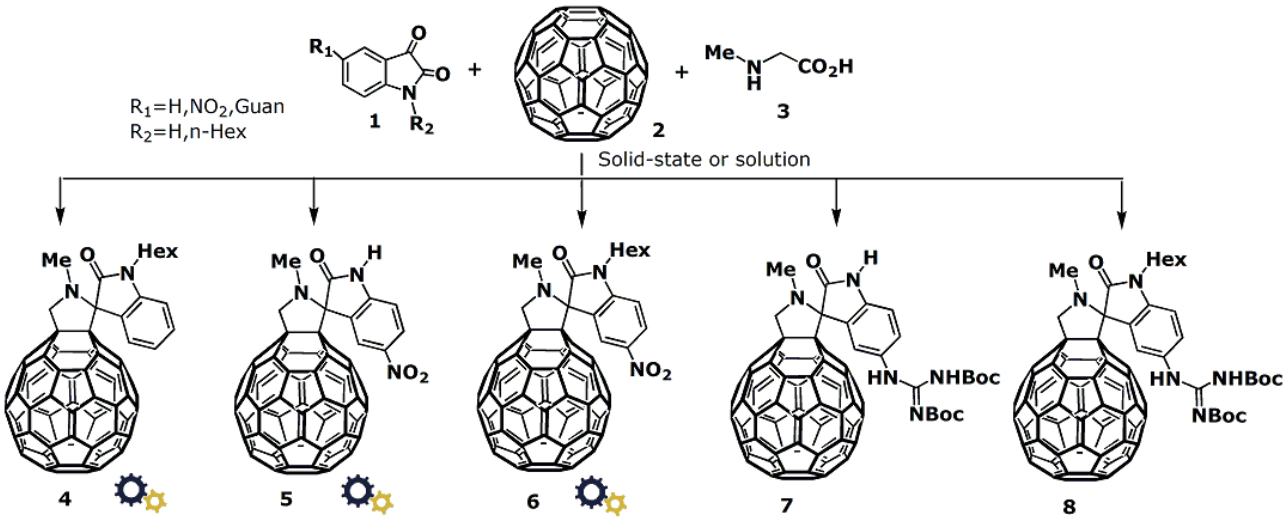

Scheme 1

Theoretical results. Experimental results were augmented with a quantum-chemical computational study. The M062X/6-31G(d,p)//SMD(EtOH) density functional calculations were carried out to predict the influence of guanidine substituent on the reactivity of isatin derivatives in 1,3-dipolar cycloaddition reactions. No notable influence of substituents on the activation energies (reactivity) was determined, which is in good accordance with experimental results.

The planned travel and visit to ICR was organized in September and a lecture at ICR was held on September 11, 2023. With the financial support from this project, the results obtained were also presented as lectures at Hokkaido University, Hiroshima University, and at conferences TACC2023 (the 5th Conference of Theory and Applications of Computational Chemistry), Sapporo, and The 26th Symposium on the Society of Iodine Science, Chiba University.

Combining Tellurium Mediated Radical Polymerization and Multicomponent Polymerization towards Unique Stimuli Responsive polypeptoids/poly(N-vinyl amide)s Copolymers

Antoine Debuigne University of Liege

Objectives

This ICR project aims to develop novel stimuli-responsive and biocompatible block copolymers, incorporating segments of polypeptoid and poly(N-vinyl amide) of interest for biomedical applications. Their synthesis relies on a combination of the Tellurium-Mediated Radical Polymerization (TERP) of N-vinyl amides, pioneered by S. Yamago in Kyoto, and the Ugi-4CR multicomponent polymerization (MCR) of amino acids, developed by A. Debuigne in Liege.

Experimental methods

Synthesis of PNVP-*b*-polypeptoid copolymer by Ugi-4CR. Glycylglycine (44 mg, 0.33 mmol) and PNVP-CO_2H (3800 g/mol, 126 mg, 0.033 mmol) were dissolved in 1.0 mL of water. Formaldehyde (0.363 mmol, 29.5 µL of formaldehyde 37 wt% in water) was added to the stirred solution at room temperature followed by addition of *t*-butyl isocyanide (1.3 eq, 0.43 mmol, 0.0357 g, 49 µL). The solution was stirred at r.t. for 72 h before lyophilization. The polymer was analyzed by ^{1}H NMR and size exclusion chromatography (SEC).

Results and discussion

Preliminary attempts focused on the synthesis of block copolymers composed of a hydrophilic poly(N-vinyl pyrrolidone) (PNVP) and a thermo-responsive and biocompatible poly(peptoid-alt-peptide) (Figure 1).

Figure 1. Synthesis of PNVP-b-poly(peptoid-alt-peptide) by combination of TERP and Ugi4-MCR.

First, an acid-terminated PNVP ($M_{n\ NMR}$ = 3800 g/mol) was synthesized by TERP in bulk at 60 °C using 2-methyl-2-(methyltellanyl)propanoic acid as chain transfer agent followed by removal of the terminal tellurium moieties upon benzenethiol treatment. Inspired by a previous report (Chem. Commun. 2017, 53, 12240), the Ugi-4 MCP of the dipeptide glygly was then performed at r.t. for 72 h in water using 1.1 eq. of formaldehyde and 1.3 eq of tert-butylisocyanide in the presence of 0.1 eq of the PNVP-CO_2H. The acid function of the latter was expected to be involved in Ugi-4 reaction with the amino group of glygly leading to the anchoring of PNVP at the extremity of the poly(peptoid-alt-peptide) and the formation of the corresponding block copolymer (Figure 1). The ^{1}H NMR spectrum confirmed the formation of the poly(peptoid-alt-peptide) but SEC analysis revealed partial formation of the desired block copolymer contaminated by non-functionalized poly(peptoid-alt-peptide). At this stage, dynamic light scattering analyses did not reveal any thermoresponsive behavior of the polymer in water.

Outcomes and perspectives

The limited functionalization of the poly(peptoid-alt-peptide) chains by PNVP may originate from a diminished reactivity of PNVP-CO_2H acid function due to steric hindrance, likely caused by the too high molar mass of the PNVP chain, or from the presence of two methyl groups in the terminal acid moiety. To address this issue, new PNVP-acid derivatives with lower molar mass (1500-2000 g/mol) and primary acid functionality are currently being prepared in Kyoto and will be tested in Ugi-4 MCP in Liege.

Acknowledgment. This work was supported by the Collaborative Research Program of Institute for Chemical Research, Kyoto University (ICR 2023-49)

Development of functional molecule for efficient perovskite solar cells

Akinori Saeki　Osaka University

Surface passivation is key to the power conversion efficiency (PCE) of organic–inorganic lead halide perovskite solar cells (PSCs). Herein, we report a novel molecular concept of a C2-symmetric *syn*-type bifacial donor–π–donor (D–π–D) passivation molecule (a racemic mixture of enantiomers) with hydrophobic phenyls and hydrophilic tetraethylene glycol-substituted phenyls on each face of the indeno-[1,2-*b*]fluorene π-core (**Fig. 1**).[1] In addition to this bifacial amphiphilic π-core unit, triphenylamine, a well-established passivation donor, effectively passivated the PSC surface, facilitated hole transfer, and increased the maximum PCE from 18.43 to 19.74%. Another notable effect is the removal of remnant PbI_2 and the change in the perovskite orientation on the surface by the *syn*-type molecule. In contrast, the anti-type isomer degraded its long-term stability. We characterized the electrostatic and electronic properties of these molecules and highlighted the advantage of molecular strategy based on a bifacial structure and its stereochemistry.

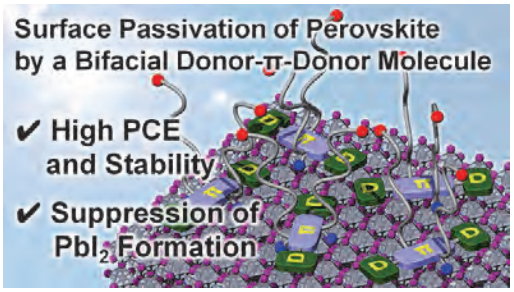

Fig. 1. Novel D-π-D molecule for passivating the surface of Pb PSC.

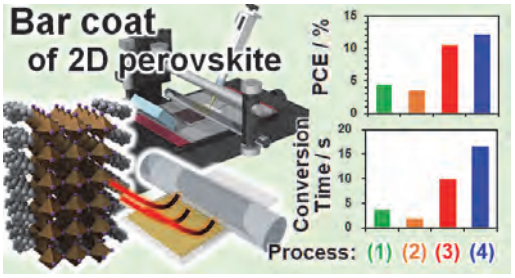

Fig. 2. Bar-coating of 2D-PSC and its correlation among PCE, anisotropic photoconductivity, and conversion time.

Understanding the effects of process variables on the large-area manufacturing of PSCs is crucial for their commercialization. In this study, we conducted a comparative analysis of four bar (blade) coating methods, along with thermal annealing or hot airflow, for two-dimensional (2D) Ruddlesden–Popper PSCs in the presence of ammonium chloride (NH_4Cl) and potassium chloride (KCl) additives (**Fig. 2**).[2] Intriguingly, the anisotropic charge carrier mobilities evaluated via time-resolved microwave conductivity exhibited a linear correlation between anisotropy and power conversion efficiency (PCE), similar to the observations in spin-coated 2D PSCs. The best PCE of 12.15% was achieved using the process involving a hot air flow after bar coating. Notably, there was a significant variation in PCE (3–12%) among the four methods, which strongly correlated with their conversion time, suggesting that slow film formation is key to achieving optimal performance. Our findings, combined with the evaluation of crystallite orientation using 2D grazing-incidence X-ray diffraction, provide a foundation for exploring large-scale 2D PSC production.

[1] N. Minoi, F. Ishiwari, K. Murotani, R. Nishikubo, T. Fukushima, A. Saeki, *ACS Appl. Mater. Interfaces* **2023**, *15*, 6708.
[2] R. Shimono, R. Nishikubo, M. Pylnev, F. Ishiwari, A. Wakamiya, A. Saeki, *ACS Appl. Energy Mater.* **2023**, *6*, 9381.

ポルフィリン二量体分子触媒の構造反応性相関に関する研究

太田雄大　山口東京理科大学

目的

各種金属ポルフィリン二量体を合成し，電気化学的な条件下で小分子（酸素，水，二酸化炭素など）活性化の反応性を検討する．X 線結晶構造解析，分光学的解析および量子化学計算を行い，分子構造と反応性の相関を明らかにする．

実験方法

ポルフィリン二量体を有機合成し，各種金属（Fe，Ni，Cu，Zn，Ru，Rh）塩により金属の挿入反応を行った。酸素還元，水の酸化，および CO_2 還元等について電解反応性を調べた．

結果と考察

X 線結晶構造解析により各種金属錯体の分子構造を決定した（図 1）．Fe ポルフィリン二量体の酸素還元反応の研究では，単量体と比べて過電圧の抑制と酸素の四電子還元選択性の向上が見られた．また，電解において分極を正側にすると水の酸化も触媒することを見出した．また，Zn ポルフィリン二量体による CO_2 還元反応ではファラデー効率 90%で CO が生成することを見出し，単量体と比べて過電圧および反応速度において優れた反応性を示すことを明らかにした．またスーパーコンピュータを利用して量子化学計算で各反応段階の熱力学的諸量の解析を行い，還元電位および pK_a を計算して反応機構について考察した．Ru ポルフィリン二量体の研究では水の酸化反応を低過電圧で触媒することを見出した。また Rh ポルフィリン二量体はグルコースの電解酸化において単量体より優れた反応性を示すことを見出し，燃料電池やセンサーへの応用に重要な知見を得た．今後これら新規なポルフィリン二量体の構造解析を行い反応性についてさらに詳しく検討する．

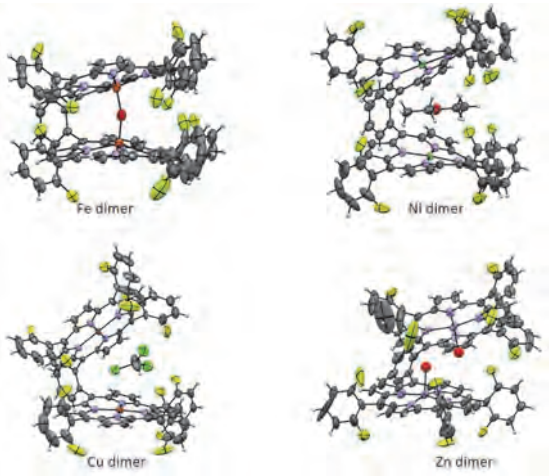

図 1 各種金属(Fe, Ni, Cu, Zn)ポルフィリン二量体の結晶構造

学会発表

1. T. Ohta, M. Mitori, T. Takeyama, M. Wakioka, T. Higaki, R. E. Cramer, Y. Ohki, “Electrocatalytic CO_2 Reduction with Cofacial Porphyrin Dimers”, 6th Symposium on Advanced Biological Inorganic Chemistry (Kolkata, India), January 2024 (Invited talk).
2. 竹山知志, 檜垣達也, 大木靖弘, 太田雄大, パックマン型ポルフィリン配位子を有する二核銅錯体による CO_2還元反応, 日本化学会中国四国大会山口大会 (山口大学, 宇部市), 講演番号: 1PA-27, 2023年11月
3. 調大輔, 竹山知志, 檜垣達也, 大木靖弘, 太田雄大, 鉄ポルフィリン二量体による酸素還元反応, 日本化学会中国四国大会山口大会 (山口大学, 宇部市), 講演番号: 1PB-27, 2023年11月

ホウ素の特性を活かした自己集合性アズレン類の合成ならびに反応・機能開拓

若林成知　鈴鹿医療科学大学

【緒言】　我々はボリルピリジンにおける分子間ホウ素－窒素配位結合に着目した分子設計により、幾つかの自己集合を達成し、超分子構築におけるユニット分子としての有用性を明らかにしてきた。例えば、アズレン共役系を組み込んだ化合物 **1** は、環状 3 量体を形成する。当合成の最終段階である、対応する臭素体における臭素／リチウム交換と続くホウ素化剤との反応は、バッチ型反応器では低収率であったが、フローマイクロリアクターを用いることによって、69%の収率まで向上した。本研究では、化学研究所の大木靖弘教授と共同し、アズレン誘導体合成におけるフローマイクロ法の有用性を、6－ブロモアズレン(**2**) を用い検討するとともに、**1** のソルバトクロミズムおよび 4－ジメチルアミノピリジン（DMAP）添加に伴う色調変化を検討した。

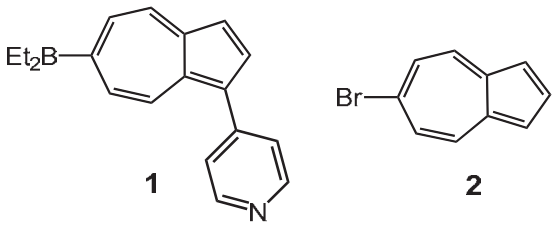

【結果と考察】　フローマイクロ法で、種々の温度（－78～0 °C）と滞留時間（0.056～3.16 秒）で、**2** に *n*-BuLi、次いでベンズアルデヒドを反応させ、生成物の収率を検討したところ、－40 °C、0.22 秒で目的のアルコール体が最高収率 76%で得られることが分かった。同反応をバッチ法で行うと、収率は－78 °C で 33%、0～－60 °C では 6～9%に過ぎなかった。フローマイクロ法では、求電子剤としてベンズアルデヒドのほか、クロロトリメチルシラン、塩化トリブチルすず、イソプロピルピナコールボレートを用いた場合にも、反応は良好な収率で進行した。従って、6 位置換アズレン誘導体合成において、フローマイクロ法は有用であることが示唆される。

化合物 **1** はクロロホルム中、532 nm に吸収極大を示し赤色を呈する。THF、ピリジン、クロロホルム/エタノール（1:1）中、吸収スペクトルの変化はなく、ソルバトクロミズムは観測されなかった。しかし、**1** のクロロホルム溶液に、DMAP のクロロホルム濃厚溶液を加えると吸収は 549 nm まで長波長シフトし、587 nm には等吸収点が観測された（**Figure 1**）。得られた生成物の NMR、ESIMS スペクトルから、**1** と DMAP との 1:1 錯体が形成されたものと考えられる。現在、色調変化の過程を詳細に検討中である。

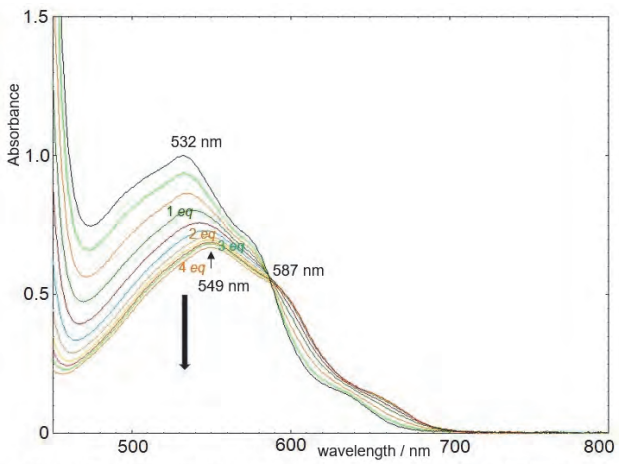

Figure 1. Spectral changes of **1** upon the addition of DMAP.

【成果報告】若林成知，宅見正浩，大木靖弘，永木愛一郎，第33回基礎有機化学討論会，岡山，1P009，2023.9.

電気化学的・光化学的手法を用いた分解型有機合成

稲木信介　東京工業大学

【背景】近年、有機合成に有用なアルキルラジカルの生成法として、可視光照射を用いて反応性基質を直接励起する方法が注目されている。2,2′-(Pyridine-2,6-diyl)diphenol （PDP）とボロン酸やトリフルオロホウ酸塩を反応させると、ホウ素アート錯体が形成される。共同研究者である大宮は、この PDP ホウ素アート錯体に青色光を照射することによって、炭素–ホウ素結合が開裂し、アルキルラジカルが生成する（下図）。このように、PDP ホウ素アート錯体は有用なラジカル前駆体である一方で、錯体形成後の精製が煩雑である点や、アルキルラジカル生成後に PDP 骨格を有する副生成物が生じるなどの課題がある。本研究では、上記の課題を解決するために、PDP ホウ素アート錯体の高分子化を目的とした。これにより、各工程における単離や精製操作が簡略化されるとともに、よりサステイナブルなアルキルラジカル源としての利用できる。

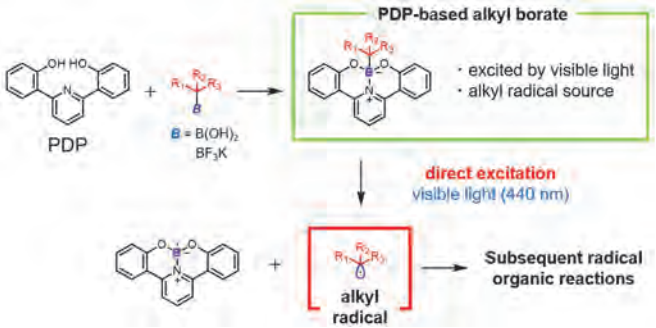

【実験・結果・考察】ビニル PDP（**1**）とスチレンを 1:9 の割合でラジカル共重合し、得られた **2** の脱メチル化反応を行うことによって、PolyPDP（**3**）を合成した（下図）。次に、**3** とフェニルエチルボロン酸との反応を試みたところ、80%の導入率でホウ素錯体の形成に成功した。合成した Poly(PDP borate)（**4**）は再沈殿操作によって容易に精製が可能であった。さらに、ラジカル捕捉剤である TEMPO 存在下、**4** の光照射分解反応を行った。**4** のジクロロメタン溶液に 440 nm の青色光を照射したところ、48%収率でフェニルエチルラジカル–TEMPO 付加体（**6**）が得られた。可視光照射によるホウ素–炭素結合開裂が効率的に進行し、アルキルラジカルが生成したことが示唆される。光照射反応後の高分子 **5** は再沈殿操作により回収可能であり、続く酸処理によって PolyPDP（**3**）へと再生できると考えられる。

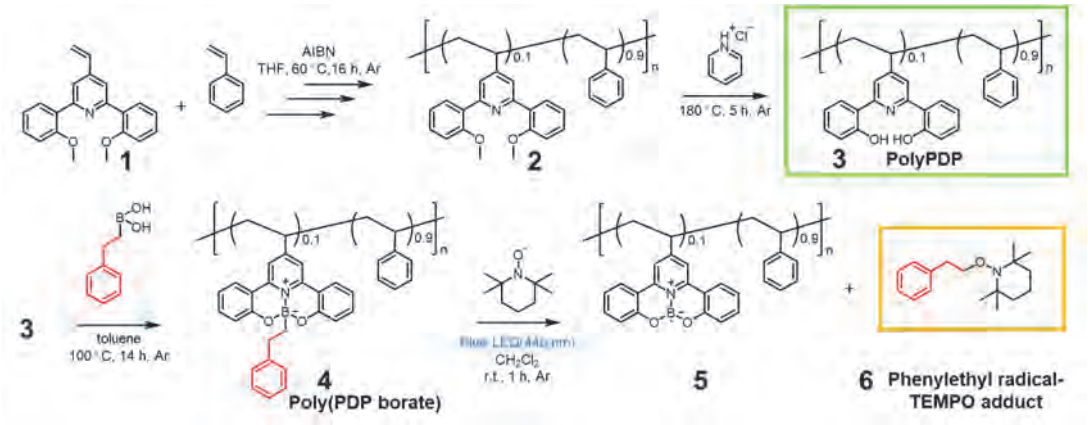

Light-driven Organosulfur Catalysis for Sugar Modification

Go Hirai Kyushu University

C-Glycoside analogues are known to possess numerous biological activities and are structurally diverse. C-Glycosylation using glycosyl donors as the precursors of anomeric radical is useful approach for the construction of C-glycoside analogues and has been actively studied in recent years. Several groups have developed C-glycosylation using unprotected C1-sp^3 glycosyl donors as an anomeric radical precursor. Specifically, Shoda reported the Giese type C-glycosylation of glycosyl xanthates without protecting groups through the anomeric radical formation using 2,2'-azobis(isobutyronirtile). Niu and Koh independently reported the Ni-catalyzed cross-coupling reaction of non-protected glycosyl donors with aryl halide. Our group and Niu independently developed Giese radical addition using protecting-group-free glycosyl sulfinates and Michael acceptors.

Earlier, Ohmiya group developed directly photo-excitable borates generating alkyl radical under visible light irradiation. These borates can work as alkyl radical source concomitantly with a strong single-electron reductant ($E_{1/2}$ = ca. –2.0 V vs. SCE in MeCN) under visible light irradiation that can be easily oxidized under mild reaction conditions. In particular, 2,2′-(pyridine-2,6-diyl)diphenol (PDP)-based borate provided higher functional tolerance and chemical stability. Based on this knowledge, we designed and synthesized that PDP-type glycosyl borate generating unprotected anomeric radical under visible light irradiation. The glycosyl borate can be available from the corresponding trifluoroborate in simple operation. The borate applied to Giese radical addition without photoredox catalysts or any additives, enabling the introduction of Csp^3 fragment at an anomeric position with α-isomer selectivity.

We selected 2,2'-(4-(trifluoromethyl)pyridine-2,6-diyl)-diphenol (**PDP$_{CF3}$**) as the tridentate ligand. After optimizing the reaction conditions, we succussed synthesizing PDP-type glycosyl borate **2** from benzyl-protected glycosyl trifluoroborates **1**. The borate **2** could be given in good yield using **PDP$_{CF3}$**, silicon dioxide (SiO_2) and triethylamine (NEt_3) in toluene (right). This transformation of **2** to unprotected glycosyl borate **3** was achieved by using palladium hydroxide on carbon under H_2 gas atmosphere.

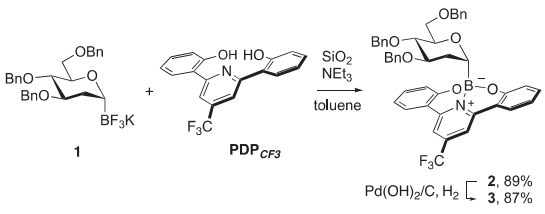

We attempted to apply unprotected glycosyl borate to photo-mediated Giese addition reaction (right). The reactions of glycosyl borates **3** with benzyl acrylates or *tert*-butyl acrylates in an MeCN/methanol mixed solvent under blue LED irradiation (440 nm) provided the C-glycoside products with complete α-selectivity (**5a**, **b**). Similarly, acrylonitrile was also applicable (**5c**).

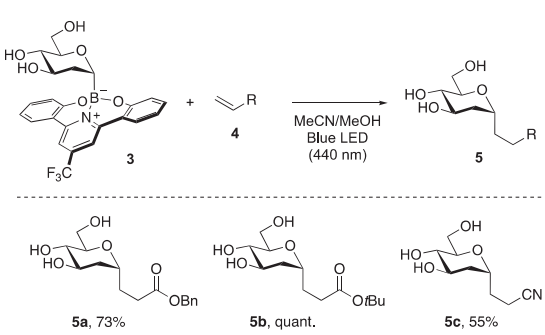

Controlling of Secondary Structure in Polysiloxane Main Chain and Application for Chiral Silica

Tomoyasu Hirai Osaka Institute of Technology

Chiral silica is focused on various kinds of fields such as template, catalysis, and separation materials. So far, chiral silica is prepared using sol-gel reaction using tetraethoxysilane in the presence of surfactants. As chiral silica thus obtained possess quite large nanocavity, functional molecules cannot selectively accommodate in it. Recently, we have reported preparation of polymethacrylate-functionalized polyhedral oligomeric silsesquioxane with well-controlled stereoregularity (*it*-PMAPOSS). The polymer formed preferred-handed helical conformation when small amount chiral dopants were mixed with *it*-PMAPOSS and the helical conformation was kept during calcination process, leading to a chiral silica with helical structure. Here, we report encapsulation behavior of functional molecules into a chiral silica prepared from *it*-PMAPOSS.

Chiral silica is prepared same method as previous report. Achiral pyranine is known to exhibit specific fluorescence emissions depending on its acid dissociation state and was selected as the achiral PL molecule. Pyranine was dissolved in MeOH and H_2O to obtain 0.5 wt% clear solutions, and the chiral silica was immersed in these solutions for 2 d at room temperature. The chiral silica immersed in the pyranine/MeOH and pyranine/H_2O solutions exhibited blue and green emissions, respectively, upon UV irradiation at 340 nm (Figure 1a). CPL measurements were performed to evaluate the effect of the solvent on the iCPL. Figure 1b shows the CPL spectra of the enantiomeric chiral silica in pyranine/MeOH and pyranine/H_2O solutions. Symmetrical mirror-imaged CPL emission spectra were obtained for the enantiomeric chiral silica/pyranine in MeOH and H_2O. This suggested that the achiral luminophores were placed along the helically structured chiral silica, leading to an iCPL in the excited state. The chiral silica immersed in the pyranine/H_2O solution exhibited a green CPL emission at 520 nm, whereas that in the pyranine/MeOH solution exhibited a blue CPL emission at 436 nm. This indicates that chiral silica acted as a nano-sized fused quartz cell to encapsulate functional materials and solvents along the helical nanocavities.

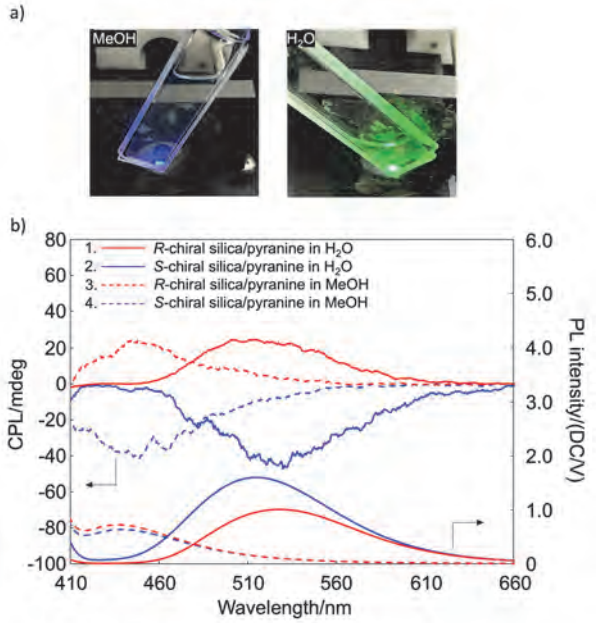

Figure 1. a) Photographs of chiral silica/pyranine in MeOH (left) and H_2O (right) upon UV irradiation at 340 nm, and b) CPL and corresponding PL spectra of chiral silica associated with pyranine under excitation at 340 nm.

Reference

Hirai et al., *JACS Au*, **2023**, *3*, 2698.

カルバゾロファンを側鎖に持つポリマーの合成とホール輸送及び CPL 材料への応用

谷敬太　大阪教育大学

【目的】カルバゾール発色団は、そのポリマー体であるポリ（*N*-ビニルカルバゾール）(PVK)がホール輸送剤として注目を浴びてきた。しかしながら PVK 中でホール移動を担うカチオンラジカルの問題点として、モノマーとダイマーのカチオンラジカル部位が共存するために、ダイマー部位がホール移動のトラップサイトとして作用することが指摘されてきた。この問題の解決策として本研究ではダイマー部位のみが存在するカルバゾロファンを側鎖に持つポリマーを合成する。円偏光発光（CPL）は多くの場合、不斉を持つ化合物からの発光である。[3.4]系の部分重なり型カルバゾロファンは面不斉を持つのでそのポリマー体の合成は新規な CPL 材料の開発にも繋がる。

【実験と実験結果】

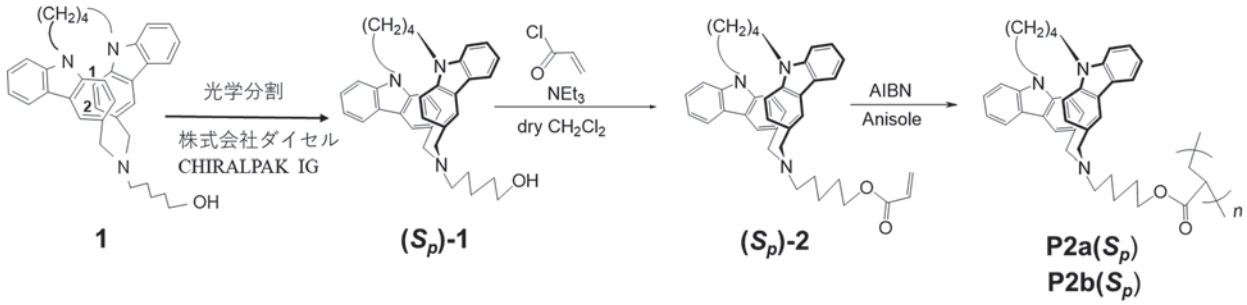

光学分割して得られた**(*S*p)-1** に NEt_3 存在下で塩化アクリロイルを反応させ単量体**(*S*p)-2** を得た。単量体濃度 10wt%のアニソール溶液中に、AIBN(開始剤濃度 3mol%)を加え、脱気封管後、24 時間、60℃で反応させたところ、良好な転化率(83％)でラジカル重合が進行した。反応後、反応溶液に貧溶媒であるヘキサンを加えて固体を析出させ、さらに THF で洗浄して THF 可溶部ポリマー**P2a(*S*p)** と THF 不溶部ポリマー**P2b(*S*p)**を得た。GPC (0.5wt%NEt_3-$CHCl_3$ 混合溶液、検量線 PMMA) より、精製ポリマー**P2a(*S*p)**と**P2b(*S*p)**の数平均分子量は、それぞれ 5000 と 11000 であることが分かった。

【考察】**P2a(*S*p)**と**P2b(*S*p)**の ^{1}H NMR スペクトルからカルバゾロファンポリマーであることはわかったが、CD スペクトルで吸収が現れなかった。ポリマーの VT-NMR から 60℃ではラセミ化が進行したと考えられるので、ラセミ体の **2** を用いてより温和な条件（30℃、40℃、50℃）でのラジカル重合を検討した。その結果、最も低い 30℃でもラジカル重合が進行することがわかったので今後、この温度で**(*S*p)-2** を重合し、キラルなポリマーへと導く予定である。

【成果報告：学会発表】

[1] 城・千原・黄瀬・辻井・前野・田中・梶・谷ら　重合基を有するカルバゾロファン誘導体の合成とそのラジカル重合、第 33 回基礎有機化学討論会、2P063
[2] 城・千原・黄瀬・辻井・前野・田中・梶・谷ら　光学活性なアクリルエステル部位を有する[3.4](3,9)系カルバゾロファン誘導体の合成とそのラジカル重合、第 72 回高分子討論会、1Pd012
[3] 城・正木・黄瀬・辻井・前野・田中・梶・今井・谷ら　光学活性な[3.4](3,9)系カルバゾロファン誘導体の合成とそのラジカル重合　日本化学会第 104 春季年会、E1113-1pm-05

Elucidation of design principles of covalent organic solid solutions

Mitsuharu Suzuki Osaka University

Objective

An important goal in chemistry is the adept linking of different molecular units to create sophisticated functional materials. We are currently engaged in studies aimed at constructing multicomponent covalent organic frameworks (COFs), considering the effectiveness of their high structural order and design flexibility toward achieving this goal. Within this exploration, we recently discovered that some multicomponent COFs allow for structural adjustments akin to solid solutions. In other words, it was found that their compositions and lattice constants can be continuously tuned without significantly compromising crystallinity. The objective of this research is to systematically investigate the design and synthesis of such "covalent organic solid solutions", aiming to gain insights for the development of intricate functional materials. In this fiscal year, the focus has been on distinguishing reaction scenarios of condensation reactions among two types of nodes and one type of linker to form, in ideal cases, imine-linked ternary 2D COFs.

Results and discussion

TAPB and TAPT were chosen as the node monomers and connected through either DMTA or DHTA, linkers with distinct hydrogen-bonding modes and thus varying linking strengths (Fig.1). Despite their similar lateral dimensions, TAPB and TAPT are significantly different in conformation; TAPB is expected to be nonplanar, while TAPT favors to be planar in the solid state. Consequently, homo-stacking (TAPB/TAPB or TAPT/TAPT) is thermodynamically more stable than hetero-stacking (TAPB/TAPT). The central question addressed in this study is: *To what extent is the homo-stacking dominant over the hetero-stacking*? Our systematic screening of different monomer combinations and ratios strongly suggests the frequent occurrence of the hetero-stacking in the ternary 2D COFs (Fig. 1). The prevalent formation of the thermodynamically less favored hetero-stacking leads to two conclusions; (1) a highly random distribution of the two types of node monomers, providing further support of frequent formation of COFs having solid-solution-like structures; and (2) the substantial challenge of combining planar and nonplanar monomers in 2D COFs. Indeed, the ternary COFs are consistently obtained only with DHTA, the stronger linker, but DMTA.

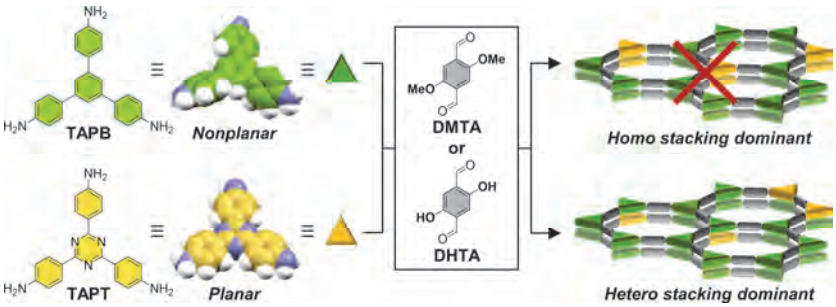

Fig. 1. Chemical structures of the COF monomers employed in this study, and schematic drawing of the expected structures of 2D COFs.

Outputs

(1) Edamitsu, M. et al. The 13th CSJ Chemistry Festa, P8-100, October 2023. (2) Edamitsu, M. et al. The 31st Symposium on Organic Crystals, P-38, November 2023.

発光性基底三重項ジラジカルの合成と物性

清水章弘　大阪大学

基底三重項のジラジカルは、不対電子の向きが揃うため、有機磁性材料として有望である。近年の様々な合成手法の開発や不安定化学種を取り扱う装置の普及に伴い、いくつかのジラジカルが合成・単離され、電子状態や基礎的性質が解明されている。しかし、不安定であるために取り扱いは難しく、機能性材料としての応用研究は進んでいない。したがって、空気中でも安定な基底三重項ジラジカルの創出が求められている。

我々は最近、トリアンギュレン誘導体 **1** の中央の炭素原子を窒素カチオンに置き換えた、窒素ドープトリアンギュレンカチオン **2a** を設計・合成し、**2a** が空気中でも取り扱えるほど安定な基底三重項ジラジカルであり、近赤外発光を示すことを見出している。本研究では **2a** の安定性に対する置換基の効果を解明するために、*tert*-ブチル基のない **2b** を設計し、その合成と安定性の評価、基礎物性の解明に取り組んだ。

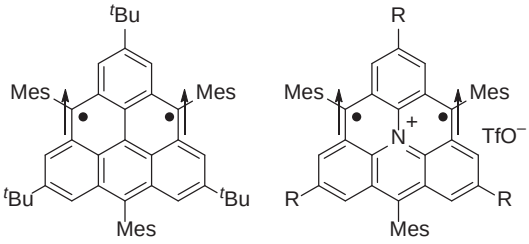

1　　**2a**: R = ^{t}Bu, **2b**: R = H

2b は市販品から 5 段階で合成した。X 線結晶構造解析は行えていないが、ESR スペクトル (Figure 1) などにより、その構造を同定し、**2a** と同様に不対電子が分子全体に広く非局在化していることを明らかにした。また、空気中での安定性を明らかにするために、UV スペクトルの時間経過を測定したところ (Figure 2)、24 時間後でもスペクトルの形状がほとんど変化せず、*tert*-ブチル基がなくても高い安定性を有することを明らかにした。また、近赤外発光 (850 nm) を示すことを明らかにした。

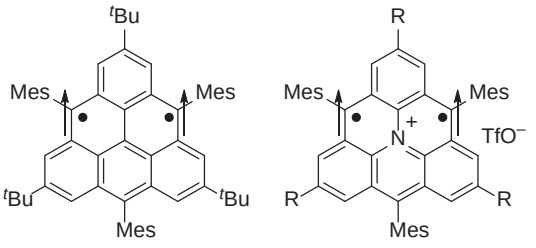

1　　**2a**: R = ^{t}Bu, **2b**: R = H

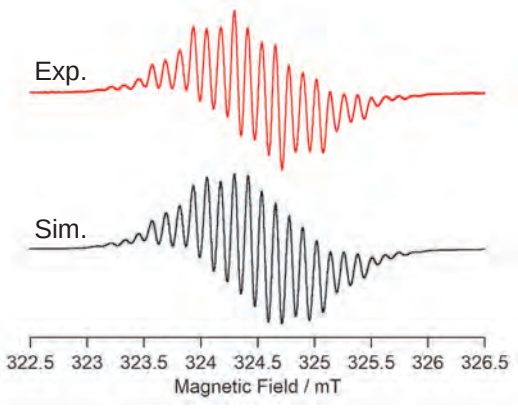

Figure 1. 2b の ESR スペクトル

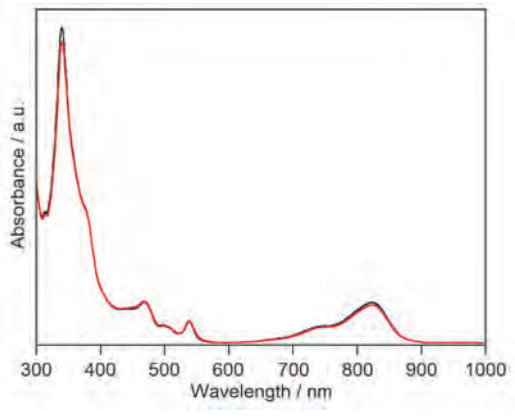

Figure 2. 2b の UV スペクトル

Reference

1) Arikawa, S.; Shimizu, A.; Shiomi, D.; Sato, K.; Takui, T.; Sotome, H.; Miyasaka, H.; Murai, M.; Yamaguchi, S.; Shintani, R. *Angew. Chem. Int. Ed.* **2023**, *62*, e202302714.

フロー反応装置による官能性ビニルテルリド合成を鍵とする重合反応の開発

永木愛一郎　北海道大学

共同研究者である化学研究所の山子教授のグループは、湾曲したπ共役系を有する環状分子であるシクロパラフェニレンの合成において、白金錯体などの遷移金属錯体を用いる全く新しい方法を世界に先駆けて開発した。しかし、選択的合成の鍵となる環化前駆体の環構造制御過程の解明は未だ途上であり、副生成物としていくつかの異なる環サイズを有する環化前駆体の形成が示唆されている。この過程では、速度論的な環形成に続く熱力学的な環組み換えにより、望まない環状中間体が生成すると考えられる。ゆえに最初に生成した環化生成物が続けて分子間で反応しない条件で反応できれば望みの生成物の収率をあげることが可能になる。

本研究では、フロー反応を用いることで、この条件を満たすことができる可能性に着目した。すなわち、①遷移金属錯体によりフロー中でカップリング素子を形成し、②基質の濃度と反応時間の精密制御を行うことで、環構造形成のためのカップリング制御を達成できると期待される。本研究では、申請者のフロー合成技術と共同研究者が有する高度なマクロ分子合成技術、ならびに化学研究所の先端分析機器を相乗的に活用することにより目的を達成可能になると考え、研究を行ってきた。

結果として、熱的に不安定なジアリールクプラート中間体を含むさまざまなアリールクプラートの酸化的カップリングにより，立体障害の大きなビアリールを選択的に合成する手法の開発を達成した。中間体のクプラートは熱的に極めて不安定であり，通常のバッチ反応条件での制御は困難である。また、クプラートの発生にはしばしば有機リチウム種を用いる必要があり、官能基化されたクプラートの発生は困難である。そこで申請者が得意とするフローマイクロリアクターを用いた反応の精密制御によって反応条件をコントロールすることで、立体障害の大きいビアリールの生成を確認した。今後の研究においてさらなるフロー条件の検討で高選択性や基質適用範囲の拡大を目的として研究を行う予定である。

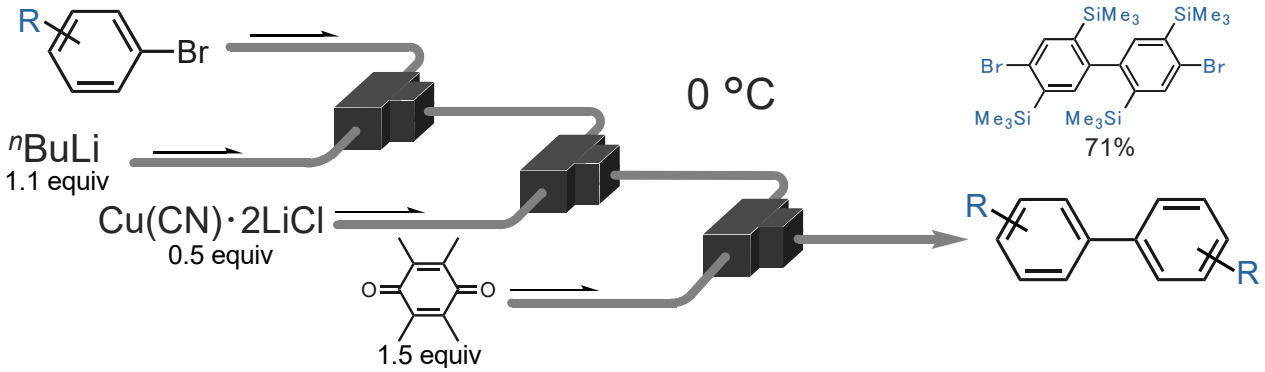

大環状共役系における電子の非局在性の荷電・スピン・励起状態依存性の研究

岸亮平　大阪大学

【目的】電子の運動状態、局在性や非局在性を制御することは、物質の機能を探求する鍵である。化学研究所の共同研究者である茅原、山子らにより合成法の開発が進められている環状共役系である[1.1]および[2.2]パラシクロファン誘導体では、隣接する 2 つのベンゼン環のイプソ位炭素同士が空間的に接近する箇所がある。この場合、結合を介した Through-bond (TB)共役と、空間を介した Through-space (TS)共役とが共存する興味深い共役構造を有し、それに起因する新奇な物性や機能の発現が期待される。そのような TB/TS ハイブリッド型の共役系の電子の非局在性は、TB 共役系と TS 共役系の相互作用の強さのバランスにより決まる。そこで、TB 共役系、TS 共役系それぞれの相互作用の強さと、系全体の電子の非局在性の関係を理論的に明らかにすることを目的とした。

【理論、結果、考察】図 1 のように TB 共役系の分子が 2 箇所で TS 相互作用し、平行に積層したモデルを考える。積層分子数が $n = 2$ のときは、前述のパラシクロファンの中性状態のモデルに対応する。TB および TS 共役部分の共役の強さが、Hückel 分子軌道（HMO）法の結合積分に相当する量 β_{TB}, β_{TS} により表される場合、系全体への電子の非局在性や HOMO-LUMO ギャップ（$\Delta\varepsilon_{HL}$）はその比 β_{TB}/β_{TS} に応じて変化すると考えられる。しかし、β を具体的な TB 共役系の分子や積層距離において推算することは簡単ではない。そこで、容易に計算できるジラジカル因子 y を用いて、$\beta_{TB}/\beta_{TS} \sim (1-y_{TB})/(1-y_{TS})$と近似できると仮定し、系全体の $\Delta\varepsilon_{HL}$ が 0 となるための y_{TB} と y_{TS} の条件式を導出した。y_{TB} は TB 共役系の分子種により、y_{TS} は分子種と分子間の積層距離により決まるが、これは量子化学計算で容易に見積ることが出来る。条件式の妥当性を検証するため、前述のパラシクロファンの部分構造である *p*-quinodimethane など種々の TB 共役系の積層距離を変えたモデルを構築し、スピン射影(P)UHF レベルで y_{TB} と y_{TS}、ならびに系全体の y_{total} を計算した。$y_{total} = 1$（つまり $\Delta\varepsilon_{HL} \sim 0$）となる場合の y_{TB} と y_{TS} は、前述の条件式の直線付近にプロットされ（図 2）、導出した条件式は、$\Delta\varepsilon_{HL} \sim 0$ となる積層距離の予測に活用できることが示された。本研究に関する論文は現在投稿中であるが、共役の強さを y により評価する方法は、パラシクロファン系の電子の非局在性の解析[1]においても有効であると期待される。また、π 共役分子の集積系の電子酸化状態における電荷分布の非局在性の理論解析にも成功した[2]。

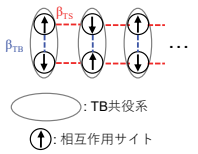

図 1. 計算モデル

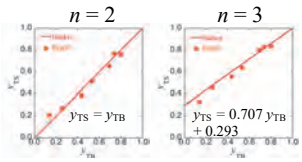

図 2. 計算結果

【成果報告】[1] 鳥越優河, 茅原栄一, 岸亮平, 山子茂, “[1.1]および[2.2]パラシクロファンのジカチオンにおける三次元芳香族性に関する理論化学的研究”, 日本化学会第 104 春季年会（発表予定）.

[2] W. Yoshida, Y. Shigeta, H. Matsui, H. Miyamoto, R. Kishi, Y. Kitagawa, *Bull. Chem. Soc. Jpn.*, 2024, DOI: 10.1093/bulcsj/uoae009.

マクロ環骨格内に導入したラジカルの化学：SOMO-HOMO エネルギー逆転

安倍学　広島大学

目的：ラジカルなどの開殻系化学種に関する研究は，化学反応の活性種としてのみならず，次世代のソフト磁性材料や量子メモリ材料として，活発に推進されている。不対電子が収まる SOMO 軌道は，通常，２電子が軌道に収まっている HOMO よりもエネルギー準位が高いが，HOMO よりもエネルギー準位が低くなる場合が数例報告されており，系統的に行われておらず，その化学は一般化されていない。その大きな理由は，SOMO-HOMO 逆転現象をもつ分子が偶発的に見いだされてきたことと，これまでの研究では，ニトロキシドなどのモノラジカルに限られていたためである。最近，安倍らは，量子化学計算によって，シクロパラフェニレン(CPP)骨格内に存在するラジカル(n**R**)，ニトロキシド(n**NO**)，カルベン(n**C**)，ジラジカル(n**DR**)が SOMO-HOMO 逆転現象を示すことを見出した(*OL*, 2021, 4955; *ACS Omega*, 2021, 22773; *AJC*, 2021, 827)。本研究では，それらのラジカルを実験的に発生し，その特異な電子状態から生まれる新奇な反応性と物性を探索・精査し，ラジカル化学に新たなブレイクスルーをもたらす研究に挑戦する。

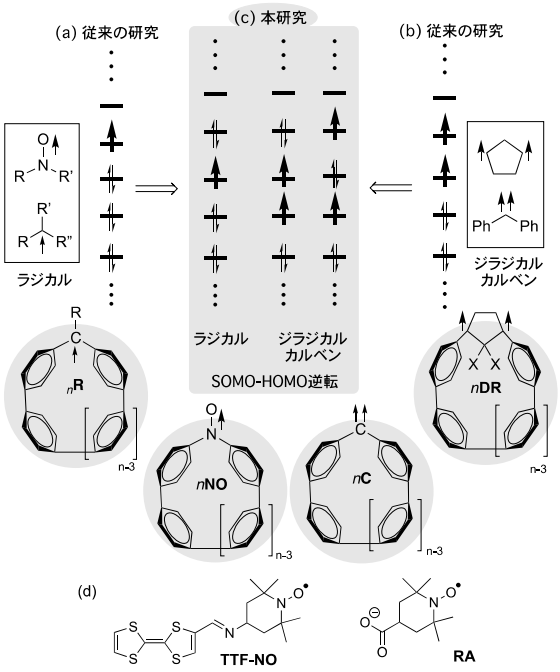

実験方法・実験結果・考察：CPP 骨格内にニトロキシルラジカルやカルベンを発生し，その化学特性を調査することを開始した。メタ位にアミノ基を有する CPP ニトロキシルやカルベンが，SOMO-HOMO 逆転現象を示すことが量子化学計算によって判明したため，対応する CPP アミンとケトンの合成を開始し，その合成に成功した。

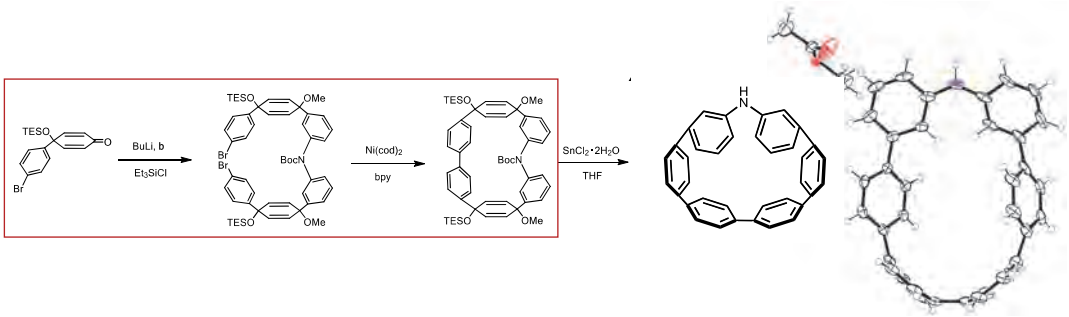

成果報告：SOMO-HOMO 逆転を有するニトロキシルラジカルの設計と合成，電子スピンサイエンス学会，2023 年 11 月 3–5 日，神戸大学；シクロパラフェニレン内カルベンの電子状態に関する研究日本化学会年会，2024 年 3 月 18–21 日

Synthesis and Functionally Development of Donor-Acceptor Cycloparaphenylene Derivatives through Reorganization of Macrocyclic Gold Complexes via Dynamic Gold-Carbon Bonds

Yoshitaka Tsuchido　Tokyo University of Science

[*n*]Cycloparaphenylenes ([*n*]CPPs, where *n* represents the number of phenylene groups), composed of 1,4-linked phenylene units, have garnered significant interest due to their distinctive π-conjugated structures and physical characteristics. Starting with the pioneering works in 2009-2010, [*n*]CPPs with various ring sizes and functional groups have been successfully synthesized. However, there are no examples of functionalization of all benzene rings of [*n*]CPPs with a small ring size, especially smaller than [7]CPP, due to the strong ring strain and the steric hindrance of the substituents that hampers their synthesis.

In this study, we have successfully synthesized a new [6]cycloparaphenylene derivative with twelve methoxy groups at the 2,5-positions of all benzene rings by utilizing our developed CPP synthesis method *via* a macrocyclic gold complex (Y. Tsuchido et al. *Angew. Chem. Int. Ed.* **2020**, 59, 22928). This molecule exhibited a significantly higher oxidation potential and guest inclusion ability due to the electron-donating ability of the methoxy groups and the tubular molecular conformation. Furthermore, we succeeded in synthesizing a [2]rotaxane from the inclusion complex composed of **1** and hexamethylene diisocyanate *via* the urea-forming reaction with adamantylmethylamine. Surprisingly, upon two-electron oxidation of the [2]rotaxane, the ^{1}H NMR signals of the methylene protons of the axle molecule shifted significantly to -14.5 ppm (Figure 1), which is due to the shielding effect by a diatropic ring current on the CPP macroring by the appearance of the in-plane aromaticity (S. Yamago et al. *J. Am. Chem. Soc.* **2015**, *137*, 82).

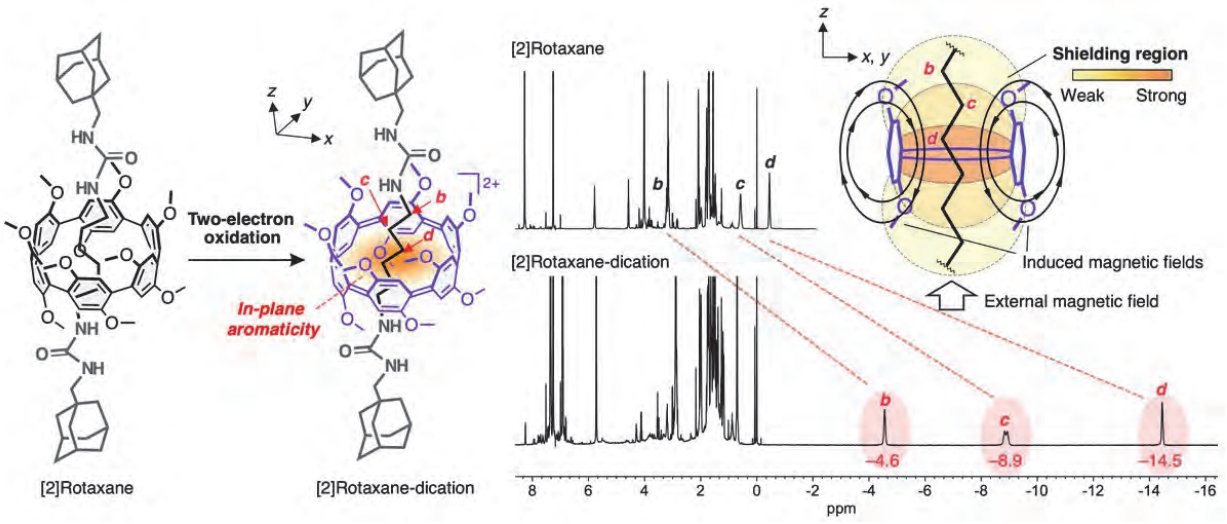

Figure 1. Chemical oxidation of [2]rotaxane. Right: ^{1}H NMR spectra (400 MHz, $CDCl_3$, r.t.) of [2]rotaxane before (top) and after (bottom) chemical oxidation upon addition of 2 equivalents of Magic Blue.

【成果報告】

N. Narita, Y. Kurita, K. Osakada, T. Ide, H. Kawai, Y. Tsuchido, *Nat. Commun.* **2023,** 14, 8091.

Trace metal elemental and isotopic composition in the North Pacific Ocean: sources and internal cycling (4)

Tung-Yuan Ho　Academia Sinica

Objectives:

The major objective of this extended joint study is to investigate the sources and internal cycling of dissolved and particulate trace metals in the water column of the Northwestern and subarctic Pacific Ocean and to evaluate the impacts of lithogenic and anthropogenic aerosols on the cycling processes. Prof. Yoshiki Sohrin is my host at ICR, Kyoto University.

Methods:

Through the Japanese GEOTRACES GP-02 subarctic Pacific Ocean transect study carried out in 2017 with Prof. Yoshiki Sohrin's and other Japanese research groups, we have collected seawater and particulate samples in the sampling sites during the cruise. Trace metal elemental and isotopic composition in both dissolved and suspended particulate samples were determined by my Ph.D. student (C.-C. Hsieh) by using HR-ICPMS and MC-ICPMS. The detailed information of the sampling and pretreatment procedures are described in two of our previous papers (Liao et al. 2020; 2021).

Result and Discussions:

Dr. Chih-Chiang Hsieh, currently a postdoctoral fellow in my laboratory, has finished the measurement of Fe isotopic composition in the GP-02 samples and has been preparing a manuscript (Hsieh et al. in prep). Moreover, Dr. Hsieh and my master student (Yi-Ning Ho) had visited Prof. Sohrin's laboratory in September 2023 for a month and finished all of the pretreatment and elemental analysis of the sediment trap samples of Japanese Time Series station in the Northwestern Pacific Ocean. These new results are under preparation for publication.

Publications:

Prof. Sohrin's and my laboratory members have kept close interaction in the research topics proposed. During the past three years, we have published three papers and the other two collaborative papers are under preparation.

Takano, S., W.-H. Liao, **T.-Y. Ho**, and **Y. Sohrin** (2022) Isotopic evolution of dissolved Ni, Cu, and Zn along the Kuroshio through the East China Sea. *Marine Chemistry* doi.org/10.1016/ j.marchem. 2022.104135.

Liao, W.-H., S. Takano, H.-A. Tian, H.-Y. Chen, **Y. Sohrin**, and **T.-Y. Ho** (2021) Zn elemental and isotopic features in the sinking particles of the South China Sea: the implications to its sources and sinks. *Geochimica et Cosmochimica Acta* doi: 10.1016/j.gca.2021.09.013.

Zheng, L., T. Minami, S. Takano, **T.-Y. Ho**, and **Y. Sohrin** (2021) Sectional distribution patterns of Cd, Ni, Zn, and Cu in the North Pacific Ocean: relationships to nutrients and importance of scavenging. *Global Biogeochemical Cycles* doi: 10.1029/2020GB006558.

Resolving the structure-dynamics-property relationship in polymer nanocomposites under uniaxial stretching-III

Tadanori Koga　Stony Brook University

Objective. Tires are a key component of the automotive supply chain, and as the only vehicle part that touches the road, they contribute significantly to vehicle safety and fuel efficiency. The overarching goal of this proposal is to advance the molecular understanding of a strain-induced softening phenomenon (i.e., the Payne effect) in filler-reinforced elastomers that affects the rolling resistance, grip, and durability of automotive tires. We use in-operando X-ray photon correlation spectroscopy (XPCS) under uniaxial stretching to understand the structural dynamics of the filler network under deformation.

Experimental. The so-called *speckle echo* XPCS technique under oscillatory deformation allows us to capture the irreversible nanoscopic rearrangements of fillers associated with yielding of a material[1]. A crosslinked silica (SiO_2, the diameter of 17 nm)/polybutadiene (PB, M_w=350 kg/mol) sample was used. Sulfur (1.6 wt%), vulcanization agents (stearic acids, N-t-butyl-2-benzothiazole sulfonamide (1.0 wt%), biphenyl guanidine (1.0 wt%), and a silane coupling agent (SI69, 16 parts per hundred rubber) were also compounded together by using a Banbury mixer. The filler concentration was 30% by volume, which is above the percolation threshold (~14%). About 1-mm thick sheet of the sample was mounted between two clamps of a tensile stage. When the structure and corresponding dynamics of fillers change ("out-of-equilibrium") on the time scale of the experiments, a one-time correlation function (g_2), which describes the equilibrium dynamics of fillers, does not correctly describe such a phenomenon. Therefore, a two-time correlation function $C(q, t_1, t_2)$ is required, which defines the intensity-intensity autocorrelation for any respective times t_1 and t_2 in the time series. The details of the XPCS analysis have been described elsewhere.[2]

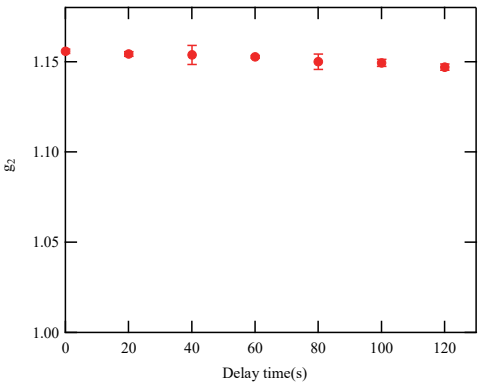

Fig.1. Echo-peak amplitudes for the crosslinked SiO_2/PB rubber (the filler loading of 30 %) at q = 0.037 nm^{-1} in the direction perpendicular to the strain as a function of delay cycle at 5 % strain. No decay was observed within the time window, indicating reversible (elastic) structural deformation during oscillatory deformation.

Results. We recorded speckle patterns and compared them at a given stretching amplitude and oscillation frequency from which g_2 was determined in the directions parallel and perpendicular to the stretching direction. g_2 shows periodic peaks corresponding to "echoes" in the speckle patterns. The change in stretching between extrema leads to gradients in the particle displacements that significantly alter the speckle pattern even for modest strain values. Thus, $g_2 \approx 1$ at $t = (n + 1/2)T$, where n is an integer (periods of oscillation), and T is a repeat time for the stretching (~ 15 s for the measurement). On the other hand, at $t = nT$, the strain returns, and the speckle pattern is recovered, causing g_2 to rise above one. If the deformation is linear and reversible, the echoes follow the static equilibrium dynamics. Instead, if the deformation is nonlinear, the peaks of the echoes are attenuated. This attenuation provides a measure of the "nanoscopic" irreversibility of the filler rearrangements. The dynamic storage and loss modules were measured under a strain sweep condition (at a frequency of 1 rad/s). The result showed that the critical strain magnitude for the linear-nonlinear deformation was 1%. The XPCS data for 5% strain at room temperature (Fig. 1) showed that a fresh cross-linked SiO_2/PB sample exhibits reversible structural deformation during oscillatory deformation in the stretching direction and in the direction perpendicular to the stretching at the scattering vector (q) < 0.03 nm^{-1} where mass-fractal structures were evident in the SAXS profile. This suggests that the origin of the observed strain-induced softening phenomenon is not due to a pervasive concept (i.e., rupture and rebirth of filler network structures), but the contribution of a rubbery matrix at the given strain. Further systematic experiments will provide material design insights for advanced automotive tires.

References

1. Rogers, M. C.; Chen, K.; Andrzejewski, L.; Narayanan, S.; Ramakrishnan, S.; Leheny, R. L.; Harden, J. L., Echoes in x-ray speckles track nanometer-scale plastic events in colloidal gels under shear, *Phys. Rev. E*, 90, 062310, 2014.

2. Yavitt, B. M.; Wiegart, L.; Salatto, D.; Huang, Z.; Endoh, M. K.; Poeller, S.; Petrash, S.; Koga, T., Structural dynamics in UV curable resins resolved by in situ 3D printing X-ray photon correlation spectroscopy, *ACS Appl. Polym. Mater.*, 2, 4096-4108, 2020.

High Frequency Response of Polymeric Liquids: Rheology and Dielectric Relaxation

Sathish K. Sukumaran　Yamagata University

Typically, experiments performed at a constant temperature (isothermal conditions) are used to investigate the response of polymeric liquids to applied fields. Interpretation of the experimental results relies on the assumption that the system temperature is not significantly affected by the applied field and remains uniform throughout the system. Under this widely used and often applicable assumption, isothermal response functions are appropriate for a quantitative description of the system. If, however, the experimental time scale is shorter than the thermal equilibration time scale, the aforementioned assumptions of constantcy and uniformity of the system temperature are likely invalid. An experimentally relevant case is investigations of (short time)/(high frequency) characteristics where adiabatic response functions might be more appropriate. To investigate this, the theoretical and experimental expertise of ICR (Sato), and the computational, theoretical and experimental expertise of international (Watanabe; Changchun) and domestic (Sathish; Yamagata) researchers were combined to form a collaboration between ICR and several international and domestic research partners.

The effect of isothermal and adiabatic conditions on the linear dynamics and viscoelasticity of polymer melts was investigated using computer simulations. The polymer chains were modelled as Lennard-Jones beads connected by finitely extensible nonlinear elastic springs and the motion of the beads were simulated using molecular dynamics. Isothermal conditions (NVT ensemble) were simulated using a Langevin thermostat. In the adiabatic simulations, the system was decoupled from the thermostat to prevent mutual energy exchange. Oscillatory shear deformation of sufficiently small amplitude (linear regime) was imposed at several frequencies and the storage modulus, G’, and the loss modulus, G’’, were determined. Negligible difference was found between the isothermal and the adiabatic G’ and G’’. This implied that, at least in the linear regime investigated here, the imposed conditions had negligible effect on the relaxation times or equivalently, the dynamics of the polymer chains. Under adiabatic conditions however, the system temperature progressively increased with time and the temperature increase under high frequency oscillatory shear deformation was significantly larger than under low frequencies. Needless to add, the increase in temperature under adiabatic conditions cannot be sustained indefinitely without affecting both the state of the system and its response to the external field. We are currently investigating the response when shear deformation (oscillatory and step) is applied for longer times. Based on these results, we plan to investigate the more more difficult nonlinear response regime in the future.

Ultrafast Exciton Dynamics in Thermally Activated Delayed Fluorescence Molecular Aggregates with Heterogeneous Conformational Distribution

Hikaru Saotome Osaka University

Excitons play an essential role in photo-energy conversion and their spatiotemporal diffusion is a key factor for dominating the fundamental performance of optoelectronic devices. Especially in amorphous solids such as organic photovoltaic and light emitting materials, excitons propagate in ten nanoscale heterogenous environments. One of the origins of the heterogeneity is broad distributions of intra- and intermolecular structures therein, which makes the exciton diffusion dynamics more complicated than at the molecular level. In the present work, to reveal an impact of the conformational heterogeneity on the photophysics of MA-TA (Figure 1a), which is a blue emissive thermally activated delayed fluorescence molecule, we investigated the exciton diffusion dynamics in MA-TA aggregates using time-resolved fluorescence spectroscopy and imaging.

We first measured time-resolved fluorescence spectra of MA-TA neat films (Figure 1b). A prompt fluorescence band appears at 455 nm immediately after photoexcitation and is shifted toward the longer wavelength in picosecond and nanosecond timescales. A weak fluorescence band, which is attributable to delayed fluorescence, remains at and after 50 ns. The fluorescence anisotropy decays on a similar timescale and converges into 0 within 10 ns. These results indicate that excitons produced upon the photoirradiation diffuse toward the surrounding molecules in different conformations with the lower excitation energy and lose memory of polarized photoexcitation. This exciton diffusion behavior was also characterized by a time-resolved imaging technique. Figure 1c shows temporal evolution of exciton profile plotted as a function of position in the film. The temporal broadening of the exciton profile intuitively shows the spatial diffusion of excitons, and the detailed analysis quantifies the diffusion coefficient (D) and length (L_D) of MA-TA. The thus obtained D and L_D values are typically in the range of 10^{-2}-10^{-1} cm^2/s and 50-200 nm, which strongly depend on the position inside of the film. Taken together, the time-resolved spectroscopy and imaging in the present work successfully visualized the exciton diffusion in the intrinsically heterogeneous environments of MA-TA films.

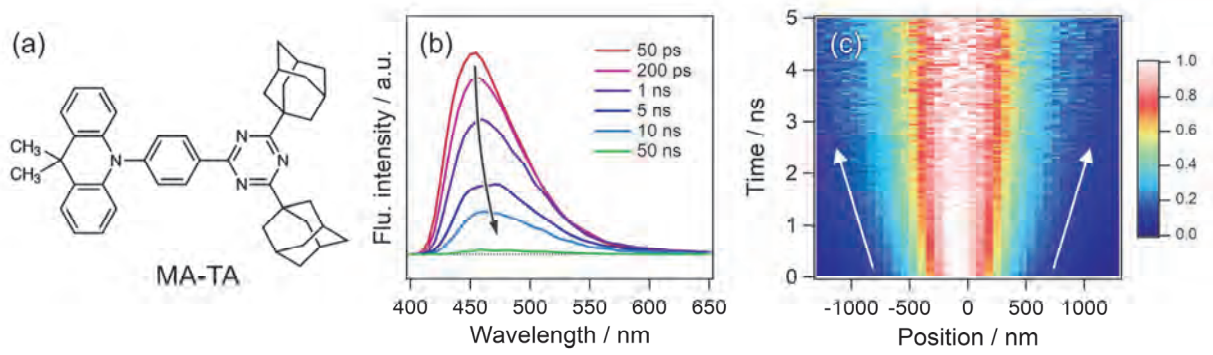

Figure 1. (a) Chemical structure of MA-TA. (b) Time-resolved fluorescence spectra of a neat MA-TA film. (c) Temporal evolution of exciton profile plotted as a function of position. The profile was normalized at each time for clarity of temporal broadening of the exciton distribution.

高い発光効率を有する半導体中における新奇光現象の探索

小島一信　大阪大学

省エネ化が叫ばれるようになって久しい近年、高耐圧かつ低損失にて電流の整流や電圧変換を行うダイオードやトランジスタのようなパワーデバイスや、電気・光エネルギーを相互に変換する発光ダイオード（LED）や半導体レーザ、太陽電池といった光デバイスの高効率化が強く求められている。このため、これら半導体デバイスの性能、とくに効率は格段の進歩を遂げており、パワートランジスタの電力変換損失はわずか数%、青色 LED の発光効率は 80%を超えている状況にある。一方、熱エネルギーを電気的に制御する熱電変換素子に関しても、多結晶半導体や金属材料を用いた研究があるが、単一ペルチェ素子の冷却効率は 5%程度であり、上で述べたような半導体デバイスの各種効率に比して低い水準にある。もし、高い冷却効率を持つ半導体熱電変換デバイスが実現され産業化、また普及価格にて社会実装されれば、その省エネ性を活かして様々な分野における応用が考えられる。このような背景の下、我々は現在、高効率太陽電池向け材料として知られるハロゲン化金属ペロブスカイト半導体の発光内部量子効率（IQE）を 100%に近づける取り組みを進めている。IQE とは、励起された電子正孔対が光子を発生する確率のことであり、100%に近い場合は種々の新奇現象の発現が期待できる。その中の一つである発光冷却は、LED 構造を発光層のバンドギャップ（E_g）よりやや低いエネルギー（E_{ex}）で光励起（もしくは電気的にバイアス）して励起させ、発光に含まれる光子 1 つ当たり E_g - E_{ex} だけ物質から熱エネルギーを奪う現象である。本研究では、半導体の光物性研究において著名な研究者であり、近年では上記のペロブスカイト半導体の物性研究、特にフォトンリサイクル現象の重要性の指摘など、当該研究分野の第一線にて活躍されている京都大学 化学研究所の金光義彦 教授と共同し、半導体発光冷却現象の効率増強技術の探索を行った。

図 1 に実験的に得られた試料の発光および吸収スペクトルを示す。図からも分かる通り、発光冷却のために E_{ex} を定価さえると、吸収係数が急激に低下することが分かる。そこで、光共振器の導入による吸収率の増大を目指し、共振器長と共振器ミラーの反射率をパラメータとした数値シミュレーションを行い、特定の条件下であれば、試料の吸収係数が微小であっても、励起光をほぼ 100%吸収させることができる構造を見出すことができた。今後は、実際に共振器を備えた発光冷却デバイスを作製し、その冷却能力を定量する予定である。

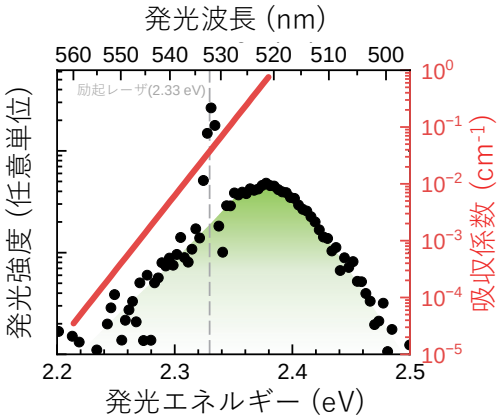

図 1　試料の発光・吸収スペクトル。

Stoichiometry of bioactive trace metals in the Osaka Bay and its inflowing river waters

Yuzuru Nakaguchi　Kindai University

Purpose) In order for phytoplankton to grow and proliferate, various trace metals such as manganese (Mn), iron (Fe), cobalt (Co), nickel (Ni), copper (Cu), zinc (Zn), cadmium (Cd), among others, are required, similar to nitrogen and phosphorus. Nutrients such as carbon, nitrogen, phosphorus, and others are known to be incorporated into phytoplankton in specific ratios. This ratio is referred to as the Redfield ratio and is typically expressed as C:N:P = 106:16:1. Similar stoichiometry applies to trace metals, and this is referred to as the Extended Redfield Ratio. Vu and Sohrin demonstrated the validity of the Extended Redfield Ratio through multi-element analysis of dissolved metals in seawater. In this study, the stoichiometry of biologically active trace metals in Osaka Bay was discussed through the analysis of biologically active trace metals in Osaka Bay and its tributary rivers.

Experimental) Seawater samples were collected at various depths in Osaka Bay on February 1, 2023, using a Niskin sampler. Sea water samples for the measurement of dissolved metals (dMs) were filtered through a 0.22 μm PTFE filter. After filtration, the samples were adjusted to a pH of 2 by adding high-purity hydrochloric acid (Ultrapur-AA-10). Nutrients (NO3+NO2, PO4, Si(OH)4) were measured using the automatic analyzer QuAAtro (BL tech, Inc.).

Stoichiometry of biologically active trace metals based on the dissolved metal-to-phosphorus (dM/P) ratio in Osaka Bay.

Figure 1 shows the average values of dissolved Al, Mn, Fe, Co, Ni, Cu, Zn, Cd, and phosphorus concentrations (dMs/P) in surface seawater samples collected at depths ranging from 0m to 20m in Osaka Bay. It also displays the average values of metal-to-phosphorus ratios (M/P) in phytoplankton bodies, based on the studies by Ho et al. (2007, 2009). In Osaka Bay, the dM/P ratio exhibited higher values than the M/P ratio of phytoplankton for all dMs, excluding dFe/P. This result indicates that dissolved Al, Mn, Co, Ni, Cu, Zn, and Cd in the seawater of Osaka Bay can supply sufficient amounts for the growth of phytoplankton. On the other hand, dFe/P exhibited lower values than the M/P ratio of phytoplankton.

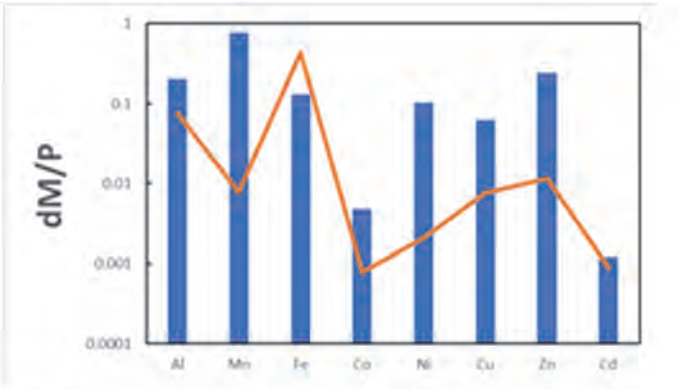

Fig. 1　Bar plots of dM/P ratios at shallow water <20 m in the Osaka Bay and line of the M/P ratio that has been observed in natural phytoplankton (Ho et al. 2007, 2009)

This result suggests that in Osaka Bay, dFe may not supply a sufficient amount for the growth of phytoplankton, depleting faster than other essential nutrients and trace metals. It implies the possibility of primary production in Osaka Bay being limited by dFe.

Achievement Report) 1. Tachibana,M., Zheng, L., Sohrin, Y., Eguchi, M., Nakaguchi, Y., Distribution of Dissolved Biologically Active Trace Metals in the Osaka Bay, The Japanese Society of Oceanography, Kyoto University (Sep., 2023)

2. Nakaguchi, Y., Tachibana, M., Shirai, S., Shimizu, T., Eguchi, M., Zheng, L., Sohrin, Y., Research on Biologically Active Trace Elements in Osaka Bay, Geochemical Society of Japan, Tokyo University of Marine Science and Technology (Sep., 2023)

3. Shimizu, T., Tachibana, M., Sugimoto, Y., Nakaguchi, Y., The Relationship between Trace Metals and Fluorescent Organic Compounds in the Yamato River and Osaka Bay, The Japanese Society of Humic Substances Science, Soka University (Nov., 2023)

イオン液体の金属錯体担持型高分子包接膜による金属イオンの高選択的膜分離に関する研究

向井浩　京都教育大学

【目的】　金属資源の循環的利用は、持続可能な開発に必要な要件の一つと言える。希少金属資源の回収に適した方法の一つに液液抽出法がある。一方、高分子包接膜を用いた液膜輸送は、液液抽出と同じ原理、特徴を持ちながら、揮発性・有害性のある有機溶媒を用いない点などで優れている。イオン液体を用いた高分子包接膜は、膜の安定性に優れ、これを用いた金属イオンの膜分離への展開が期待される。先に Li^+ と Co^{2+} の液膜輸送実験において、Li^+ と Co^{2+} の混合溶液から Co^{2+} のみが輸送されることを見出し、Li^+ と Co^{2+} の相互分離が可能であることが示唆された。リチウムイオン電池からの Li と Co の分離回収への応用が期待される。しかし、混合溶液からの Co^{2+} の除去率と、膜を通過させる輸送率が不十分であるといった課題があった。そこで、予め Co^{2+} の錯体を担持させた高分子包接膜を用いることで、高い輸送率と分離能を有する液膜輸送系の開発を企図した。特に、除去率と輸送率の向上を目指し、これらの経時変化を解析する実験的研究を行った。

【方法】　**(1) イオン液体含有高分子膜の作成**　キレート試薬 1-phenyl-3-methyl-4-benzoylpyrazol-5-one (BMPP) を 0.05 mol kg^{-1} 含む疎水性 IL 1-butyl-3-dodecylimidazolium bis(trifluoromethanesulfonyl)-imide ($[C_4C_{12}im][Tf_2N]$) 1.0 g に、tetrahydrofuran 5 g に溶かした polyvinyl chloride (PVC) 0.1 g を加え、内径 49 mm のガラス製シャーレ内に 3 日以上静置して円形の膜を作成した。**(2) 金属錯体担持型高分子包接膜** **(1)** の膜を 0.13-40$\times10^{-5}$ mol dm^{-3} $Co(NO_3)_2$ の水溶液に浸漬し、緩やかに 24 時間撹拌した。水溶液中の Co の減量から、膜中の Co 錯体の担持率を求めた。**(3) 液膜輸送**　**(2)** の膜を PVC 製 U 字形液膜輸送セルの中央に挟み込み、膜の両側の容器に、HNO_3 で pH を調節した供給相水溶液（$[Co^{n+}] = 2.0\times10^{-5}$ mol dm^{-3}, $[CH_3COONa] = 0.01$ mol dm^{-3}, $[NaClO_4] = 0.1$ mol dm^{-3}, pH 5）と受容相水溶液（$[CH_3COONa] = 0.01$ mol dm^{-3}, $[NaClO_4] = 0.1$ mol dm^{-3}, pH 1）を、それぞれ 30 cm^3 入れた。両水相を一定時間撹拌後、pH、体積、金属濃度を測定し、各相中の金属イオンの存在率を算出した。

【結果と考察】　Co 錯体の担持率が異なる高分子包接膜を用いて、Co^{2+} の供給相からの除去率と、受容相への輸送率が、どのように変化するのかを調べた。ここで Co 錯体の担持率は、配位子 BMPP（HL）が 1:2 錯体 CoL_2 を生成すると仮定し、膜中の全配位子により生成可能な Co 錯体に対する含有 Co 錯体の割合として定義した。24h の液膜輸送において、担持率 0.02 以上で 0.96-1 の高い除去率が得られ、担持率 0.22 以上で輸送率が 1 を超えた（1 を超えるのは、担持された Co 錯体の受容相への溶出による）。以上より、供給相中の Co^{2+} のほぼ全量が受容相へ輸送されたと見なすことができる。金属錯体担持型高分子包接膜を用いることで, 除去率、輸送率共に高い結果が得られた。

担持率 0.41 の膜を用いて輸送の経時変化を調べ、供給相－液膜相、液膜相－受容相それぞれの界面での輸送の違いを調べた。供給相から液膜相へは一定の速さで輸送が行われ、12h でほぼ頭打ちとなった。一方、液膜相から受容相への輸送は、3h まで急激に輸送が進行し、それ以降緩やかに輸送が継続した。以上から、供給相－液膜相の輸送が律速であり、12h で除去と輸送が完了することが示唆された。より最適な担持率を探ることで、効率的な輸送と分離に改良できると思われる。

プラズモニック合金ナノ粒子を設計するための理論的指針の構築

飯田健二　北海道大学

[目的] 自然界の限られた資源を有効活用するためには、様々な元素を組み合わせて高性能な物質・材料を創造していくことが求められる。可視域に局在表面プラズモン共鳴（LSPR）吸収を示す材料の場合、周期表 11 族の金属（Cu，Ag，Au）のみが使われてきた。しかし近年、*B*2（塩化セシウム）型や *C*1 型の合金ナノ粒子が可視域に LSPR 吸収を示すことが京大化研寺西研究室にて見いだされた。

我々は、合金ナノ粒子の LSPR 特性を制御するための理論的指針を構築することを目的として、第一原理計算を進めてきた。2023 年度は、*C*1 型構造を持つ $PtIn_2$ ナノ合金の光励起の機構を解析し、Au ナノ粒子との違いを明らかにした。

[計算手法] 本研究では、直径数 nm のナノ粒子の光電子物性を原子スケールで明らかにすることが求められる。そのために、高い並列化効率を有する第一原理計算プログラム SALMON を用いて、光励起電子ダイナミクスをシミュレーションした。結晶構造から直径約 3 nm の $Pt_{249}In_{432}$ ナノ粒子（図 1(a)）を切り出して計算した。比較のために、Au_{561} ナノ粒子（図 1(b)）の計算も行った。

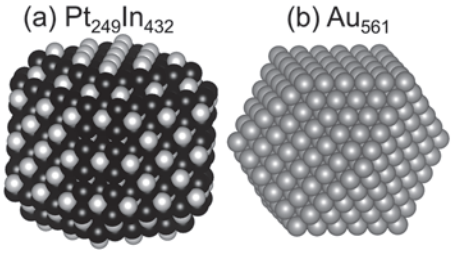

図 1. 対象とした(a)$Pt_{249}In_{432}$ ナノ粒子と(b)Au_{561} ナノ粒子 [3]。

[結果と考察] 光吸収スペクトルを計算したところ、$Pt_{249}In_{432}$ では 2.8 eV に、Au_{561} では 2.3 eV にて LSPR に由来するピークが見いだされた。LSPR は自由電子の集団運動で発現するが、その励起エネルギーは d 電子のバンド間遷移に強く依存する。しかし $Pt_{249}In_{432}$ では、In の d 電子のエネルギーが非常に低いため、LSPR に寄与する d 電子の数は Au_{561} より遥かに少ない。従って、電子構造のみからでは $Pt_{249}In_{432}$ が可視光にて LSPR 吸収を示すことを説明できない。

LSPR 発現の機構を明らかにするために、光励起電子ダイナミクスを解析した。その結果、Au_{561} では、LSPR に由来する大きな電子分極がクラスター表面で生じ、クラスター内部では各原子近傍で d 電子が分極していた。この d 電子の分極は LSPR のエネルギーを低下させる。$Pt_{249}In_{432}$ では、クラスター表面にて Au_{561} と同じく大きな分極が生じ、クラスター内部では Au_{561} よりも大きな変位の分極が見いだされた。この内部での大きな変位の分極は、少ない電子で効率的に LSPR のエネルギーを低下させる。$PtIn_2$ ナノ合金について、原子レベルの幾何的特性が LSPR の機構を決定づけていることが明らかになった [3]。

[論文（謝辞あり）]

[1] K. Iida, T. Takeuchi, R. Katsumi, and T. Yatsui, *J. Phys. Chem. A*, **127**, 7718 (2023).

[2] T. Chiba, K. Iida, S. Furukawa, and J. Hasegawa, *Phys. Chem. Chem. Phys.*, **25**, 9454 (2023).

[3] H. Takekuma, R. Sato, K. Iida, T. Kawawaki, M. Haruta, H. Kurata, K. Nobusada, and T. Teranishi, *Adv. Sci.*, 2307055 (2024).

固体イオンセンサーを指向した発光性ランタノイド錯体の集積化と膜構造解析

三枝栄子　大阪公立大学

【背景・目的】

ランタノイド錯体の発光は、色純度が高く長寿命であることから、発光材料や医療用センサーなどに利用されている。ランタノイドイオンに水など溶媒分子が配位すると発光強度は著しく減少するが、我々が開発した環状ポリアミンにコレステリル基を導入したキレート配位子を用いた錯体 **EuL** (Fig. 1)は、水溶液中でもランタノイドイオンから強い発光を得ることに成功している [1]。この両親媒性錯体は、水溶液中で安定な会合コロイドを形成し、内部の疎水場が水の配位を抑制するため、水溶液中でも長寿命発光を示す。またコロイド溶液中において、膜中にアニオン性ゲスト分子、イオンを包摂し、発光強度の変化を目視で観察することができることが分かっており、本研究では、固体薄膜で同様のゲスト認識素子として活用できるか検討することを目的としている。これまでの共同研究成果として、**EuL** 錯体を用いて水面上単分子膜を形成し Langmuir-Blodget (LB) 法により基板上へ集積することに成功した。転写膜の分子配向性や発光特性の評価から、両親媒性錯体は非常に安定な単分子膜を形成することがわかった。しかしながら、配位子のみの薄膜が配向膜であったのに対し、**EuL** 錯体の薄膜は配向性が見られず、先行研究で報告されている選択的なゲスト認識 [2] の挙動を膜構造から説明するには至らなかった。そこで今回、**EuL** 錯体の成膜条件を改めて検討し、各条件下での膜構造解析を行った。

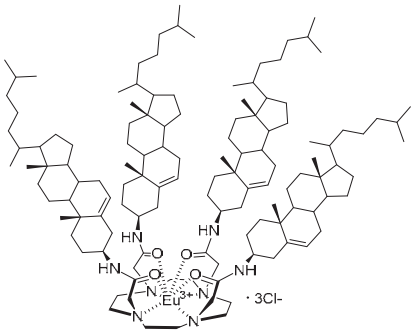

Fig.1 Structures of lanthanide complex [**EuL**]·**3Cl**.

【実験方法】

EuL 錯体を水面上に展開し、水面上膜の圧縮圧 5, 10, 25 mN の 3 水準で成膜を行った。圧縮圧を変えて作製した薄膜を Si 基板上に転写した。また、積層数を 3 層と 9 層の 2 水準で作製し、pMAIRS 法と MAIRS2 法を用いた赤外分光分析による膜構造解析を行った。

【実験結果・考察】

配位子のみの場合､圧縮圧 25 mN で成膜するとカルボニル基が面内方向に配向した膜が得られる。pMAIRS スペクトルから、錯体の場合、同じ条件では表面圧力が高すぎるのではないかと考えたが、いずれの場合も配向性は見られなかった。金属中心の電荷反発が膜構造に大きく影響していると考えられる。また圧縮圧が低いとき膜密度が低くなり、pMAIRS 測定ではバックグラウンドノイズが大きく目的ピークを観測することが困難であった。MAIRS2 を用いると、目的の C=O 伸縮、NH 変角の吸収を観測することができた。以上のように、成膜条件および測定方法の最適化を行うことができた。

【文献】1) T. Sagami *et al., Chem. Commun*., **2017**, *53*, 3967. 2) T. Michinobu *et al,. J. Am. Chem. Soc*., **2006**, *128*, 14478.

新規ハイブリッド型部分フッ素化リン脂質二分子膜の構造・物性の解析

園山正史　群馬大学

【目的】　生物化学分野への展開を念頭に、部分フッ素化リン脂質の設計指針を得るための物理化学的な研究により、リン脂質 Dimyristoylphosphatidylcholine（DMPC）の 2 本の疎水鎖末端にパーフルオロアルキル基(R_f, C_nF_{2n+1})を部分的に導入したアナログ分子群 Fn-DMPC（n＝2, 4, 6, 8）は、R_f鎖長依存的な際だった膜物性を示すこと等を私たちは明らかにして来た。本研究では、DMPC の一方の疎水鎖末端を部分フッ素化した新規 Hybrid 脂質群 Fn-Hybrid（n＝4, 8）を新たに合成し、膜物性・構造を調べることにより、膜タンパク質研究への応用の可能性を探ることを目的とした。

【方法】　これまでの方法に準じて新規 Hybrid 脂質 F4-Hybrid および F8-Hybrid を合成し、水面上単分子膜を金基板に転写したＬ膜の IR MAIRS スペクトルを測定した。また、F4-Hybrid 二分子膜に膜タンパク質バクテリオロドプシン（bR）を再構成した試料（bR/F4-Hybrid）を調製し、分光学的手法によりその高次構造や光サイクルを調べた。

【結果と考察】　F4-Hybrid および F8-Hybrid の単分子膜の IR MAIRS スペクトルを測定し、F4-DMPC および F8-DMPC と比較した。その結果、n＝4, 8 のいずれにおいても、2 本の疎水鎖に Rf 基を導入した Fn-DMPC では、CF_2 伸縮振動の IP 成分と OP 成分の間に波数シフトおよび強度の違いが観測され、1250 cm^{-1} 付近に観測されるバンドを含めて、フォノン由来の性質が見られた。このことは、Fn-DMPC は高い二次元分子集合性を有することを示しており、自発的な分子集合が弱い n=4 の分子も人工的に一定の密な膜を調製することが可能であると考えられる。一方、Fn-Hybrid では、MAIRS スペクトルにはフォノンに特徴的なバンドは観測されなかった。

可視円二色性スペクトルから、天然類似の三量体構造を形成する F4-DMPC の場合と異なり、bR/F4-Hybrid は単量体であることが強く示唆された。一方、過渡吸収測定によると、bR/F4-Hybrid は天然類似の約 100 ms の光サイクルを有することがわかった。したがって、F4-Hybrid は非天然構造を形成するにもかかわらず、天然類似の機能を発現できる可能性が示唆された。

【成果報告】

- Hasegawa et al., Phonon modes controlled by primary chemical structure of partially fluorinated dimyristoylphosphatidylcholine (DMPC) revealed by multiple-angle incidence resolution spectrometry (MAIRS), J. Chem. Phys. (2024) 160(6), 064704. doi: 10.1063/5.0190441
- 中川原ら、一方の疎水鎖末端をフッ素化した新規リン脂質 F4-Hybrid に再構成した膜タンパク質バクテリオロドプシンの特徴、第 49 回生体分子科学討論会（2023 年 6 月 2 日）、他 1 件。

フッ素系樹脂の摩耗に伴う分子配向変化の観測

粕谷素洋　公立小松大学

フッ素樹脂は優れた自己潤滑性を示すため，固体潤滑剤として自動車や船のエンジン内ピストン摺動部等に用いられている．一方で，フッ素樹脂は耐摩耗が課題となっており，フィラー等の添加による改善が行われてきたが，そもそも摩耗中の高分子鎖挙動やフィラーの役割について，分子レベルでは分かっておらず，さらなる摩耗特性の改善にはその化学的過程の理解が必要な状況である．

申請者はこれまでシリコン系水潤滑材料やゴム-氷間における摩擦挙動を含む界面分子挙動を精密摩擦試験と分光手法を組み合わせて評価することで，新規な分子レベルの摩擦・潤滑機構を解明してきた（例： J. Phys. Chem. 2013, Soft Matter 2019，光化学 2021）．現在，同様の手法を医療用高分子材料やフッ素樹脂等，摩擦分野で重要な他の樹脂に展開すべく，研究を進めている．

これらの研究を通して，申請者は分子情報，特に配向を直接観測可能な分光手法が摩擦・摩耗の機構解明には必要，という着想を得て，本申請の共同研究者である京大化研長谷川教授の開発した多角入射分解赤外分光法(IR-MAIRS)を摩擦界面の評価法として展開することを着想し，昨年度から共同研究を進めている．具体的には MAIRS2 法を適用して，摩耗前後のフッ素樹脂の分子配向と集合構造の変化を評価可能であることを示した．一方で摩耗に伴う分子配向変化は 2 軸配向となり，MAIRS2 法では評価に限界があるという課題も見出すことができた．

そこで本年度は，2 軸配向 pIR 試料の評価に有効な pMAIRS 法を同様の試料系に適用して，摩耗に伴う 2 軸配向変化が評価可能かどうかを示すことを目的として研究を進めた．実験としては，シリコンウェハにスピンコート法により成膜したフッ素樹脂薄膜（ポリ（フルオロアルキルアクリレート）をもう一枚のシリコン基板と接触・せん断させ，前後での pMAIRS スペクトル変化を試料の向きを 90 度変えて比較した（右図）． 1150 cm^{-1} 周辺の CF_2 伸縮振動および 1700 cm^{-1} 周辺の C=O 伸縮振動に由来するピークは摩擦前では測定の向きで変化がないのに対して，摩擦後の試料では摩擦方向に平行(p//F)な方が垂直方向（p⊥F)よりも大きくなり，摩擦方向への分子配向変化を観測可能であることを見出した．

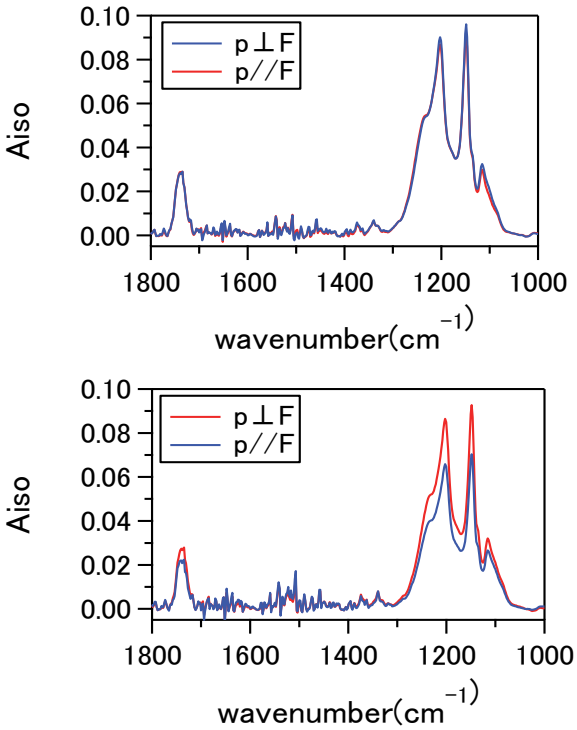

図　フッ素樹脂薄膜の摩耗に伴う面内配向．

以上の結果より，pMAIRS 法が摩耗に伴う 2 軸配向変化の評価に適用可能であることを示すことができた．これらの成果の一部については，トライボロジー会議 2024 春にて発表予定である．

Isolation and Identification of Active Gibberellins in the basal land plant *Marchantia polymorpha*

Takayuki Kohchi　Kyoto University

Gibberellins (GAs) are important plant hormones that regulate plant growth and development. The physiological functions induced by GAs have been elucidated at the molecular level. The biosynthetic genes and receptors of GAs have been isolated mainly from *Arabidopsis* and rice plants. However, the origin and evolution of the GA signaling are largely unknown. Under the International Collaborative Research Program of the Institute for Chemical Research, Kyoto University, in collaboration with Dr. Shinjiro Yamaguchi and Dr. Kiyoshi Mashiguchi, we focused on a model bryophyte *Marchantia polymorpha,* which is the sister lineage of vascular plants. *M. polymorpha* lacks the enzymes that catalyze the final steps of canonical GA biosynthesis but can produce GA precursors such as *ent*-kaurenoic acid (KA) or GA_{12}. The biosynthesis of KA and GA_{12} was upregulated by far-red light (FR)-enriched conditions, while disruption of GA biosynthesis genes consistently inhibited FR-induced hyponastic growth and sexual reproduction. Treatment with another GA precursor or KA, fully rescued the mutants deficient in its biosynthesis, suggesting that a GA-related compound functions as a potent hormone in *M. polymorpha*. These results suggest that the GA system is also present in bryophytes (Sun *et al*., 2023). Considering that bryophytes lack the canonical receptor GIBBERELLIN INSENSITIVE DWARF1 (GID1), the co-evolution of GAs and their receptors is thought to have been crucial during the evolution of land plants, although the active GA molecules (GA_{Mp}) and their receptors in *M. polymorpha* are still unknown.

To identify GA_{Mp}, a bioassay method was developed for *M. polymorpha*. Fractionated samples were prepared from extracts using the two-phase partition method. A bioassay was conducted using the timing of sexual organ formation as an indicator, since GA biosynthetic mutants of *M. polymorpha* have delayed sexual organ formation.

Further analysis revealed that the fraction contained low polar acidic substances that accumulated and contributed to the restorative effect. The study found that a specific fraction, analyzed in detail using HPLC and reversed-phase columns, had a restorative effect on sexual organ delay in GA biosynthesis mutants. The structure of GA_{Mp} will be determined in future studies by combining mass spectrometry and NMR.

Sun, R., Okabe, M., Miyazaki, S., Ishida, T., Mashiguchi, K., Inoue, K., Yoshitake, Y., Yamaoka, S., Nishihama, R., Kawaide, H., Nakajima, M., Yamaguchi, S., and Kohchi, T. Biosynthesis of gibberellin-related compounds modulates far-red light responses in the liverwort *Marchantia polymorpha*. Plant Cell 30, 4111-4132 (2023). doi: 10.1093/plcell/koad216.

モデル二次元シート状高分子の調製と精密キャラクタリゼーション

土肥侑也　名古屋大学

【目的】　二次元方向のみに架橋を持つシート状高分子は、その異方的分子構造に起因して特徴的物性を示すことが期待される。しかし、モデルシート状高分子の合成報告例は少なく、その性質は十分理解されていない。筆者らは最近モンモリロナイト（MMT）中のナノ平面空間中を鋳型としてメチルメタクリレート（MMA）モノマーを平面重合し、二次元シート状高分子試料（2d-PMMA）の調製及びキャラクタリゼーションを行った[1]。本研究では、同試料の希薄溶液中の回転半径 R_g 及び流体力学的半径 R_h を、サイズ排除クロマトグラフィー（SEC）との同時測定により評価した。

【実験】　試料は過去に合成して得られた 2d-PMMA-γ15 を用いた[1]。同試料を SEC と多角度光散乱、準弾性光散乱、粘度の同時測定（SEC-MALS-QELS-viscometry 測定）より評価した。

【結果と考察】　Figure 1 に、2d- PMMA-γ15 の SEC プロファイルを実線で示す。なお 28 分以降のピークは溶媒由来で、18~28 分の主ピークは線状、10~18 分の副ピークはシート状の分子が含まれることを確認済みである[1]。Figure 1a に、単分散線状（L-）PMMA の測定結果も示す。Figure 1a には 2d-PMMA-γ15 と単分散 L-PMMA の R_h（≥ 10 nm）もプロットした。過去に測定した R_g データでは、低溶出時間の副ピーク部で 2d-PMMA-γ15 の R_g が L-PMMA に比べて同溶出時間で有意に低かった[1]のに対し、Figure 2a では R_h が 2d-PMMA-γ15 と線状 PMMA でよく一致している。この挙動は、高度分岐高分子で見られる[2]。Figure 1a より、L-PMMA を基準として R_h と溶出時間の関係を見積り、過去に測定した R_g データを R_h で割った結果を Figure 1b に示す。Figure 1b より、市販多分散線状 PMMA は R_g/R_h 値が 1.5 程度と線状ガウス鎖で予想される値[2]と概ね近いのに対し、2d-PMMA-γ15 は副ピーク部で明らかに R_g/R_h 値が 1 より低く、低溶出時間ほどその値が低いことを確認した。この結果は、2d-PMMA-γ15 の副ピーク部に含まれる目的のシート状高分子が、より低溶出時間側ほど高分岐度を有することを示唆する。

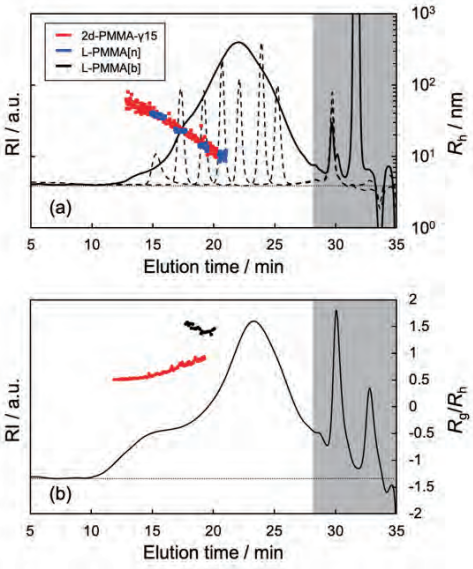

Figure 2. SEC profiles of 2d-PMMA-γ15 (left axes), plotted with (a) R_h and (b) R_g/R_h (right axes) against elution time. In panel a, SEC profiles of commercial monodisperse L-PMMA samples are shown together as dashed curves, while in panel b, R_g/R_h of a commercial polydisperse L-PMMA is plotted.

【成果報告】

- Y. Doi, “Preparation, characterization and dilute solution rheology of two-dimensional sheet-shaped poly-(methyl methacrylate)”, 19th International Congress on Rheology, Athens, Greece, Aug. 4, 2023.
- 土肥侑也、「二次元シート状 PMMA の調製と希薄溶液レオロジー」第 71 回レオロジー討論会、1A03、松山、2023/10/19

【参考文献】　[1] Y. Doi, et al. *Polym. J.* **2023**, *55*, 957.　[2] W. Burchard, *Adv. Polym. Sci.* **1999**, *143*, 113.

Spin signals in a ferrimagnetic film near the compensation temperature

Atsufumi Hirohata　University of York / Tohoku University

Objectives: We aim to develop a ferrimagnetic Heusler-alloy film, in which the magnetic properties will be controlled by substituting the constituent element to achieve compensated ferrimagnetism (effectively the same as antiferromagnetism).
Experimental Methods: Originally we proposed to grow polycrystalline antiferromagnetic and (compensated) ferrimagnetic films using a sputtering system at the University of York. Unfortunately the sputtering system was down until August 2023 and has only been available with a thin sputtering target with the thickness of almost 1 mm as of today. Accordingly we deposited ferrimagnetic films compensated at room temperature at the Ono Laboratory in Kyoto University and patterned them into Hall bars for the measurements of the spin Hall and anomalous Nernst effects.
Outcomes and Analysis: Due to the delay in the shipment of facilities from York, we have used a probe station and a measurement setup in Tohoku University but we could not complete the measurements. We will continue to characterise the samples fabricated to evaluate a possible effect of compensation on the spin Hall and anomalous Nernst effects.
Publications: None.

Characterization of quantum magnon using hybrid magnonic systems

Kab-Jin Kim　KAIST

Objective:
The goal of the study focuses on nonlinear control of magnon-magnon coupling in the synthetic antiferromagnet.

Experimental methods:
We generated and detected propagating spin-waves in the CoFeB/Ru/CoFeB synthetic antiferromagnet (SAF) using micro-patterned coplanar waveguide (CPW) antennae which determine wavelength of the spin-waves and 25.6GHz-cover RF signal processing vector network analyzer (VNA). By changing the in-plane field increment, we obtained the clear magnonic *f-H* (frequency-field) map from the SAF with respect to excitation power -20dBm to +10dBm.

Experimental results:
The spin-wave spectra in the SAF exhibit two distinct modes, which are out-of-phase (optic) and in-phase (acoustic) rotaion modes. As excitation geometry, the acoustic mode becomes dominant when the angle between field and CPW is 0 degree and the optic mode becomes dominant for 90 degrees. At the degree 45 degree, the two modes coexst and they show strong magnon-magnon coupling due to exchange symmetry breaking for interlayers caused by dynamic dipolar interaction. As increasing RF-excitation power, we observed abrupt transition between optic-to-acoustic bands and it losts its intrinsic magnonic anti-crossing gap over 0dBm. Furthermore, we found the hysteretic behavior of the SAF spin-wave spectra with respect to field sweep direction.

Discussion:
The magnonic nonlinear anti-crossing gap tunability has potential for developing future quantum magnonic technonlogy owing to nonlinear phenomena such as magnon BEC, deterministic quantum entanglement. Our research not only provides one-step further explanation of the nonlinear nature of magnons but also helps to make magnon-based stochastic p-bit processor. Furthermore, it can be applicable to the nonlinear neuromorphic reservoir computing someday.

Non-reciprocity of spin wave propagation generated by orbital Hall effect in transition metal dichalcogenides

Sanghoon Kim University of Ulsan

“Quasi-particles” is one of the most intriguing and fundamental idea in the condensed matter physics. *Magnons* are *resultant quasi-particles from collective modes of spin excitations* in a magnetic solid. The concept of magnon has been essentially introduced to understand many spin-related phenomena, for example, ultrafast spin dynamics and current-induced magnetic auto-oscillation. Such quanta of spin waves give rise to even more exotic phenomena such as quantum Bose-Einstein condensation, magnonic black holes, spin pumping, spin Seebeck effect, and magnon-related transports. Especially, the magnon propagation, called as magnonic currents, has been proposed as a source of the future data technology replacing electronics without Joule heating-induced power dissipation [1]. Therefore, the unequivocal identification of magnon characteristics is highly demanded for realizing future magnonic applications.
“Unidirectional Spin Hall magnetoresistance (UMR)” is a novel magnon-related phenomenon observed in ferromagnet (FM)/heavy metal (HM) bilayer structures. Not like other MRs, UMR is a non-linear effect that violates Onsager reciprocity, being odd under either magnetization or current reversal. This state-of-the art phenomenon has two main origins in debating; one is electron-magnon scattering in a FM layer, and the other is spin accumulation at the FM/HM interface [2-4]. Since this method is also relatively easy to adopt to various environments for the magnon study, we developed a way to measure pure magnon effect with this method. This will be also efficient way to observe the magnon-related phenomena in the transition metal dichalcogenides (TMDC) which requires narrow environmental window to study.

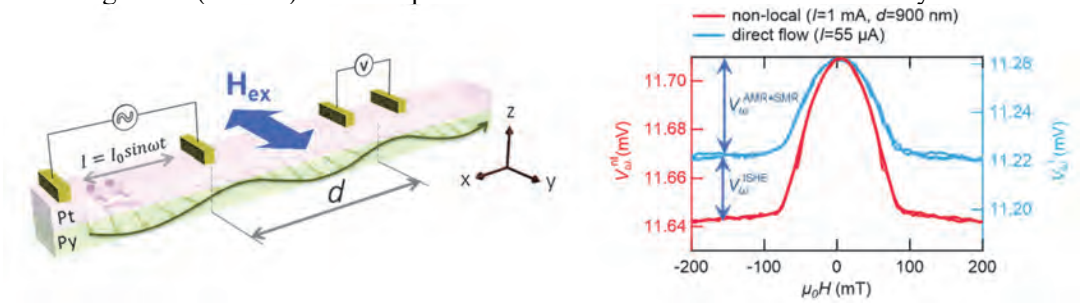

Figure 1. Non-local harmonic voltages in the Pt/Py wire. (left) Schematic illustration of the non-local measurement geometry with the Pt/Py nanowire. (right) Measured local and non-local voltages of the device.

As a result, we, for the first time, demonstrate that the inverse spin Hall effect *via* spin pumping for high energy magnon is superior to that for low energy magnons. The importance of our work is as follows. First, we revealed that the high energy magnons are much more efficient for spin pumping and spin current generation. The performance of magnonic devices depends on conversion efficiency between propagating magnons and spin current generation. Therefore, our findings will be important step toward for application of magnonic devices. Second, we have developed the harmonic voltage model in order to precisely extract the magnon contribution from the nonlocal UMR signal and understand corresponding characteristics of magnons. Therefore, our model can be broadly utilized to understand not only the magnon-based UMR, but also various spin-related transport phenomena with non-local geometries especially for TMDC systems. This work is now under preparation for submission to a journal.

Reference

[1] Nat. Phys. 11, 453 (2015); [2] Nat. Phys 11, 570–575 (2015); [3] Phys. Rev. Lett. 117, 12722 (2016); [4] Appl. Phys. Express 12, 063001 (2019)

Research toward stable NV centers at shallow region and spin dynamics in diamond

Gopalakrishnan Balasubramanian　Helmholtz-Zentrum Dresden-Rossendorf

Recently, NV centers in diamond have been significantly interested as a candidate for a resource for quantum sensing with nanoscale spatial resolution and ultra-high sensitivity. By utilizing nanoscale shallow NV centers, applications for nanoscale imaging and nanoscale nuclear magnetic resonance were demonstrated. In recent years, we have reported that NV centers located at nano-level depths created by ion implantation in phosphorus-doped diamond can lengthen T_2 and improve charge stability [1]. For this reason, the importance of phosphorus doping in diamond is increasing. Conventionally, phosphine has been used to dope diamonds with phosphorus using chemical vapor deposition (CVD), but phosphine is highly toxic and explosive, making the synthesis process dangerous and requiring expensive equipment to detoxify it. In this research, phosphorus-doped diamond was synthesized using tertiary-butylphosphine (TBP), which has significantly lower explosiveness and toxicity than phosphine. Although there have been researches of synthesis using TBP, TBP has a low boiling point and there were issues in controlling the doping concentration.

Toward these issues, Kyoto University group synthesized Phosphorus doped n-type diamond using TBP [2]. We demonstrated that by optimizing synthesis conditions such as synthesis pressure, we were able to suppress nitrogen contamination while controlling the incorporation amounts of phosphorus into the diamond sample [2]. Hall measurements confirmed n-type conduction in measured samples prepared under different growth conditions. It was demonstrated that the spin coherence time (T_2) was increased to more than 2 ms in the sample. Optically detected magnetic resonance spectra indicated that all measured NV centers were aligned along the [111] direction. This study provides appropriate CVD conditions for growing phosphorus-doped n-type diamonds with perfectly aligned NV centers exhibiting long spin coherence times, paving the way to developing and applying diamond quantum sensing devices.

Reference

[1] A. Watanabe, T. Nishikawa, H. Kato, M. Fujie, M. Fujiwara, T. Makino, S. Yamasaki, E. D. Herbschleb, N. Mizuochi, *Carbon,* 178, 294 (2021).

Published paper and presentation

[2] R. Kawase, H. Kawashima, H. Kato, N. Tokuda, S. Yamasaki, M. Ogura, T. Makino, N. Mizuochi, *Journal of Applied Physics*, 132, 174504 (2022).

[3] R. Kawase, H. Kawashima, H. Kato, N. Tokuda, S. Yamasaki, M. Ogura, T. Makino, N. Mizuochi, “Synthesis of P-doped diamond using tert-butyl phosphine toward the high sensitivity quantum sensor of the NV center”, Hasselt Diamond Workshop 2024 - SBDD XXVIII, Feb. 28 – Mar. 1, 2024, Hasselt, Belgium.

Research on the efficiency enhancement of the NV centers creation in nanodiamond

Takuya F. Segawa　ETH Zürich

NV centers in diamond are interested as a candidate of a resource for quantum sensing with nano-scale spatial resolution and ultra-high sensitivity. For the life science application, the NV centers in nanodiamonds are significantly interested as a nanoscale probe for dynamics, magnetic field, electric field, temperature, and pH in a living cell. Among the applications, temperature sensing at the subcellular level has attracted significant interest because the temperature in living cells reflects thermodynamics and plays an important role in regulating cell activities, in particular researchers have demonstrated that the membrane vesicles in cells can be modulated by temperature. However, the common bio probe used to investigate these phenomena often suffers from photobleaching or high cytotoxicity. The photostable and biocompatible diamond probe therefore represents a promising tool for long-term monitoring of cellular activities, notably with millikelvin sensitivity in living cells.

Half-field signals in electron paramagnetic resonance (EPR) spectroscopy are recorded as a reliable method to quantify NV^- centers in nanodiamonds. Enhancing the efficiency of creating the NV centers in nanodiamonds is required for a higher sensitivity of the NV sensor. We measured the EPR spectrum of the NV center in nanodiamonds, which were produced by various methods. One of the main targets in the project is detonation nanodiamonds (DND) because it is the smallest class of diamond nanocrystal capable of hosting various color centers with a size akin to molecular pores around 30-40 nm. We measured half-field EPR spectra (ν = 9.87 GHz) of electron irradiated DNDs with 2 MeV electrons and 1 MeV electrons at a fluence of 5×10^{18} e-/cm^2, which are reported in [1]. We measured nanodiamonds which contains various nitrogen and other impuriy concentration. In addition, we measured TEM (Transmission Electron Microscopy) and DLS (Dynamic Light Scattering) to estimate the size of nanodiamonds. We found the appropriate condition to observe efficiently the characteristic optically detected magnetic resonance (ODMR) NV^- signal in DND subjected to boiling acid surface cleaning. We discussed and analyzed the EPR spectra and enhancement of the efficiency of the creation of the NV centers in nanodiamond. We also evaluate the temperature sensitivities in each sample, which is an important figure of merit of DND and important for application in life science. The results and information obtained are important for higher sensitivity and the life science application of the NV sensor.

Reference

[1] F. T.-K. So, A. I. Shames, D. Terada, T. Genjo, H. Morishita, I. Ohki, T. Ohshima, S. Onoda, H. Takahsima, S. Takeuchi, N. Mizuochi, R. Igarashi, M. Shirakawa, T. F. Segawa, *The Journal of Physical Chemistry C*, 126 (11), 5206-5217 (2022).

Research toward high sensitive NV quantum sensor in diamond

Jörg Wrachtrup　Stuttgart University

Recently, negatively charged nitrogen-vacancy (NV^-) centers in diamond have been significantly interested as a candidate for a resource for quantum sensing with nanoscale spatial resolution and ultra-high sensitivity. Toward high sensitive NV quantum sensor in diamond, charge state instabilities have been a bottleneck for implementing solid state spin systems and pose a major challenge to the development of spin-based quantum technologies. In this project, we investigate the stabilization of NV^- centers in phosphorus-doped diamond at liquid helium temperatures. Photoionization of phosphorous donors in conjunction with charge diffusion at the nanoscale enhances NV^0 to NV^- conversion and stabilizes the NV^- charge state without the need for an additional repump laser. The phosphorus-assisted stabilization is explored and confirmed both with experiments and our theoretical model. Stable photoluminescence-excitation (PLE) spectra are obtained for NV^- centers created during the growth as shown in Fig. 1. The fluorescence is continuously recorded under resonant excitation to real-time monitor the charge state and the ionization and recombination rates are extracted from time traces. We find a linear laser power dependence of the recombination rate as opposed to the conventional quadratic dependence, which is attributed to the photo-ionization of phosphorus atoms. [1]

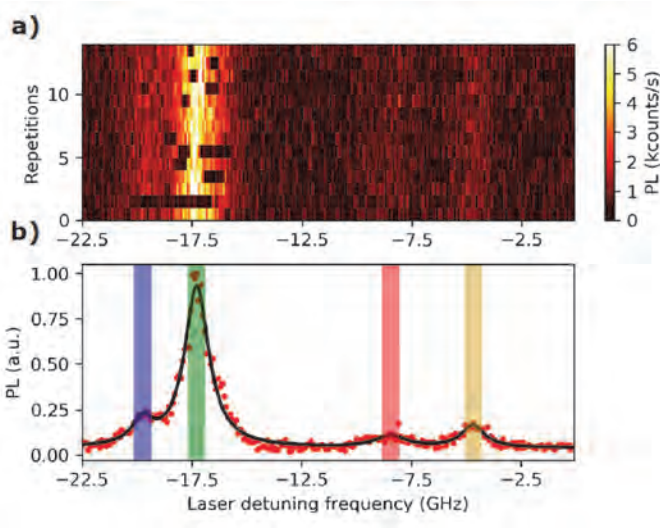

Fig. 1, Stable photoluminescence excitation (PLE) spectrum of an NV center created during growth in the phosphorus-doped diamond. (a) PL intensity as a function of laser detuning (detuned from 636.60 nm) in several individual repetitions. Sharp changes in the PL intensity indicate NV ionization or recombination events. The measurements show a stable but broad PLE spectrum of NV^- over multiple repetitions. (b) PLE spectrum averaged over multiple repetitions in (a). The circles are experimental data and the solid line is fit with a multi-Lorentz function. Blue, green, red, and yellow marked regions correspond to 4 different observed peaks.

Published paper

[1] J. Geng, T. Shalomayeva, M. Gryzlova, A. Mukherjee, S. Santonocito, D. Dzhavadzade, D. Dasari, H. Kato, R. Stohr, A. Denisenko, N. Mizuochi, J. Wrachtrup, "Dopant-assisted stabilization of negatively charged single nitrogen-vacancy centers in phosphorus-doped diamond at low temperatures", npj Quantum Information, **9**, 110 (2023).

Study on the spin injection using perpendicularly magnetized ferromagnetic conductor film

Masaaki A. Tanaka　Nagoya Institute of Technology

The injection of spin-polarized electrons from ferromagnetic electrodes into non-magnetic materials (spin injection) is one of the hottest topics in the spintronics research field. Recently, two types of cobalt-ferrite (001) thin films, insulative Fe-rich cobalt-ferrite (I-CFO) and conductive Fe-rich cobalt-ferrite (C-CFO, $Co_yFe_{3-y}O_4$), with perpendicular magnetic anisotropy were successfully fabricated on MgO (001) substrates [1]. The first-principles band-structure calculation suggested that the electronic structures of C-CFO have half-metallic characteristics and it was found that the perpendicularly magnetized C-CFO films can be a candidate material for spin injection. In this study, the spin injection using the perpendicularly magnetized C-CFO films was investigated.

I-CFO(20 nm)/C-CFO(y=0.6, 20 nm)/MgO (2.0 nm)/Co (1.0 nm)/$\{Tb/Co\}_n$ (15 nm) (MTJ-1) and I-CFO(20 nm)/C-CFO (y=0.6, 20 nm)/MgO (2.0 nm)/ C-CFO (y=0.2, 10 nm)/Pt (3.0 nm) (MTJ-2) films were grown on MgO (001) substrates using the pulsed laser deposition and electron beam deposition techniques. The C-CFO films grown on the I-CFO buffer layers can be expected to decrease antiphase boundaries because both C-CFO and I-CFO are inverse spinel structures. The out-of-plane hysteresis loops of these films show that the C-CFO films exhibit PMA. The MTJs with a junction diameter of several μm were fabricated using photolithography and dry etching by an ion-milling method. The whole microfabrication process was carried out at ICR, Kyoto University. The current-voltage and magnetoresistance (MR) measurements of the MTJs were performed using a four-probe method.

The current-voltage measurements indicated that the MTJs show good tunneling properties. Figure 1 shows the MR curves at 150 K. The tunnel magnetoresistance (TMR) effect caused by the magnetization switching of the bottom CFO and top ferromagnetic (Co/$\{Tb/Co\}_n$ or CFO) layers was observed. The TMR ratio of the MTJ-1 and MTJ-2 at 150 K were −4% and +5%, respectively. The sign difference between the TMR ratio of the MTJ-1 and that of the MTJ-2 reflected the difference in electronic structures between the Co and CFO layers. Therefore, the spin injection using the perpendicularly magnetized C-CFO layer was successfully observed.

[1] M. Morishita *et al.*, Phys. Rev. Materials **7**, 054402 (2023).

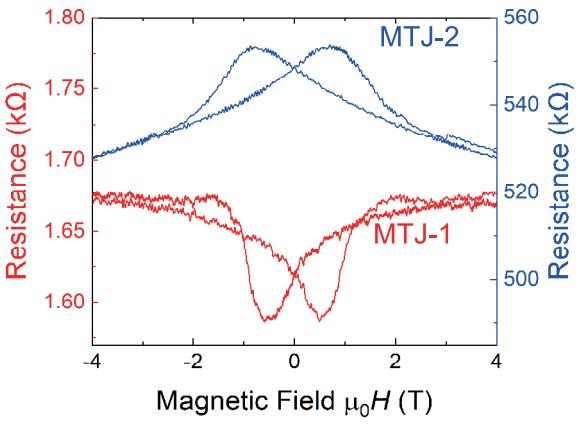

Fig. 1 Magnetoresistance curves of MTJ-1 (Red) and MTJ-2 (Blue) at 150 K.

新規 Fe 基 $D0_3$ 型合金薄膜の開発と熱電効果の機構の解明

長浜太郎　山口大学

目的：熱電効果は今後のエネルギーハーベスティングにおける核心的な技術であり、高機能な熱電材料の開発は喫緊の課題である。その中で、最近、ゼーベック効果に続く新たな熱電効果として、強磁性体で観測される異常ネルンスト効果が注目されている。これは、熱勾配と磁場を印加するとその外積方向に電圧を生じる効果で、高機能熱流センサーなどの高機能なデバイス応用が簡便に実現可能である。その物理については近年理解がすすみ、電子状態から決まる内因性ネルンスト効果と、ゼーベック効果と異常ホール効果に起因するネルンスト効果の和として理解されている。内因性ネルンスト効果に関しては、近年トポロジカル物性の理解が進んだことによって、特異なバンド構造に基づいた巨大な異常ネルンスト効果を示す物質の開拓が進んでいる。最近では $D0_3$ 型の結晶構造を持つ Fe_3Al などがワイル磁性体やノーダルウェブと呼ばれる電子状態に起因する巨大な異常ネルンスト効果を示すことが報告された。本研究では同構造の合金である Fe_3Sn を作製し、結晶構造と磁性、熱電効果について調べた。

実験方法：Fe_3Sn 合金は熱力学的には六方晶系 $D0_{19}$ 構造の方が安定である。本研究では岩塩型構造をもつ単結晶基板上にエピタキシャル成長することで、立方晶系の B2 構造の薄膜を開発した。薄膜試料は分子線エピタキシー法を用いて作製した。基板には MgO(100)を用いて Fe_3Sn 合金薄膜試料の作製を行った。Fe_3Sn の製膜温度を変えた数種類の試料を作製し、XRD による結晶構造解析、SQUID による磁化測定をおこなった。さらに微細加工によりホールバー形状を作成し、熱電能および磁気抵抗効果・ホール効果などを評価した。

実験結果と考察：図 1 に XRD 測定の結果を示す。200~400 ℃で製膜した試料で立方晶を示す Fe_3Sn(222)ピークが観測され、B2 構造が得られたことがわかった。また、400 ℃まで蒸着温度の上昇とともに B2 規則度が上昇した。500 ℃で蒸着した薄膜では $D0_3$ 構造の形成を示唆する 111 ピークが観測されたが、同時に若干の異相ピークが見られた。100 ℃で製膜した試料は多結晶的であるとともに異相のピークが観測された。得られた薄膜のホールバーを作製し、電気伝導特性と熱電特性を評価した。異常ネルンスト効果は次の式で整理される。

$$S_{ANE} = \rho_{xx}\alpha_{xy} + \rho_{xy}\alpha_{xx}$$

右辺第一項は横熱電気項 S_I、第二項は異常ホール×ゼーベック項 S_{II} で、ρ_{xx} は比抵抗、α_{xy} は横熱電定数、ρ_{xy} は異常ホール抵抗、α_{xx} はゼーベック定数である。図 2 に異常ネルンスト効果の成膜温度依存性を示す。400 ℃製膜の試料に向けて S_{ANE}, α_{xy} といった ANE を特徴づける物性パラメータが上昇しており、400 ℃製膜の Fe_3Sn 薄膜試料で S_{ANE}=2.3 μV/K, α_{xy}=1.4 A/mK という最大値を得た。また、500 ℃製膜の Fe_3Sn 薄膜ではどちらの値も下がっていた。これは結晶の構造が B2 構造から $D0_3$ 構造に変化したこと、および異相が析出したことによると考えられる。400 ℃製膜の試料に向けて S_{ANE}, α_{xy} が上昇していることから B2 規則度が高いほど熱電効果が向上することが示唆され、異常ネルンスト効果が結晶品質と強く関連していることが明らかとなった。

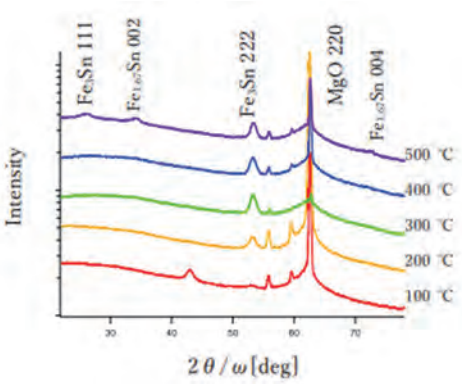

図 1　XRD プロファイルの成膜温度依存性

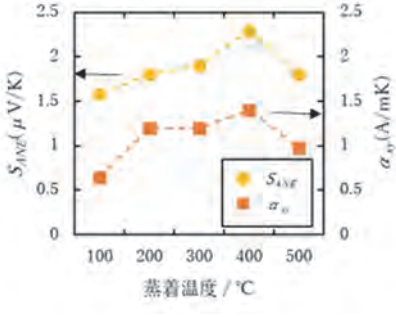

図 2　異常ネルンスト定数と横熱電定数の成膜温度依存性

成果報告:1. 相川皆子他, 第 84 回応用物理学会秋季学術講演会 2023.9.19 熊本市　2:M. Aikawa, A3 Joint Symposium of Emerging　Materials Innovation,P-34, 2023.9.1, Jeju.

Demonstration of topological phase control in chalcogenide superlattices

Misako Morota　AIST

Purpose: This study aims to realize a variety of topological materials and demonstrate new topological properties by simply changing the combination of thickness, number of layers, and number of iterations of multilayers consisting of several chalcogenide materials. Topological insulators are expected to exhibit highly efficient spin-current conversion due to their surface states caused by strong spin-orbit coupling.　Thus, the ST-FMR measurements have been performed on a bilayer sample of ferromagnetic metal CoFeB using Sb_2Te_3 as a topological insulator. To investigate the mechanism of the topological surface state and the conversion efficiency, the ST-FMR measurements have been performed on a ferromagnetic CoFeB bilayer sample using Sb_2Te_3 as a topological insulator. In this study, samples with different thicknesses of the Sb2Te3 layer were prepared and ST-FMR was measured.

Experimental: First, a Sb_2Te_3 film was deposited on a thermally oxidized silicon substrate under conditions that created a layered crystal structure, followed by 5 nm layer of CoFeB and 3 nm thick SiO_2 as anti-oxide film with keeping the vacuum in the same chamber by RF sputtering at AIST. Then, device fabrication was performed using a maskless exposure system and Ar-ion milling and finally electrodes were fabricated by sputtering at Chemical Research, Kyoto University. Four types of samples were prepared with Sb_2Te_3 film thicknesses of 5, 15, 20, and 50 nm. As a reference sample, a single layer of CoFeB 5nm was also prepared.

Results and Discussion: Figure 1 shows the ST-FMR voltages at various frequencies for the Sb_2Te_3 5-50 nm film thickness sample and the CoFeB 5 nm monolayer sample. In the Sb_2Te_3 sample, the shape of the 2 GHz voltage signal is asymmetric, which is of opposite sign to the 5 nm thick sample and the CoFeB monoatomic layer sample. Because the electrical resistance of the Sb_2Te_3 film thickness of 50 nm is equivalent to that of the CoFeB 5 nm, the ferromagnetic resonance appears to have been induced by the inductive magnetic field of the current flowing in the Sb_2Te_3 layer. On the other hand, it remains to be conclusively confirmed that the observed voltage is due to ST-FMR generated by spin injection from Sb_2Te_3. Further detailed analysis will be continued.

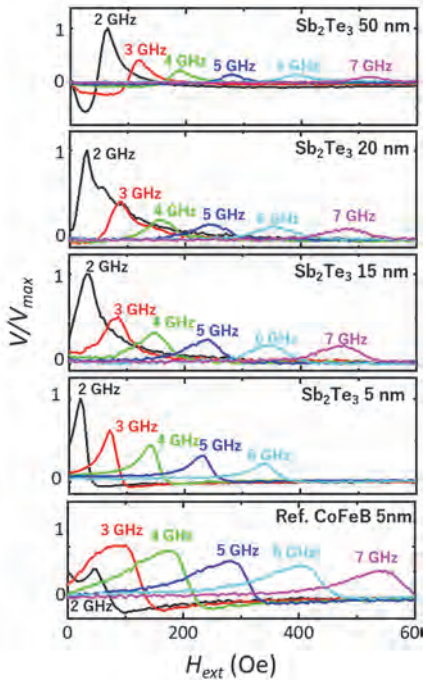

Fig. 1. Normalized voltage for Sb_2Te_3 5, 15, 20, 50 nm-thick samples and CoFeB monolayer sample to maximam voltage of each thickness of the Sb_2Te_3 layer measured under frequencies of 2-7 GHz.

ダイヤモンド量子センサのための表面状態研究

徳田規夫　金沢大学

【緒言・目的】ダイヤモンド中の窒素 - 空孔複合体(NV)中心は優れたスピン特性及び光学特性を有する。他材料と比べ特筆すべき点は、NV 中心ではスピンを室温において光検出・操作できる点である。そのスピンをプローブとし、NV 中心を用いた磁気センサ、電場センサ、温度センサに関して、近年、優れた実証研究がなされてきた。特に、表面からナノレベルの深さに存在する NV 中心は、高い空間分解能を実現することが期待されるが、表面付近ではスピンコヒーレンス時間（T_2）が短くなって感度が低下することや、電荷状態の不安定化が知られていた。近年、我々はリンドープダイヤモンドにイオン注入法により作製したナノレベルの深さに存在する NV 中心では、T_2の長時間化と電荷の安定性を向上できることを報告していた[1]。このことから、ダイヤモンドへのリンドーピングの重要性が高まっている。従来、化学気相成長(CVD)法によるダイヤモンドへのリンドーピングではホスフィンが用いられてきたが、ホスフィンは毒性及び爆発性が高く、合成作業に危険が伴い、無毒化のために高額な装置を導入しなくてはならないという問題点があった。本研究課題では、ホスフィンと比較して格段に爆発性・毒性が低いターシャリーブチルホスフィン(TBP)を用いてリンドープダイヤモンドを合成した。これまでも TBP を用いた合成研究例はあったが、TBP は沸点が低く、ドーピング濃度を制御する点に課題があった。

【実験と結果】リンドープダイヤモンドは、原料ガスに水素で希釈した高純度 ^{12}C メタンを用いて、ARIOS 社製のマイクロ波プラズマ CVD 装置によって、Ib(111)基板上に合成した。二次イオン質量分析法により不純物濃度を測定した。ホール測定から、n 型伝導性を示すことを確認した。今回、我々は、合成圧力等の合成条件を最適化することにより、ダイヤモンド試料中の不純物を、微量のリンが取り込まれつつ、窒素混入を抑制できたことを実証した[2]。T_2の測定は、室温下で自作の共焦点顕微鏡を用いたハーン・エコー法で行い、NV 軸の方向は光検出磁気共鳴測定により確認した。更に、最適化した条件での合成試料で、長い T_2 を有する単一 NV 中心が生成していることを確認した。これは T_2を短くする不純物を抑制できたためと考えられる。SIMS により窒素濃度を抑制できていることも定量的に確認している。更に、NV 軸の配向性についても、[111]方向への高い配向性を確認した。また、新たな量子センシング手法を考案し、実証した[3]。これらの成果は、今後の量子センシング応用研究にとって重要な結果である。

【参考文献】[1] A. Watanabe, T. Nishikawa, H. Kato, M. Fujie, M. Fujiwara, T. Makino, S. Yamasaki, E. D. Herbschleb, N. Mizuochi, "Shallow NV centers augmented by exploiting n-type diamond", *Carbon*, 178, 294 (2021).

【成果報告】[2] R. Kawase, H. Kawashima, H. Kato, N. Tokuda, S. Yamasaki, M. Ogura, T. Makino, N. Mizuochi, “Synthesis of P-doped diamond using tert-butyl phosphine toward the high sensitivity quantum sensor of the NV center”, Hasselt Diamond Workshop 2024 - SBDD XXVIII, Feb. 28 – Mar. 1, 2024, Hasselt, Belgium.

[3] H. Tabuchi, Y. Matsuzaki, N. Furuya, Y. Nakano, H. Watanabe, N. Tokuda, N. Mizuochi, J. Ishi-Hayase, "Temperature Sensing with RF-Dressed States of Nitrogen-Vacancy Centers in Diamond", *Journal of Applied Physics*, 133, 024401 (2023).

量子センサの高感度化に向けたリンドープダイヤモンド合成と量子科学技術研究

牧野俊晴　産業技術総合研究所

【緒言・目的】ダイヤモンド中の NV 中心は、量子科学技術分野において精力的に研究され、特に固体中のスピンとしては群を抜く長いスピンコヒーレンス時間を持つことにより、高い量子センサ感度が実現し、磁場、電場、温度、圧力、pH などの高感度センサとして幅広い分野での応用が期待される。更なる高感度化に対し、課題の一つとして、電荷状態が負電荷状態から中性状態になってしまう不安化の問題があり、本研究課題では、電荷状態の安定化に取り組んだ。

【実験と結果】以前、我々は、リンドープ n 型ダイヤモンド中の NV 中心の負電荷状態状態が安定化すること、及びスピンコヒーレンス時間の長時間化が実現することを報告していた。今回、n-i-n 接合を CVD 合成法により作製し、電荷状態の安定化について定量的に調べ、理論的解析を行った。i 層中のＮＶ中心においては不純物濃度が抑えられ、原理的に不純物の磁気ノイズとしての影響を抑えることができ、一方で、n 型膜の影響で、電荷状態の安定化が期待できるのではないかと考えた。図 1 (c)に、フォトルミネッセンスにおけるゼロフォノン線積分強度から見積もった NV^-電荷状態の NV^-と NV^0 状態の和に対する割合を示した。図 1 (b)には計算から得られたバンド図を掲載している。n-i-n 接合において、i 層中にあるＮＶ中心が、n 型膜の近くで NV^-電荷状態が安定化されることが理論的に期待され、図 1 (c)に示した通り、その安定性が示された[1]。

更に、低温にいてはフォトルミネッセンスにおけるゼロフォノン線のシフトが電荷状態の不安定性からシフトしてしまう課題があったが、リンドープダイヤモンドを用いることにより安定化を実証できた[2]。

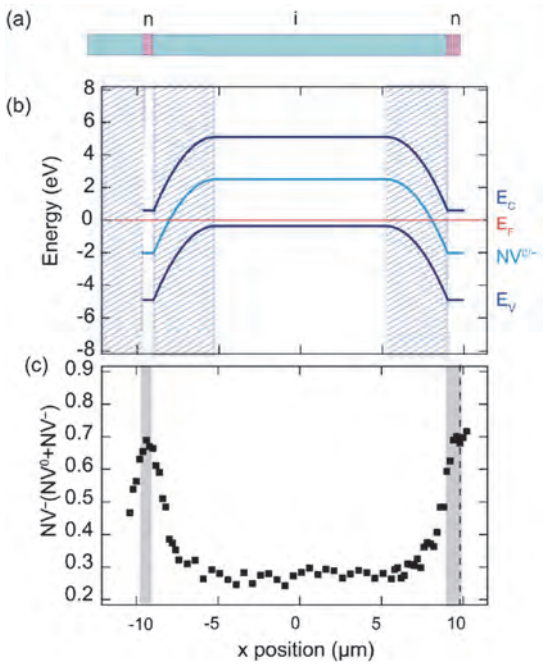

図１　n-i-n 接合による NV^-電荷状態の安定化．(a) n-i-n 接合の概略図．(b) n-i-n 接合のバンド図．(c) フォトルミネッセンスにおけるゼロフォノン線積分強度から見積もった NV^-電荷状態の NV^-と NV^0 状態の和に対する割合．

【成果報告】[1] M. Shimizu, T. Makino, H. Kato, M. Fujiwara, M. Ogura, N. Mizuochi, M. Hatano, "Charge states of nitrogen-vacancy centers in Fermi level controlled diamond n-i-n junctions" *Journal of Applied Physics*, **133**, 214401 (2023).

[2] J. Geng, T. Shalomayeva, M. Gryzlova, A. Mukherjee, S. Santonocito, D. Dzhavadzade, D. Dasari, H. Kato, R. Stohr, A. Denisenko, N. Mizuochi, J. Wrachtrup, "Dopant-assisted stabilization of negatively charged single nitrogen-vacancy centers in phosphorus-doped diamond at low temperatures", *npj Quantum Information*, **9**, 110 (2023).

Role of PIP5K Genes in Pollen Tube Development

Li-Jia Qu Peking University

Objectives: Phosphoinositides—a class of glycerophospholipids—serve as signaling molecules on membranes in eukaryotic cells. Of seven structurally possible phosphoinositides that are different in their phosphorylated positions on the inositol residue, phosphatidylinositol 4,5-bisphosphate [PtdIns(4,5)P_2] is localized mainly to the plasma membrane and involved in various cellular processes including cytoskeletal organization, membrane trafficking, and signal transduction for gene expression through physical interaction with various regulatory proteins. Phosphatidylinositol 4-phosphate 5-kinase (PIP5K), which produces PtdIns(4,5)P_2 by phosphorylating PtdIns(4)P, is thought to be a key enzyme responsible for the spatiotemporal pattern of PtdIns(4,5)P_2 in higher plant cells, where some of the phosphoinositide metabolic pathways found in animal or fungal cells are missing. We have identified a set of PIP5K genes the complete loss of functions of which caused male sterility. Pollens with the multiple mutations were found to be defective of pollen tube development. In this study, an essential role of PIP5K in pollen germination was investigated.

Experimental Methods: T-DNA or transposon tagging mutant lines of the *PIP5K4*, PIP5K5, and *PIP5K6* genes were obtained from public organizations for biological resources. Loss-of-function mutant lines for the genes were established, and crossed with one another to obtain multiple mutant lines. Single and multiple mutant lines of the *PIP5K4–6* genes were examined for their phenotypes in pollen development and germination by microscopic observation, and transformed with the gene encoding the PtdIns(4,5)P_2 fluorescent marker protein 2xmCHERRY-2xPH^{PLC}.

Results and Discussion: We investigate *pip5k4pip5k5pip5k6* triple mutant pollen grains, which were obtained from heterozygous triple mutants, for processes of the pollen development and germination by detailed microscopic observation. Although the triple mutant pollen grains were apparently normal in their morphology, they couldn't germinate under germination conditions. Spatiotemporal localization of the PtdIns(4,5)P_2 fluorescent marker protein 2xmCHERRY-2xPH^{PLC} as seen in the wild type was abolished in the triple mutant pollen grains, which exhibited swelling and rupture of the pollen wall, but neither the conspicuous protruding site nor site-specific deposition of cell wall materials for germination. These data indicate that PIP5K4–6 and their product PtdIns(4,5)P_2 are essential for pollen germination, possibly through the establishment of the germination polarity in a pollen grain.

Publication: Kato, M., Watari, M., Tsuge, T., Zhong, S., Gu, H., Qu, L.-J., Fujiwara, T., Aoyama, T. (2024) Redundant function of the *Arabidopsis* phosphatidylinositol 4-phosphate 5-kinase genes *PIP5K4-6* is essential for pollen germination. *Plant J.* 117:212-225.

Molecular mechanisms of mRNA processing governing 3'UTR ends by using plant as a model system

Artur JARMOLOWSKI　Adam Mickiewicz University

Objectives: The biology in 3' end regulation of pre-mRNA remained un-chartable due to the difficulty in obtaining loss-of-function animals. By utilizing the plant system, both teams were able to analyze null mutants of genes encoding CFI subunits, for the first time. My team, has revealed many regulations involved in pre-mRNA processing, such as posttranscriptional coordination of splicing and miRNA biogenesis in plants. The interest in comprehending the machineries involved in giving rise to variation of transcripts, eventually extended to 3' UTR length determination and its regulation. The ICR team has discovered that CSN, a signaling hub that utilizes upstream signals such as starvation/irradiation in mammals and light/dark in plants, directly bound mRNA processing complexes, such as SF3b and CFI. We aim to put our complementary skills together to understand the molecular mechanisms involved in mRNA 3'UTR processing.
Experimental results: We have discovered that, AtCFI25a, AtCFI59, and AtCFI68 each pulled down all components of the CFI, confirming that these subunits form the plant CFI complex. Furthermore, either AtCFI59 or AtCFI68 was essential for nuclear localization of the smallest subunit, AtCFI25a. Mutants with single loss-of-function for AtCFI59 or AtCFI68 showed no obvious morphological defects compared to wild-type plants, while the double mutant displayed pleiotropic morphological defects, identical to those previously reported for AtCFI25a loss-of-function plants. Moreover, these morphological defects correlated with alterations in the usage of 3' UTR cleavage and polyadenylation sites. *atcfi25a*, *atcfi25a atcfi25b* and *atcfi59 atcfi68* double mutants showed widespread changes in the choice of cleavage and polyadenylation sites. In most cases, more proximal cleavage and polyadenylation sites were used, leading to shorter 3' UTRs.
Discussion: We favor our hypothesis that diverse yet temporal-regulated transcript usages are key to respond to specific environmental stimuli. In particular, genes involved in light intensity, light harvesting, photosynthesis and cold responses showed significant dependence on AtCFI function. Furthermore, transcripts coding for AtCFI subunits showed altered 3' end processing in these mutants, suggesting self-regulation of AtCFI.

Presentations: Zhang X, Szewc L, Nomoto M, Garcia-León M, Kato M, Yura K, Rubio V, Tada Y, Furumoto T, Staiger D, Aoyama T, Jarmolowski A, Tsuge T*. “Cleavage Factor I is essential for maintaining the diversity at the 3' ends of mRNA in plants.” The 33rd ICAR, 2023.06.05-09, Chiba JAPAN.

Publication in preparation: “Plant Cleavage Factor I complex is essential for precise cleavage and polyadenylation site determination”

Exploiting AtMYB60 regulation for water use efficiency and drought resistance in crops

Massimo GALBIATI　National Council of Research

Objectives: We propose improving drought-resistance traits by focusing on a MYB transcription factor identified as a key element in stomatal opening/closure regulation. Increasing temperature and reduced precipitations is a serious threat to crop productivity worldwide. Drought-resistance involves complicated combination of different physiological pathways. Therefore, dissecting processes to simple cascaded of events is important. My group identified clusters of DOF-binding motifs ([A/T]AAAG), located in the regulatory genomic region upstream of the AtMYB60 start codon, as GC-specific *cis*-element conferring cellular specificity to the *AtMYB60* expression. DOF-type Zn-finger transcription factors, including *SCAP1*, were recognized as the *trans*-elements which bind to these motifs to activate AtMYB60 expression in guard cells. ICR-group has been working on the CSN that is involved in both proteolysis and pre-mRNA processing. The latter is represented by the binding to SF3b involved in splicing, and the CFI in cleavage and polyadenylation. Together we will find a novel model system for drought regulation.
Experimental results: Through complementary collaboration following progress has been achieved this year. Two different promoter was exploited to drive expression of the AtMYB60:GFP translational fusion, namely the well-characterized 1.3kb native AtMYB60 promoter and, the CaMV35S constitutive promoter ($MYB60_{pro}$:MYB60:GFP and $CaMV35S_{pro}$:MYB60:GFP, respectively). Binary vectors were generated for these constructs and introduced into Arabidopsis. As a result, stable transgenic Arabidopsis lines carrying $MYB60_{pro}$:MYB60:GFP and $CaMV35S_{pro}$:MYB60:GFP constructs have been produced. Over 15 independent T1 lines have been selected for each construct. All lines were self-propagated to produce T2 seeds which have been used for the selection of lines harboring a single copy insertion for either construct.
Discussion: Having the platform being plowed this year, the long-term goal of the collaboration is to provide a thorough understanding of the AtMYB60 regulation in guard cells to assist the design of innovative strategies for the breeding of novel resilient crop varieties. For detailed update and practical discussion on the progress, I visited ICR for an interactive seminar titled “Deciphering the transcriptional regulation of stomatal activity” (2023.11.16-28). Further continuous work will address both the post-transcriptional and post-translational regulation of AtMYB60, to fully exploit its potential for modulating the water use efficiency and drought resistance in plants.

Chromatin, epigenetic and proteolytic regulation of RNA processing in plant morphogenesis

Vicente RUBIO　National Center of Biotechnology

Objectives: We focus to understand molecular mechanisms bridging proteolysis to mRNA processing in the general processes of environmental adaptation. Taking advantage of the resources in the plant system, Arabidopsis was used as a model organism to investigate CRLs, DCAFs, CSN and their binding factors, that are highly conserved among kingdoms. To date, plants have utilized these protein complexes in adaptation to light environmental changes. CFI (cleavage factor I) is a complex that binds CSN in mammals and plants, and is involved in processing 3' UTR ends of mRNAs. In my group, “tandem affinity purification” and “protein detection” system was systematically applied to analyze CFI-interacting proteins using different bait and environmental conditions. Results were examined against the DCAF list that revealed novel overlaps in certain proteins categories.
Experimental results: Through complementary collaboration with Dr. Tsuge's group at ICR, numerous proteins have been listed up as interacting partners for CRLs, DCAFs, CSN and their binding factors. However, it remains unclear which network is the key network linking proteolysis to mRNA processing regulation. We revealed that Arabidopsis CFI25a subunit interacts with CFI25a, CFI59, and CFI68, confirming that an intact CFI complex could be formed in plants. CFI25b, a homolog of CFI25a, will be examined to seek dynamic composition diversity of the CFI complex. Six out of 8 subunits composing the CSN protein complex was also identified. Interestingly, an overrepresentation of proteins involved in proteolysis led us to believe that CSN-CFI interaction could be a key link between proteolysis and mRNA processing regulation.
Discussion: We favor our hypothesis that diverse yet temporal-regulated transcript usages are key to respond to specific environmental stimuli. For detailed update and practical discussion on the progress, I visited ICR for an interactive seminar titled “Dangerous liaisons: COP1 and DET1 regulatory loops in controlling plant development” (2023.10.06-14). Further collaboration will gain understanding of the key general platform for gene expression regulation *via* proteolysis and transcriptional regulation.

Presentations: Zhang X, Szewc L, Nomoto M, Garcia-León M, Kato M, Yura K, Rubio V, Tada Y, Furumoto T, Staiger D, Aoyama T, Jarmolowski A, Tsuge T*. “Cleavage Factor I is essential for maintaining the diversity at the 3' ends of mRNA in plants.” The 33rd International Conference on Arabidopsis Research, 2023.06.05-09, Makuhari Messe, Chiba JAPAN.

Publication in preparation: “Plant Cleavage Factor I complex is essential for precise cleavage and polyadenylation site determination”

Self-Assembling Compounds That Selectively Inhibit Protein Phase-Separation

Lu Zhou　Fudan University

Compartmentalization is a defining characteristic of life. Cells organize their contents into organelles, which have classically been considered as membrane-separated architectures. However, a growing number of studies have revealed newly defined types of organelles that form via liquid–liquid phase separation (LLPS), a physical process whereby components in a solution separate into two coexisting phases. In this research, we collaborated with the Uesugi group of ICR to develop self-assembling compounds that selectively inhibit the phase separation of particular proteins.

Through rigorous screenings involving 1002 compounds, our Fudan lab has identified a self-assembling compound termed D008, demonstrating an affinity for a subset of proteins within the proteome. Detailed proteome analysis of proteins binding to D008 has identified 174 entities that co-precipitate with D008 in PBS. A Gene Ontology (GO) analysis of these proteins has highlighted their involvement in critical cellular processes such as mRNA splicing and mRNA processing. Notably, among the proteins exhibiting significant binding affinity with D008, HNRNPA2B1 emerged prominently. This RNA-binding protein, recognized as an LLPS-forming that plays a role in mRNA processing and translation, was successfully isolated through pulldown assays using D008 at 50 μM. Subsequent experiments involving RNase-treated lysates did not exhibit co-precipitation of HNRNPA2B1 with D008, indicating a dependence on RNA for their interaction.

Given D008's interactions with an array of RNA-binding proteins, initial expectations suggested a potential modulation of protein translation. However, assessments in Hela cells revealed no discernible impact on protein translation, potentially attributed to D008's limited cell permeability. To elucidate these findings further, ongoing collaborative efforts with the Uesugi group at ICR involve *in vitro* translation assays with D008. We also plan to determine whether D008's self-assembling properties are imperative for any observed effects on protein translation.

Development of Cancer Vaccine Adjuvants with Optimized Safety Profiles

Yan-mei Li　Tsinghua University

The development of synthetic cancer vaccine adjuvants has been an area of active research. One promising class of small-molecule anti-cancer adjuvants are agonists of TLR7/8 that usually sense viral single-stranded RNA to elicit a Th1-type cellular innate immune response. In this collaborative research with ICR, we extended ICR's previous discovery of a self-assembling vaccine adjuvant named cholicamide, with the goal of identifying a potent cancer vaccine adjuvant with an improved safety profile. Our collaboration resulted in a cholicamide derivative (cholicamide β) as a non-cytotoxic small-molecule cancer vaccine adjuvant that stimulates antigen-presenting cells to induce antigen-specific T-cell activation in cells and *in vivo*. In FY2023, we focused on the safety profile of cholicamide β in cells and *in vivo* to complete the study. This collaboration with ICR and other institutions in Japan resulted in our publication in *J. Med. Chem* in 2023.

Our collaboration assessed the *in vivo* safety profiles of cholicamide and cholicamideβ as adjuvants for influenza vaccines. Animal studies indicated that cholicamideβ has a higher level of safety as a vaccine adjuvant than cholicamide does. Our collaboration also analyzed the gene expression levels of 17 safety biomarkers and confirmed the excellent safety profile of cholicamideβ.

Collectively, these results support the idea that cholicamideβ maintains a high safety profile despite its potent cytokine-inducing activity. Our investigation underscores the immunostimulatory potency of cholicamideβ in dendritic cell activation, devoid of any cytotoxic effects. Furthermore, when coupled with a peptide antigen, this simple self-assembling small-molecule enhanced antigen-specific T-cell response, with consequent tumor regression *in vivo*. In light of these findings, cholicamideβ emerges as a prospective avenue for translation, potentially defining a novel category of small-molecule adjuvants for cancer vaccines.

Publication

Zhuo, S., Noda, N., Hioki, K., Jin, S., Hayashi, T., Hiraga, K., Momose, H., Li, W., Zhao, L., Mizukami, T., Ishii, K., Li, Y., Uesugi, M.　*J. Med. Chem.* 66(18), 13266–13279 (2023)

Red and Near-Infrared Multi-Resonance Thermally Activated Delayed Fluorescence Emitters

Christin Bednarek　KIT

Objectives

Aim of this project is the fine tuning of long-range charge-transfer (LRCT) and short-range charge-transfer (SRCT) in TADF emitters comprising a multi-resonance (MR) core which is decorated with conformation confined donor moieties. While Donor-Acceptor (D-A) type TADF emitters are typically designed around a twist between D- and A-segments facilitating reverse intersystem crossing (RISC) *via* LRCT state, MR emitters rely on an intrinsic SRCT of their molecular core structure. Alternative donor conformations i.e., quasi-axial, are known to also occur in some diarylamine type donors (phenothiazine or dibenzoazepine (DBZ)). While they were investigated in D-A type emitters a study of their impact in MR-type emitters (e.g. emission profiles) remain due.

Experimental Methods

Synthesis of the compounds was done using flash chromatography for purification, Chemotion software for research data management and were/will be characterized *via* NMR, IR, MS, and photophysically (KIT/University of St. Andrews). Quantum mechanical calculations were conducted on high performance computing clusters of the German state of Baden-Wuerttemberg (bwhpc).

Outcomes

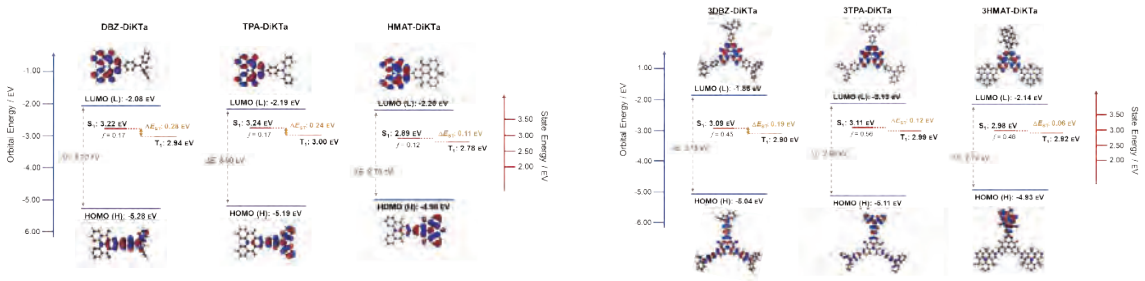

Frontier molecular orbitals and state energies calculated *via* DH-TDA-DFT/B2K-PLYP/def2-SVP//PBE0-D3(BJ)/6-31G** in gas phase.

Mono- and trisubstituted DiKTas were obtained via SUZUKI coupling in high yields. Monosubstituted emitters show dominating LRCT features and broad FWHM, trisubstituted emitters show a range of SRCT and LRCT depending on donor conformation (FWHM < 40 nm for 3DBZ-DiKTa). The latter compounds are regarded more interesting for OLED fabrication. Suitability for vacuum deposited devices was investigated via TGA and sublimation attempts revealing limited stability above 300 °C. We suggest the fabrication of solution processed devices at Kyoto University (Kaji Group).

Analysis

Photophysical characterization will be completed at KIT for monosubstituted emitters and at University of St. Andrews for trisubstituted emitters. Further characterization regarding devices will be conducted at Kyoto University (Kaji Group) in September 2024.

	λ_{PL}[a/b] [nm]	FWHM[a/b] [nm]	PLQY[b]	HOMO[c] [eV]	LUMO[c] [eV]	ΔE_{redox} [eV]	ΔE_{ST} [eV]	τ_{promt} / $\tau_{delayed}$ [ns / µs]
DBZ-DiKTa	536 / 551	73 / 72	0.91	-5.37	-3.01	2.36	-	-
TPA-DiKTa	539 / 551	77 / 77	0.87	-5.31	-3.02	2.29	-	-
HMAT-DiKTa	583 / 576	105 / 87	0.96	-	-	-	-	-
3DBZ-DiKTa	541	44	-	-5.33	-3.05	2.28	-	-
3TPA-DiKTa	537 / 551	54 / 58	0.93	-5.37	-3.07	2.30	0.13	14 / 131
3HMAT-DiKTa	572	95	-	-	-	-	-	-

a 10^{-5} M toluene solution. Excitation at 340 nm.
b 2 w% mCP film (N_2 atmosphere). Excitation at 340 nm.
c CV data in degassed DCM with 0.1 M $[nBu_4N]PF_6$ as the supporting electrolyte and Fc/Fc^+ as the internal reference; scan rate of 100 mV/s.

Preliminary photophysical data of all 6 target compounds.

Publications

Preliminary results were presented on the 2nd Core-to-Core meeting in a research poster (*Chemical Letters* poster prize. Publication with device data in e.g. *Advanced Optical Materials* is planned for end of 2024.

Construction of heterologous protein secretion system at low temperatures by using cold-adapted microorganisms

Xianzhu Dai　Southwest University

[Background and objectives]

Bacteria secret membrane-embed nanoparticles from their membrane surface. These particles carry various biological components, such as polysaccharides, phospholipids, proteins, and nucleic acids, and play crucial roles in bacterial activities, including biofilm formation and infection. In this study, we focused on the application of bacterial extracellular membrane vesicles (EMVs) as a platform for the secretory production of heterologous proteins. We employed *Shewanella vesiculosa* HM13 as a model strain, known for producing a substantial quantity of EMVs harboring a single major cargo protein, P49. In a previous study, it was observed that P49 was secreted through the Type 2 secretion system and binds to the EMV surface via the interaction with the surface polysaccharides. This system is expected to be useful in transferring the desired proteins to EMVs without any modifications of membrane components, such as membrane phospholipids and membrane proteins. This year, we attempted to elucidate the physiological roles of enzymes involved in the synthesis of EMV surface polysaccharides.

[Results and Discussion]

Genes, *wecA3N* and *wecA3C*, coding for the N- and C-terminal halves of a predicted undecaprenyl-phosphate α-N-acetylglucosaminyl 1-phosphate transferase (WecA) was found from a P49-coding gene containing gene cluster. WecA catalyzes the first reaction of the synthesis of O-antigen polysaccharides of bacterial surface polysaccharides, lipopolysaccharides (LPS) and capsular polysaccharides (CPS). This strain has additional WecA homologs, WecA1 and WecA2. Surface polysaccharides analysis of the cells and EMVs indicated that this strain produces lipooligosaccharides lacking O-antigen polysaccharides and CPS. Gene disruption of all three *wecA* genes resulted in the disappearance of CPS from the cells and EMV. At the same time, the major P49 disappeared from cells and EMV fractions and was detected in the supernatant after removal of EMVs. Interestingly, the EMV production level of this mutant was significantly decreased than that of the parent strain. Transmission electron microscopic observation of the all-*wecA*-deletion mutant demonstrated that abnormally protruding and balloon-like membrane structures were formed on the cell surface of this mutant. The loss of CPS, mislocalization of P49, and reduced production levels of EMVs observed from the all-*wecA*-deletion mutant were partially recovered by the introduction of plasmids expressing either wecA1, 2, or 3. These results suggest that the CPS regulates EMV localization at P49 as well as EMV production; *S. vesiculosa* HM13 is expected to produce large amounts of EMVs via the blebbing and pinching-off process, while the CPS is involved in the later step of EMV production.

Structural and functional analysis of the surface polysaccharides of outer membrane vesicles released by bacteria

Maria Michela Corsaro　University of Naples Federico II

Objectives:

The aim of this research has been the determination of the primary structure of the capsular polysaccharides (CPS) isolated from the cells of the *nfnB* mutant of *Shewanella vesiculosa* HM13. Previous studies suggested that the affinity between CPS and P49 is reduced in the mutant that lacks *nfnB*, a gene in the close vicinity of the P49 gene, and therefore we focused on the structural analysis of CPS from this mutant. The group of the ICR partner researcher (Prof. Tatsuo Kurihara) furnished the sample, and the characterization was performed by 2D-NMR spectroscopy.

Experimental:

To determine the primary structure of CPS isolated from the water extract of the *nfnB* mutant strain of *S. vesiculosa* HM13, the purified sample was analysed by chemical methods and two-dimensional NMR spectroscopy. The absolute configuration of the sugars was determined by obtaining their acetylated octyl glycosides and analyzing them by gas-chromatography mass spectrometry (Leontein et al. 1978) on an Agilent Technologies GC-MS 5977 instrument. Mono- and two-dimensional homo- and heteronuclear spectra (^{1}H-^{1}H COSY, TOCSY, NOESY, ^{1}H-^{13}C DEPT-HSQC and HMBC) were acquired using Bruker Avance 600 MHz spectrometer equipped with a Cryoprobe. ^{13}C NMR spectrum was recorded using Bruker 400 MHz spectrometer at 298K. All the chemical shifts were referenced to external sodium 3-trimethylsilyl-(2,2,3,3-$^{2}H_4$)-propanoate (TSP, δ_H 0.00) and 1,4-dioxane in D_2O (δ_C 67.40), respectively.

Results:

Monosaccharide compositional analysis obtained after derivatization in acetylated methyl glycoside and acetylated octyl glycosides disclosed the presence of D-glucose (D-Glc) and 2-acetamido-2-deoxy-D-glucose (D-GlcN). Preliminary inspection of ^{1}H detected β-configured residues, along with a signal at δ 2.02 ppm, which was consistent with the glucosamine acetyl group and confirmed by ^{13}C NMR spectrum. The punctual structure, obtained by 2D NMR spectroscopy, allowed us to establish that the CPS consists of a disaccharide repeating unit constituted by GlcNAc and Glc (Scheme 1).

⟶ 3)-β-GlcNAc-(1⟶4)-β-Glc-(1⟶

Scheme 1

Leontein Karin, Lindberg Bengt, Lönngren Jörgen. Assignment of absolute configuration of sugars by g.l.c. of their acetylated glycosides formed from chiral alcohols (1978). Carbohydrate Research, 62, 2, 359-362.

High pressure synthesis of the metastable rare-earth nickelates with Ni-site substitutions for synchronizing their electronic phase transition and potential magnetic transitions

Jikun Chen University of Science and Technology Beijing

- **Objectives:** Synthesizing metastable *RE*NiO_3 with Ni-site substitutions by other 3d-transition metals (*TM*) and exploring the respective impact on both electronic phase and/or magnetic transition properties. In addition, a molten salt assisted heterogenous growth of other metastable perovskite oxides exhibiting potential electronic phase and/or magnetic transition properties will be also performed, aiming at reducing the synthesis pressures and amplifying the synthesis amount. The investigations were performed together with Shimakawa-lab in ICR.
- **Experimental Methods:** GPa-high pressure synthesis of *RE*$Ni_{1-x}TM_xO_3$ and also other analogous metastable perovskite oxides with potential electronic phase and/or magnetic transition properties were performed at the Shimakawa lab, ICR, aiming at fundamental explorations. Meanwhile, the same materials were also gown in the lab of the candidate via a different route of a molten salt assisted heterogenous growth at MPa oxygen pressures, aiming at amplifying their synthesis amount.
- **Outcomes:** A series of *RE*$Ni_{1-x}TM_xO_3$ covering a large variety of both *RE* and *TM* compositions were successfully synthesized. Their metal to insulator transition properties were systematically investigated. Furthermore, the synthesis of other metastable material family (e.g., *RE*$Cu_3Fe_4O_{12}$, $BiCu_3Co_4O_{12}$) were also explored by both routes. The potential heterogenous nucleation of the metastable perovskite oxide such as *RE*$Cu_3Fe_4O_{12}$ at the presence of molten salts such as LiCl was observed to reduce the synthesis pressure (e.g., from 9 GPa to 6 GPa).

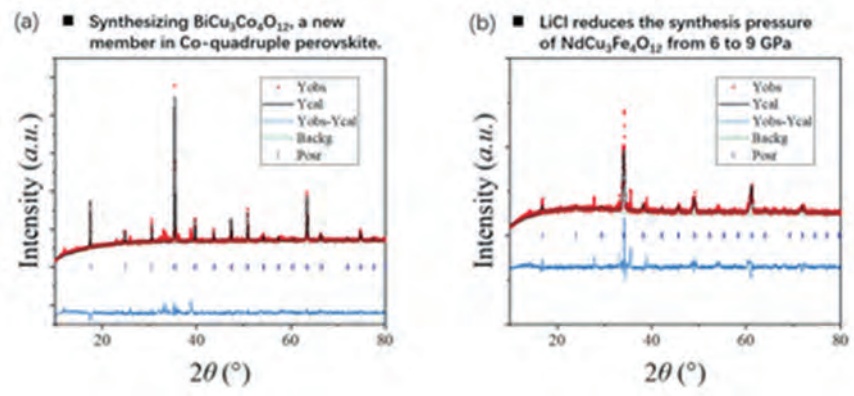

- **Analysis:** X-ray diffractions with structural refinements, Temperature dependence of material resistivity using PPMS for temperature ranges of 2-400 K and CTA system for 300-700 K. X-ray absorption spectroscopy for the Ni-3d and O-2p edges.
- **Publications:** 2 publications are in prepare.

Formation of authigenic $CaCO_3$ on the ocean floor below the compensation depth

Pinghe Cai　Xiamen University

Objectives: By working with **Prof. Yoshiki Sohrin at ICR**, this project aims to solve the mechanism that controls the formation of authigenic $CaCO_3$ on the deep ocean floor where no preservation and accumulation of $CaCO_3$ would be expected.

Experimental methods: Sediment and porewater samples were collected along a transect in the North Pacific Ocean (Figure 1). Radium-226 (^{226}Ra) and thorium-230 (^{230}Th) in sediments were measured using a high-sensitivity ICP-MS. Porewater profiles of dissolved Ca and K^+ was analyzed using an ICP-OES. Dissolved inorganic carbon (DIC) in porewater were determined by Apollo SciTech Dissolved Inorganic Carbon Analyzer.

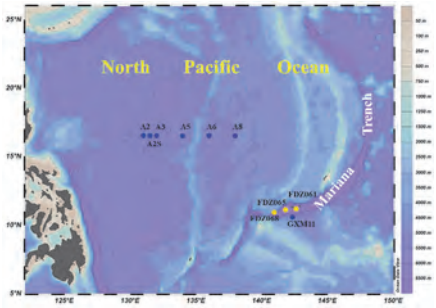

Figure 1. Sampling stations in the East China Sea

Experimental results: Our porewater measurements reveal a strong correlation between Ca^{2+} consumption and K^+ production (Figure 2). The relationship of the two major cations shows that the porewater concentration of Ca^{2+} declines with the rise in K^+, and the stoichiometry ratio of Ca^{2+} and K^+ changes (-1:4.1) is very close to the value (-1:4) predicted by illite weathering:

$$4KAl_3Si_3O_{10}(OH)_2 + 2CO_2 + CaCl_2 + 8H_2O \rightarrow$$

$$6Al_2Si_2O_5(OH)_4 + 2KCl + K_2CO_3 + CaCO_3\downarrow$$

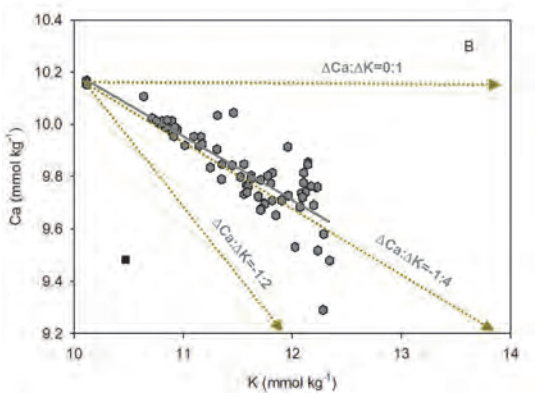

Figure 2 Plot of dissolved Ca^{2+} vs. K^+

Discussion: We attribute this unexpected phenomenon to the delicate coupling of mineral illite weathering into kaolinite to aerobic respiration of sedimentary organic carbon, a process that consumes protons and results in near-surface sediment porewaters becoming saturated with respect to calcite.

Outcome report : Not yet available.

Fabrication of nanotopographical polymer surfaces for bactericidal properties-V

Maya Endoh　Stony Brook University

Objective. After COVID-19 pandemic, the significant efforts have been made to design effective antibacterial surface coatings. Antibacterial surfaces are typically based on liquid-repellent (superhydrophobic) or bactericidal properties. Moreover, inspired by the topography of certain insect wings, developing nanostructured surfaces have provided a potential pathway toward drug-free antibacterial surfaces, which may be vital in the ongoing battle against antimicrobial resistance. Block copolymer (BCP) self-assembly receives a great attention due to its ability to produce long-range nanoscale periodic structures. We have developed synergistic surfaces combining bacteria-releasing and bactericidal properties against *Escherichia coli* (*E. coli,* a Gram-negative bacterium) using BCP lithography[1]. To produce viable antibacterial nanostructured surfaces, it is important to understand what the most effective morphology and structural dimension is. In this report, we investigate the bactericidal efficacy between "nanowalls" developed from BCP lamellae morphology and "nanopillars' developed from BCP cylinder morphology.

Experimental. Polystyrene-*block*-poly(methyl methacrylate) (PS-*block*-PMMA) diblock copolymer with $M_{n,PS}$=18500 g/mol, $M_{w,PMMA}$=18000 g/mol, polydispersity (M_w/M_n)=1.06 for lamellae morphology was purchased from Polymer Source Inc., and PS-*block*-PMMA with $M_{n,PS}$=44600 g/mol, $M_{w,PMMA}$=51200 g/mol, polydispersity (M_w/M_n)=1.12 for lamellae morphology was supplied by prof. Takenaka. Additionally, PS with M_w=30,000 g/mol (M_w/M_n=1.06, Pressure Chemical Co.) was used to prepare a "non-preferential" surface coating (hereafter assigned as "PS nanocoating") for the development of perpendicular oriented microdomains in block copolymer thin films deposited on silicon (Si) substrates[1]. The detail of the sample preparation process is explained in Ref. 1. The height of nanowalls and nanopillars are both about 10 nm and the space between the structures are both around 20 nm.

Results & Discussion. We Incubate *E. coli* in standard Luria-Bertani (LB) broth solution up to 36h at 37 °C. We set the maximum incubation time to 36 h, since *E. coli* incubated in LB medium undergoes a loss of viability of 99% of the cells after 3 days, regardless of the environmental conditions. To measure the efficacy of bactericides, we stained all bacteria by Hoescht 33342 (cell-permeable blue dye) and dead *E. coli* by propidium iodide which is a red-fluorescent DNA dye and used fluorescent microscopy to count them. As shown in Fig. 1, nanopillar surface doesn't have many blue or red dots which implies that there are not many bacteria on the surface, while we see so many blue dots on PS planar surface indicating there are many live *E. coli* attached on the flat PS surface. This tendency was shown for the entire incubation period until 36 h. Fig.2a indicates that the ratio of dead *E. coli* adhered on the nanopillars and nanowalls reached nearly 80% and 70%, respectively after 12 h of contacting to *E. coli* solution, while almost 50% *E. coli* on the flattened PS surface can survive for 3 days. Moreover, nanopillars shows more efficacy of killing *E. coli* than nanowalls. Fig 2b shows the ratio of dead bacteria in the LB broth which indicates the bacteria releasing properties of the surfaces. Interestingly, the PS nanopillars and PS nanowalls exhibit high "dual" (bactericidal and bacteria releasing) properties. This result indicates that the nanopatterned surface (especially cylindered nanopillar-surface) shows the resistance to the bacterial adsorption and high-bactericidal functionality. Topographical surface stays clean without much residual after the debris takes off from the surface.

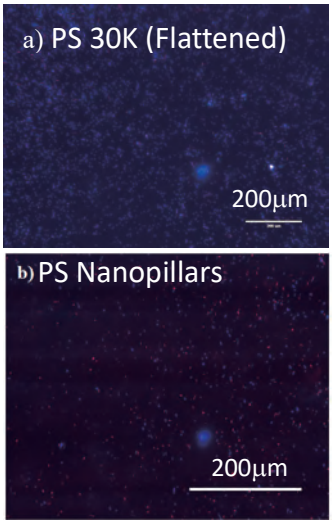

Figure 1. Fluorescent microscopy image after 12h of incubation period. Blue dots indicate *E.coli* on the surface stained Hoescht 33342 and red dots indicate dead *E. coli* stained by propidium iodide.

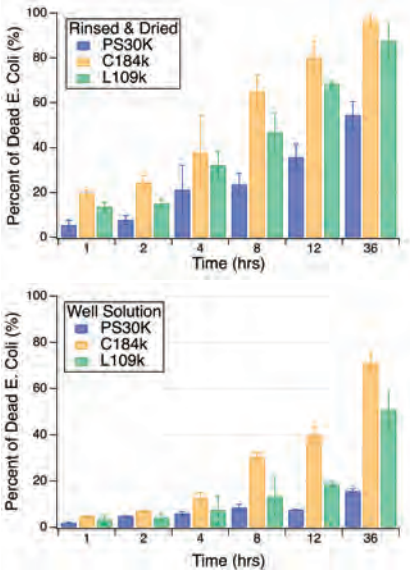

Figure 2. Time dependence of the percentage of dead *E. coli* (a) adhered onto the nanopatterned surfaces, (b) in solution (LB broth) for the planar PS thin film (15 nm thick), PS nanopillars, and PS nanowalls.

Outcome Reports. This result will be presented at American Chemical Society (ACS) March Meeting 2024 (3/17/24 – 3/21/24).

Reference

1. Structure-Based Design of Dual Bactericidal and Bacteria-Releasing Nanosurfaces (D. Salatto, Z. Huang, P. T. Benziger, J.-M. Y. Carrillo, Y. Bajaj, A. Gauer, L. Tsapatsaris, B. G. Sumpter, R. Li, M. Takenaka, W. Yin, D. G. Thanassi, M. Endoh, T. Koga), *ACS Appl. Mater. Interfaces,* 2023, 15, 2, 3420-3432.

Fabrication of novel cell culture substrates using well-defined porous materials

Chiaki Yoshikawa National Institute for Materials Science

Objective

Porous polymers, including polymer monoliths, are used frequently in the fields of chromatography and separation due to their high mass-transfer efficiency and low hydrodynamic resistance. Among the several types of polymer monoliths, those based on epoxy resins have attracted much interest, because they have a well-defined, three-dimensional bicontinuous structure comprised of both a porous channel and a resin skeleton. Prof. Tsujii group (ICR, Kyoto University) has recently developed the application of epoxy-resin-based monoliths by controlling their shapes to form membranes (disks) and particles.[1] Most importantly, their monolithic materials were prepared with special care not to possess a non-porous polymeric surface (a "skin" layer). The surface "skinless" is most important characteristic for solute permeation to the interior of the monolithic materials. Thus, the monoliths confer significant advantages in terms of skinless surfaces, permeability to solutes, and controllable structures and pore sizes. We thus postulate that the monoliths are beneficial for cell culture substrates which can exchange small molecules across the membrane to apply tissue engineering fields. In this study, we studied the monolith disks as cell culture substrates. Herein, we used a MG63 cell, osteosarcoma cell line derived from human. First, we seeded MG63 cells on the monolith disks having different pore sizes. Then, we confirmed the effect of the monolith pore sizes on cell viability and morphology.

Experiments

The monolith disks were prepared according to the previous reports (Fig. 1).[1] The monolith disks were placed in a 24-multiwell culture plate. The MG63 cells were seeded on the monolith disks (2×10^4 cells/well) and incubated for 24 h. Proliferation and viability test of MG63 were evaluated with the Premix WST-1 Cell Proliferation Reagent. The adherent cells were stained with Alexa fluoro 555 and mounted with Prolong Gold antifade reagent with DAPI, coloring nuclei in blue and actin filaments (F-actin) in red, respectively (Fig. 2).

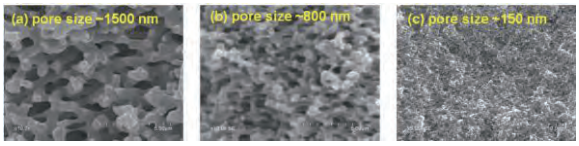

Figure 1. SEM images of the monolith disks with different pore sizes.

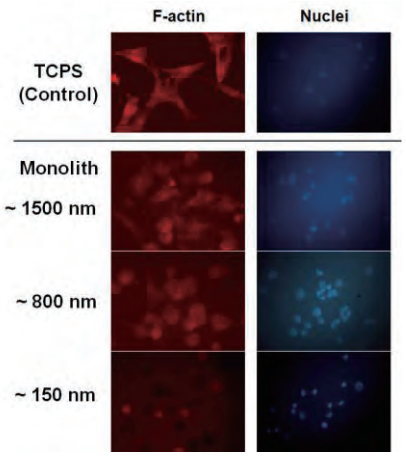

Figure 2. Fluorescent images of the adherent cells on TCPS and monolith disks with different pore sizes (Magnification: 40×).

Results and Discussion

As shown in Fig. 1, the monolith disks with different pore sizes were successfully prepared. The cell viability test confirmed that the cell little died independent of pore sizes. It indicates that the material itself and the pore sizes were harmless to cells.

The attachment of MG63 cells were evaluated on the monolith disks with different pore sizes (Fig. 2). Typically, MG63 has fibroblast morphology as observed on TCPS (control). However, MG63 cells adhered on the monoliths less stretched, and the shapes became more round with decreasing pore sizes. This result suggests that the pore sizes, namely, surface morphology of the monolith disks affect cell attachments, hence, their biological functions. To confirm this, we are now investigating the cell functions by gene expression analysis.

Reference

1. K. Sakakibara, H. Kagata, N. Ishizuka, T. Sato, Y. Tsujii. *J. Mate. Mate. Chem. A*. **2017**, *5*, 6866-6873.

Interdisciplinary Approach to Nanostructured Materials for Applications

Jean-Pierre Bucher Université de Strasbourg

We summarize here the progress on two fronts of our interdisciplinary project for which Professor T. Teranishi is our ICR contact.

Structural changes of inorganic nanoparticles

In 2023, Teranishi's group investigated the structural changes of Pd nanoparticles (NPs) in the presence or absence of triphenylphosphine (TPP) ligand at around 280 °C. It was found that we could obtain face-centered cubic Pd NPs without TPP, while the presence of TPP gave amorphous PdP_x NPs in the size range of 6–42 nm. Such phase change will be detected by HR-TEM in Banhart's group (Strasbourg) under a laser pulse by means of electron diffraction.

Self-organization of single molecule magnets (SMM's) by means of macrocycle networks and LT-STM characterization.

$TbPc_2$ SMMs synthezised in Strasbourg (Ruben's group) have been sent to Nagoya where they will be incorporated in the synthesis of the 2D-crystal made of properly functionalized π-conjugated macrocycles (Tanaka's group).

Simultaneously Tanaka's group has undertaken the synthesis of the proper ligand to grow the macrocycle. After varying the ligands bound to the macrocycle, 2D arrays have been successfuly formed on Au(111), as evidenced by STM in collaboration with Onoe's group. Furthemore, by using STM/STS, they found that C_{60} molecules are selectively incorporated into the nanospace of the macrocycle with no significant interactions between C_{60} and Au(111) surface. In Strasbourg, M. Boero in collaboration with Bucher's group, pursued the molecular dynamics calculation of 2D networks of self-assembled $TbPc_2$ SMM's. It is found that changing the ligand of the Tb SMM's to a more bulky version is a viable approach for changing the pitch of the network. This result, if validated by the experiment, will deepen our knowledge on these double-decker SMMs in interaction with their environment.

Search for four-wave-mixing in the vacuum
- Unveiling dark components in the Universe –

Kensuke Homma　Hiroshima University

Purpose and Method

The aim of this study is to investigate Four-Wave-Mixing (FWM) phenomena within a vacuum environment, with the goal of shedding light on the dark components present in the Universe. To this end, we have developed and refined an ultra-high vacuum chamber at ICR for this purpose. Within this vacuum chamber, two-color laser pulses are combined collinearly and focused into the vacuum along the same optical axis. If photon-photon interactions occur within this vacuum setting, the production of intrinsic FWM photons through the stimulated interaction $\omega+\omega\rightarrow(2\text{-u})\omega+\mathrm{u}\omega$ is expected to be amplified. Here, ω represents the energy of the creation laser pulse, while $\mathrm{u}\omega$ denotes the energy of the inducing laser pulse with $0<u<1$. The energy of the signal photon generated in this scattering process corresponds to $(2\text{-u})\omega$.

Progress and Achievements

We have furthermore extended the search by increasing laser intensity and developing a new method to handle backgrounds from atomic FWM processes, in particular, from the optical elements included in the searching system. We have succeeded to newly install a camera with image intensifier in order to capture the 2-dimensional image of the weal background FMW photons from the optical components.

In parallel, in order to access to a higher mass range of dark components, we have upgraded the current two-beam setup design to a 3-beam collider design, where the creation laser beam is split into two focused colliding beams and the inducing laser beam is further focused into the collision point.

We summarize the published papers relevant to this subject during FY2023 as follows.

Published papers:

[1] Challenge of search for cosmological dark components with high-intensity lasers and beyond, K. Homma, O. Tesileanu, Y. Nakamiya, Y. Kirita, C. Chiochiu, M. Cuciuc, G. Giubega, T. Hasada, M. Hashida, F. Ishibashi, T. Kanai, A. Kodama, S. Masuno, T. Miyamaru, L. Neagu, V. Rodrigues, M. Rose, S. Sakabe, J. Tamlyn, S. Tazlauanu, and S. Tokita (The SAPPHIRES collaboration), The European Physical Journal A, Vol. 59, no. 5, 109(2023).（acknowledge the support by ICR）

[2] Design and Construction of a Variable-Angle Three-Beam Stimulated Resonant Photon Collider toward eV-Scale ALP Search, Takumi Hasada, Kensuke Homma, Yuri Kirita, Universe 9 (2023) 8, 355.（acknowledge the support by ICR）

Advanced Oxygen – mediated Flow Chemistry

Thomas Wirth　Cardiff University

Molecular oxygen is the most appealing reagent to perform oxidation reactions. Yet, lower reactivity of molecular oxygen from its ground state (triplet oxygen, $^3O_2$) generally requires high pressure and temperatures for oxidation reactions. In contrast, the excited singlet oxygen ($^1O_2$) is highly reactive with different organic molecules even under very mild conditions. This report is a continuation of previous research with the Nakamura group (ICR partner researcher). Initially, we had to overcome difficulties as the starting material **1** for the proposed research was no longer commercially available. We therefore successfully developed the following synthesis route:

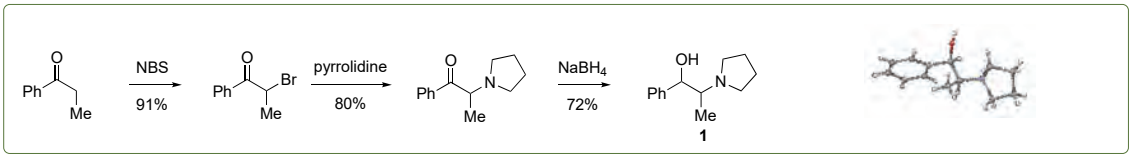

This approach was discussed with the Nakamura research group during a very interesting and fruitful visit in October 2023. Very recently, we have made a larger amount of the material and are currently in the process of investigating the reaction of **1** with an electrochemically generated superoxide radical anion ($O_2^{\bullet-}$). We were able to identify about 20-30% of the product **2**, while also the side products **3** and **4** are formed in the reaction. We are now changing the electrochemical reaction conditions to further optimize the yield of **2**. These results are not yet available and, therefore, cannot be included here. We are, however, confident that we can obtain the reaction product with higher yield and will then also investigate gold nanoclusters (AuNCs) which have been shown by Nakamura and coworkers to be efficient photocatalysts for oxidative cyclization of amino alcohols (*ACS Catal.* **2021**, *11*, 13180-13187).

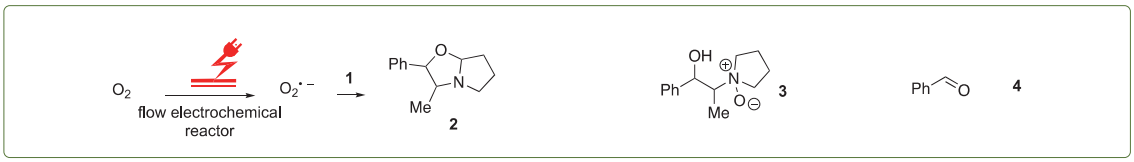

We will also proceed and employ alternative singlet oxygen sources (photochemical approaches, use of endo-peroxides) to effect the transformation, also investigating modified starting materials and include solvent modifications in the experiments.

Synthesis and characterization of raw and polymerized Asian lacquer samples: towards the development of a comprehensive collection of lacquer reference samples for materials science and conservation studies

Bonaduce Ilaria　University of Pisa

Urushi or Japanese lacquer is a natural product originating from the sap of the *Toxicodendron vernicifluum* tree. The sap is a water-in-oil emulsion composed of alk(en)ylcatechols (60-80%), water (10-30%), gum (3-6%) and enzymes (2-3%). It has long been employed as a coating and adhesive material for both practical and aesthetic purposes. Nevertheless, the complex nature of the cross-linked and heterogeneous material formed upon polymerization, and the fact that urushi formulations often include mixtures of several other components, have, so far, hindered a systematic and in-depth characterization of this material. The goal of this collaboration is to establish a comprehensive collection of realistic lacquer reference samples to improve our understanding of the role of lacquer components and additives in the chemical and physical properties of natural and artificial lacquer formulations. This knowledge would benefit the research in both art conservation (identification and conservation of ancient urushi artifacts) and materials science (development of new artificial lacquers).

The collaborators have selected and characterized unpolymerized urushi samples (raw and kurome-processed) and pigments (red ochre and carbon black). They have then successfully created several films of pure urushi and urushi mixed with the pigments (Figure 1). This was carried out under the supervision of Prof. Shimode, a renowned urushi artist, who explained how to mix urushi with pigments and guided the collaborators in the preparation of the samples following traditional recipes. The collaborators also visited a urushi shop, where they heard about the techniques used to obtain urushi from the raw sap. Finally, on 2024/2/2 a workshop was held at ICR where the collaborators presented their current research work related to urushi and discussed the future directions for this collaboration: i) refining the main research questions; ii) designing a new set of model samples to expand on the ones prepared during the visit; iii) defining the best methodological approaches for the molecular characterization of the polymerized samples, following the preliminary work carried out on the fresh materials.

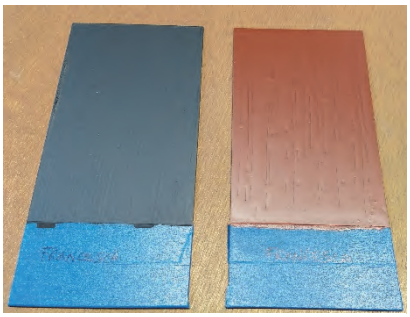

Figure 1 Left: polymerized film of black urushi. Right: polymerized film of red urushi.

Novel strategy for intracellular delivery of nanomedicines

Sílvia PUJALS　Institute for Advanced Chemistry of Catalonia

Nanomedicine arose 20 years ago with the promise of selectively delivering drugs to target sites, thus increasing their effectivity while minimizing undesired side effects. However, despite the great promise behind nanomedicine for drug delivery very few products have been approved for patient use. This poor translation into clinic comes from different factors, some of them being a poor characterization of the nanomaterials or a simplistic model to evaluate them. Poor cellular uptake efficacy of these nanomedicines is also a big obstacle. Sílvia PUJALS (PI) is a specialist on preparation of nanoparticles being applied for nanomedicine. She has also strong background of nanomaterials characterization and intracellular behavior using various microscopic techniques (including electron microscopy and super resolution microscopy). Shiroh Futaki is an expert on intracellular delivery of nanomedicines. This joint research aims to establish novel approaches for stimulating cellular uptake of nanomedicines created by Pujals group (IQAC) with the know-hows of Futaki group at ICR, Kyoto University. Thus, Sílvia PUJALS has visited the ICR, Kyoto University, in December, 2023, to give lectures and research discussions with the members of the Futaki laboratory. Aiming at a possible continuation and development of the collaboration, Sílvia PUJALS has applied for a research grant ("I-LINK" 2023) from the Spanish National Research Council (CSIC), entitled "Elucidating membrane remodelling in nanocarriers trafficking by advanced microscopy", which has been approved, while inviting an Israeli research team. The research team is now discussing the actual collaboration plan and possible procedures to apply for a more prestigious grant as the nest stage of the collaborative project.

Structural and functional analysis of curvature-inducing peptides and their applications

Anne S. Ulrich　Karlsruhe Institute of Technology

Spatiotemporal structural alterations in cellular membranes are the hallmark of many vital processes. In these cellular events, the induction of local changes in membrane curvature often plays a pivotal role. Many amphiphilic peptides can modulate membrane curvature, but there is little understanding of specific structural factors that direct the curvature change. Epsin-1 is a representative endogenous protein thought to initiate invagination of the plasma membrane upon clathrin-coated vesicles formation. Its N-terminal helical segment (EpN18) plays a key role in inducing positive membrane curvature. This study aimed to elucidate the essential structural features of EpN18 to understand general curvature-inducing mechanisms better, and to design effective tools for rationally controlling membrane curvature. Structural dissection of peptides derived from EpN18 revealed the decisive contribution of hydrophobic residues to (i) enhancing membrane interactions, (ii) helix structuring, (iii) inducing positive membrane curvature, and (iv) loosening lipid packing. The analog EpN18-L, in which all hydrophobic amino acids other than tryptophan were replaced with leucine, has the highest hydrophobicity and intrinsic helicity among all studied peptides, and it shows the strongest activity in terms of curvature induction and loosening of lipid-packing. Furthermore, this peptide promoted cytosolic translocation of R8 through the cell membrane, significantly more effective than the parent EpN18. As a conclusion from these studies, we also realized that a benign membrane-sculpturing peptide could be turned into a harmful membranolytic one once the membrane interactions become too strong. It would be interesting to confirm how transferable the results obtained in this study are to other curvature-modulating peptides or membrane-active peptides in general. A better understanding of these peptide-membrane interactions will lead to more rational approaches to modulating membrane curvature using peptides. Such tools should help to accurately regulate cellular phenomena related to membrane re-organization and, for instance, facilitate intracellular drug delivery, inhibit virus-cell fusion, prohibit biofouling, etc.. These results have been published in *Chemistry – A European Journal* [1].

[1] Nishimura et al., *Chem. Eur. J.* **2023**, 29, e202300129.

Molecular mechanisms for the inactivation of a growth hormone in rice

Zuhua He　Chinese Academy of Sciences

Objectives: Gibberellins (GAs) are a class of plant hormones that regulate diverse developmental processes, including seed germination, leaf expansion and stem elongation. They are tetracyclic diterpenoid carboxylic acids that are biosynthesized from the methylerythritol phosphate pathway in the plastid. Bioactive GAs play critical roles in promoting growth, including internode (stem) elongation of rice. The *elongated uppermost internode 2* (*eui2*) mutant of rice shows a tall phenotype due to its elongated uppermost internode. Because of this reason, this mutant has been utilized in hybrid rice breeding in order to eliminate panicle enclosure in male sterile parents. Previously, we have shown by map-based cloning that EUI2 is a functionally-uncharacterized protein that belongs to the α,β-fold hydrolase superfamily. In collaboration with Shinjiro Yamaguchi's group, we have previously characterized the rice *eui* mutant and found that *EUI* encodes a cytochrome P450 enzyme that deactivates GAs via 16α,17-epoxidation. Based on these results, we speculated that EUI2 might act as an epoxy hydrolase and further deactivate epoxidated GAs in the uppermost internode of rice. In fact, our collaboration showed that EUI2 protein could hydrolyze epoxy GAs *in vitro*. In addition, we determined the levels of endogenous 16α,17-epoxy GAs in wild type and the *eui2* mutant by LC-MS/MS analysis.

Experimental methods: Various 16,17-modified GA derivatives were chemically synthesized, and their biological activities were determined using GA-deficient rice seedlings. Endogenous levels of epoxy GAs in another genetic background of WT and *eui2* mutant rice plants were determined by LC-MS/MS using deuterium labeled epoxy GAs as internal standards.

Experimental results: Previously, we chemically synthesized 16,17-modified GA_4 derivatives. We found that many of them are weakly, but significantly active in promoting the elongation of uppermost internodes of rice. In addition, our data also showed that the biological activity of the hydrolyzed product (16,17-dihydroxy GA_4) was much weaker. This finding suggests that EUI2 plays a role in further deactivating epoxy GA_4. Previous X-ray crystallographic analysis of the GA_4-GID1 complex suggested that C-17 plays an important role in closing the lid of the GID1 receptor through hydrophobic interaction. Therefore, the introduction of a hydroxyl group at C-17 may inhibit this hydrophobic interaction. This would explain why 16,17-dihydroxy GA_4 (EUI2 product) is nearly inactive. To confirm the results obtained before, we analyzed endogenous epoxy GAs in another genetic background of WT and *eui2* mutant rice plants. Consistent with the previous data, the *eui2* mutant accumulated epoxy GAs at much higher levels than does WT.

Publications: In preparation (we have prepared a first draft of the paper).

Analysis of novel transporters for strigolactones or their biosynthetic intermediates

Yunde Zhao　University of California San Diego

Objectives: Strigolactones (SLs) are carotenoid-derived plant hormones that regulate various processes of plant growth and development. They are also secreted from plant roots into the rhizosphere and function as allelochemicals for symbiosis with arbuscular mycorrhizal fungi and for stimulating seed germination of parasitic plants. Classical grafting studies have suggested that SL and/or its biosynthetic intermediate(s) can move from roots to shoots, but much has not been fully elucidated about SL transport. Previously, we likely have identified novel transporters for SLs or intermediates for SL biosynthesis in rice. The knockout mutants of the transporters increased tiller numbers, which are phenotypically very similar to those well-characterized SL biosynthesis mutants and signaling mutants. The physiological and biochemical roles of the identified transporters need to be experimentally demonstrated.

Experimental methods:

Our group

• Phenotypic and genetic interaction studies of the mutants whose ability to transport SLs or SL biosynthetic intermediates have potentially been compromised.

• Generation of additional mutants using CRISPR/Cas9 gene-editing technology.

ICR partner researchers (Dr. Kiyoshi Mashiguchi, Prof. Shinjiro Yamaguchi)

• Analysis of the endogenous levels of SLs and SL biosynthetic intermediates by LC-MS/MS to find transporters' substrate(s).

• Elucidation of SLs and SL biosynthetic intermediates that can move from roots to shoots

• Evaluation of transporters' export/import activity toward the candidate compound(s).

Experimental results: We further conducted genetic studies on the putative SL transporters this year. By the last year, ICR partner researchers found that two SL biosynthetic intermediates, carlactone and carlactonoic acid (CLA), might be able to move from roots to shoots in Arabidopsis. In addition, they detected novel SL-related compounds in xylem sap in Arabidopsis and rice. This year, they have revealed the chemical structure of an SL-related compound commonly observed in Arabidopsis and rice. These results suggest that this compound is a common SL that moves from roots to shoots among species. This compound should be analyzed in the knockout mutants of the transporter candidates.

Publications: No publications from the collaboration in FY2023.

Cycloparaphenylenes and Chiral Fullerenes for Supramolecular Architectures in Chiroptical Applications

Matthew Fuchter　Imperial College London

The objective of this project was to explore, for the first time, the complexation of chiral fullerenes with cycloparaphenylenes (CPPs), with the expectation that such complexation would modify the chiroptical behaviour of the chiral fullerene. We were particularly interested in potential chirality transfer from the chiral guest to the non-chiral host.
[10]CPP, [11]CPP and [12]CPP were provided by our ICR project partner Prof. S. Yamago. The chiral bis-PCBM derivatives have been previously synthesized and separated in our group whereas a chiral open cage fullerene (cOCF) was provided by Prof. Y. Murata from ICR and separated into enantiomerically pure sample by our group using chiral HPLC. The complexation was studied using fluorescence titrations and the chiroptical properties were studied using CD-spectroscopy in combination with UV/Vis. Chirality transfer was further evaluated using circular polarized fluorescence spectroscopy.
Initially we attempted complexation of several chiral bis-PCBM derivatives with [11]CPP or [12]CPP. However, we observed no or only negligible quenching of the CPP emission, indicating no formation of the corresponding supramolecular complex.
In parallel we examined a chiral open cage fullerene (cOCF) derivative, which was found to be much easier to separate into its enantiomers and show a stronger chiroptical response than our chiral bis-PCBMs. We found strong quenching of the emission of [10]CPP in toluene upon addition of the cOCF, indicating the formation of a complex.
Subsequent UV/Vis and CD studies in solutions containing different ratios of cOCF and [10]CPP revealed a lowering of chiroptical activity for the complex compared to the pure cOCF. This interesting observation was further underpinned by computational studies performed by a collaborator, Prof. M. Zwijnenburg (University College London). These showed that a widening of the angle between the electric and magnetic transition dipole moments in the complex was responsible for the reduced chiroptical activity.
Circular polarized luminescence studies did not provide any detectable signal indicating that there is no measurable chirality transfer from the cOCF to the emissive [10]CPP.
Overall, our data so far shows how it is possible to manipulate the transition dipole moments of the supramolecular complex over the host or guest. Informed by this, we plan to continue our studies to design host-guest complexes in which complexation can lead to an enhancement of the chiroptical response.
Currently we are preparing a publication with the results obtained during this project.

Chiral cyclophenylene with a [2.2]paracyclophane core

Stefan Bräse　Karlsruhe Institute of Technology

Introduction. Cyclophane is a general term used to describe a cyclic hydrocarbon in which two or more aromatic rings are bridged together. The most well-known compound is [2.2]paracyclophane ([2.2]PCP, **1**), in which the benzene ring is bridged at the para position by two ethylene chains (Figure 1). Due to the close proximity of the two bridgehead carbons with a distance of 2.83 Å, which is significantly shorter than the sum of the van der Waals radius of the sp^2 carbon, [2.2]PCP possesses the trough-space (TS) interaction that occurs between the two benzene rings that face each other. Our laboratory has already synthesized [2.2]PCP derivatives with various substituents and elucidated their unique physical properties.[1)]

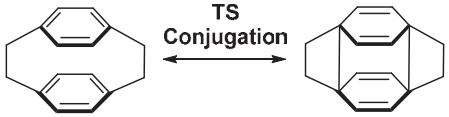

Figure 1. [2.2]paracyclophane ([2.2]PCP) and its resonance structure

We are interested in incorporating [2.2]PCP skeleton into the cycloparaphenylene, which is a π-conjugated oligomer with interesting physical properties derived from its ring structure. We have anticipated that the introduction of PCP can be expected to perturb the electronic structure of the cycloparaphenylene skeleton through TS conjugation. In this study, we considered using the cyclooligomerization of [2.2]PCP derivatives with Pt or Au complexes reported by Yamago[2)] or Tsuchido[3)], respectively, for the synthesis of cycloparaphenylenes. As there are several [2.2]PCP precursors for the cyclooligomerization, the feasibility of the synthesis has been estimated based on theoretical calculations.

Results and Discussion. There are seven possible [2.2]PCP isomers as precursors for [2.2]PCP-embedded cycloparaphenylenes (Figure 2a). We determined the structures, strain energies, and frontier orbitals of the cyclic trimers and tetramers obtained from these isomers at the B3LYP/6-31G* level of theory. Figure 2b shows the most stable isomers of cyclic tetramers and trimers formed from *para*- and pseudo *para*-precursors (Figure 2b). Strain energies of the cyclic tetramers are 170 and 158 kJ mol^{-1}, and those of the trimers are around 260 kJ mol^{-1}, which are significantly smaller than the parent [12] and [9]cycloparaphenylenes (205 and 280 kJ mol^{-1}, respectively). The results indicate that the synthesis of these cyclic oligomers is feasible. The analyses of frontier molecular orbitals indicate that the TS conjugation is less efficient than the conjugation among the paraphenylene units, except for the cyclic trimer formed from pseudo *para*-precursor (data are not shown here). Therefore, the synthesis of this molecule should be most interesting. The synthesis is currently underway.

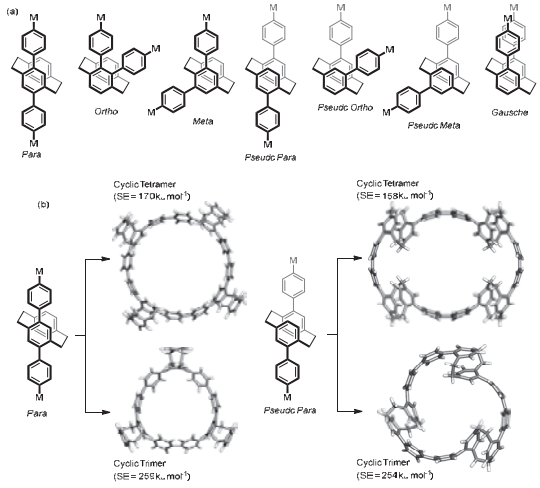

Figure 2. a) Possible [2.2]PCP isomers for the cyclooligomerization and b) the most stable structures and strain energies of the selected cyclic tetramers and trimers

Conclusion. Structures, strain energies, and frontier orbitals of cyclic tetramers and trimers formed from [2.2]PCP derivatives have been studied theoretically. The results indicate that these molecules are synthesizable and may have unique electronic properties.

References. 1) Hassan, Z.; Spuling, E.; Knoll, D. M.; Bräse, S. *Angew. Chem. Int. Ed.* **2020**, *59*, 215. 2) Yamago, S.; Watanabe, Y.; Iwamoto, T. *Angew. Chem. Int. Ed.* **2010**, *49*, 757. 3) Tsuchido, Y.; Abe, R.; Ide, T.; Osakada, K. *Angew. Chem. Int. Ed.* **2020**, *59*, 222928.

Development of Multi-dimensional Perovskite Light-emission and Photo-response Materials

Hao-Wu Lin　National Tsing Hua University

Developing high-performance halide perovskite optoelectronic devices, especially for photoresponse applications (e.g., solar cells, photodetectors), and light emission applications (e.g., light-emitting diodes). The research topics of this study encompass the syntheses, properties, and applications of multi-dimensional perovskites.

We initiated the project with three-dimensional multi-cation perovskites. The device structure is illustrated in Figure 1. The hole-transporting layer in the devices utilized 3PATAT-C3, a chemically adsorbed monolayer, developed by Prof. Wakamiya at Kyoto University.[1] It is noteworthy that the hole-collecting monolayers exhibit minimal parasitic absorption while providing conformal coverage on rough surfaces. The subsequent layers of halide perovskite, electron-transporting layers, interfacial layers, and electrodes were all vacuum-sublimed and developed by Prof. Hao-Wu Lin's group at NTHU.

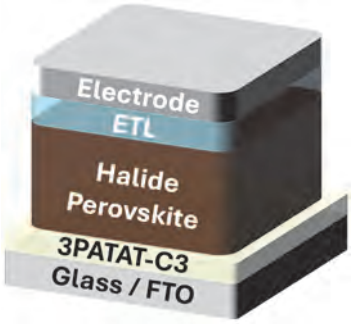

Fig. 1. Device structure of the perovskite photoresponse device.

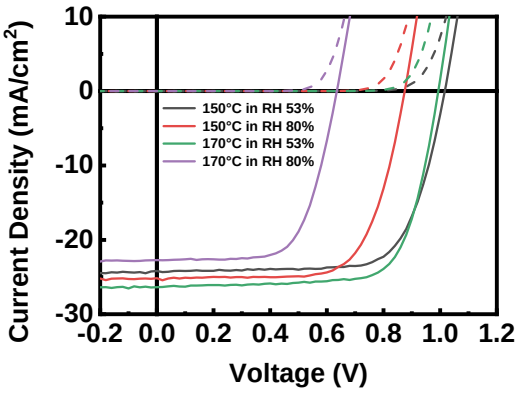

Fig. 2. Current density-voltage curve of the devices under 1-sun illumination.

The morphologies of vacuum-deposited perovskites and device performance were significantly influenced by the 3PATAT-C3 underlayers. The current best device characteristics and external quantum efficiency (EQE) spectra are presented in Figures 2 and 3, respectively. Through a comparison of EQE spectra with optically simulated results, we suspect that the lower response in the blue wavelength region is attributed to a thin layer of residual PbI_2. Further optimization as well as their applications in light-emission diodes are still ongoing.[2]

With the promising outcomes of this green-solvent process, we believe that our collaboration could not only enhance the research quality on both sides but also have substantial impacts on halide perovskite studies and the industry.

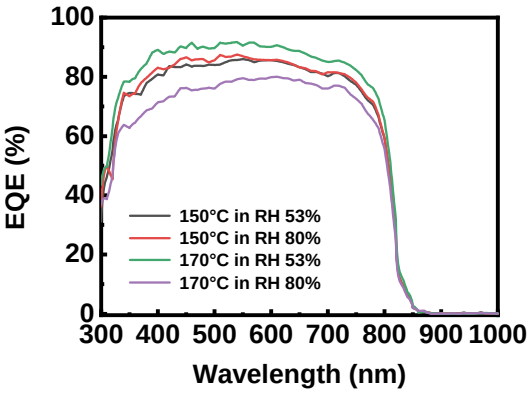

Fig. 3. External quantum efficiency spectra of the devices.

[1] M. A. Truong, T. Funasaki, L. Ueberricke, W. Nojo, R. Murdey, T. Yamada, S. Hu, A. Akatsuka, N. Sekiguchi, S. Hira, L. Xie, T. Nakamura, N. Shioya, D. Kan, Y. Tsuji, S. Iikubo, H. Yoshida, Y. Shimakawa, T. Hasegawa, Y. Kanemitsu, T. Suzuki, A. Wakamiya, *J. Am. Chem. Soc.* **2023**, *145*, 7528.

[2] C.-A. Hsieh, G.-H. Tan, Y.-T. Chuang, H.-C. Lin, P.-T. Lai, P.-E. Jan, B.-H. Chen, C.-H. Lu, S.-D. Yang, K.-Y. Hsiao, M.-Y. Lu, L.-Y. Chen, H.-W. Lin, *Adv. Sci.* **2023**, *10*, 2206076.

Precise synthesis and viscoelastic properties of ring polymers with high purity and high molecular weight

Atsushi Takano　Nagoya University

Introduction A ring polymer has topologically interesting molecular architecture with no chain ends and it is considered as a model polymer to clarify the topological effect on physical properties such as viscoelastic properties. The dynamics of ring polymers were theoretically predicted by several models such as lattice-animal model[1] and fractal loopy globule model[2], when the molecular weight of the rings is high enough to penetrate each other, it is predicted that they form strong entanglement as branched polymers. But high molecular weight ring polymers have not been experimentally synthesized so far because of the synthetic difficulty. In this study, ring polybutadienes (PBs) with relatively high molecular weight and high ring purity was prepared, and the melt rheology was measured and the dynamics of high molecular weight ring polymers was discussed.

Experimental A series of ring PBs with the molecular weight ranging 10k ≤ Mw ≤ 50k and with high ring purity (>99.5%) were carefully prepared by anionic polymerization and HPLC separation techniques[3]. Purity of rings was checked by interaction chromatography (IC) analyses[3]. The dynamic viscoelastic measurements of the linear/ring PBs were carried out by frequency sweep measurements with the temperature ranging -25°C ≤ T ≤ 25°C.

Results and Discussion Figure 1 shows the angular frequency ω dependence of the storage and loss moduli, G'(ω) and G"(ω) for high molecular weight sample, ring-50k, compared with the linear counterpart (linear-50k). The entanglement molecular weight (M_e) of PBs was calculated from G^0_N as M_e=2.1k. Linear-50k exhibits relatively long rubbery plateaus since the entanglement number is larger (M_w=50k=23M_e), while ring-50k did not reveal definite rubbery plateaus. It is confirmed that the longest relaxation times and zero-shear viscosities for the ring-50k and linear-50k are almost comparable, therefore it seems that this high molecular weight ring PB start entanglement each other as predicted by the theories mentioned above.

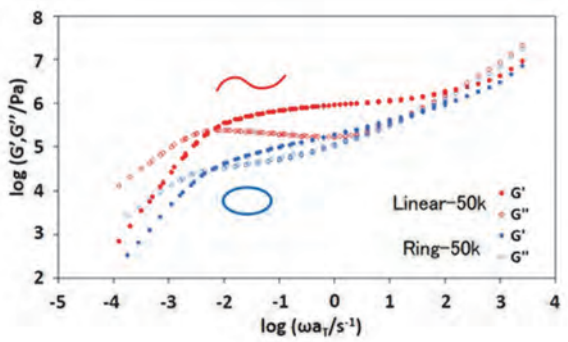

Figure 1: Master curves of G'and G" for ring/linear PBs (Mw=50k) at $T_{ref.}$=-15°C.

References

1. M, Rubinstein.; *Phys. Rev. Lett.* **1986**, 24, 3023-3026
2. T, Ge.; S, Panyukov.; M, Rubinstein.; *Macromolecules*. **2016**, 49, 708-722
3. Y, Doi.; K, Matsubara.; Y, Ohta.; T, Nakano.; D, Kawaguchi.; Y, Takahashi.; A, Takano.; Y, Matsushita.; *Macromolecules* **2015**,48,3140-3147

Correlation of concentration and orientation fluctuations in mixture of liquid crystal/solvent isotropic one-phase state

Ryoko Shimada　Japan Women's University

The dynamics in liquid crystal (LC)/solvent mixtures in the isotropic one-phase state can be characterized with the correlation of fluctuations of the concentration of LC molecules ϕ and the orientational order parameter of LC molecules Q. Despite extensive studies on the kinetics of the phase separation of various LC/solvent systems, this correlation was not fully understood. Our previous studies focused on a model mixture of 4-cyano-4'-pentylbiphenyl (5CB) and dimethyl phthalate (DMP) at a DMP concentration w_{DMP} = 3.1 wt% to reveal that the kinetic viscosity ν and the dielectric relaxation time τ_ε, reflecting the fluctuations of ϕ and Q, showed temperature (T) dependence that positively deviated, on a decrease of T, from the dependence in respective high-T asymptotes.[1, 2]

Based on this finding, this study was devoted for the dynamic light scattering (DLS) of the DMP/5CB mixtures with w_{DMP} = 3.1 and 5.0 wt%. Since the decay of the DLS signal was too fast and its time-constant, detecting the dynamics of the fluctuation of ϕ, was not determined very accurately. However, as a preliminary result, no angular dependence of the auto-correlation function was observed for those mixtures, indicating lack of the diffusive mode in the mixtures. Fig. 1 compares the DLS decay time τ_{DLS} and the dielectric relaxation time τ_ε in DMP/5CB mixture (w_{DMP} = 3.1 and 5.0 wt%). The DLS decay time τ_{DLS} was ~ten times longer than the dielectric relaxation time τ_ε, and the positive deviation of τ_{DLS} from its high-T asymptote is much stronger than that of τ_ε. This result suggests the correlation between the fluctuations of ϕ and Q: Faster fluctuation of Q (reflected in τ_ε) enhances the slower fluctuation of ϕ passively through coupling of rotational and translational modes of 5CB molecular motion. Further study is now planned for this hypothesis.

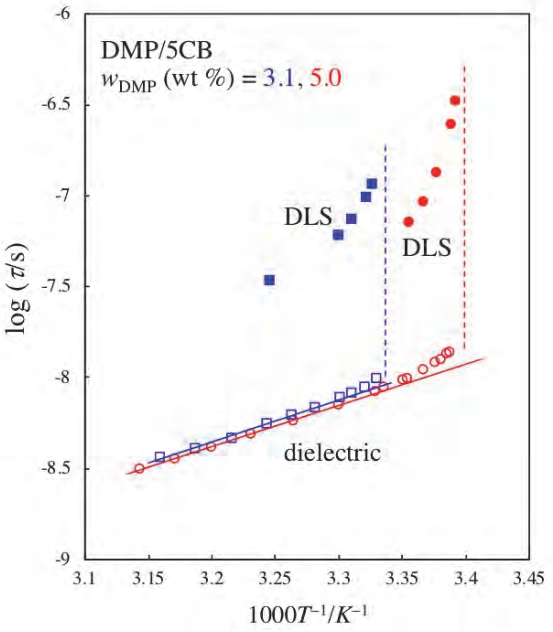

Fig. 1 Comparison of DLS decay time and dielectric relaxation time in DMP/5CB Mixture (w_{DMP} = 3.1 and 5.0 wt.%). Broken lines show $1/T_{IN}$, respectively.

1. R. Shimada and H. Watanabe, *J. Soc. Rheol. Japan*, **48**, 199 (2020).
2. R. Shimada et al., *Soft Matter*, **17**, 6259 (2021).

Evaluation of Mechanical Properties for Polymer Elastomers with Pseudo-Rotaxane Type Cross-Links

Osamu Urakawa　Osaka University

A movable crosslinking network (MCN) is a supramolecular network with high flexibility and toughness[1]. We investigated the dynamics of MCN consisting of a poly(methyl acrylate), poly(ethyl acrylate), and poly(butyl acrylate) backbone threaded through acetylated γ-cyclodextrins (AcγCD), which are connected to other chains. The threaded AcγCD moieties that act as movable crosslinking points can slide along the polymer backbones. We analyzed their sliding dynamics through viscoelastic and broadband dielectric spectroscopy (BDS) measurements. BDS measurements revealed that the relaxation mode, called "slow mode," appeared in the glass-to-rubber transition region (Fig. (a)). We ascribed this mode to the rotational motion of the rotaxane-type CD moieties via sliding motion on the polymer backbone as schematically shown in Fig.(b) [2]. The concentration of the rotaxane-type CDs (C_{eff}) was determined from the dielectric relaxation strength $\Delta\varepsilon$ ($\propto C_{\mathrm{eff}}$) of the slow mode. Fig.(c) shows that $\Delta\varepsilon$ decreases with increasing polymer chain thickness (r_{nAA}). We analyzed the rubbery plateau modulus G_N of MCNs, determined from the viscoelastic measurements for all samples with different polymer structures and various CD concentrations. The elastic modulus component due to rotaxane crosslinking was determined by subtracting the entanglement contribution from G_{N}. We found that those moduli were proportional to C_{eff} for each system. However, the proportionality coefficient decreased with decreasing r_{nAA}. This result suggests that fluctuations of the crosslinking points are more likely to occur for thinner chains.

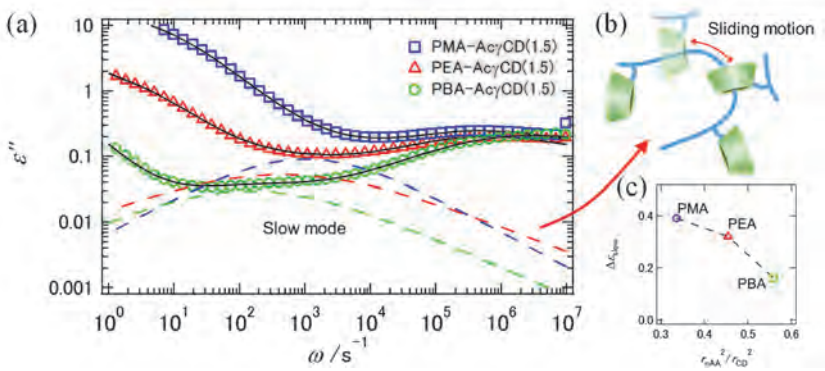

Figure (a) Dielectric loss cures for MCNs; (b)Schematic illustration of MCN; (c) $\Delta\varepsilon$ vs. r_{nAA}.

References

1) Ikura, R.; Park, J.; Osaki, M.; Yamaguchi, H.; Harada, A.; Takashima, Y. *Macromolecules* **2019**, 52(18), 6953−6962.
2) Kashiwagi, Y.; Urakawa, O.; Zhao, S.; Takashima, Y.; Harada, A.; Inoue, T. *Macromolecules* **2021**, 54(7), 3321–3333.

植物細胞の原形質流動におけるリン脂質の関わり

上田晴子　甲南大学

【目的】植物細胞では，小胞体をはじめとした細胞小器官がアクチン・ミオシン XI 依存的に高速で流動しており，この現象は原形質流動とよばれている．これまでの研究から，ミオシン XI が小胞体膜に結合し，アクチン繊維上を滑り運動しながら配向の揃った繊維束を構築することで，原形質流動を促進することがわかってきた．アクチンの重合・脱重合は厳密な制御を受けていることから，原形質流動にはアクチン繊維の動態がひとつの鍵になると考えられる．そこで本研究では，アクチン繊維の組織化を制御することが知られるリン脂質に着目し，原形質流動への関与を解析した．

【実験方法，結果，および考察】生体膜の成分であるリン脂質の影響を解析するためには，代謝酵素を利用した遺伝学的な手法が有効であると考え，2 種類の酵素に注目した．ホスホリパーゼ D (PLD) は，ホスファチジルコリンからホスファチジン酸とコリンを生成する酵素であり，一方のホスファチジルイノシトール 4 リン酸 5 キナーゼ (PIP5K) は，ホスファチジルイノシトール 4,5 二リン酸 [$PI(4,5)P_2$] を生成する酵素である．モデル植物シロイヌナズナは，これらの酵素をそれぞれ 12 および 11 遺伝子コードしており，共同研究者である青山博士らによって，さまざまな細胞機能における特異性と冗長性が報告されている．そこで，*pldζ1 pldζ2* 二重変異体および *pip5k1 pip5k2* 二重変異体に小胞体を可視化する蛍光マーカーを導入した形質転換体を作製し，野生型の小胞体パターンと比較した．その結果，*pldζ1 pldζ2* 二重変異体の一部の細胞で，小胞体の運動が抑制され，その分布パターンに異常が観察された．分布パターンの変化にはアクチン繊維の影響が強く示唆されたため，アクチン繊維を同時に可視化して，小胞体とアクチン繊維の関係を詳細に比較する必要がある．本研究で注目した酵素群は，植物の成長分化のみならず，ストレス応答に関与する例も報告されている．観察した *pldζ1 pldζ2* 二重変異体はいずれも野生型と同様に生育したが，小胞体の異常には程度の差があったことから，解析ごとの微妙な生育環境の差などが影響した可能性が考えられた．今後，これらの変異体を用いて乾燥状態をはじめとした生育条件の変化による小胞体の運動性や分布パターンに与える影響を調べ，原形質流動におけるリン脂質の関与を明らかにすることで，さまざまな環境ストレスに対する植物の生存戦略の解明の一端につながることが期待される．

Real-Time Visualization of Cellular Phase-Separating Proteins

Kazuya Kikuchi　Osaka University

Objectives

A growing number of proteins contain disordered regions of low-sequence complexity which induces protein condensation via liquid-liquid phase separation (LLPS). Although these protein condensates initially have liquid-like properties, they can also age into more solid-like states, leading to many diseases. The goal of the present collaboration is to develop a new chemical technique that allows us to monitor the transition of liquid-liquid phase separation into the more solid or viscous state in live cells.

Results

Together with the Uesugi group of ICR, we developed a new chemical technique that detects the status of protein condensates. This fluorescence-based technique uses a unique protein labeling method (PYP method) that has been developed by our group in Osaka. The PYP method takes advantage of the relatively small size of PYP protein for visualizing proteins of interest fused with PYP. First, HEK293 and U2OS cells were transfected with each of 17 plasmids that encode a PYP protein fused to 17 different phase-separating proteins. The addition of a PYP ligand fluorescent probe into the culture medium permitted the detection of the 17 PYP fused phase-separating proteins in live cells under a confocal microscope. To monitor the formation of solid-like condensates, we performed pulse-chase analysis, in which PYP ligand probes with different colors were added at different time points. We found that solidified protein condensates were labeled only by Orange probe, while the remaining liquid protein condensates were double-labeled with both Orange and Far-red probes. These results were further confirmed by FRAP technique (Fluorescence recovery after photobleaching).

The new method allowed us to analyze solid aggregates and liquid condensates quantitatively. Sorting of the cells harboring those proteins by a FACS machine facilitated ranking the 17 phase-separating proteins to identify the highly aggregating protein under different conditions. The use of this method for genetic or chemical screenings may lead to the discovery of factors and molecules that mitigate the liquid-to-solid transition of particular pathological proteins.

Remote Control of Cells by Synthetic Small Molecules

Makiya Nishikawa　Tokyo University of Science

The ICR's Uesugi group achieved a milestone in cell magnetization by utilizing synthetic paramagnetic tyrosine (m-YR1). The primary objective of the collaborative research conducted in FY2023 was to refine the robustness of their cell-magnetization technique with the goal of precise control over transplanted cells within animals.

In conjunction with the Uesugi group, our team previously explored the feasibility of manipulating the metastasis location through the application of a magnetic field. Melanoma cells, magnetized using the Uesugi group's established method, were introduced via tail vein injection into mice equipped with a neodymium magnet positioned in the chest. Unfortunately, the directed migration of magnetized melanoma cells to the lungs was not clearly observed in the presence of an external magnetic field. This limitation may be attributed to the insufficient magnetic responsiveness of the artificial melanin within the mouse body.

In FY2023, the Uesugi group and our team endeavored to enhance cell magnetization to broaden the applicability of the methodology. By selectively incorporating melanogenic enzymes into HEK 293 cells, they effectively extended the functionality of the system to non-melanocytes. Simultaneously, we analyzed the stability of synthetic paramagnetic tyrosines (m-YR1). LC-MS analysis of m-YR1 revealed a notable decline in peak intensity within 12 hours. Our investigation identified the instability of m-YR1 stemming from the hydrolysis of the imine bond in the salen structure, leading to the dissociation of Fe (III) and subsequent loss of magnetism. This discovery presented an avenue for enhancing compound stability through the design of distinct analogs of m-YR1.

Pursuing this objective, we synthesized m-YR2 and m-YR3. In aqueous conditions, the half-life of m-YR1 was determined to be 9.56 hours, whereas m-YR2 and m-YR3 exhibited half-lives of 11.18 hours and 104 hours, respectively. Notably, m-YR2 and m-YR3 displayed heightened stability in water, prompting us to proceed with in vitro experiments. Comparative analysis among the three analogs, m-YR1-3, revealed superior alignment in m-YR2-treated samples in contrast to m-YR1 and m-YR3. This outcome signifies the greater efficacy of m-YR2 for our intended future applications.

量子化学計算と原子スケール分光による
ドナー・アクセプター分子系の探求

木村謙介　理化学研究所

近接したドナー(D)分子とアクセプター(A)分子により形成される電荷分離(CT)励起子の挙動は、光-電子変換、熱活性化遅延蛍光、光化学反応といった様々な機能の根源である。これらの現象には、ナノメートルスケールの局所領域で起こる励起子の挙動が重要であることから、高い空間分解能を有する光学測定手法が必要となる。しかしながら、従来の光を用いた測定手法では、光の回折限界が数百ナノメートルであることから空間分解能が不十分であった。研究代表者らが理化学研究所の Kim 研究室にて開発に従事してきた走査トンネル顕微鏡(STM)をベースとした発光測定手法は、トンネル電流を励起源として用いることで単一分子を可視化しつつ光学測定を行うことが可能であり、ナノメートルスケールで近接した DA 分子系の空間的な配置を決定したうえで光学測定ができると期待される。加えて、可視化によりモデル DA 分子系は構造をよく規定出来ることから、計算化学との親和性が高い。これらの検討に基づき、共同研究者である梶教授らによる化学研究所のスーパーコンピュータシステムを用いた量子化学計算と組合わせ、DA モデル分子系の学理構築を目指している。

昨年度の研究課題(2022-82)では、Mg フタロシアニン(MgPc)を D 分子、HAT-CN を A 分子として用い、近接させたときの DA 分子系からの新規な発光現象観測に成功した。図 1a のインセットに示した、STM 像で可視化された DA 分子系の構造に基づき量子科学計算を進めるなかで、このように DA 分子が横並びに近接した二量体ではπ-π相互作用が弱いことから MgPc 本来の発光と CT 発光の波長変化が小さく、実験的にも計算的にも議論が難しいことが分かった。そこで本年度は A 分子の二次元膜を作製し、その上に D 分子を吸着させることでπ-π相互作用が強い DA 分子系の作製を目指した。具体的には、Au(111)上に成長した NaCl 膜上に A 分子として C_{60} の分子膜を作製した(図 1b のインセット)。730 nm 近傍にメインピークを持つ STM 発光スペクトルが得られ、C_{60} の蛍光由来の発光であると結論づけた。また C_{60} 分子膜を詳細に STM 観察すると、分子ごとにコントラストが異なることが観測された。このコントラストの違いは C_{60} 分子の配向の違いに由来しており[1]、この分子膜の上に D 分子を吸着させると、種々の配向の DA 接合を作成できることが期待された。

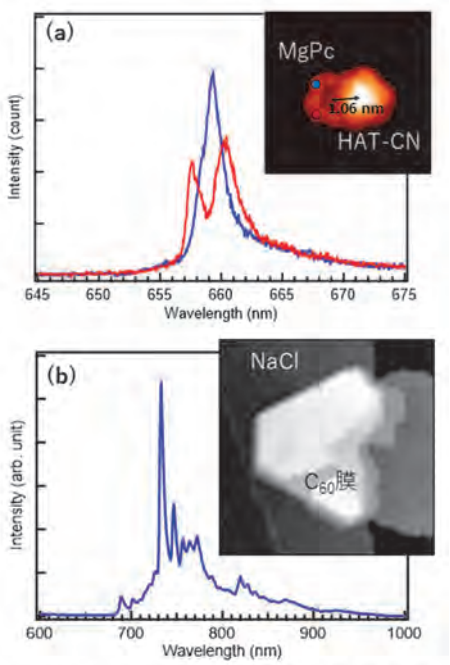

(a) MgPcとHAT-CN二量体のSTM発光スペクトルとSTM像。二量体内の探針を置く位置(赤丸・青丸)によってスペクトル形状が異なる。
(b) NaCl/Au(111)上に成長したC_{60}分子膜のSTM発光スペクトルとSTM像(50 x 50 nm^2)。

本研究に関しての具体的な成果報告は未だ行えていないが、逐次、学会発表および論文化を目指し研究を進めていく。

[1] F. Rossel *et al., Phys. Rev. B* 84, 075426 (2011).

Analysis of membrane lipid-dependent fermentation stress response in acetic acid bacteria

Yosuke Toyotake　Ritsumeikan University

[Introduction] Acetic acid bacteria (AAB) utilize phosphatidylcholine (PC) as a primary component of their membrane phospholipids (PLs). We previously created a PC-deficient mutant from *Acetobacter pasteurianus* SKU1108 and discovered that PC plays an important role in tolerance to low pH and high temperatures, as well as in resistance to organic acids, detergents, and oxidative conditions. PC is critical for maintaining the membrane integrity, but the exact relationship between the lack of PC, the resulting membrane disturbance, and the increased stress sensitivities remains unclear. One of the difficulties in studying this relationship is that AAB synthesize PC from other PL molecules, making it challenging to precisely control PC production to isolate its effects. To overcome this obstacle, we developed a new living cell system based on the SKU1108 strain. This system allows us to control PC production in a choline-dose-dependent manner, providing a unique opportunity to study how variations in membrane PC content influence the physicochemical properties of the membrane and the stress tolerance of this strain.

[Results and Discussion] AAB synthesize PC from phosphatidylethanolamine (PE) using PE *N*-methyltransferase (PmtA). We previously constructed a *pmtA*-deletion mutant (Δ*pmtA*) from the wild-type strain using the pKOS6b-mediated homologous recombination system. We then applied this system to introduce the gene encoding PC synthase (Pcs), a protein that condenses CDP-diacylglycerol with external choline, derived from *Pseudomonas aeruginosa*, into the specific location on the Δ*pmtA* genome (Fig. 1A). The resulting recombinant was named Δ*pmtA*+*pcs*.

To confirm the insertion of the *pcs* sequence, both the Δ*pmtA*+*pcs* and the wild-type genomes were subjected to PCR using the primers depicted in Fig. 1B. A distinct fragment (~ 1,500 bp) was obtained from Δ*pmtA*+*pcs* only when using pcs-ck-Fw and ck-Rv primers. On the other hand, a distinct fragment (~ 1,500 bp) was obtained from the wild-type only when using pmt-ck-Fw and ck-Rv primers (Fig. 1C). These results indicated that the *pcs* sequence was inserted at the genome location where *pmtA* sequence is located in the wild-type genome.

To confirm the phenotypes, Δ*pmtA*+*pcs* cells were grown in the medium with or without choline hydroxide (choline), and their PL compositions were analyzed by the thin layer chromatograhy. We found that Δ*pmtA*+*pcs* cells produced large amounts of PC and showed the acetic acid torelance similar to wild-type cells only when supplemented with choline in the medium. Thus, we successfully constructed a choline-dependent PC producing mutant of AAB.

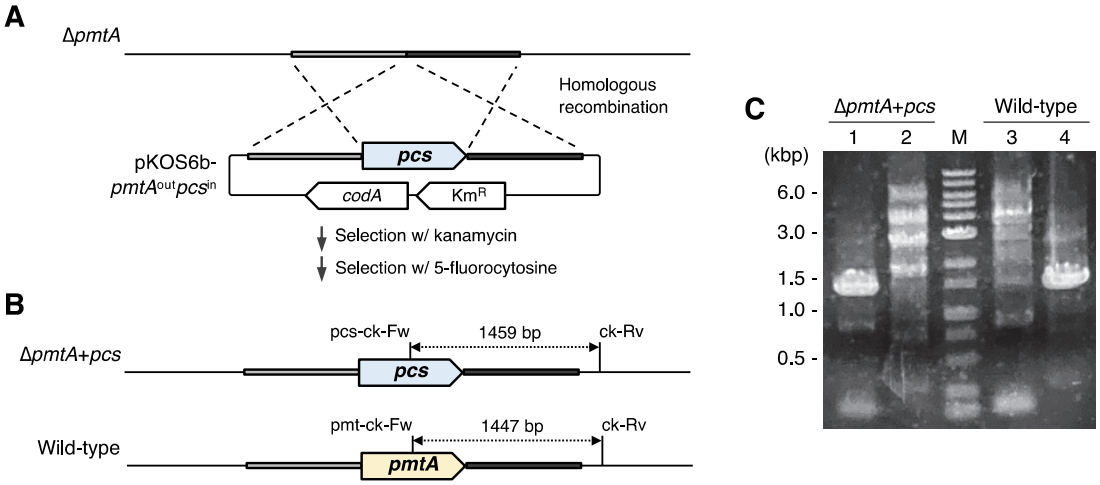

Fig. 1 Genetic engineering and analysis of the choline-dependent phosphatidylcholine (PC) producing mutant (Δ*pmtA*+*pcs*). (**A**) The plasmid pKOS6b-*pmtA*^{out}*pcs*^{in} harboring the upstream (light gray) and the downstream (dark gray) regions of *pmtA* connected by *pcs* was introduced into the *pmtA*-deletion mutant (Δ*pmtA*). Through homologous recombination between the pKOS6b-*pmtA*^{out}*pcs*^{in} and the genome, a plasmid-integrated Km^{R} recombinant was obtained. A second homologous recombination between two corresponding regions of the genome yielded a choline-dependent PC-producing mutant (Δ*pmtA*+*pcs*), in which *pcs* was inserted into the designated location on the genome. (**B**) The genomic difference between Δ*pmtA*+*pcs* and wild-type is depicted. The locations of *pcs* in Δ*pmtA*+*pcs* and *pmtA* in wild-type are identical. The primers used for PCR are indicated as pmt-ck-Fw, pcs-ck-Fw, and ck-Rv. (**C**) PCR-amplified DNA from the Δ*pmtA*+*pcs* genome using pcs-ck-Fw and ck-Rv (lane 1) or pmt-ck-Fw and ck-Rv (lane 2) and from the wild-type genome using pcs-ck-Fw and ck-Rv (lane 3) or pmt-ck-Fw and ck-Rv (lane 4) are shown. The DNA size maker is placed in the center (lane M). The genome and plasmid are not depicted to scale.

Studies on the structures and functions of two alanine dehydrogenases in *Geobacillus kaustophilus*

Taketo Ohmori　Osaka Institute of Technology

Introduction: Alanine dehydrogenase (AlaDH, EC 1.4.1.1) catalyzes the NAD-dependent reversible oxidative deamination of L-alanine to pyruvate. This enzyme is broadly distributed among various microorganisms and plays an important role in both alanine utilization and synthesis. In *Bacillus subtilis*, AlaDH is related to the energy supply during spore formation and is necessary for normal sporulation. We found that *Geobacillus kaustophilus* has two putative AlaDH genes (*GK2752* and *GK3448*, amino acid sequence identity: 75%) within its genome by using GenomeNet Database Resources. We constructed the expression vectors of *GK2752* and *GK3448*, respectively, and overexpressed these recombinant proteins using *Escherichia coli*. Both recombinant proteins showed the AlaDH activity. Furthermore, expression analysis of AlaDH revealed that the GK3448 enzyme is expressed only in the vegetative cells of *G. kaustophilus*. In this research, to understand the physiological function of the two AlaDHs in *G. kaustophilus*, we attempted to characterize the enzymatic properties of the two AlaDHs and to identify the AlaDH expressed in the spores.

Methods: To prepare the spores, *G. kaustophilus* was grown in the Difco sporulation medium. AlaDHs in spores were purified by ammonium sulfate precipitation, Dye-ligand chromatography and preparative Native-PAGE. The N-terminal sequence of the purified AlaDH was determined by protein sequencer PPSQ31A. The recombinant GK2752 and GK3448 enzymes were overexpressed by *E. coli* BL21(DE3), purified to homogeneity, and characterized in detail.

Results and Discussion: AlaDH expressed in spores was homogeneously purified by the method described above. N-terminal sequence analysis revealed that N-terminal sequence (12 amino acid residues, MKIGIPKEIKNN) of the purified AlaDH exhibited 100% identity with that of GK2752 enzyme. This result demonstrated that AlaDH from *GK2752* gene is expressed in only spore state of *G. kaustophilus*. These and previous results suggest that, in *G. kaustophilus*, two AlaDHs play distinct physiological roles at different growth stages. As results of functional analyses of the two recombinant enzymes, both enzymes showed high stability against low and high pHs and high temperature (70°C). Kinetic analyses showed that the activities of both enzymes proceeded according to the same sequentially ordered Bi-Ter mechanism. For oxidative deamination, the k_{cat}/K_m value of GK3448 (49 $mM^{-1}\cdot s^{-1}$) for L-Ala was slightly higher than that of GK2752 (31 $mM^{-1}\cdot s^{-1}$). Furthermore, for reductive amination, the k_{cat}/K_m value of GK3448 (1103 $mM^{-1}\cdot s^{-1}$) for pyruvate was also somewhat higher than that of GK2752 (937 $mM^{-1}\cdot s^{-1}$). Both enzymes showed substrate inhibition by L-Ala at concentrations above 12 mM, as well as dead-end inhibition by the product pyruvate. These results suggest that both AlaDHs exhibit similar enzymatic properties and are susceptible to several inhibitors, although the catalytic efficiency is slightly higher for GK3448.

Functional analysis and applications of extracellular vesicles produced by intestinal bacteria

Shino Yamasaki　Kansai University

Introduction:

The human gut hosts a diverse intestinal bacterial microbiota, which produces metabolites that can affect host physiology. Additionally, extracellular vesicles (EVs) produced by these bacteria are involved not only in bacterial– bacterial interactions but also in bacterial–host interactions such as host colonization and immune regulation. Herein, we analyzed the functions of intestinal bacteria-derived EVs and the associated EV-stimulated biological responses in the host.

Results:

1. Immunomodulatory effects of intestinal bacteria-derived EVs

The EV-producing ability of intestinal bacteria derived from human feces and immunostimulatory activity of the produced EVs were investigated. Gram-negative *Parabacteroides distensions* and *Megamonas funiformis* exhibited high EV-producing ability, whereas that of gram-positive *Ruminococcus gnavus* was less. *M. funiformis*-derived EVs induced interleukin-6 production in murine macrophage-like J774A.1 cells; therefore, *M. funiformis* is regarded as a high-EV-producing strain with immunostimulatory activity.

On the other hand, we showed that *Lactobacillus* and *Bifidobacterium* bacteria-derived EVs caused the activation of the toll-like receptor 2 on the surface of host immune cells for the elicitation of immunostimulatory effects. Fluorescence microscopy observation revealed that these EVs were localized on the surface layer of cells. We demonstrated the mechanism of action of EVs on host cells.

2. Proteomic analysis of EVs from *Shewanella vesiculosa* HM13

A psychrotrophic Gram-negative bacterium, *Shewanella vesiculosa* HM13, isolated from horse mackerel intestinal contents, produces abundant EVs. This bacterium secretes P49 as a major EV cargo. *S. vesiculosa* HM13 is expected to be useful as the host for production of foreign proteins as cargoes of EVs. Proteomic analysis of EVs from the P49-deficient mutant and its parent strain identified 211 and 130 proteins, respectively. The results showed that EVs of this strain contain predicted lipoproteins, HM705 and HM2707. Disruption of the genes coding for these proteins caused increase and decrease of EV production, respectively, shedding light on EV biogenesis mechanism.

金属酸化物の電気化学的制御と新奇物性探索

土屋敬志　物質・材料研究機構

機能性材料である遷移金属酸化物の構造・物性は遷移金属の価数と密接に関連している。水素や酸素などの脱挿入によって遷移金属の価数を制御することは、酸化物の新奇機能を開発やデバイス応用にも有用である。電界で制御可能な電気化学的な酸化還元反応を利用した場合には、可逆的に価数を変調でき、またプロトン注入によって新物質相の発見にもつながる。これまで我々は、ゲート層としてプロトン伝導性電解質であるナフィオンを用いたトランジスタ構造デバイスが遷移金属酸化物の電気化学的制御、さらにはプロトン注入による新物質開発に有用であることを明らかにしてきた。

本課題では、酸化物中で複数の価数状態を取りうることが可能なFeおよびCoを含んだ酸素欠損型ペロブスカイト酸化物Sr(Fe,Co)Oxに着目した。パルスレーザー堆積法で作製したSr(Fe,Co)Oxエピタキシャル薄膜をチャネルとし、ナフィオンをゲート層としたトランジスタ構造における電気化学的な水素脱挿入によって、Sr(Fe,Co)Ox薄膜の構造および電気抵抗の制御を行った。図1aに示すのはプロトン注入前後におけるSFCO薄膜のX線$2\theta/\theta$回折パターンである。どの組成の薄膜においても，黒矢印で示すように，プロトン注入後にはプロトン含有相の形成による新たなピークが見られた。一方で，弾性反跳検出分析（ERDA）の結果からは，薄膜中へ注入された水素量はFe/Co組成比に依存し，Co量の増加ともに水素量が増加することが分かった。またX線回折の結果からはCo量が0.3以上の薄膜では酸素欠損の規則配列に由来した(0 0 3/2)反射が観測されており，Sr(Fe,Co)Ox格子中の酸素欠損の規則配列が水素注入時における酸素欠損の形成を抑制する結果、SFCOへの水素の蓄積が促進されたと理解できる。また、図1bに示すように、Sr$(Fe_{0.5}Co_{0.5})O_{2.5}$薄膜においては、その電気抵抗が電気化学的な水素の脱挿入によって三桁にもわたって変調できることも見出した。

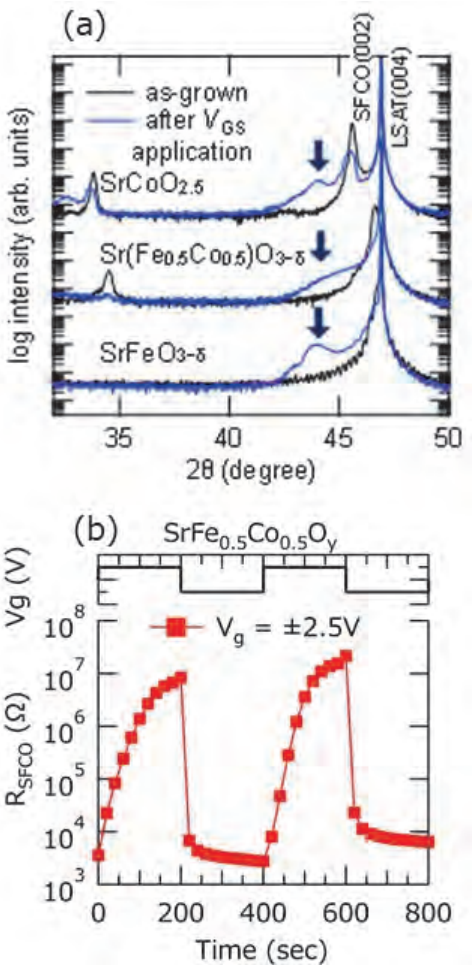

図１：(a)プロトン注入前後におけるSFCO薄膜のX線$2\theta/\theta$回折パターン．(b) $Sr(Fe_{0.5}Co_{0.5})O_{2.5}$薄膜におけるプロトン脱挿入に伴う抵抗変化

界面活性剤を含浸させた溶媒含浸樹脂による希土類元素の分離

倉橋健介　大阪公立大学工業高等専門学校

１．目的

希土類元素は小型で磁力の強い希土類磁石に使用されるほか、電池や触媒、発光材料といった日本の主要な製造業にて欠かすことのできない元素であることから、安定供給のため廃棄物や廃水から希土類元素を回収することが重要な課題となっている。我々の研究グループでは、溶媒抽出法に比べ、人体に有害な揮発性有機溶媒の利用が少ない固相抽出による Eu の分離において、多孔性樹脂に界面活性剤のみを含浸させた溶媒含浸樹脂（SIR）を用いることで、他の抽出剤の助けなく Eu を樹脂相へ吸着することが可能であり、また酸を用いることなく Eu の回収が可能であることを見出した。本研究では、この溶媒含浸樹脂を利用したレアアースの分離法を確立するため、他の金属元素との分離選択性を解明することで、分離法の最適化を試みた。

２．実験方法

Amberlite XAD-7HP をエタノールで洗浄し、減圧乾燥機で 1 日乾燥させた多孔性樹脂 1 g に、面活性剤として Sodium dodecyl sulfate (SDS)を 0.2 mmol 溶解させたエタノール溶液 20 mL を調製し、1 日間含浸させた。減圧留去で溶媒を除き、減圧乾燥機で 1 日間乾燥させて SIR を調製した。10.02 mM Eu, Zn と、緩衝剤として 0.05 M クロロ酢酸ナトリウムを含む水相を HCl，HNO_3, NaOH で任意の pH に調整し、この水相 2.5 mL に SIR 0.1 g を加え、恒温振とう機で 2 時間振とうさせた。振とう後、3000 rpm で 5 分間遠心分離を行い、水相を 2 mL 分取して pH を測定した。水相を採取後の樹脂に、1 M の HCl を 2 mL 加え、恒温振とう機で 15 分間振とうすることで逆抽出を行い、遠心分離の後に水相を分取した。抽出前、抽出後、逆抽出後の水相に含まれる金属濃度を、誘導結合プラズマ発光分光光度計(ICP-OES)を用いて測定し、抽出率および逆抽出による回収率を算出した。

３．結果と考察

水相の pH を 0.5～3.5 まで変化させて SIR への Eu と Zn 抽出率を測定したところ、Eu 抽出率は pH とともに増加し、pH 1.97～2.45 では 70%以上に達したが、pH 3 以上では低下した（図 1）。一方、Zn の抽出率も pH とともに増加したが抽出率は低く 20%以下だった。また、水相における Eu と Zn の初期濃度を、Zn が Eu の 10 倍となるように調製して同様の実験を行ったところ、抽出率の差は Eu と Zn が同濃度の場合と大きく変わらなかった。以上の結果から、SDS を含浸させた SIR を用いて、水相の pH を 2.4 とした抽出操作を 5 回繰り返すことで 10 倍存在した Zn を Eu の 5%未満とできると考えられる.

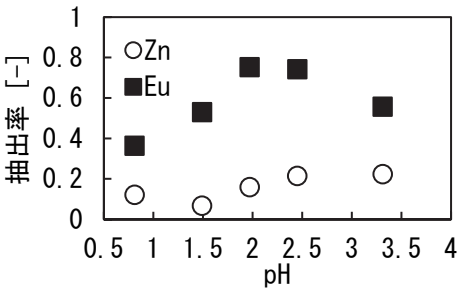

図 1　SDS を含浸させた SIR への Eu と Zn 抽出率の pH 依存性

４．成果報告

1） 小松智葉ら，第 26 回化学工学会学生発表会，オンライン開催，2024. 3.

ポリマーブラシ付与複合微粒子系潤滑添加剤の開発

大野工司　大阪公立大学

【目的】潤滑剤は、工業製品および製造工程における可動部品間の摩擦と摩耗を低減するために日常的かつ広範囲に使われている。近年の潤滑剤に関する研究課題の一つとして、その性能と効率を向上させられる機能性添加剤の開発があげられる。それにより、経済および環境問題の解決に取り組み持続可能な社会の実現に向けて貢献できると期待される。潤滑液添加剤として微粒子の利用が検討されているが、微粒子の粒径、形状、表面特性などの構造パラメーターが潤滑特性に及ぼす影響について十分には理解されていない。そこで、本研究では、表面開始リビングラジカル重合により、構造パラメーターの異なる各種ポリマーブラシ付与複合微粒子を合成することを行った。

【結果および考察】表面開始原子移動ラジカル重合(SI-ATRP)により、シリカナノ粒子表面およびチタンカーバイト系ナノシート表面をポリマーブラシで修飾することを行った。

ポリマーブラシ付与シリカナノ粒子の合成：直径 15 nm のシリカナノ粒子を ATRP 開始基含有シランカップリング剤で処理することにより、その表面に開始基を付与した。さらに、SI-ATRP によりポリメタクリル酸メチル(PMMA)をグラフトし、ポリマーブラシ付与シリカナノ粒子を合成した。シリカナノ粒子上の PMMA 鎖のグラフト密度は 0.7 chains/nm^2 と算出され、高密度グラフト化が進行したことが明らかとなった。重合条件を変えることにより、グラフト鎖の分子量が 2000～40000 まで異なる複合微粒子を合成でき、いずれの試料においても高密度グラフト化を確認した。また、**図 1** の透過型電子顕微鏡(TEM)写真が示すとおり、ポリマーブラシ付与シリカナノ粒子の凝集物は全く観察されなかったことから、極めて高い分散性が明らかとなった。

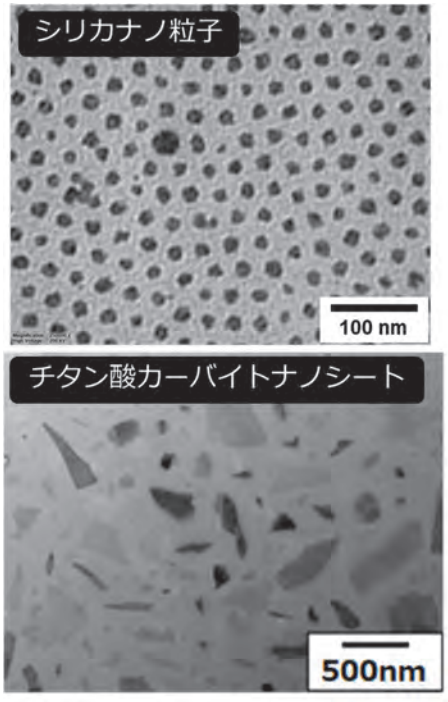

図 1. ポリマーブラシを付与したシリカナノ粒子および MXene の TEM 写真

ポリマーブラシ付与ナノシートの合成：チタンアルミニウムカーバイドを HCl および LiF で処理することにより、チタンカーバイト系ナノシート(MXene)を合成し、さらに ATRP 開始基を有するシランカップリング剤を用いて MXene 表面を修飾した。開始基固定化 MXene 表面からの ATRP は制御されて進行し、構造の明確なポリマーをグラフトすることに成功した。得られたポリマーブラシ付与 MXene は、全く凝集することなく極めて高い分散性を示した（**図1**）。

今後、上述した複合微粒子の潤滑液添加剤として機能を摩擦・摩耗試験を通じて評価する予定である。

3D プリンタを用いたモノリスの 3 次元構造制御

村瀬浩貴　共立女子大学

多孔材料は，各種の分離フィルタ，各種電池セパレータ，透湿防水布としての快適性衣料，海水淡水化膜や水浄化膜などの環境関連材料，血液透析膜や細胞培養基材などの医療材料など幅広い分野で利用されている。これまで，様々な多孔材料が実用化されてきたが，モノリス(Monolith)は３次元ネットワーク状の骨格構造を持ち，ネットワークの骨格サイズと，その空隙である連続空孔のサイズを独立に制御できる次世代多孔材料として注目されている。京都大学化学研究所の辻井敬亘教授と榊原圭太氏（元化学研究所助教、現産業技術総合研究所）は，界面化学的手法を駆使して，重合誘起スピノーダル分解を経由するエポキシ系ポリマーモノリスで新規な多孔材料を創生してきた。一方，報告者はこれまで、Additive Manufacturing（AM，3D Printing とも呼ばれる）の技術を応用して，新規な構造を有する複合繊維や繊維−樹脂複合型布帛の開発，セルロースナノファイバーの３次元造形に取り組んできた。本研究では AM の技術と，辻井教授らの界面制御技術・高性能モノリス合成技術を融合し，３次元構造を制御した新規ポリマーモノリスを創生することを目的とする。

前年度までは 3D プリンタを用いてポリマーモノリスの鋳型を作製する検討を実施してきたが，今年度は新たな試みとして 3D プリンタで直接ポリマーモノリスを造形する技術検討に着手した。3D プリンタの一つの形式として光造形方式がある。この方式では、紫外線照射によりモノマーを重合しながら造形する。造形用樹脂として多く用いられるのは紫外線硬化型エポキシ系樹脂である。まず、市販されている 3D プリンティング用の紫外線硬化樹脂（SK 本舗, Water Washable 10K Resin Neo Clear）と孔形成剤（Poly ethylene glycol）が混合可能であるか調査した。今回は Polyethylene glycol として融点が室温以上の物（キシダ化学, PEG2000）を使用した。PEG2000 を 80℃に加熱して溶融し，紫外線硬化樹脂と混合すると透明な混合物を得ることができた。均一に混合できたと推定する。この透明な混合物をスライドガラスに 80℃で加熱しながら滴下しカバーガラスで封止した。この溶液を徐冷しながら紫外線を 90 秒間照射すると白濁した硬化物が得られた。白濁した硬化物をカミソリで割断し、断面を走査型電子顕微鏡（日本電子製, JSM-IT200）で観察した結果が図 1 である。不完全ではあるが、相分離による多孔化が実現できていることが確認でき、光造形型 3D プリンタでモノリスを任意の形状に造形できる可能性が拓けた。今後は、最適な孔形成剤を選定し、実際に光造形型 3D プリンタでのモノリス造形を検討してゆく。

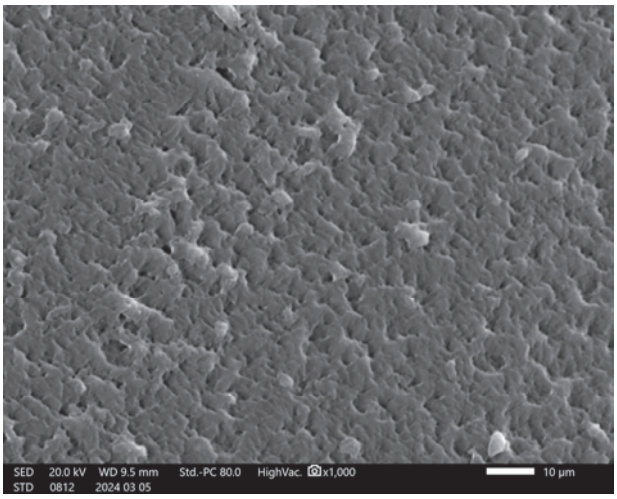

図 1.　3D プリンタ用紫外線硬化樹脂を用いた多孔構造

ポンププローブ過渡吸収分光法を駆使した三次元量子ドット超格子の超短時間光熱変換現象の解明

江目宏樹　山形大学

目的

光エネルギーと熱エネルギーとの変換を利用した機器が次々と提案されている。持続可能な近代的エネルギーを確保するため、太陽光エネルギーの有効利用は重要な課題である。太陽熱収集において、粒子構造体を活用しているが、その熱変換機構に関して、未だ検討できていない因子も多く、本質的な理論解明がなされているとは言い難い。すなわち、粒子構造の最適化や共鳴現象の活用によって増強されたプラズモンによる光エネルギーの吸収が、どのように熱エネルギーに変換されるのか、明らかにされていない。

化学研究所で独自に開発された Cu2-xS 量子ドット超格子ロッドは、迅速な一段階の液相法で得られる自立可能な三次元量子ドット集合体である。Cu2-xS 量子ドットは Cu+欠陥量（x）によってホール密度やバンドギャップを制御でき、かつ電圧印加や電子線照射により結晶構造が変化して異なる電子的特性を示すなど、電子材料として特異な挙動を有する。格子構造と光熱変換の関係を明らかにすることができれば、新たな熱回収性能の制御因子を提案し、これまで実現されてきた光からの熱エネルギー回収性能を超える新たな熱輸送制御技術をも実現できる可能性がある。

本研究は太陽光熱利用の技術革新を目指し、三次元量子ドット超格子の光－熱エネルギー変換メカニズムの解明を目的とする。具体的には光熱変換過程の超短時間計測を図り、研究を遂行する。

実験方法

Cu2-xS 超格子ナノロッドは化学的液相法により合成した。また、比較物質として単分散の Cu2-xS の合成も実施した。作製された試料に対し、光が物質に吸収される過程における、超短時間の電子励起状態の緩和過程や温度拡散過程などをフェムト秒過渡吸収分光光度計を用いて評価した。

結果と考察

単分散の Cu2-xS と Cu2-xS 超格子ナノロッドのブリーチング緩和過程の比較を図に示す。分散状態・超格子状態に関わらず、ブリーチング緩和は短い時間（約 2.0 ps）で終了する。超格子状態は分散状態に比べて吸光度変化の変化量が小さい。これが粒子構造の特徴なのか、光透過の問題なのか、検証するため、今後、装置の改造が課題となる。

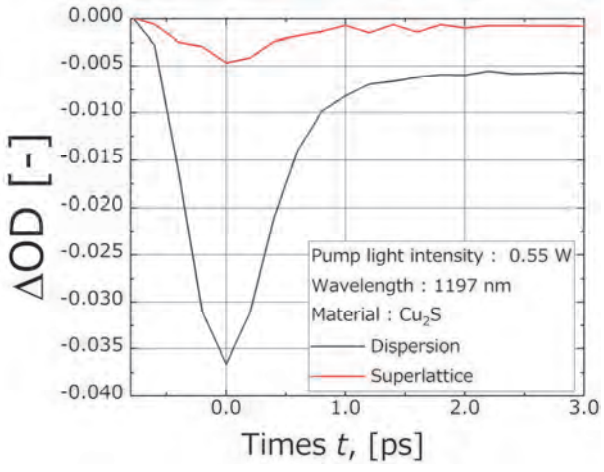

図　単分散の Cu2-xS と Cu2-xS 超格子ナノロッドのブリーチング緩和過程の比較

CdS/CdTe タイプ II 型二量体単一ナノ粒子を用いた世界最小ダイオードの室温動作

真島豊　東京工業大学

ナノギャップ電極間に単一半導体量子ドットを架橋すると、量子化したエネルギー準位を介した共鳴トンネル現象を観察することができる。タイプ II 型二量体ナノドットでは、電子と正孔の波動関数が異なる空間に閉じ込められているため、量子ドット内に内部電界を有している、本研究では、CdS/CdTe タイプ II 型二量体単一ナノドットをナノギャップ電極間に架橋し、内部電界に由来する世界最小の単一ナノ粒子ダイオード特性を観察すると共に、室温動作を実現することを目的とした。

電子線リソグラフィと独自の無電解金めっきを用いて、10 nm のギャップ長を有するヘテロエピタキシャル球状 Au/Pt ナノギャップ電極を作製した。寺西研究室にて合成した粒径 10 nm 程度のタイプ II 型 CdS/CdTe 二量体ナノドットを、アルカンジチオールを用いてナノギャップ間に化学吸着した。

得られた素子の電流－電圧特性を示す。9 K において±0.5 V 程度の範囲でクーロンブロッケード現象が観察され（図 1 (a)）、電流の立ち上がりは理論曲線（赤破線）とよく一致した。ゲート変調特性も観察されたことから、本素子は単電子トランジスタとして動作している。さらに同じ素子において±1.5 V 程度で非対称なさらなる電流の立ち上がりが観察された（図 1 (b)）。この整流性は、室温においても若干観察された。室温における電流値は数倍の増大に留まっているため、この電流はトンネル伝導が支配的である。この整流性の起源については、現在再現性を含め検討中である。

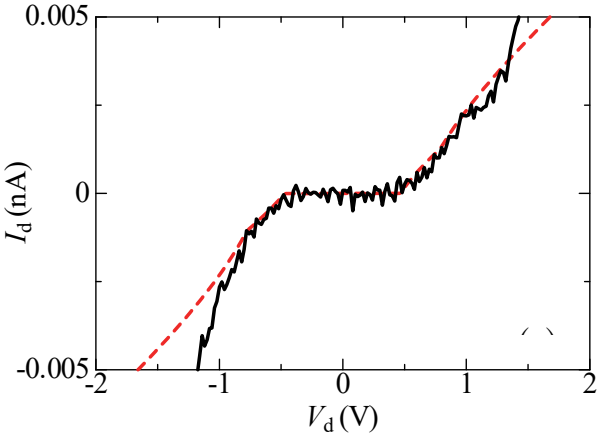

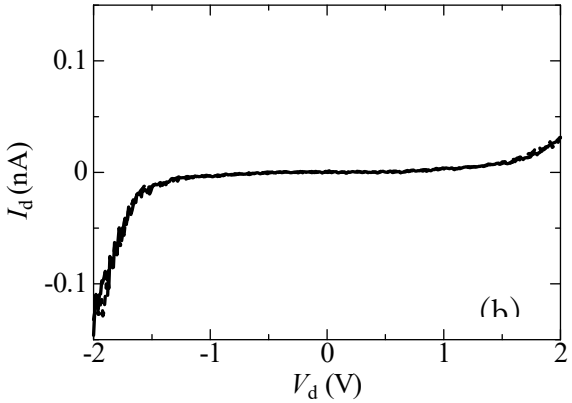

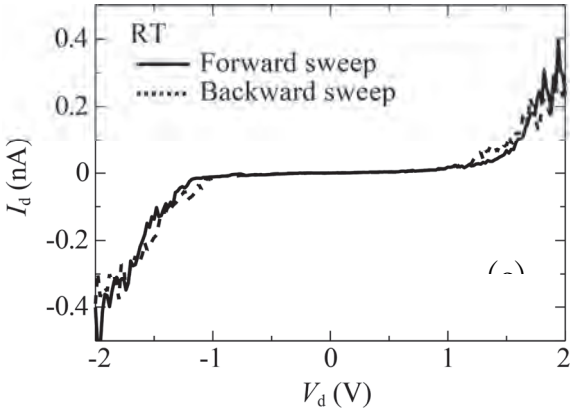

図 1 (a) ナノギャップ電極を用いた単一 CdS/CdTe 素子における、微少電流領域の電流―電圧特性（9 K)。赤破線は、クーロンブロッケード現象の理論解析結果。(b) 同素子における電流―電圧特性(9 K)。(c) 同素子における電流―電圧特性(室温)。

担持金属－金属酸化物クラスター複合化による協奏的触媒機能の創出

山添誠司　東京都立大学

近年，金属酸化物クラスター（ポリオキソメタレート，POM）を保護配位子とした金属ナノ粒子の合成および触媒応用が注目されている．しかし，担体に担持した不均一系触媒としての応用や Au 以外の金属への適用，金属-POM の協奏機能 の報告は限定的である．本研究では，担持 Ag ナノ粒子に POM を修飾し，本手法の汎用性を示すとともに，アルコールとアニリンの N-アルキル化反応へ適用した．

Al_2O_3 担持 Ag ナノ粒子触媒（Ag/Al_2O_3）は含浸法により調製した．Ag の担持量が 0.5wt.%となるように $AgNO_3$ 水溶液に Al_2O_3 を懸濁させ 353 K で蒸発乾固した．大気下，673 K で 5 h 焼成し，5% H_2 流通下，673 K で還元し，Ag/Al_2O_3 を得た．Ag に対し過剰量の$[Nb_6O_{19}]^{8-}$を含む $K_8Nb_6O_{19}$ 水溶液に Ag/Al_2O_3 を懸濁し，10 min 撹拌後，洗浄・回収し，真空乾燥することで$[Nb_6O_{19}]^{8-}$を修飾した Ag/Al_2O_3（Nb6-Ag/Al_2O_3）を得た．試料は走査透過電子顕微鏡（STEM）及びエネルギー分散型 X 線分析（EDX）及び X 線吸収分光により評価した．N-アルキル化反応はベンジルアルコールとアニリンを基質とし常圧反応容器にて行った．

STEM 測定から，Al_2O_3 担持 Ag ナノ粒子は平均粒径 3.0 nm で高分散に担持されており，EDX 分析から Ag ナノ粒子上に$[Nb_6O_{19}]^{8-}$が選択的に修飾されたことを明らかにした．Nb6-Ag/Al_2O_3 の Nb-K 殻広域 X 線吸収微細構造（EXAFS）は前駆体である $K_8Nb_6O_{19}$ 溶液の EXAFS と酷似しており，$[Nb_6O_{19}]^{8-}$は元の構造を保って修飾されたと結論した．以上より，本研究で用いた簡便な修飾法は担持 Au ナノ粒子のみならず，担持 Ag ナノ粒子にも適用可能な汎用的な修飾法といえる．

図 1 には，ベンジルアルコールとアニリンの N-アルキル化反応の収率を示す．Nb6-Ag/Al_2O_3 は本反応に対して 80%程度の転化率と高いイミン選択性を示した．Ag/Al_2O_3 に塩基として Cs_2CO_3 を加えると，N-アルキル化生成物である benzylideneaniline とイミノ基が水素化された N-phenylbenzylamine が生成し，イミン収率は約 40%であった．一方，塩基無しの Ag/Al_2O_3 もしくは Al_2O_3 に $K_8Nb_6O_{19}$ を含浸担持した触媒（$Nb6/Al_2O_3$）では活性，選択性ともに低かった．以上より本反応には Ag ナノ粒子と塩基の共存が重要であると結論した．このように，Ag ナノ粒子への塩基性の$[Nb_6O_{19}]^{8-}$の修飾により，外部塩基を加えることなく，選択的にクロスカップリング反応を進行させ，目的物のイミンが得られる不均一触媒系を構築した．

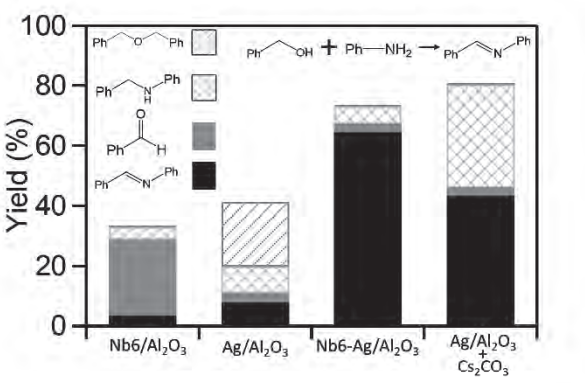

図 1 アルコールとアニリンの N-アルキル化反応の生成物収率.

本成果は *ACS Catal.* への投稿を予定している。

積層 CNT ターゲットへの高強度レーザー照射による高エネルギー電子生成に関する実験研究

松井隆太郎　京都大学

研究背景と目的：集光強度領域が $10^{18\text{-}19}$ W/cm^2 のフェムト秒高強度レーザーを物質に照射することで生成する相対論プラズマは、小型の粒子線癌治療装置や核融合炉の開発、高エネルギー宇宙線の生成起源の解明をはじめとした医療・産業・学術への幅広い応用が期待されている。我々は先行するシミュレーション研究により、ターゲットに波長オーダ（サブμm）の微細構造を付与し、それらを適切に設計・配置することで、プラズマの自己組織化過程を通じた準定常強磁場の生成と相対論プラズマの保持や、プラズマ指向性・電子温度の制御が可能であることを見いだしている[1]。特に、nm オーダのミクロな繊維状炭素の集合体であり、ロッド径を極限まで下げた媒質と位置付けられるカーボンナノチューブ（CNT）は、レーザー照射により高線量の相対論電子が生成されることから、癌治療への利用可能性が指摘されてる[2]。本研究では、レーザー生成プラズマの保持・制御を実現することで、粒子線治療や核融合に資するプラズマの新機能の創出を目指して、CNT に高強度レーザーを照射する実験を行い、レーザーとの相互作用特性と発生する高エネルギー電子の空間分布を調べた。

実験方法：本学エネルギー理工学研究所の松田一成教授から貸与の CNT を用いて、これに高強度レーザーを照射する実験を実施した。具体的には、厚さ 500 μm のシリコン基板上に作製された高さ 300 μm の CNT に対して、パルス幅および集光径が 40 fs と 5 μm（FWHM）で集光強度が 2×10^{19} W/cm^2 の京大化研・T^6 レーザーを CNT の軸方向（上面方向）、および、軸に垂直な方向（側面方向）から照射し、CNT の側面と上面の 2 方向に設置した同一の性能を有する電子スペクトルメータ(ESM)を用いて電子エネルギースペクトルの空間分布特性を調べた。

結果と考察：**図 1** は、(a)側面照射・(b)上面照射で得られた、CNT の上面方向の電子エネルギースペクトルである。どちらの場合も、500 keV 付近の領域に特徴的な平坦構造（**図の赤点線領域**）が現出していることが確認できる。一方で、側面方向では、上面・側面照射のどちらの場合においても、このような特徴的な構造は見られず、スペクトルは（微細構造を持たない）固体平板に照射した場合と似た構造となっていた。すなわち、CNT は、レーザーの照射方向に依らず、生成プラズマが上面方向に異方性を持つ媒質であることが明らかとなった。今後、プレパルスの影響を検証するとともに、この異方性を促進して方向性を持った高エネルギーの電子ビームとして取り出すなどの可能性を追求する。

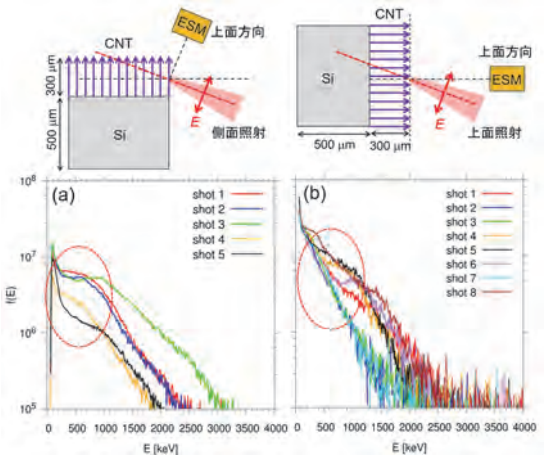

図 1　(a)側面照射・(b)上面照射における、CNT の軸方向（上面方向）の電子エネルギースペクトル。

成果報告：松井隆太郎，升野振一郎，橋田昌樹，阪部周二，時田茂樹，岸本泰明他，「レーザー駆動高エネルギー密度バルクプラズマの生成・制御に向けた CNT ターゲットの異方性の検証と新機能の創出」（口頭），レーザー学会学術講演会第 44 回年次大会．2024 年 1 月 19 日，東京。

参考文献：[1] R. Matsui, Y. Kishimoto *et al.*, International Conference on High Energy Density Sciences 2023, April 21st, 2023, Yokohama. [2] Dante Roa *et al.*, *Photonics* **9**, 403 (2022).

高強度レーザーと構造性媒質との相互作用による準定常強磁場の生成と検証

岸本泰明　京都大学

【計画全体の目的】集光強度が I~10^{18-20} W/cm^2 の高強度レーザーをサブμm オーダの微細構造を有する物質(構造性ターゲット)に照射することにより高エネルギー密度状態のプラズマを生成するとともに、その過程において現出するプラズマの自己組織化機能や構造形成機能を制御することにより、kT オーダの準定常強磁場の生成やそれによる生成プラズマの慣性時間を超えた保持(閉じ込め)を実現できる可能性を提案者等が指摘してきた[1]。これらは、自然界にない nm レベルの人工的な物質と光との相互作用の制御により新機能を創出するメタマテリアル概念に、高強度レーザー照射によって生成されるプラズマの要素を取り入れた非線形領域のメタマテリアル科学と位置付けられる。これが実現すれば、中性子を出さない究極の核融合である陽子・ホウ素(P-B)反応などの新たな応用が期待される。本研究では、ナノ工学と材料工学を用いて構造性ターゲットを作製するとともに、これに京大化研 T^6 レーザーを様々な視点から照射する実験を実施することにより、上記の仮説を検証することを目的とする(図 1 参照)。

【2023 年度の成果】上記の目標のもと、本年度は、前年度の成果をもとに、1)実験配位での磁場生成過程を再現・評価するシミュレーション、2)それを実験で検証するための高アスペクト比の各種ターゲットの開発、3)T^6 レーザーによるターゲット照射実験の実施等 に関する研究を進めた。

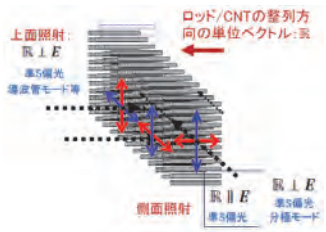

図 1: シミュレーションおよび実験で想定した.ロッド集合体への照射レーザーの方向と偏光の関係。

1)　図 2 は、サブμm サイズのロッド集合体にパルス長が 30fsec で 10^{19} W/cm^2 レベルの高強度レーザーを斜め照射したときに生成されたプラズマの β 値(上図)と位相空間(下図)のシミュレーション結果を表す。ロッド集合体の間隙に沿って電流路が形成されるとともに、それが $\nabla p=\mathbf{J}\times\mathbf{B}$ の平衡条件を満たしながら、陽子・ホウ素核融合に必要な数 100 keV のバルクプラズマを psec オーダで生成できることを確認した。尚、psec オーダの電流は $\mathbf{J}_{diamag}=(\mathbf{B}\times\nabla p)/\mathbf{B}^2$ による反磁性電流によって自己無撞着に維持される。

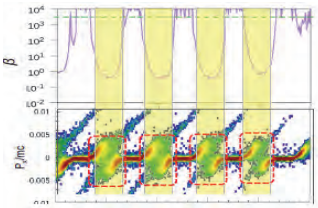

図 2: ロッド集合体へのレーザーの上面入射時に形成された磁場によりプラズマ β 値(上図)と位相空間(下図)

2)　非線形領域のメタマテリアル様の特性の一つとして、臨界密度を大きく上回ってプラズマ化したロッド集合体中を分極波としてレーザー光が伝播する特性が指摘されている[1]。この実験検証を 2024 年度に検討しているが、そのためには、より小さな半径でアスペクト比が大きなロッド集合体の作製が不可欠である。2023 年度は従来のリソグラフィー過程をネガ型からポジ型に変更することでよりアスペクト比が 50 に及ぶ精緻なターゲトを作製する方法論の開拓および条件出しを行い、対応する実験系の検討・構築を行った。

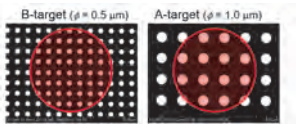

図 4: 同じ空間充填率 p=0.2 でロッド径が Φ=1μm(左)および Φ=0.5μm(右)の異なったロッド集合体へのレーザー照射実験。

3)　上記 2)で作製したターゲットを用いて、同じ空間充填率で半径が異なる二つのロッド集合体(Φ=1 μm および 0.5 μm)に対して上面方向から高強度レーザーを照射し、異なった方向からの電子エネルギーのスペクトルを 2 台の ESM で同時計測する実験を行った。その結果、半径が小さいロッド集合体(Φ=0.5 μm)のスペクトルは大きい場合(Φ=1.0 μm)に比べて高エネルギー成分が少なくバルクのエネルギーが低いことなど、理論・シミュレーションで予測した傾向が観測された。

参考文献:[1]Y. Kishimoto, et al., 10th IFSA 2017, St Malo, France, September 11-15 (2017).

[2] 岸本泰明, 松井隆太郎他: 2023年1月20日:物理学会2023年秋季大会 (東北大学2023年9月19日)。

細胞外小胞の標的細胞への移行メカニズムの解明

江口暁子　三重大学

研究代表者は、慢性肝疾患の病態進行過程において、障害肝細胞由来細胞外小胞(障害 HC-EV)と正常肝細胞由来細胞外小胞（正常 HC-EV）による標的細胞の活性化には、違いがあることを明らかにしている。しかし、障害 HC-EV と正常 HC-EV の標的細胞への取り込み量や取り込み経路の違いについては、全く解明できていない。そこで、本研究は、障害 HC-EV が細細胞間情報伝搬経路としてマクロピノサイトーシスを介して各種標的細胞へ取り込まれる機構を解明し、障害 HC-EV に特異的な取り込み経路を同定することを目的とする。この研究過程において、取り込み量の測定や取り込み経路の可視化等、様々な化学的な実験要素が必須となるため、化学研究所・二木史朗博士が開発した実験系を利用するために共同研究を実施することとした。本年度は特に、共同研究者である二木史朗博士がこれまでの研究で培ったマクロピノサイトーシス等の細胞への取り込み経路の実験条件を利用して、各種阻害剤を用いて細胞内移行経路に関して検討することで、障害 HC-EV と正常 HC-EV の標的細胞への取り込み経路を明らかにすることを目指した。

まず、腓腹筋の標的細胞である骨格筋細胞や腎臓の標的細胞であるメサンギウムへの取り込みを検討した。標的細胞に種々の取り込み阻害剤を添加した後、この障害マウスから HC-EV を精製し、近赤外細胞膜蛍光標識色素である PKH26 で標識した肝細胞由来 HC-EV を加え、共焦点顕微鏡とフローサイトメトリーにて取り込みを観察した。その結果、骨格筋細胞では Pitstop2 の添加により取り込み阻害がみられ、クラスリン依存性エンドサイトーシスが主取り込み経路であることがわかった。一方、メサンギウムでは nystatin と wortmannin の添加により取り込み阻害がみられ、カベオラ依存性エンドサイトーシスとマクロピノサイトーシスが主な取り込み経路であると推定された。肝細胞由来微粒子はフォスファチジルセリンを有することから、骨格筋細胞やメサンギウム細胞における PS 受容体の種類について検討した。その結果、細胞種により PS 受容体の発現量は異なることがわかった。現在、各細胞で発現が一番高い PS 受容体に注目し、PS 受容体を介した肝細胞由来微粒子の取り込みについて検討を進めている。

エクソソームの細胞内への送達設計

中瀬生彦　大阪公立大学

エクソソームは細胞が分泌するナノスケールの脂質小胞であり、生体における細胞間情報伝達に重要な役割を果たしている。内包した核酸・タンパク質等の生理活性分子を他細胞に送達できることや、生体由来で毒性が少ないことが予期されることから、エクソソームの特徴に注目した新たなDDSの開発が臨床治験も含め世界中で行われている。しかし、特に核酸を含む薬物の内包化や細胞内送達の効率など、技術的な問題点も多く残っており、本研究を通してエクソソームの効率的な細胞内送達法が開発できれば、エクソソーム DDS の実用化や治療への応用観点から大きなインパクトをもつ。

エクソソームの効率的細胞内への送達の試みの一つとして、研究代表者インクジェットシステムと膜透過性ペプチドを用いた簡便かつ細胞を傷つけない新たな細胞内導入技術の開発を進めた。蛍光標識したウイルス由来の膜透過性ペプチド（FHV coat (35-49)）をインクジェットプリンターのインクカートリッジ部分に相当するヘッド部分に入れ、ヒト子宮頸がん由来 HeLa 細胞に吐出し、細胞内移行を観察した。液滴の吐出スピードが増すほど、細胞膜通過および細胞内への移行効率が上昇することが確認でき、類表皮がんや乳がん細胞でも同様にFHVペプチドの高効率な細胞内移行を確認できた。このインクジェットシステムは、1滴をピコリットルレベルで制御できるだけでなく、1秒間で1,000回の連続高速吐出も可能であり、細胞膜を損傷させること無く目的分子が通過し、細胞内へ高効率に到達できるといった画期的な技術となりうる。狙ったがん細胞群に細胞死を誘導させるため、PAD（pro-apoptotoc domain）ペプチドの細胞内導入実験を行った。PADペプチドは細胞内に入ると、ミトコンドリアの膜を損傷させ、細胞死を誘導するが、PADペプチドだけでは細胞内への移行効率が低く、抗がん剤としては使用できない。本研究では、PAD ペプチドに FHV ペプチドを結合させ、さらにインクジェットシステムを用いた結果、高効率にがん細胞群に導入し細胞死を誘導することに成功した。さらにエクソソームも、stearyl-R8を用いて表面修飾することで、高効率でがん細胞内への導入が可能であることが確認できた。この成果は論文として発表するとともに、京都大学、大阪公立大学、JSTよりプレスリリースを行った。

論文：Omura M, Futaki S, Nakase I et al. Inkjet-Based Intracellular Delivery System that Effectively Utilizes Cell-Penetrating Peptides for Cytosolic Introduction of Biomacromolecules through the Cell Membrane. ACS Appl Mater Interfaces. 2023, 15, 47855-47865. doi: 10.1021/acsami.3c01650.

プレスリリース：膜を傷つけず細胞内に薬を届ける新技術！―インクジェットプリンター技術の活用でがん細胞に直接アプローチ―
https://www.kuicr.kyoto-u.ac.jp/sites/topics/231005/　(2023年10月5日)

Functional analysis of non-canonical strigolactones as plant hormones and root-derived signals

Yoshiya Seto　Meiji University

【The aim of this study】 Strigolactones (SLs) are plant hormones that regulate shoot branching, as well as being known to be rhizosphere signals that control symbiotic and parasitic relationship with arbuscular mycorrhizal fungi and root parasitic plants, respectively. SLs are biosynthesized from carotenoids via a key intermediate molecule called carlactone (CL). In a model plant, Arabidopsis, CL is further converted into carlactonoic acid (CLA) by a cytochrome P450 monooxygenase, MORE AXILLARY GROWTH1 (CYP711A). We previously identified a methyl esterified derivative of CLA, methylcarlactonoate (MeCLA) in Arabidopsis, and found that MeCLA can interact with the Arabidopsis SL receptor protein, AtD14. On the other hand, CL and CLA were not able to interact with AtD14, suggesting that the methyl esterification step is critical to convert a biologically inactive precursor to a bioactive hormone molecule. Conventional SL molecules have the tricyclic lactone ring part (ABC-ring) that is connected to another butanolide lactone part (D-ring) via an enol ether bridge. However, CL derivatives lack BC ring system, and possesses only A and D rings. After the discovery of CL derivatives, structurally similar molecules have been isolated from various plant species. Currently, these new types of SL molecules are classified to be ‘non-canonical’ SLs, whereas the conventional SLs are called ‘canonical’ SL (Fig. 1). Although, these new types of SL molecules have been identified, the functional difference between canonical and non-canonical SLs are not fully understood. In this collaborating project with Prof. Shinjiro Yamaguchi in ICR, Kyoto University, we planned to clarify the biological role of non-canonical SL using an important crop, tomato. MeCLA is thought to be a common precursor for non-canonical SLs, thus we aimed to identify the CLA methyltransferase in tomato (*Solanum lycopersicum* CLA methyltransferase; SlCLAMT), and analyze its physiological role.

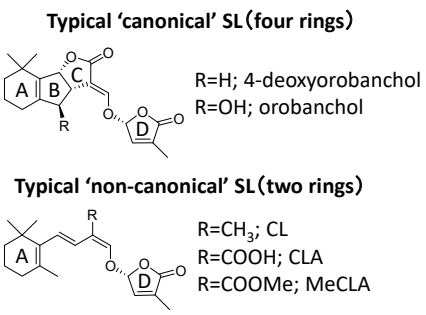

Fig. 1. Structures of ‘canonical’ and ‘non-canonical’ SL

【Results】 We made the *SlCLAMT* knockout mutants by genome editing and analyzed its phenotype. We found that the *slclamt* mutant showed an increased shoot branching phenotype and the phenotype was very similar to that of the *ccd8* knockout mutant, which is defective in an earlier step of SL biosynthesis. We also analyzed endogenous SLs in the *slclamt* mutant and found that possibly OH-CLA is highly accumulated in this mutant. We detected a possibly hydroxylated MeCLA (OH-MeCLA) in the *d14* mutant, in which the receptor gene is deficient. We also found that the *slclamt* mutant produces canonical SLs such as solanacol and orobanchol. These results indicate a distinct physiological role between canonical and non-canonical SL, and that non-canonical SLs have a crucial function in shoot branching inhibition in tomato.

超分子化学による合成ポリマーの精密配列制御

灰野岳晴　広島大学

当研究室は，カリックス[5]アレーン（C5A）がフラーレン(C_{60})の良いホストとして働くことを見出した。また，この C5A と C_{60} のホスト–ゲスト錯形成を超分子ブロックポリマー構築の駆動力に用いることで，ポリメチルメタクリレートとポリスチレンの超分子ジブロックポリマーの合成に成功した[1]。この結果から，C5A と C_{60} の強いホスト–ゲスト錯形成能は両親媒性ブロックポリマー形成の駆動力として有効であると考え，今回新たに，親水性と疎水性のポリマーを連結した両親媒性の超分子ジブロックポリマーの構築を目的とした。C5A に親水性のポリエチレングリコール（PEG）を導入した poly-**1** と C_{60} に疎水性のポリスチレン（PS）を導入した poly-**2a** および poly-**2b** を合成し，poly-**1** と poly-**2a** または poly-**2b** を混合することで，C5A が C_{60} を包接し，両親媒性ジブロックポリマーである poly-**1•2a** および poly-**1•2b** を形成すると考えられる(Fig. 1)。

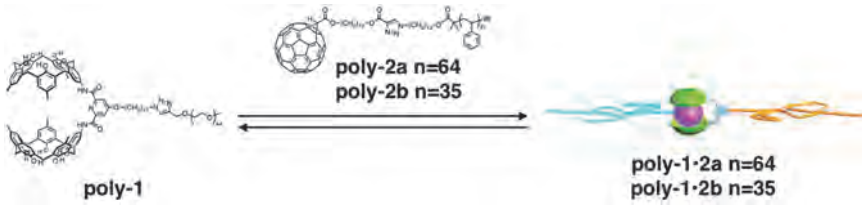

Fig. 1 Amphiphilic block copolymers were formed through host–guest interactions of C5A and C_{60}.

得られた poly-**1** と poly-**2a** の会合体形成を確認するため，UV スペクトル測定を行った（Fig. 2a)。poly-**2a** の溶液に poly-**1** を滴下していくと，400nm から 500nm にかけて吸収スペクトルの増加が観測された。この波長領域において poly-**1** は吸収をもたないため，このスペクトル変化は会合体由来であると考えられる。UV スペクトル測定の結果から，25℃における poly-**1•2a** の会合定数は 1.81×10^4 L mol^{-1} と見積もられた。これは，先行研究で報告されている会合定数と近い値を示したため親媒性の違うポリマーでも問題なく会合体を形成することが示唆された。続いて，DOSY 測定により拡散係数を調べることにより，会合体形成の確認を行った（Fig. 2b)。poly-**1** および poly-**2a** それぞれの溶液と poly-**1** と poly-**2a** の混合溶液について拡散係数を見積もったところ，poly-**1** と poly-**2a** の混合溶液の拡散係数は，poly-**1** および poly-**2a** のみの拡散係数より減少した。拡散係数は溶液中に存在する化学種の大きさに反比例することから，混合溶液では大きな構造体，すなわち poly-**1•2a** が生成していることが示唆された。また，短いポリマーである poly-**2b** と poly-**1** の混合物を用いて測定を行ったところ同様の傾向が見られたことから，poly-**1•2b** の生成が示唆された。

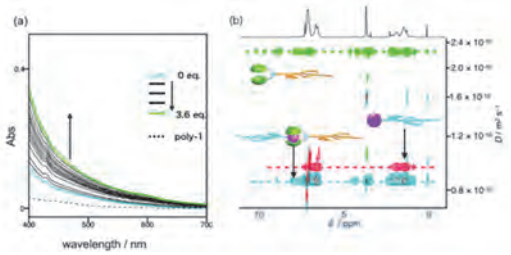

Fig. 2 (a) Changes in the UV spectra of poly-**2a** (2.0×10^{-5} mol L^{-1}) upon the addition of poly-**1** at 298K in toluene. (b) 2D DOSY spectra of poly-**1** (10 mmol L^{-1}), poly-2 (10 mmol L^{-1}) and a mixture of poly-**1** (10 mmol L^{-1}) and poly-**2a** (10 mmol L^{-1}) at 298K in chloroform-*d*.

発表論文

1. Hirao, T.; Haino, T. *J. Porphyr. Phthalocyanines* **2023**, *27*, 966 - 979.
2. Hirao, T.; Kishino, S.; Haino, T. *Chem. Commun.* **2023**, *59*, 2421-2424.
3. Nitta, N.; Kihara, S.-i.; Haino, T. *Angew. Chem. Int. Ed.* **2023**, *62*, e202219001.
4. Arimura, S.; Matsumoto, I.; Sekiya, R.; Haino, T. *Angew. Chem. Int. Ed.* **2024**, *63*, e202315508.
5. Fujimoto, H.; Hirao, T.; Haino, T. *Bull. Chem. Soc. Jpn.* **2024**, *96*, in press. DOI: 10.1093/bulcsj/uoad016

Determine the three-dimensional structure of $^{13}C=^{18}O$ labeled α-synucln(61-95) in the Langmuir-Blodgett film and supported phospholipid bilayer by MAIRS2

Chengshan Wang　Middle Tennessee State University

A. Objectives:

1. $^{13}C=^{18}O$ labeled α-syn(61-95) containing residues 61-95 of α-synuclein will be synthesized and purified.
2. Screen the conformation and orientation of specific amino acid residue of α-syn(61-95) in Langmuir-Blodgett film.
3. Screen the conformation and orientation of specific amino acid residue of α-syn(61-95) in supported phospholipids bilayers.

B. Experimental methods:

Peptide of ^{13}C labeled α-syn(61－95) at position 68G was synthesized via solid phase (Fmoc) chemistry and purified by semipreparative reversed-phase high-performance liquid chromatography (RP-HPLC) on Waters Breeze 2 separation system equipped with 1525 EF binary pump. The success of the synthesis and the purity of the peptide were confirmed by a Waters SYNAPT q-TOF tandem mass spectrometer. The surface pressure-area (π−A) isotherm of α-syn(61－95) were conducted in a A Kibron μtrough. The Langmuir-Blodgett (LB) films of α-syn(61－95) were made by transferring the α-syn(61－95) Langmuir monolayers to quartz slides and silicon (Si) slides under the surface pressure 6 mN/m under various time as mentioned in the Results. p-Polarized Multiple-Angle Incidence Resolution Spectroscopy (pMAIRS) measurements were performed on the Nicolet IS50 FT-IR spectrometer (Thermo Scientific, Waltham, MA) equipped with a pMAIRS accessory. The LB film monolayer of the ^{13}C labeled α-syn(61－95) at position 68G on Si substrate was put in the pMAIRS accessory and the IR beam transmitted trough the sample.

C. Experimental results:

The stability study of Langmuir monolayer of α-syn(61－95) is shown in Figure 1A. The α-syn(61－95) Langmuir monolayer was compressed to a surface pressure of 6 mN/m and the surface pressure was kept constant over two hours. The surface pressure (solid line curve) and area (dashed line curve) were monitored over the entire experiment. The molecular area decreased more than 30 % within the first one hour. After that, the molecular area decreased only about 1% for the second hour compression. To clarify the decreasing of the area, unlabeled α-syn(61－95) monolayer was transferred to Si substrate after two hours compression and the pMAIRS results are shown in Figure 1B. Similar to the published results with the

compression for only 15 minutes, the peak position of amide I band in both IP and OP spectra is at 1658 cm^{-1} which is the characteristic peak of α-helix. However, the intensity of the peak at 1658 cm^{-1} in OP result was lower than that transferred at 6 mN/m for 15 minutes as previously published. The tilt angle of the amide I transition moment after two hours compression is 21.2°, also significantly lower than ~31 ° for the monolayer with the compression for only 15 minutes. A peak at 1715 cm^{-1} arised in the OP result (the bottom curve in Figure 1B). This novel peak indicates a new conformation. To validate the conformation change, ^{13}C label was introduced into the backbone carbonyl at 68G. The pMAIRS results of the ^{13}C labeled α-syn(61－95) is shown in Figure 1C with similar IP result, which mainly detected the regular amide I band at 1658 cm^{-1}. However, a novel peak at 1685 cm^{-1} was detected in the OP result in addition to the regular and ^{13}C amide I band at 1658 and 1625 cm^{-1}, respectively. 1625 cm-1 is the ^{13}C amide I band of helix, with the regular band at 1658 cm^{-1}. Similarly, 1685 cm^{-1} is also 30 cm^{-1} lower than that at 1715 cm^{-1} and they are from the same conformation. Due to the spontaneous detection of the peak at 1685 and 1625 cm^{-1}, equilibrating conformations are detected at 68G.

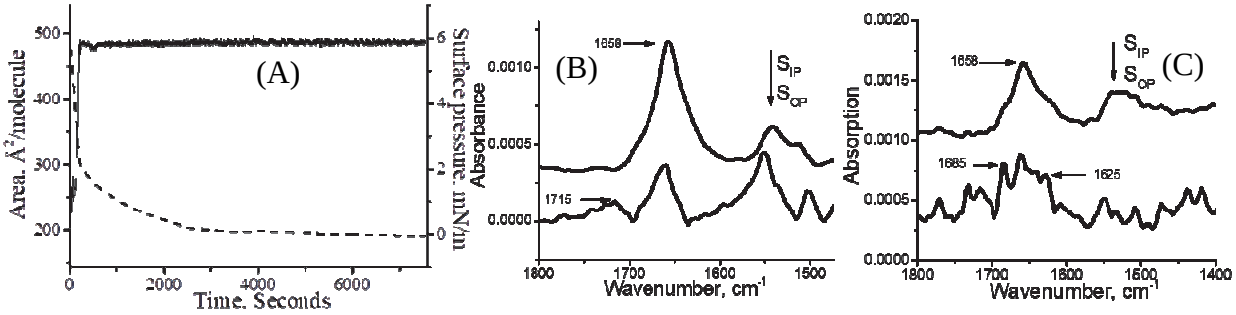

Figure 1. (A) Stability study of pressure-area isotherm of the α-syn(61－95) on pure water, (B) p-MAIRS results of the LB monolayer of unlabeled α-syn(61－95) transferred after two hours compression. (C) p-MAIRS results of the LB monolayer of the ^{13}C labeled α-syn(61－95) transferred after two hours compression.

D. Discussion

X-ray crystallography, NMR, and cryo-EM are the major methods to determine protein's structure. However, neither of them can elucidate high resolution structure of membrane proteins in monolayer structure, especially with equilibrating conformations. MAIRS is shown here to be able to detect equilibrating conformations in a specific residue for membrane proteins even in monolayer structure. Thus, MAIRS can supplement the techniques above for membrane protein's structure.

E. Publication.

One paper about Figure 1 is *in preparation* by Wang C., Akinleye T., D. Ogunmola, O. Olahanmi, and Hasegawa T. for high quality journal.

High-efficacy protein chemical synthesis

Hironobu HOJO　Osaka University

Our research goal is to develop methods that enable the synthesis of a wide variety of proteins. To realize such synthesis we are developing a chemical method such as a thioester method and a ligation method, in which a building block has an auto-activating unit. Based on these basic researches, we are synthesizing membrane proteins with trans-membrane and juxta-membrane regions for structural studies. We are also synthesizing a chemically modified histone using developing ligation auxiliaries for extended chemical ligation. This project aims to invite five world-wildly prominent professors in chemical biology and protein synthesis to discuss the scope and limitation of current strategies in synthesis of proteins with complicated structures. The five German professors are experts on protein synthesis, came to Shiga to attend the 19th Akabori Memorial Conference held in May 16-20, 2023. Taking advantage of this opportunity, we discussed the possibility of collaboration among ICR-Kyoto University, IPR-Osaka University, and German Universities to construct new scientific networks between Germany and Japan, and ICR-Kyoto University and IPR-Osaka University as well.

The participants and discussion topics included:

Christian Hackenberger, FMP Berlin:
Coming full circle: Peptide-conjugates and additives for intracellular protein delivery

Dirk Schwarzer, Universität Tübingen:
Establishing Sortase-Catalyzed Multi-Peptide Assemblies by Ligation Site Switching

Oliver Seitz, Humboldt Universität zu Berlin:
Ligation Auxiliaries Capable of Base Catalysis

Carlo Unverzagt, Universität Bayreuth:
Chemoenzymatic Semisynthesis of Bikunin, an N,O-Glycosylated Proteoglycan

Valentin Wittmann, Universität Konstanz:
Investigation of Protein O-GlcNAcylation by Metabolic Glycoengineering

Hironobu Hojo, Osaka University:
A Novel Peptide Condensation Method Using Dipicolylamino Group as the Leaving Group

We also organized a special seminar on “Breakthroughs in Chemical Biology and Structural Analysis of Proteins” held at IPR-Osaka University on May 20, 2023.
http://www.protein.osaka-u.ac.jp/seminar/20230520/

In this seminar, other than German researchers, around twenty Japanese scientists, who are mainly working on the peptide, protein and glycoprotein synthetic fields, got together and actively discussed on the recent progress in the field, not only of chemical synthesis but also of their functional and structural analyses. As we took a sufficient discussion time, the discussion extended to the future advances of these fields. These active discussions were very valuable for graduate and undergraduate students who participated (ca. 10 person). The students also had a chance to talk personally with the excellent German professors and received much stimulation from them in point of their way of researches.

Finally, we appreciate the support of the ICR, Kyoto University, in making these opportunities for research exchange and discussion possible.

Modulation of in-cell protein-protein interactions using mid-sized peptides

Hirokazu Tamamura　Tokyo Medical and Dental University

Protein-protein interactions (PPIs) are difficult targets for typical small molecule ligands. Mimicking folded domains of proteins, we can modulate the function of a particular protein with metabolically stable synthetic molecules. Therefore, strategies for developing structured mid-sized peptides that display protein-like functionality are highly demanded in drug discovery. Five German professors, including Professors Ines Neundorf (Universität zu Köln), Norbert Sewald (Universität Bielefeld), Roderich Süßmuth (Technische Universität Berlin), Hans-Achim Wagenknecht (Karlsruhe Institute of Technology), and Armin Geyer (Universität Marburg), who are experts on peptide-based medicinal chemistry and PPI, came to Shiga to attend the 19th Akabori Memorial Conference held in May 16-20, 2023. Taking advantage of this opportunity, this project aimed to exchange information on the related research being conducted in each laboratory and to pursue the possible collaboration among ICR-Kyoto University, Institute of Biomaterials and Bioengineering (IBB)-TMDU, and German Universities to construct new scientific networks between Germany and Japan, and ICR-Kyoto University and IBB-TMDU as well.

The research topics included:
- Taking advantage of PTM to design bioactive peptides altering localization and function of distinct intracellular proteins (Ines Neundorf);
- Late-Stage Diversification of Peptides (Norbert Sewalt);
- The oligoarylamide antibiotic Albicidin – mode-of-action and resistance (Roderich Süßmuth);
- The Concept of Photozymes: Small Peptides with Photocatalytic Activity (Hans-Achim Wagenknecht);
- Chemical Synthesis of Peptide Natural Products (Armin Geyer)
- Development of Anti-SARS-CoV-2 Agents Learned from Anti-HIV Agents (Hirokazu Tamamura)

We have also had related topics from German and Japanese participants in the Akabori Memorial Conference, as follows: Thioether-mediated Sulfenylation of the Indole Ring of Tryptophan; Selective Immunomodulation by Lipid- and Glyco-conjugate Antigens;

Investigation of Protein O-GlcNAcylation by Metabolic Glycoengineering; Tackling cancer with ^{211}At-radiopharmaceuticals; Development of Dioxetane-Containing Chemiluminophore Toward Biological Imaging Study; Chemoenzymatic Semisynthesis of Bikunin, an N,O-Glycosylated Proteoglycan; Glycopeptide Libraries via Chemical Glycosylation with Human N-Linked Oligosaccharides.

There was agreement on the importance of continuing the research exchange and that the next meeting should be held in Germany in 2025.

The 17th International Workshop for East Asian Young Rheologists

Tadashi Inoue　Osaka University

【Purpose of project】The ICR budget was used to organize the 17th International Workshop on Young Rheologists in East Asia (IWEAYR-17). The purpose of this workshop is to promote international exchange among young faculty and graduate students in cooperation with researchers from various countries in East Asia in several research fields, such as polymer science and materials science since the first workshop launched. IWEAYR keeps allowing participants to present their research results and discuss and exchange research ideas in a friendly atmosphere. This year, IWEAYR-17 was held in Pusan, Korea. There were nearly 180 participants, partly due to the reduced impact of COVID-19 and partly due to vigorous promotion by the Korean organizers. The ICR budget was effectively utilized to support the participation of as many Japanese researchers as possible.

【Place and schedule of workshop】IWEAYR - 17 was held from January 23 - 26, 2024, at the Pukyong National University Busan, Korea, chaired by Professor Kyu Hyun of Busan University, Korea.

【Purpose of the workshop】The purpose of this workshop is to promote international exchange and collaboration among young faculties and graduate students who will be the leading researchers in the field of rheology and material science in the near future and, therefore, to provide a place for research presentation and discussion, and to revitalize related fields. At the same time, in order to further develop joint research activities among several research groups, it is to provide a place for people exchange.

【Background of workshop】This workshop has been held annually since the first IWEAYR in Seoul (February 2006). After that, it was organized in Kyoto (January 2007), Shanghai (January 2008), Nakhon Ratchasima (January 2009), Busan (January 2010), Yamagata (January 2011), Beijing (February 2012), Phuket (January-February 2013), Seoul (February 2014), Fukuoka (February 2015), Shenzhen (January 2016), Pattaya (February 2017), Jeju Island (January 2018), Nagoya (January 2019), Changchun (January 2020), and Udon Thaini (February 2023) (in a circulating order of Korea, Japan, China, and Thailand). There have been some changes in the organization of the workshop due to various circumstances in the hosting countries; every IWEAYR has served as a place for faculties and graduate students to engage in international exchange and collaboration.

【Participants】Professor Kyu Hyun, the organizer, worked extensively to organize IWEAYR-17 very well, and therefore, the conference was conducted with meticulous attention to detail. The number of participants in this IWEAYR-17 was 42(26) professors and 134 (84) students, which was the highest level from the first one. (Numbers in () are the numbers of participants IWEAYR-16). The breakdown by country was Japan 37 (35), Korea 114(71), China 15(0), Thailand 10(10), Bangladesh 1(0) and Germany 1(0). The main participants were:

Kyung Hyun Ahn, Professor,	Seoul National University,	Korea,
Kyu Hyun, Professor,	Pusan National University,	Korea,
Wei Yu, Professor,	Shanghai Jiaotong University,	China,
Visit Vao-soongnern, Asso. Prof.	Udon Thani Rajabhat University,	Thailand
Hiroshi Watanabe, Professor,	Kyoto University,	Japan
Yumi Matsumiya, Asso. Professor,	Kyoto University,	Japan

Hiroshi Suzuki Professor, Kobe University, Japan

Group Photo

Excursion

Professor Kyu Hyun

【Overview of IWEAYR-17】Total number of submitted papers was 13(Long Oral)+8(Short Oral) + 41(Poster). On the first day, the session started with 10 Long oral presentations given by mostly Ph.D. students. After lunch, the short oral presentations (24) by master course students were presented before the poster presentations (25). On the second day, similarly, long oral presentations (10), also short oral presentations (34), and Poster presentations(15). Then, a group excursion was organized. The six best presentation awards of students supported by the Society of Rheology, Japan and Korea-Australia Rheology Journal were chosen by the professors' vote.

At this conference, there were many studies related to rheology and polymer science on new materials. In addition, there was basic research on the analysis of various rheological properties and hierarchical structures of polymers. Some issues, such as theory, simulation, and flow control of soft matter, were also presented.

IWEAYR has been held in the order of Korea, Japan, China, and Thailand. This year's IWEAYR in Busan marks the fifth round. The author has attended most of those workshops, and IWEAYR-17 was the most active and gorgeous in terms of the number of participants, receptions, etc., and it showed new directions and possibilities for the workshop. Although many of the professors who were involved in the establishment of IWEAYR are about to retire, the author has a feeling that IWEAYR will continue in the future to maintain the science and friendship among the four Asian countries.

【Summary】 All students enjoyed the workshop and were able to befriend students from neighboring countries. They also could feel the active science community in East Asia. In conclusion, IWEAYR-17 successfully achieved its purpose from the beginning. Finally, the author should note that the next IWEAYR-18 will be held in Kobe, JAPAN, in connection with the Pacific Rim Conference on Rheology 2025.

固体核磁気共鳴分光法による新たな代謝解析法の開発と がん細胞生物学への応用

伊藤貴浩　京都大学

がん患者の予後に大きな影響を与える要因のひとつが、がんの悪性化・進展の有無である。好気的解糖現象に代表されるように、がん細胞が正常細胞とは異なる代謝様式を示すこと、遺伝子変異によって細胞代謝の変化が誘導され腫瘍の発生に直接寄与すること等が解明されてきた。一方で、転移、治療抵抗性の獲得など、がんの悪性化過程における代謝変動の役割や意義については殆ど解析されていない。細胞内代謝の分析では質量分析器を用いる手法が現在の主流だが、これらの技術では細胞の破壊が必須で、がん細胞内の代謝活動を連続的に観察することは不可能である。本研究で我々は細胞内代謝を動的・リアルタイムに捉えることを目指して、固体核磁気共鳴分光法(NMR) の手法であるマジック角回転（MAS, Magic Angle Spinning）と高分解能 NMR を組み合わせた High Resolution NMR MAS (HR-MAS) 技術を生きた細胞に適用する系の構築を目指した。

まず、がん細胞の増殖とヒトにおけるがん病期進行に必須であることが明らかになっている分岐鎖アミノ酸代謝と骨髄性白血病細胞に焦点を絞り検討を行った。ヒト骨髄性白血病細胞株 U937, HL60, K562 等において分岐鎖アミノ酸代謝酵素 BCAT1 および 2 が発現していることをイムノブロット法により確認した。次に、分岐鎖アミノ酸の一つであるバリン(Val)およびその前駆体となるケトイソ吉草酸(KIV)の炭素がすべて安定同位体 ^{13}C で置換されている化合物を入手した。^{13}C -Val あるいは ^{13}C -KIV を含む培養液にヒト白血病細胞 K562 を懸濁し、HR-MAS ローターに封入したものをサンプルとした。このサンプルを化学研究所共同利用機器である Bruker 社 Avance III 800US Plus NMR System を用いて、マジック角回転 3.2kHz、300K 定温条件下にて ^{1}H-^{13}C HSQC シグナルを測定した。128 スキャン分、約 4 分間の測定を単位時間スペクトルとし、1~2 時間程度にわたって経時的に取得した（図 1 ）。Val および KIV の側鎖に存在する 6 つのメチル基に依存して、0.9~1.1ppm の領域に、Val および KIV 特異的なスペクトルをそれぞれ同定できた。この側鎖メチル基の有無をもとに、KIV 消失あるいは Val 産生を分単位で経時的に追跡することに成功した。図 1 に示すように、^{13}C -KIV を添加直後から経時的に ^{1}H-^{13}C HSQC スペクトルを取得して 22 系列分、約 90 分間の測定を行ったところ KIV が時間経過とともに消失し、代わって ^{13}C -Val に由来するシグナルが出現することがわかった。この KIV から Val への変換反応は KIV 添加１０分後から観察されはじめ、1 時間後にはほぼ全ての検出可能 KIV が Val に変換されることがわかった。一方、同様の追跡実験を ^{13}C -Val 添加条件で行ったところ KIV の産生は検出されなかった。したがって、ヒト骨髄性白血病細胞では、KIV から Val 産生反応は起こる一方で、Val を KIV に脱アミノ化する反応は起こらないことが示唆された。また、ピーク下面積の測定から KIV, Val の相対的定量も可能であった。KIV と Val を基質としてアミノ基転移反応を触媒する酵素 BCAT1 の酵素活性阻害薬を添加して Val 産生を追跡・定量したところ、阻害薬添加群では Val 産生量が顕著に抑制

された。この Val 産生抑制効果は、K562 細胞のみならず、HL60, U937 といった他のヒト骨髄性白血病細胞においても観察された。さらに、BCAT1 遺伝子の発現を short hairpin RNA (shRNA) を用いた RNAi により抑制し、この細胞における Val 産生を定量したところ、阻害薬処理と同様に産生量の低下を観察した。以上の結果は KIV から Val への変換反応が BCAT1 によって触媒されていることを示している。

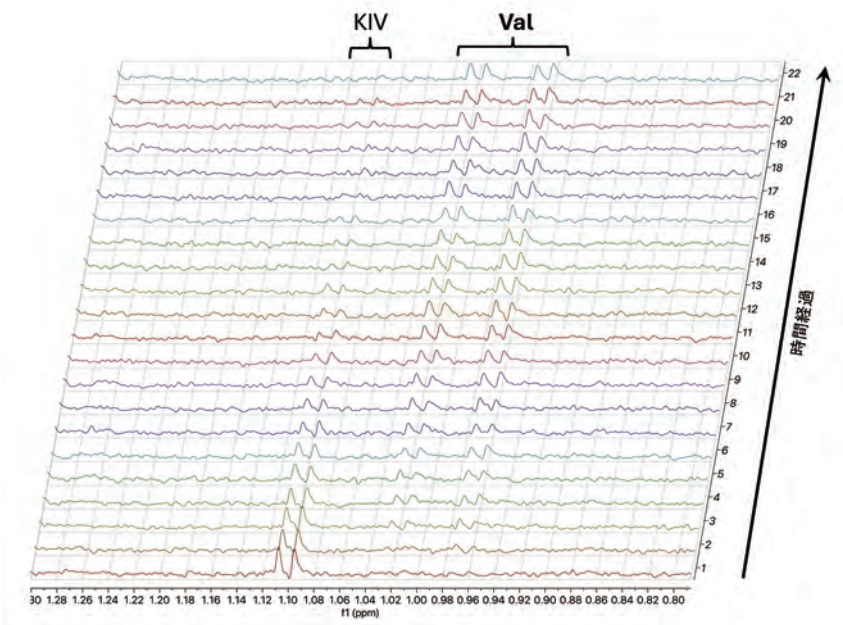

図 1　ヒト骨髄性白血病細胞株 K562 による KIV>Val 変換反応のリアルタイム検出。^{13}C -KIV を添加直後から約 4 分毎に取得した ^{1}H-^{13}C HSQC スペクトル 22 系列分(約 90 分間)を示す。1.1ppm 付近の KIV 由来ダブレットが時間経過とともに消失し、代わって ^{13}C -Val に由来する 2 つのダブレットが 0.96-1.04ppm 領域に出現することがわかった。この KIV から Val への変換反応は KIV 添加 1 0 分後から観察され、 1 時間後にはほぼ全ての検出可能 KIV が Val に変換されることがわかった。

今回構築した代謝解析法を組織レベルで適用可能か否かを明らかにするため、マウスから単離した肢骨を用いて、同様に KIV からの Val 産生を観察可能か、検討した。野生型マウス前肢骨を外科的に摘出し ^{13}C -KIV を含む組織培養液に浸した状態で HR-MAS ローター内に封入して細胞懸濁液と同様の手法をもちいて ^{1}H-^{13}C HSQC シグナルを掲示的に測定した。その結果、K562 細胞の場合と同様に 0.9~1.1ppm の領域に特徴的なダブレットを検出できた。細胞の場合と同様、KIV 添加後 15 分後から Val 由来シグナルが得られ、組織内でも同様の変換が生じていることを示唆する結果を得た。細胞を用いた場合と比較し、バックグランドノイズが高い傾向にあり、SN 比の改善が必要であることも明らかになった。今後はその他の単離組織を用いた代謝分析にも応用できるよう、技術的な改良を加えていく計画である。以上に記載した本研究成果は投稿準備中である。本研究により、細胞内代謝を動的に捉えることが可能な、がん細胞の新しい代謝解析法を確立できた。このような全く新しい領域融合的研究を可能にして頂いた化学研究所分子材料化学研究領域の梶宏典教授、前野綾香技術員および化学研究所共同利用・共同研究の枠組みに深く感謝致します。

Microstructural Investigation by Atomic Resolution Transmission Electron Microscopy of Novel Alloys

Natthaphol CHOMSAENG　Burapha University

Objectives

We have investigated and characterized high entropy alloys in collaboration with Associate Prof. Dr. Mitsutaka HARUTA, Division of Electron Microscopy and Crystal Chemistry. For advanced ARM-TEM was used to study unknown phase of high entropy alloys, and TEM-EELS was used to confirm their chemical composition. This work was supported by the Collaborative Research Program of Institute for Chemical Research, Kyoto University (Grant No. 2023-139).

Experiment Results

1. AlCrFeNiCu and AlCuAgZnSn high entropy Alloys for high strength application

This work aims to clarify the effects of phase stability and therefore the mechanical properties of AlCuCrFeNi quinary alloy systems. In order to elucidate the phase transformation, electron microscopy and spectroscopy are much needed for the analysis. The alteration of aluminium contents in this system would promote mechanical stability at high temperature environment due to the phase evolutions. The AlCuCrFeNi alloys were prepared by a direct arc melting method with different mount of aluminium contents shown in Table 1.

Table 1. The mole ratio/% of AlCuCrFeNi alloys

	Al	Cu	Cr	Fe	Ni
$Al_{0.5}$CuCrFeNi	10.0	22.5	22.5	22.5	10.0
$Al_{1.0}$CuCrFeNi	20.0	20.0	20.0	20.0	20.0
$Al_{2.5}$CuCrFeNi	50.0	12.5	12.5	12.5	12.5

The as cast alloys were investigated using JEM-ARM200F transmission electron microscope. TEM micrographs, selected area diffraction patterns, and EELS data were carefully collected. The as cast microstructures consist of dendritic regions, interdendritic regions, intermetallic phases, and carbides. The Cr/Fe ratios in the interdendritic regions characterized by EELS showed that the increasing of Al content affects the Cr/Fe ratios and correlated to the crystal structure transformations from the FCC structure to the BCC structure.

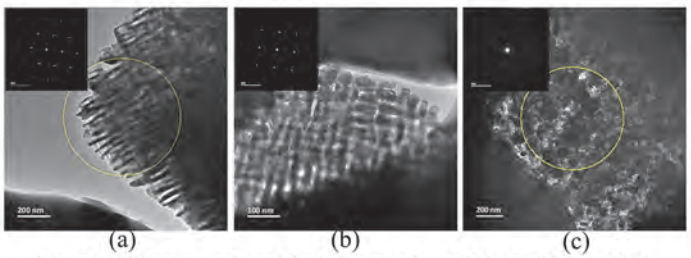

Figure 1. TEM micrographs and the SADP as an inset of (a) $Al_{0.5}$ (b) $Al_{1.0}$ (c) $Al_{2.5}$

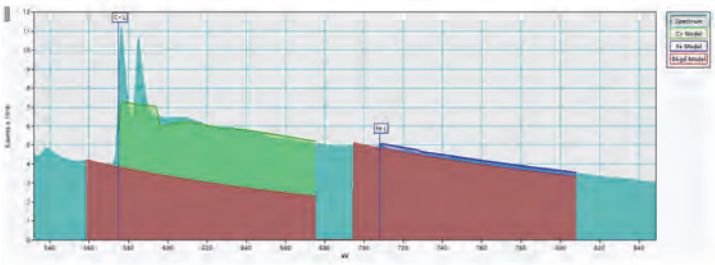

Figure 2. EELS spectrum of $Al_{0.5}$CuCrFeNi

Electron Energy Loss Spectroscopy and High-Resolution Transmission Electron Microscopy of Novel Functional Materials

Torranin Chairuangsri Chiang Mai University

Objectives

We have investigated and characterized three functional materials in collaboration with Associate Prof. Dr. Mitsutaka HARUTA, Division of Electron Microscopy and Crystal Chemistry: (i) HRTEM was used for studying nanostructures on FeOx/C nanocomposite for potential use as anode in LIBs and EELS was used for identifying phases in the as-prepared anode materials, (ii) *in situ* heating experiment of NASICON base, sodium titanium phosphate glass has been performed in JEM ARM-200F for studying its crystallization behavior by TEM and EELS, and (iii) Cross-sectional thin foils of oxides formed by high temperature oxidation in high chromium cast irons with Si addition were prepared by FIB and characterized by STEM-EDS and EELS.

Experimental Results

I. Novel FeOx/C nanocomposite for potential use as anode in LIBs

The carbon matrix structure of the C/FeOx nanocomposite material (WH0.03) was identified using HRTEM and EELS, with the results illustrated in Fig. 1. Figs. 1(a) and 1(b) depict the presence of graphitic domains scattered in an amorphous structure. The d-spacing of each domain was measured to be 0.34-0.39 nm in length, close to the d_{002} of graphite. EELS spectrum in Fig. 1(c) shows two peaks, at 287 eV and 290–300 eV, which implied that the material was close to amorphous, but not entirely. Raman spectroscopy in Fig. 1(d) supports that sp3 carbon in raw material (WH) was transformed into sp2 carbon in both amorphous and graphitic structures.

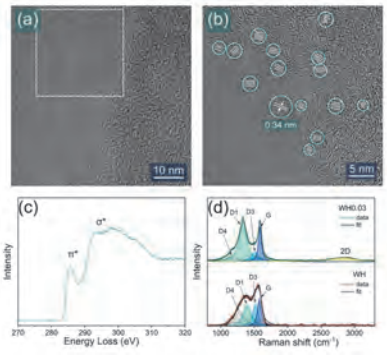

Figure 1

II. NASICON base, sodium titanium phosphate glass

In situ heating experiment was performed from 600 ºC to 800 ºC for 30 minutes. *Ex situ* and *in situ* results were different. The sample heat-treated in an electrical furnace (*ex situ*) remained in an amorphous state, showing no noticeable Bragg peak, On the other hand, *in situ* heating resulted in the presence of crystalline phase (BF-TEM image in Fig. 2(a) and SAED spot pattern in Fig. 2(b)). DF-TEM image (Fig. 2(c)) revealed the position of corresponding crystalline phase, mostly at the edge of sample. Ti L-edge EELS spectrum of the crystalline phase suggests that TiO_2 phase was crystallised, which is different from the $Na_3Ti_2(PO_4)_3$ phase previously reported in the literature.

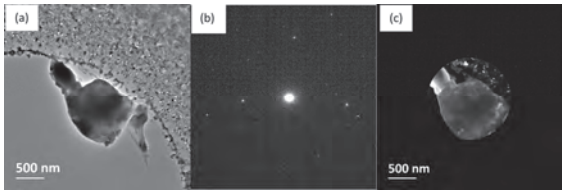

Figure 2

III. Oxides formed by high temperature oxidation in high chromium cast irons with Si addition

Oxides formed by high temperature oxidation in 31 wt.% Cr-1.1 wt.%C high chromium cast irons with 0.3, 1, 2 and 3wt.% Si addition have been investigated. Cross-sectional thin foils were prepared (e.g. Figs. 3(a-b) in the 0.3wt%Si iron). STEM-EDS maps (Figs. 3(c-f)) revealed the Si-rich oxide layer formed between the Fe-rich and Cr-rich oxides. Fine structures in O K-edge and Cr L-edge EELS spectra were found to be useful for distinguishing these oxides.

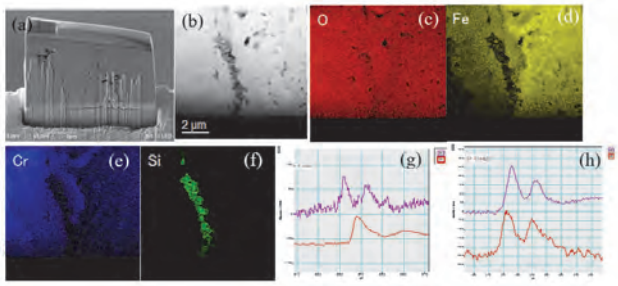

Figure 3

Outcome

1. W. Yodying, T. Sarakonsri, N. Ratsameetammajak, K. Khunpakdee, M. Haruta, and T. Autthawong, Crystals, 2023, 13(2), 280; https://doi.org/10.3390/cryst13020280
2. W. Yodying, T. Autthawong, O. Namsar, T. Kiyomura, M. Haruta, H. Kurata, T. Chairuangsri, and T. Sarakonsri, J. mater. Sci.: Mater. Electron., 2023, Recycling Water Hyacinth Stem Waste for Cost-Effective Production of Carbon/FeOx Nanocomposite Anodes for Sustainable Fast-Charging Lithium-Ion Batteries. (submitted manuscript)

Tackling the Electronic Instability of Charge-Density Waves by Electron Energy-Loss Spectroscopy

Ming-Wen Chu　National Taiwan University

This project aims at understanding the nature of the correlated charge order of charge-density waves (CDWs) in quantum matters, which are inherently weakly-correlated and supposedly not subject to the electronic ordering. The material of interest chosen for this collaboration project with Prof. Mitsutaka Haruta at Institute for Chemical Research (ICR) is the Dirac semimetal GdSbTe. The GdSbTe consists of the square-net Sb and rumpling Gd-Te layers, with the Sb-4*p* states of the square net dictating the linearly-dispersing bands near the Fermi level. Meanwhile, the Te and Gd bands are further away from the Fermi level and, therefore, less relevant to the electronic characteristic of the GdSbTe. The significant band width of the linearly-dispersing bands is tied to weak electronic correlations. Notably, the GdSbTe manifests the correlated CDW ordering, with the simultaneous presence of two sets of CDW-modulated wave vectors. The possibility of the crystalline twinning effect is ruled out by careful dark-field imaging and the two sets of CDW modulations consist of an inherent electronic characteristic of the GdSbTe. For convenience, we assign them as the degenerate CDW domains (q_a- and q_b-CDW domains).To dig out the electronic origin for the domain formation, we conducted momentum(q)-dependent electron energy loss spectroscopy (q-EELS) on the respective q_a- and q_b-CDW domains in ICR (August, 2023). We observed the bulk plasmon at ~16 eV, which is the dynamical oscillation of all valence electrons, and also the weak excitation at ~1.65 eV due to the plasmon oscillation of carriers at the Fermi surface. Intriguingly, the q_a- and q_b-CDW domains manifest a discernible shift in the bulk plasmons, implying that either the number or the mass of the free valence electrons in respective domains is different. Moreover, a gentle difference in the spectral weight in the ~1.65-eV excitation is accompanied. These intriguing electronic hints shall shed light on the emergence of concomitant CDW domains in the GdSbTe and we are working on the grand detail of the materials physics and chemistry. The next tun of q-EELS experiments is planned for later in the year 2024.

High-pressure synthesis of transition metal oxides with novel physical properties

Kunlang Ji　University of Edinburgh

Objectives: High pressure-high temperature (HPHT) synthesis is used to stabilize unusual oxidation states and coordination environments in transition metal oxides, resulting in interesting physical properties. In collaboration with Professor Shimakawa in ICR at Kyoto University, a unique high-pressure multianvil apparatus which reaches up to 20 GPa and 2273 K is available to use. This equipment provides a good opportunity for synthesize the double corundum/perovskite with small tolerance factor and develop their potential multiferroics.

Experimental methods: I was able to visit Shimakawa lab at ICR for carrying out research between September and October 2023. The preparation of the $Mn_{2-x}Co_xScSbO_6$ (x = 0.5, 1 and 1.5) precursor mixtures were performed via conventional solid-state route under ambient pressure. The precursor mixtures were then loaded into the pressure cell and synthesized under required temperature and pressure in Shimakawa lab. Their structures were characterized using x-ray diffraction methods and their physical properties were explored using a Quantum Design PPMS and MPMS-SQUID.

Outcomes: $Mn_{2-x}Co_xScSbO_6$ recovered from high pressure has two polymorphs, double perovskite (DPv) and double corundum. Incorporation of small Co^{2+} at A-sites in (double) perovskites is very unusual. Rietveld refinements shows that all these solid solutions have the $P2_1/n$ DPv structure, with phase purities up to ~90%. High temperature Synchrotron X-ray data of x = 1 shows a structural phase transition from DPv to a $R3$ corundum type structure above 270 ° C. $Mn_{2-x}Co_xScSbO_6$ is also remarkable for showing a large negative thermal expansion on heating above 400 ° C for all solid solutions. Magnetic measurements and powder neutron diffraction confirmed very rich and different magnetic properties for DPv and double corundum polymorphs.

Analysis: The magnetic structures for DPv and corundum phases have been under investigation using low temperature powder neutron diffraction collected at ILL, Grenoble. The large cation redistributions between Mn^{2+}, Co^{2+} and Sc^{3+} are the potential reason resulting in larger negative thermal expansion. Considering the close positions of Mn^{2+}, Co^{2+}, and Sc^{3+} in periodic table, high temperature neutron powder diffraction is necessary to confirm the cation redistributions. And this experiment has been accepted in J-PARC using BL08 SuperHRPD.

Publication: K. Ji, Y. Shimakawa, J. P. Attfield et al., In preparation.

Elucidation of Hydrogen and Helium Retention Behavior in Fusion Materials

Mitsutaka Miyamoto Shimane University

W was chosen as the plasma-facing material in the ITER divertor region because of its high melting temperature, high thermal conductivity, and low sputtering erosion yield. In the ITER DT (deuterium-tritium) phase, the W divertor will be exposed to burning plasma of high density helium (He) and hydrogen isotopes. Behavior of the H isotopes in W is an important consideration because they influence the plasma operation parameters via re-emission. Previous studies have shown that the retention properties of the H isotope in W are significantly affected by the He pre-irradiation, suggesting the contribution of He bubbles [1,2]. However, direct evidence of the effect of He bubbles on H retention remains elusive. In this Joint Research, the effects of He irradiation on H isotope retention in W were precisely evaluated from a microscopic viewpoint using the aberration-corrected scanning TEM combined with electron energy-loss spectroscopy (STEM-EELS) at ICR, Kyoto University.

Fig. 1 displays the (a) HAADF image and corresponding (b) sample thickness and areal densities of the (c) D and (d) He atoms for the sample post-irradiated with D^+ at R.T. after He^+ pre-irradiation and annealing of ~1573 K. Although there are small facets in some of the bubbles, they have an approximately spherical structure, as shown in (a) and (b). In addition, the elemental mappings clearly show the localization of the D and He atoms in the bubble. Although the localization of the H isotope in Be has been reported on the inner surface of the bubble [3], both of the D and He atoms show high areal densities at the central part of the bubble, indicating the absence of localization of the bubbles for W. This result is also inconsistent with the tendency of H to diffuse to the bubble periphery, as predicted by the molecular dynamics simulation [4], suggesting that H exists in molecular form in large bubbles. In this experiment, the dependence of bubble pressure on bubble size and shape was also investigated, showing that the trend was different for deuterium and helium. More detailed evaluation of this dependence will be performed in the future under extended experimental conditions.

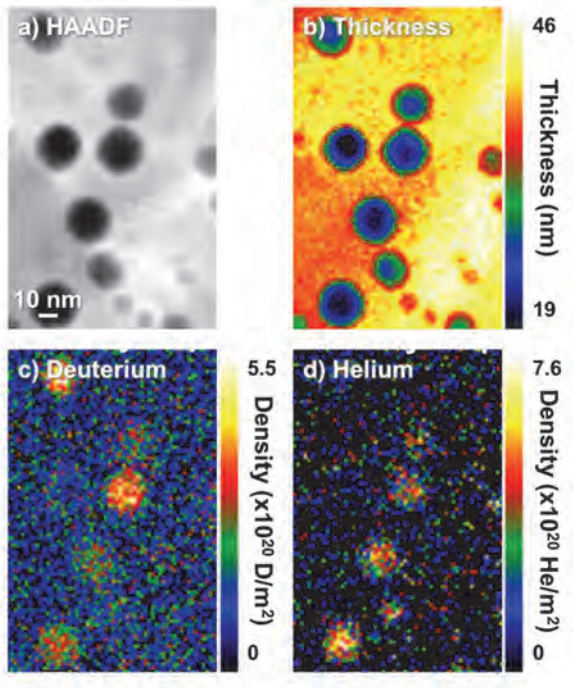

Fig. 1 (a) HAADF image and corresponding (b) sample thickness and areal densities of the (c) D and (d) He atoms for the sample irradiated with combined deuterium and helium ions.

[1] Y. Sakoi et al., J. Nucl. Mater. 442 (2013) S715
[2] M. Miyamoto et al., Nucl. Fusion 49 (2009) 065035
[3] M. Klimenkov et al., Micron 127 (2019) 102754
[4] N. Juslin, B.D. Wirth, J. Nucl. Mater. 438 (2013) S1221

Nano structural analysis of $Cs_4PbBr_6/CsPbBr_3$ composite for the development of a scintillator for fast electron beam detection with high efficiency

Hikaru Saito　Kyushu University

It has been reported that $CsPbBr_3$ nanoparticles embedded in Cs_4PbBr_6 matrix ($CsPbBr_3/Cs_4PbBr_6$ nanocomposite) exhibit high photoluminescence (PL) quantum yield [1]. Recently we have found sub-nanosecond cathodoluminescence (CL) decay from $CsPbBr_3/Cs_4PbBr_6$ nanocomposite by using Hanbury Brown-Twiss interferometry, which is applicable to high performance scintillator for fast electron beams [2]. Furthermore, the CL efficiency increased in areas irradiated with electron beams. To elucidate this phenomenon, in this study we analyzed a Cs_4PbBr_6 thin film by electron energy-loss spectroscopy (EELS).

We fabricated a Cs_4PbBr_6 thin film by thermal evaporation. Fig. 1a shows an annular dark field-scanning transmission electron microscopy (ADF-STEM) image obtained from the Cs_4PbBr_6 at a probe current of 4.5 pA. The EELS spectrum obtained from this area (Fig. 1b) shows characteristic peaks of Cs_4PbBr_6 [3]. By using the electron beam with an increased current up to 8.4 pA, a local area indicated by the red square (Fig. 1c) was intensively irradiated. Then, EELS mapping was conducted in the same area at the probe current of 4.5 pA. There is almost no change in the spectrum overall, and only the presence of Cs_4PbBr_6 can be confirmed (blue spectrum in Fig. 1d). However, the spectrum drastically changed only in the intensively irradiated area (red spectrum in Fig. 1d). The bandgap onset of 2.3 eV can be recognized in the red spectrum instead of the decreased peak at 4 eV, suggesting the generation of $CsPbBr_3$ particles [3] by electron beam irradiation. This is consistent with the previously observed CL intensity increasing by electron beam irradiation.

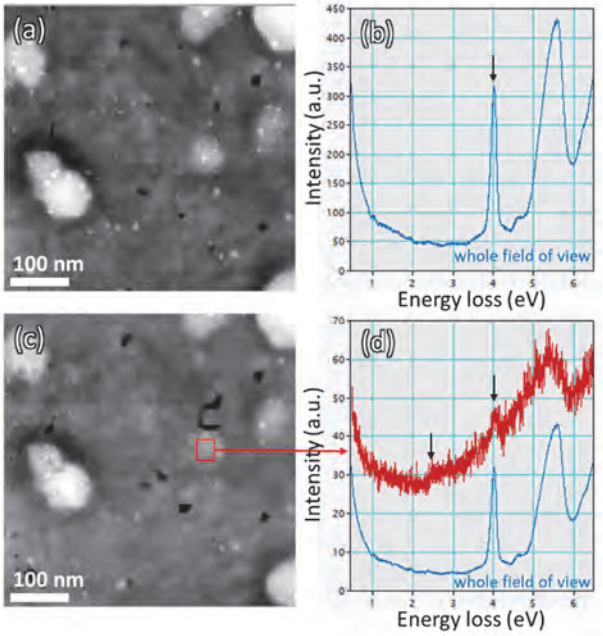

Fig. 1 (a) ADF-STEM image and (b) EELS spectrum obtained from a Cs_4PbBr_6 thin film before intensive electron beam irradiation. (c) ADF-STEM image and (d) EELS spectra obtained from the Cs_4PbBr_6 thin film after intensive electron beam irradiation. The red spectrum was extracted from the area irradiated under the high current condition.

[1] Y. M. Chen et al., *ACS Appl. Mater. Interfaces*, **10**, 15905 (2018).
[2] T. Kubota et al., *Appl. Phys. Express*, **17**, 015005 (2024).
[3] C. de Weerd et al., *J. Phys. Chem. C*, **121**, 19490 (2017).

Optimization of laser irradiation conditions for high-quality ion beam generation by laser-driven ion acceleration mechanism

Sadaoki Kojima　National Institutes for Quantum Science and Technology

Background & Objectives:

When a high-intensity laser exceeding 10^{18} W/cm^2 is irradiated onto a thin foil target, a strong sheath field (~TV/m) is generated at the rear surface of the target, ions are accelerated up to multi-MeV from small interaction region (μm). National Institutes for Quantum Science and Technology (QST) in Japan have progressed toward developing a compact laser-driven ion injector by using the TNSA mechanism for heavy-ion radiotherapy called “Quantum Scalpel”. The ion beam specification for medical applications typically requires high energy, high fluence and low emittance. Much novel research is under way to improve beam performance.

Methods & Results:

Ion beam emittance (transverse emittance) is an important parameter that determines beam focusing and transport performance. In a typical emittance diagnostic, the transverse momentum spread is determined from the spatial profile of the beamlet extracted by a slit or pinhole. In particular, laser-accelerated ions have a small spatial beamlet profile because the ion beam is generated by a small source of micrometer scale. A two-dimensional dosimeter and readout system with micrometer spatial resolution is necessary to diagnose small changes in this spatial profile. Two-dimensional profile measurements of laser-driven ions utilize a radiochromic film (RCF) and it has micrometer spatial resolution. On the other hand, the spatial resolution of commercially available flatbed scanners (GT-X980), a commonly used reading system, is limited to approximately 83.3 μm (high contrast spatial resolution with MTF ≥ 0.8) due to artifacts such as scattering of RCF transmitted light. In this study, we develped a test bench microdensitometer (TBMD), and its optical performance, dose equivalent response, and spatial resolution characteristics with MTF were evaluated. The TBMD had a minimum readout focal diameter of 13 μm, and its high contrast spatial resolution with an MTF of ≥0.8 is about 11.9 μm. Ion beam emittance were diagnostics for several laser and target conditions. It was found that the emittance of the laser-accelerated proton beam is more than one order of magnitude better than that of the current accelerator beam.

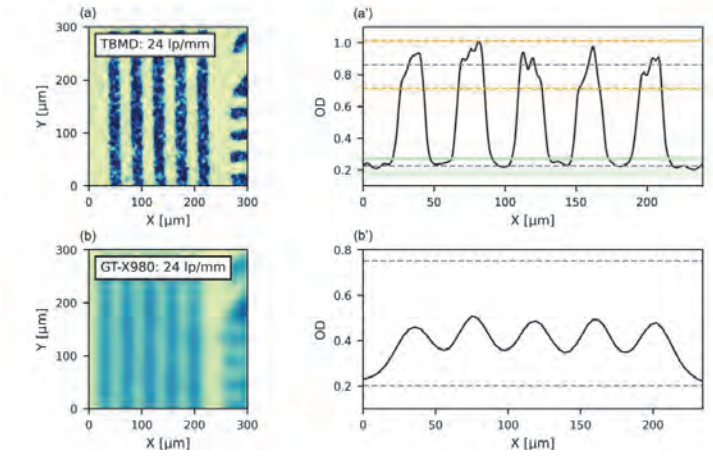

FIG. 7. (a) and (b) show the measured profiles at the 24 lp/mm line pattern on the TBMD and GT-X980. The color contrast between (a) and (b) is uniform. (a′) and (b′) show the line profile of the OD at the red dashed line in (a) and (b).

スギ木質組織構造の効率的化学分解過程から先端化学物質生産をめざした質量分析解析

秦野修　奈良県立医科大学

目的： 本研究は再生可能資源である木質バイオマスから、主成分であるセルロースやリグニン等を、先端化学材料（CNF など）を含む有用化学物質への効率的変換/利用法の開発を目的とする。化学研究所・中村研究室では、種々の触媒と過酸化水素水を用いて、新奇な木材の効率的分解/合成/利用法の開発を行っている。この際、有機酸触媒等を木粉や木材チップに直接作用させ、軽量で高剛性を実現できる新規材料として注目されるセルロースナノファイバー（CNF）様の構造物が容易に得られることを見出している。

申請者は、スギ木幹部の薄い切片を作成して、形態学的側面から、これらの触媒反応による組織構造の前後変化を可視化（Imaging）する系を構築した。この際、光学顕微鏡と SEM を併用して、リグニン、セルロース等の存在部位を可視化し（光学顕微鏡）、SEM を用いて電顕レベルの形態学的変化を追跡する系を構築した（CLEM 法: 光学・電子顕微鏡相関法）。本研究は、過酸化水素水と触媒等による木材分解過程を、主に切片を用いた組織形態学的変化と、FT-ICR MS を用いた分解産物の解析に重点を置き、木材から先端化学材料等の有用化学物質への効率的分解/合成/利用法の開発・解析を行うことを目的とする。

実験方法、実験結果、考察：

申請者は、R4 年に薄いスギ木幹部切片を用いることにより、触媒を用いず、過酸化水素水のみで、効率的に木質切片を分解できることを明らかにした。本実験系は、薄い切片（0.009 mm）とごく微量の反応液(0.04 ml 可）を用いて、簡便に触媒のスクリーニングが可能である。本年度（2023 年）は、この薄い切片を用いた簡便なスクリーニング系を用いて、４種の酸と、１種の塩基について、過酸化水素水への添加量を変化させて、スギ分解の触媒効果を検討したところ、1 種の弱酸について、新奇に触媒効果が示唆された。又、セルロース分解のモデル実験系として、濾紙片（3 x 5 mm）を用いて、これら 5 種溶液による分解作用を調べたところ、過酸化水素水に加えて１種の弱酸と１種の強酸にセルロース分解作用を認めた。

一方、FT-ICR MS を用いて、主に MALDI 法で、スギ切片の過酸化水素水分解産物を解析したところ、分解産物中に、セルロースの構成成分である、グルコースの単量体(C6H12O6)、2 量体（セロビオース、C12H22O11）、3 量体（セロトリオース、C18H32O16）の Na 付加体に相当するピークを、組成式から計算される ***m/z*** 値に比べて、極く微小の誤差(1 ppm 未満)で検出できた（MALDI Matrix として、DHB（2,5-dihydroxybenzoic acid）を使用）。

又、同じくスギ切片の過酸化水素水分解産物を、Girard-T 試薬でカルボニル基（ケトン基、アルデヒド基）を誘導体化後に、CHCA (α-Cyano-4-hydroxycinnamic acid) を Matrix として、MALDI 法で検出したところ、リグニン由来と思われるカルボニル化合物のピークを検出した。又、FT-ICR MS は、超高分解能（質量分解能＞100 万）であるため、安定同位体解析から組成式を推定可能であり、これらピークの組成式について、極く微小な誤差(1 ppm 未満)で推定できた。一方、中村研究室の実験系でも、スギ木質の触媒分解産物中に NMR, FT-IR 等でカルボニル化合物を含むことが明らかになっている。

今後は、主に薄い切片を反応系として用い、過酸化水素水のみ、及び触媒添加によって得られる分解産物（化合物）の同定を、超高分解能質量分析機（FT-ICR MS）を用いて行うと共に、光顕（リグニン、セルロース等の変化の可視化）、および電顕レベルの超微形態学的変化の解析を行っていきたい。又、申請者は、本 FT-ICR MS 機を用いて、カルボニル化合物誘導体化の質量分析イメージング解析系を構築しており、分解過程の木材切片の質量分析イメージング解析を行っていきたい。

Theoretical design of low-dimensional silicon material embedded in a flat two-dimensional sheet and exploration for operating principles

Masae Takahashi Tohoku University

【Objectives】Two-dimensional (2D) Dirac materials represent a special class of quantum matters that host linearly dispersing Dirac cones. Dirac cones categorized as type-I exhibit a tilted anisotropic linear dispersion in all k directions, together with a point-like Fermi surface. Most recently, we designed a silicon-based type-I Dirac material Si_2Be with a planar configuration based on first-principles calculations. Here, we report findings on the thermal stability, mechanical properties, and thermal conductivity of our recently designed silicon-based type-I Dirac material, Si_2Be.

【Computational Details】First-principles calculations were performed using CASTEP code (ver. 2018 and 2019). To investigate the thermal stability, *ab-initio* molecular dynamics simulations were carried out in the NVT ensemble. The 2D elastic constants were calculated with least squares fitting of the linear stress versus strain curve for the chosen elastic constants in the strained unit cell, where the stress tensor was calculated using first-principle calculations. The minimum thermal conductivity was determined according to the Clarke model.

【Results and Discussion】Both the in-plane Young's modulus and Poisson's ratio along an arbitrary direction are anisotropic (Fig. 1). The smaller Young's modulus compared to that of graphene (335 N m^{-1}) indicates that the Si_2Be sheets have higher flexibility compared to graphene. The minimum thermal conductivity ratio of Si_2Be to graphene is estimated to be 0.22 and 0.28 in the direction parallel and perpendicular to the 1D chains, respectively, and thus Si_2Be sheets are also expected to be good 2D heat dissipation sheets like graphene. We verified the prerequisite for a viable compound by performing ab-initio molecular dynamics simulations at various temperatures. As a result, the Si_2Be sheet was stable during the simulation time up to 8 ps at 700 K, and the Si-Si bond was stable up to 1 ps at 1000 K.

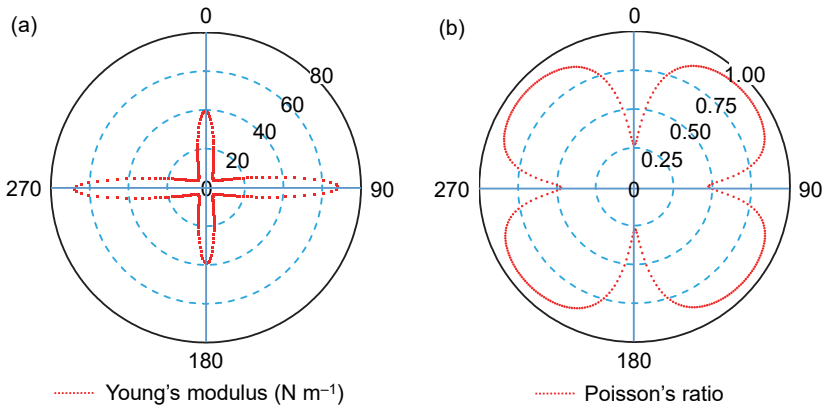

Fig. 1. Polar diagrams of in-plane (a) Young's modulus and (b) Poisson's ratio.

【Publications】[1] M. Takahashi, *Sci. Rep.* **2023**, *13*, 13182.

[2] M. Takahashi, H. Matsui, E. Kwon, Y. Ikemoto, *Chemical Physics Impact* **2024**, *8*, 100442.

[3] M. Takahashi, 11th International Conference on Materials for Advanced Technologies, June 26-30, **2023**, Suntec Singapore, Singapore (Invited talk).

2. 国際会議、シンポジウム・研究会報告

第 10 回環太平洋ラジカル化学会議（PSRC-10）
実施報告書

主　催：第 10 回環太平洋ラジカル化学会議組織委員会
共　催：京都大学化学研究所共同利用・共同研究拠点
後　援：日本化学会、近畿化学協会、有機合成化学協会
会　期：2023 年 6 月 4 日（日）～6 月 9 日（金）
場　所：京都大学　宇治キャンパス　宇治おうばくプラザ

2023 年 6 月 4 日～9 日の 6 日間にわたり、京都大学宇治キャンパスおうばくプラザで、国際シンポジウム「10th Pacific Symposium on Radical Chemistry (PSRC-10)」を開催した。

PSRC は、2004 年に第 1 回が金沢で開催されて以来、ほぼ二年ごとに各国持ち回りで開催され、今回で 10 回目となる。本来は 2 年前の 2021 年に開催予定であったが、新型コロナウイルス感染症が世界的に拡大したことの影響を受け、二度の延期を経て今回の開催となった。本シンポジウムの目的は、環太平洋地区のみならず世界の有機ラジカル化学の発展と、この分野の人々の相互交流を促進することにある。また本シンポジウムの議題は、フリーラジカル化学のあらゆる側面を網羅し、ラジカル合成反応、ラジカル重合、重要なラジカル反応のメカニズムの解明、ラジカルを利用した新しい機能性分子や材料、さらには生物学や医学に影響を与えるラジカルのあらゆる側面にわたる。これらの分野に携わる世界中の産業界や学術界の化学者が集まり、最新の発見を報告する点に本シンポジウムの意義がある。計画時は 100 人前後の参加を見込んでいたが、最終的には 18 か国から計 186 名の研究者が集い盛況な会議となった。参加者の内訳は、日本国内から 101 名、中国から 15 名、韓国から 10 名、アメリカ合衆国から 9 名、イギリスから 8 名、ドイツ、台湾から各 7 名、フランス、シンガポール、スイスから各 5 名、オーストラリア、ノルウェーから各 2 名、ベルギー、デンマーク、インド、スペインから各 1 名であった。

今回のシンポジウムでにおいて、口頭での講演はおうばくプラザ内のきはだホールで行われた。6 月 3 日は議長の山子茂教授による開会の挨拶に引き続き、大阪公立大学・国立陽明交通大学の Ilhyong Ryu 教授による 45 分の基調講演とウエルカムパーティが行われた。6 月 5 日には 25 分の特別招待講演 8 件と 20 分の招待講演 4 件が行われた。引き続き、きはだホールに併設されたハイブリッドスペースにて 2 時間のポスターセッションが行われ、若手研究者を中心に発表された 91 件の研究について活発な議論がおこなわれた。なお、ポスター発表からは 12 名の学生・ポスドクがポスター賞受賞者として選ばれ、閉会式にて表彰された。6 月 6 日から 9 日にかけては、フリンダース大学の Michelle Coote 教授、およびミシガン大学の Corey Stephenson 教授による基調講演、特別招待講演 20 件、招待講演が 20 件行われた。また研究者間の親睦を深めるため、6 月 8 日の夕刻には平安神宮会館（京都市左京区）でバンケットが行われた。

今回発表された研究のテーマは光酸化還元触媒を用いた反応開発、ラジカルを用いる精密高分子合成や材料創製、さらに複数のラジカルが相互作用する複雑分子の設計・合成や理論など、幅広い分野にわたる最近の研究成果であった。ここ数年制限されていた人の行き来が解除されたことを受け、一件だけ行われたウェブでの講演を除き、シンポジウム全体を対面で実施できたことは特筆に値する。対面開催ならではの緊迫した質疑応答や、コーヒーブレークやランチ、さらにアルコールが少し入った場でもリラ

ックスした議論が行われ、参加者の間で大いに交流を深めることができた。
今回のシンポジウムではこれらの活動を通じ、有機ラジカル化学の研究の更なる発展と研究者コミュニティの国際的交流の場を提供し、当初の目的を無事に達成したものと考えている。

最後に、本シンポジウムを開催するにあたりご支援をいただいた京都大学化学研究所国際共同利用・共同研究拠点に厚く御礼を申し上げる。

文責：山子茂

The 1st Kyoto-SKKU Workshop
実施報告書

日　時：2023 年 6 月 5 日（月）

場　所：京都大学化学研究所　共同研究棟大セミナー室

参加者：35 名（韓国側　5 名　日本側 30 名）

表記会議が京都大学化学研究所大セミナー室（CL110）で開催された。この会議はペロブスカイト太陽電池に関する機能性有機分子の設計・合成から物性の解明、さらには応用に向けた基礎化学を行っている韓国と日本の化学者が集まり、研究の活性化と相互交流の促進を目的としている。京大化研の国際共同利用共同研究拠点にて、2022 年度より採択された共同研究の一環として、今回、第 1 回目のワークショップを京都大学化学研究所で開催した。若宮がオーガナイザーを務め、国内からは、大阪大学から佐伯昭紀教授、兵庫県立大学から伊藤省吾教授、京大工学研究科から大北英生教授、化研からは、金光義彦教授、廣理英基准教授を含め 30 名が参加し、韓国側からは、成均館大学校 エネルギー科学技術研究所所長の Nam-Gyu Park 教授を含む 5 名の教授が参加した。

会議は前日夕方にレセプションを行った後、6 月 5 日（月）には開会式の際に、京都大学化学研究所（青山卓史所長）と成均館大学校 エネルギー科学技術研究所（Nam-Gyu Park 所長）の MOU の調印式を行った。その後、ペロブスカイト半導体材料、有機半導体材料およびそれらを用いた太陽電池に関する 11 件の研究発表が行われ、活発に質疑応答が行われた。また、休憩時間を利用して、若宮研究室の合成・太陽電池作製・評価装置群と金光研究室の先端分光測定装置の見学会を行った。

参加者全員が高い研究の質と密な交流に満足し、大変盛会であった。国際共同利用共同研究拠点の支援に感謝する。

MOU 調印式

第 1 回 Kyoto-SKKU Workshop 参加者の集合写真

若宮　淳志（分子集合化学研究領域）

持続可能社会創造ユニット令和 5 年度第 1 回ミーティング「PFAS 科学の再出発に向けて」開催について

題名：化研を核とした学際的な PFAS の研究

本文：

研究連携基盤の 4 つの研究ユニットのうち，私がユニット長として担当する「持続可能社会創造ユニット」は，科学・人文系にまたがる 8 つの研究所・センターによる学際研究により，単独の研究機関では成し遂げられないような地球規模での課題に取り組むことを求められており，主としてエネルギー問題と環境問題の二つに分けて取り組んでいます．その中でも，化学物質の安全性に関わる課題は，常に議論が続いているものです．

昨今，PFAS という呼称の化合物群が環境や人体への影響が懸念され，環境，科学，産業，政策などの広い分野から世界的な関心を集めています．PFAS は，有機フッ素化合物の中でも CF_2 基や CF_3 基を含む化合物群の総称で，有名な PTFE（テフロン）をはじめ，燃料電池や電解に必須のナフィオン，さらには半導体産業でも PFAS なしには製造が成り立たないなど，非常に影響力の大きな化合物群です．これほどまでに PFAS が重要視されているのは，フッ素を使わない炭化水素化合物では，求められる必要な物性が出せないからです．たとえば，水も油もはじく撥水撥油という性質は，PFAS に固有の性質です．

不思議なことに，これまで PFAS が発現する物性はほとんど理解が進んでおらず，経験を通じて機能性材料が次々に開発されてきたのは，PFAS の位置づけを材料科学の中でも特殊なものにしています．PFAS には化学的に安定で分解されにくい性質がありますが，こうしたごくわずかにわかっている性質だけに必然的に焦点が当たり，環境や人体に蓄積する機構や，毒性を発揮する機構といった本質的な分子論の構築が極めて困難で，経験重視の“科学”に甘んじてきたことは学術的な大きな問題でした．

化学研究所で 2013 年から始まった研究で，この PFAS の科学に初めての分子論（SDA 理論）が理論と実験の両面から研究され，炭化水素と本質的に違う分子論が明らかになってきました．その結果，材料科学，環境科学，毒性学などを物理的な視点と定量計算，さらには最先端の分光学などを駆使することで，長年の未踏領域に初めて挑戦できる地盤が整ってきました．

こうした状況を受けて，R5 年 6 月 30 日（金）に，宇治キャンパスのきはだホールにて今年度の持続可能社会創造ユニットの R5 年度の第 1 回ミーティングを実施しました．環境省の取り組みに詳しい経済研の廣木雅史先生に，日本の PFAS 問題への取り組み最前線をお話しいただき，そのあと SDA 理論を核として高分子科学，物理学，マルチスケールシミュレーション，分析化学，トライボロジー，疫学，体内動態学の専門家が集結し，今後の新しい PFAS 科学の進め方について話し合いました．こうした学際的に大規模な講演会は，「持続可能社会創造ユニット」の特性ともよく合い，研究連携基盤ならでは研究基盤ができつつ

あることを実感できました.

参加者は，現地とオンライン合わせて 193 名で，講師も入れると 202 名という大規模でかつ充実したなミーティングとなりました．これは，国際共同利用・共同研究拠点のご支援により実現したもので，ここで厚く御礼を申し上げます.

第２回ナノカーボンデバイス国際研究拠点セミナー
実施報告書

主　催：ナノカーボンデバイス国際研究拠点
共　催：京都大学化学研究所共同利用・共同研究拠点
後　援：京都府及び公益財団法人京都文化交流コンベンションビューロー
会　期：2023 年 10 月 4 日（水）～10 月 6 日（金）
場　所：京都大学　宇治キャンパス　宇治おうばくプラザ

2023 年 10 月 4 日～6 日の 3 日間にわたり、京都大学宇治キャンパスおうばくプラザで、第２回ナノカーボンデバイス国際研究拠点セミナー「The 2nd Seminar on International Core-to-Core Project on Nano Carbon Device Science at Kyoto」を開催した。

π共役系化合物は導電性、光吸収・発光等の豊富な機能を持ち、未来の有機光電子材料開発における鍵物質である。次世代社会を支える光情報有機材料の開発には、革新的な新規化合物の探索と共に、新しい有機合成概念とデバイス作製の融合的な創発が必須である。本国際拠点形成プログラムの目的は、日本・英国・カナダ・ドイツのグループが若手研究者の交流を交えながら、新奇な炭素ナノ分子群の創製とその材料利用への展開を行う国際研究交流拠点形成を行うことにある。2022 年 9 月に英国（Imperial College London）で開催された第 1 回のキックオフシンポジウムに続き、第２回となる国際研究拠点セミナーを京都において開催した。

会議の初日（10 月 4 日）には、日本側拠点のコーディネーターである山子教授より、本国際拠点形成プロジェクトの目的と今回開催する第 2 回ナノカーボンデバイス国際研究拠点セミナーの開催趣旨について、開会挨拶が行われた。その後、McGill 大学の Dmytro Perepichka 教授より “Design of Optoelectronic Properties in 2D Polymers and Covalent Organic Frameworks” という題目で、若手研究者向けの特別セミナー講演が行われた。15 時～16 時半の時間帯には、化学研究所の研究室および測定装置室を紹介する Lab Tour が開催された。日本側拠点の研究室の設備と最先端の測定装置が紹介され、今後の共同研究の実施に向けて情報共有が行われた。16 時半～18 時半の時間帯の Poster Session では、計 13 件のポスター発表が行われ、国内外から集まった参加者による活発な議論が行われた。その後、Poster Session と同じ会場で夕食会が開催され、引き続き研究についてのディスカッションと国際交流が行われた。

会議２日目（10 月 5 日）の午前中には、国内外の研究室の若手研究者から計 5 件の口頭発表が行われた。発表後の質疑では、詳細な測定条件や得られた結果の解釈、共同研究の可能性について、活発な議論が行われた。11 時～14 時の時間帯の Early Career Networking では、若手研究者のネットワーキング作りを目的として交流活動を行った。参加者は約 5 人程度の小グループに分かれて錦市場周辺を散策し、京都の街並みや食文化に触れる体験を共有することで、国内外の若手研究者間の情報交換と人脈形成を行うことができた。14 時～17 時半の時間帯には株式会社島津製作所 本社・三条工場の工場見学を行い、化学技術に基づくオープンイノベーションの取り組み、最先端の分析装置とその製造過程について、情報共有とディスカッションを行った。

会議３日目（10 月 6 日）の午前中には、国内外のシニア研究者から計 8 件の口頭発表が行われた。発表修了後には活発な議論が行われ、コーヒーブレイクや昼食、および、３日目午後の Group Discussion

の時間帯を含めて最先端の化学研究結果と今後の共同研究の可能性についてのディスカッションが進められた。

本国際拠点形成プログラムの主要な目的の１つは、次世代の分野融合研究を担う若手研究者の育成であり、本セミナーでは若手研究者への口頭発表賞２件とポスター発表賞４件の表彰を行った。口頭発表賞（計２件）は Jasmin Seibert (Karlsruher Institut für Technologie, Germany) と Dr. Matthew Ward (Imperial College London, UK) にそれぞれ授与された。また、英国王立化学会（RSC）がスポンサーとなる Chemical Communication Award と Faraday Discussion Award のポスター賞（計２件）が Atsuhiro Ikeno (Grad. Sch. Sci., Kyoto University, Japan) と Hiroki Sato (ICR, Kyoto University, Japan) にそれぞれ授与された。日本化学会（CSJ）がスポンサーとなる BCSJ Award と Chemistry Letters Young Researcher Award のポスター賞（計２件）が Weizhe Hu (ICR, Kyoto University, Japan) と André Jung (Karlsruher Institut für Technologie, Germany) にそれぞれ授与された。

今回の国際研究拠点セミナーでは、これらの活動を通じて、次世代のナノカーボンデバイスの実現に向けた国際的交流と若手育成の場を提供することができ、当初の目的を無事に達成したものと考えている。次回の第３回の国際研究拠点セミナーは、Label 大学の Jean-François Morin 教授が開催責任者を担当し、Quebec city (Canada) で開催される予定である。

最後に、本シンポジウムを開催するにあたりご支援をいただいた京都大学化学研究所国際共同利用・共同研究拠点に厚く御礼を申し上げる。

文責：山子茂

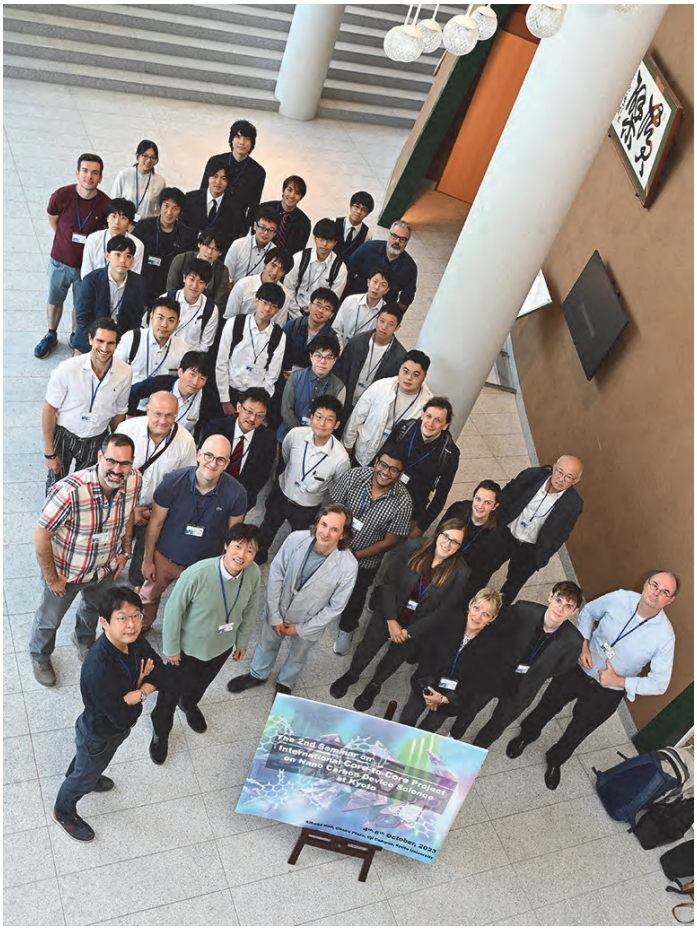

第 60 回ペプチド討論会サテライトシンポジウム:
ペプチド設計と機能拡張に関する国際ミニシンポジウム

International Mini-Symposium on Peptide Design and Functional Extension

A Satellite Symposium of the 60th Japanese Peptide Symposium

開催報告書

シンポジウム世話人　二木史朗　（化学研究所・生体機能設計化学研究領域）

趣旨：

第 60 回ペプチド討論会（大津）のサテライトシンポジウムとして、ペプチド討論会に参加する海外からの著名研究者と関連領域で活躍する日本人若手・中堅研究者を招待講演者とした「ペプチド設計と機能拡張に関する国際ミニシンポジウム」を企画した。また、一般講演としてポスター発表も受け付けた。収容人数最大 50 名程度のセミナー室で開催し討論の密度を高めることを狙った。

日時: 2023 年 11 月 11 日（土）10:00-17:00

会場: 京都大学宇治おうばくプラザ セミナー室 4/5 （講演会場） および セミナー室 1/2 (ポスター会場)

https://www.uji.kyoto-u.ac.jp/campus/obaku.html

主催: 日本ペプチド学会

協賛: 日本化学会・日本薬学会

後援: 京都大学化学研究所 国際共同利用・共同研究拠点、バイオタージ・ジャパン（株）

参加登録費: 日本ペプチド学会／協賛学会会員 3,000 円; 一般 5,000 円; 学生 無料

シンポジウム HP: https://www.peptide-soc.jp/60jps/satellite-symposium.html

招待講演者と演題:

Anna Maria Papini (University of Florence, UNIFI): The challenge of biological function optimisation through side-chain to side-chain macrocyclisation fine tuning of peptide secondary structures

Joel P. Schneider (NCI-NIH): Inhibiting Peptide Folding for Function

Jaehoon Yu (Seoul National University): Cyclohexylalanine-containing alpha-helical amphipathic peptide with eukaryotic cell penetrating ability targets cardiolipin and rescues mitochondrial dysfunction

Thimmaiah Govindaraju (Jawaharlal Nehru Centre for Advanced Scientific Research, JNCASR): Amino Acid and Peptide-guided Molecular Architectonics

Jumpei Morimoto (University of Tokyo): Alanyl-Backbone Peptoid as a Rigid Synthetic Oligomer Useful for Intracellular PPI Inhibitors

Rie Wakabayashi (Kyushu University): Supramolecular architectures based on peptides and their interaction with cells

Gosuke Hayashi (Nagoya University): One-pot peptide ligation with novel Cys protecting groups

Yoshimasa Kawaguchi (Kyoto University): Development of a Novel Endosomolytic Peptide for Cytosolic Delivery of Proteins

Takayuki Miki (University of Tokyo): Amphiphilic Peptide-Fusion Proteins Self-Assembling within Living Cells

Rui Kamada (Hokkaido University): PPM1D phosphatase regulates neutrophil subset function via alternative splicing of CEACAM3

Daisuke Fujiwara (Osaka Metropolitan University): Generation of conformationally constrained Helix-Loop-Helix peptides that inhibit intracellular protein-protein interactions

Hiroshi Inaba (Tottori University): Microtubule Engineering through Peptide Design

参加者:

招待講演者 12 名; 一般講演者(ポスター発表) 15 名; その他の参加者 14 名; 合計 41 名

(内外国人 8 名 (在日外国人学生 2 名を含む); 学生 13 名)

謝辞

Schneider 博士、Govindaraju 教授の宿泊費 (3 泊 4 日、各 71,530 円)は京都大学化学研究所 国際共同利用・共同研究拠点経費から支出していただきました。ご支援に関して、この場を借りて感謝します。

Australia-Japan Foundation Joint Conference
実施報告書

日　時：2024 年 1 月 25 日（月）
場　所：京都大学化　宇治キャンパス　きはだホール
参加者：48 名（オーストラリア側　3 名　日本側 45 名）

表記会議が宇治キャンパスきはだホールで開催された。本会議は、ペロブスカイト太陽電池の開発研究に関するもので、国際共同研究共同利用・共同研究拠点に採択いただいている橘 泰宏教授（RMIT University、オーストラリア）と若宮がオーガナイザーを務め、Australia-Japan Foundation Grant、フィルム太陽電池研究コンソーシアム、日本太陽光発電学会 ペロブスカイト太陽電池分科会の協賛を得て開催しました。オーストラリアからは Anita Ho-Baillie 教授（University of Sydney）、Udo Bach 教授（Monash University）、橘 泰宏 教授（RMIT University）の 3 名、国内からは若宮（京都大学化学研究所 分子集合解析研究領域）、金光義彦 教授（同研究所 光ナノ量子物性科学研究領域）、猿山雅亮 特定准教授（同研究所 精密無機合成化学研究領域）、大北英生 教授（同大学工学研究科）、Shen Qing 教授（電気通信大学）、早瀬修二 特任教授（同大学）、佐伯昭紀 教授（大阪大学）の 7 名が講演を行い、ペロブスカイト太陽電池に関する最新研究について、活発な情報共有・意見交換が行われました。また、休憩時間を利用して、若宮研究室の合成・太陽電池作製・評価装置群の見学会を行いました。

参加者全員が高い研究の質と密な交流に満足し、大変盛会でありました。国際共同利用共同研究拠点の支援に感謝します。

Australia-Japan Foundation Joint Conference
参加者の集合写真

第 7 回 京都生体質量分析研究会国際シンポジウム・第 521 回 生存圏シンポジウム

実施報告書

■ 主催
第 7 回京都生体質量分析研究会国際シンポジウム実行委員会
京都生体質量分析研究会
■ 共催
京都大学 生存圏研究所
京都大学 化学研究所（国際共同利用・共同研究拠点 共同研究推進室）
京都大学 エネルギー理工学研究所 （国際・産官学連携支援推進部）
京都大学 工学研究科
■ 後援
京都大学 研究連携基盤 持続可能性社会創造ユニット
■ 日時
2024 年 1 月 30 日（火）
■開催場所
京都大学 宇治キャンパス 宇治おうばくプラザ きはだホール
■Web サイト
https://www.kbmss.org/sympo7/

令和 6 年 1 月 30 日（火）に第 7 回京都生体質量分析研究会国際シンポジウムが、「質量分析が拓く持続可能社会」というテーマの下、おうばくプラザで開催されました。本シンポジウムは、現代日本が直面する「持続可能社会」という重要な社会問題に焦点を当て、質量分析分野が当問題にどのように貢献できるかについて活発な議論が行われました。
シンポジウムには、218 名（うち外国人 20 名）の参加者が集まり、基調講演と招待講演、特別招待講演が合わせて 9 件（うち海外研究者 2 件）行われました。ランチョンセミナーは 2 件、ポスター発表は 33 件実施され、若手研究者や学生による積極的な参加が見られました。また、企業スポンサー18 社の支援により、充実した懇親会も開催されました。
特に、ポスターセッションでは、通常のポスター発表だけではなく、メインステージを利用した 1 分間フラッシュトークを実施し、若手研究者の発表能力向上に寄与しました。さらに、若手研究者同士、研究者と企業技術者・開発者間の交流を促進することで、生体質量分析という進展著しい研究分野のさらなる振興につながりました。
このシンポジウムは、持続可能性への意識を高め、参加者に新たな知見とネットワークを提

供する重要な場となりました。これは宇治キャンパスの特色を活かした議論の深化を示すものであり、今後の研究発展に大きな影響を与えることが期待されます。"

最後に、本シンポジウムを開催するにあたりご支援をいただいた京都大学化学研究所国際共同利用・共同研究拠点に厚く御礼を申し上げます。

講演の様子

1分間フラッシュトークの様子

懇親会の様子

文責：増口　潔（生体触媒化学研究領域）

3. 成果発表論文

紙数の都合により、目次に記載した論文の一部についてのみ、別刷りを次頁以降に掲載する。

Reprinted from *Nature*, 616, 783–789 (2023)

Article

Mirusviruses link herpesviruses to giant viruses

https://doi.org/10.1038/s41586-023-05962-4

Received: 27 October 2022

Accepted: 16 March 2023

Published online: 19 April 2023

Open access

Check for updates

Morgan Gaïa[1,2,9], Lingjie Meng[3,9], Eric Pelletier[1,2], Patrick Forterre[4,5], Chiara Vanni[6], Antonio Fernandez-Guerra[7], Olivier Jaillon[1,2], Patrick Wincker[1,2], Hiroyuki Ogata[3], Mart Krupovic[8] & Tom O. Delmont[1,2]✉

DNA viruses have a major influence on the ecology and evolution of cellular organisms[1–4], but their overall diversity and evolutionary trajectories remain elusive[5]. Here we carried out a phylogeny-guided genome-resolved metagenomic survey of the sunlit oceans and discovered plankton-infecting relatives of herpesviruses that form a putative new phylum dubbed *Mirusviricota*. The virion morphogenesis module of this large monophyletic clade is typical of viruses from the realm *Duplodnaviria*[6], with multiple components strongly indicating a common ancestry with animal-infecting *Herpesvirales*. Yet, a substantial fraction of mirusvirus genes, including hallmark transcription machinery genes missing in herpesviruses, are closely related homologues of giant eukaryotic DNA viruses from another viral realm, *Varidnaviria*. These remarkable chimaeric attributes connecting *Mirusviricota* to herpesviruses and giant eukaryotic viruses are supported by more than 100 environmental mirusvirus genomes, including a near-complete contiguous genome of 432 kilobases. Moreover, mirusviruses are among the most abundant and active eukaryotic viruses characterized in the sunlit oceans, encoding a diverse array of functions used during the infection of microbial eukaryotes from pole to pole. The prevalence, functional activity, diversification and atypical chimaeric attributes of mirusviruses point to a lasting role of *Mirusviricota* in the ecology of marine ecosystems and in the evolution of eukaryotic DNA viruses.

Most double-stranded DNA viruses are classified into two major realms: *Duplodnaviria* and *Varidnaviria*. *Duplodnaviria* comprises tailed bacteriophages and related archaeal viruses of the class *Caudoviricetes* as well as eukaryotic viruses of the order *Herpesvirales*. *Varidnaviria* includes large and giant eukaryotic DNA viruses from the phylum *Nucleocytoviricota* as well as smaller viruses with tailless icosahedral capsids[6]. The two realms were established on the basis of the non-homologous sets of virion morphogenesis genes (virion module), including those encoding the structurally unrelated major capsid proteins (MCPs) with the 'double jelly-roll' and HK97 folds in *Varidnaviria* and *Duplodnaviria*, respectively[6]. Both realms are represented across all domains of life, with the respective ancestors thought to date back to the last universal cellular ancestor[7].

Within *Duplodnaviria*, bacterial and archaeal members of the *Caudoviricetes* exhibit a continuous range of genome sizes, from about 10 kilobases (kb) to >700 kb, whereas herpesviruses, restricted to animal hosts, are more uniform with genomes in the range of 100–300 kb. Herpesviruses probably evolved from bacteriophages, but the lack of related viruses outside the animal kingdom raises questions regarding their exact evolutionary trajectory[5]. Members of the *Varidnaviria* also exhibit a wide range of genome sizes, from about 10 kb to >2 Mb, but there is a discontinuity in the complexity between large and giant viruses of the *Nucleocytoviricota* phylum and the rest of varidnaviruses with genomes <50 kb. It has been suggested that *Nucleocytoviricota* have evolved from a smaller varidnavirus ancestor[8–10], but the complexification entailing acquisition of multiple informational genes (informational module) remains to be fully understood.

Viruses within *Caudoviricetes* and *Nucleocytoviricota* are prevalent in the sunlit ocean where they play a critical role in regulating the community composition and blooming activity of plankton[11–17]. Here we carried out a genome-resolved metagenomic survey of planktonic DNA viruses guided by the phylogeny of a single hallmark gene. The survey covers nearly 300 billion metagenomic reads from surface-ocean samples of the *Tara* Oceans expeditions[18–20]. We characterized and manually curated hundreds of population genomes that expand the known diversity of *Nucleocytoviricota*. However, most notably, our survey led to the discovery of plankton-infecting relatives of herpesviruses that form a putative new phylum we dubbed *Mirusviricota*. The mirusviruses share complex functional traits and are widespread in the sunlit oceans where they actively infect eukaryotes, filling a critical gap in our ecological understanding of plankton. Despite a clear evolutionary relationship to herpesviruses,

[1]Génomique Métabolique, Genoscope, Institut François Jacob, CEA, CNRS, Univ. Evry, Université Paris-Saclay, Evry, France. [2]Research Federation for the Study of Global Ocean Systems Ecology and Evolution, FR2022/Tara GOSEE, Paris, France. [3]Bioinformatics Center, Institute for Chemical Research, Kyoto University, Uji, Japan. [4]Institut de Biologie Intégrative de la Cellule (I2BC), CNRS, Université Paris-Saclay, Gif sur Yvette, France. [5]Département de Microbiologie, Institut Pasteur, Paris, France. [6]MARUM Center for Marine Environmental Sciences, University of Bremen, Bremen, Germany. [7]Lundbeck Foundation GeoGenetics Centre, GLOBE Institute, University of Copenhagen, Copenhagen, Denmark. [8]Institut Pasteur, Université Paris Cité, CNRS UMR6047, Archaeal Virology Unit, Paris, France. [9]These authors contributed equally: Morgan Gaïa, Lingjie Meng. ✉e-mail: tdelmont@genoscope.cns.fr

mirusviruses encode even more genes that have closely related homologues in *Nucleocytoviricota*. These remarkable chimaeric attributes of *Mirusviricota* connect two distantly related virus realms, providing key insights into the evolution of eukaryotic DNA viruses.

Genomics of marine eukaryotic viruses

DNA-dependent RNA polymerase subunits A (RNApolA) and B (RNApolB) are evolutionarily informative gene markers occurring in most of the known DNA viruses infecting marine microbial eukaryotes[9,21], which until now included only *Nucleocytoviricota*. Here we carried out a comprehensive search for RNApolB genes from the euphotic zone of polar, temperate and tropical oceans using large co-assemblies from 798 metagenomes (total of 280 billion reads that produced about 12 million contigs longer than 2,500 nucleotides)[19,20] derived from the *Tara* Oceans expeditions[18]. These metagenomes encompass eight plankton size fractions ranging from 0.8 µm to 2,000 µm (Supplementary Table 1), all enriched in microbial eukaryotes[22,23]. We identified RNApolB genes in these contigs using a broad-spectrum hidden Markov model (HMM) profile and subsequently built a database of more than 2,500 non-redundant environmental RNApolB protein sequences (similarity <90%; Supplementary Table 2). Phylogenetic signal for these sequences not only recapitulated the considerable diversity of marine *Nucleocytoviricota*[24] but also revealed previously undescribed deep-branching lineages clearly disconnected from the three domains of life and other known viruses (Extended Data Fig. 1). We reasoned that these new clades represent previously unknown lineages of double-stranded DNA viruses.

We carried out a phylogeny-guided genome-resolved metagenomic survey focusing on the RNApolB of *Nucleocytoviricota* and new clades to delineate their genomic context (Supplementary Table 3). We characterized and manually curated 581 non-redundant *Nucleocytoviricota* metagenome-assembled genomes (MAGs) up to 1.45 Mb in length (average of about 270 kb) and 117 non-redundant MAGs up to 438 kb in length (average of about 200 kb) for the new clades. We incorporated marine *Nucleocytoviricota* MAGs from previous metagenomic surveys[11,12] and reference genomes from culture and cell sorting to construct a comprehensive database enriched in large and giant marine eukaryotic double-stranded DNA viruses (thereafter called the Global Ocean Eukaryotic Viral (GOEV) database; Supplementary Table 4). The GOEV database contains about 0.6 million genes and provides contextual information to identify main ecological and evolutionary properties of MAGs containing the new RNApolB clades.

Discovery of a third *Duplodnaviria* phylum

The newly assembled *Nucleocytoviricota* MAGs contain most of the hallmark genes of this viral phylum, corresponding to the virion and informational modules[4,5] (Supplementary Table 4). They expand the known diversity of the *Imitervirales*, *Pandoravirales*, *Pimascovirales* and *Algavirales* orders within the class *Megaviricetes*. In addition, one of the new RNApolB clades exposed a putative new *Nucleocytoviricota* class-level group we dubbed *Proculviricetes*, which is represented by six MAGs exclusively detected in the Arctic and Southern Oceans (Fig. 1). The 111 MAGs from the remaining new RNApolB clades also contain key genes evolutionarily related to the *Nucleocytoviricota* informational module, including RNApolA and RNApolB, family B DNA polymerase (DNApolB) and the transcription factor II-S (TFIIS). Single-gene phylogenies place these MAGs in one (DNApolB) or multiple clades (RNApolA and RNApolB), always in between the known *Nucleocytoviricota* orders (Extended Data Fig. 2). Signal for TFIIS was weaker owing to its shorter length. Robust phylogenomic inferences of the concatenated four informational gene markers indicate that they represent a monophyletic viral clade with several hallmark genes closely related to, yet distinct from, those in the known *Nucleocytoviricota* classes (Fig. 1). We dubbed viruses in this clade the mirusviruses (*mirus* is a Latin word for surprising or strange).

The mirusvirus MAGs are organized into seven distinct subclades, M1 to M7 (from the most to least populated), with M1 and M7 being represented by 41 MAGs and a single MAG, respectively (Fig. 2a and Supplementary Table 4). Notably, however, they were devoid of identifiable homologues of the *Nucleocytoviricota* virion module, including the double jelly-roll MCP. Instead, annotation of mirusvirus gene clusters using sensitive sequence and structure similarity searches (Methods) identified a distant homologue of HK97-fold MCPs occurring in most of these MAGs (Fig. 1 and Extended Data Fig. 3). The presence of this MCP fold, shared only with *Caudoviricetes* and *Herpesvirales*, indicates that mirusviruses belong to the realm *Duplodnaviria*. Consistent with the identification of this MCP, further comparisons of HMM profiles and predicted three-dimensional (3D) structures uncovered key remaining components of the *Duplodnaviria* virion module, including the terminase (ATPase–nuclease, key component of the DNA packaging machine), portal protein, capsid maturation protease and triplex capsid proteins 1 and 2 (Fig. 1, Extended Data Fig. 4 and Supplementary Table 5). The presence of the genes encoding these proteins in mirusviruses establishes that they are bona fide large DNA viruses capable of forming viral particles similar to those of previously known viruses in the realm *Duplodnaviria*. Notably, phylogenetic inferences of the mirusvirus HK97-fold MCP recapitulated the seven subclades initially identified on the basis of DNApolB, RNApolA, RNApolB and TFIIS (Fig. 2b), indicative of a coevolution of the virion and informational modules.

The extensive sequence divergences and length disparities for proteins of the virion module between mirusviruses, herpesviruses and *Caudoviricetes* (Supplementary Table 5) prevented meaningful phylogenetic inferences for the newly expanded realm *Duplodnaviria*. Nevertheless, multiple components of this module provided critical insights clarifying the evolutionary trajectory of mirusviruses. First, the two triplex capsid proteins, which form a heterotrimeric complex and stabilize the capsid shell through interactions with adjacent MCP subunits[25], are conserved across herpesviruses but are missing in *Caudoviricetes*. Second, in herpesvirus MCPs, the HK97-fold domain, referred to as the floor domain and responsible for capsid shell formation, is embellished with a 'tower' domain that projects away from the surface of the assembled capsid[26]. The tower domain is an insertion within the A subdomain of the core HK97 fold[26,27]. In mirusviruses, the MCP protein also contains an insertion within the A subdomain, albeit of substantially smaller size (Fig. 1 and Extended Data Figs. 3 and 4). This tower domain has not been thus far described for any member of the *Caudoviricetes*, including the so-called jumbo phages (that is, phages with a very large genome[28]). Overall, the triplex capsid proteins and the MCP tower represent hallmark traits pointing to a closer evolutionary relationship between mirusviruses and herpesviruses compared to their bacterial and archaeal relatives.

Phylogenetic inferences of the DNApolB gene using the GOEV database and a wide range of eukaryotic and additional viral lineages[29] supported the evolutionary distance of mirusviruses relative to all other known clades of double-stranded DNA viruses (Extended Data Fig. 5). The monophyletic mirusvirus DNApolB was positioned as a sister clade to *Herpesviridae*, and the two clades of eukaryotic *Duplodnaviria* were most closely related to eukaryotic Zeta-type and Delta-type DNApolB sequences, together forming a strongly supported clade distinct from the DNApolB of other viruses. Taken together, the considerable genetic distances between the virion modules of mirusviruses, *Caudoviricetes* and *Herpesvirales*, the distinct 3D structures of the mirusvirus MCP (see predicted 3D structure comparisons in Extended Data Fig. 4) and the DNApolB phylogenetic inferences firmly position mirusviruses within the realm *Duplodnaviria*, but outside the two previously characterized phyla *Uroviricota* (*Caudoviricetes*) and *Peploviricota* (herpesviruses), in a separate phylum we dubbed *Mirusviricota*.

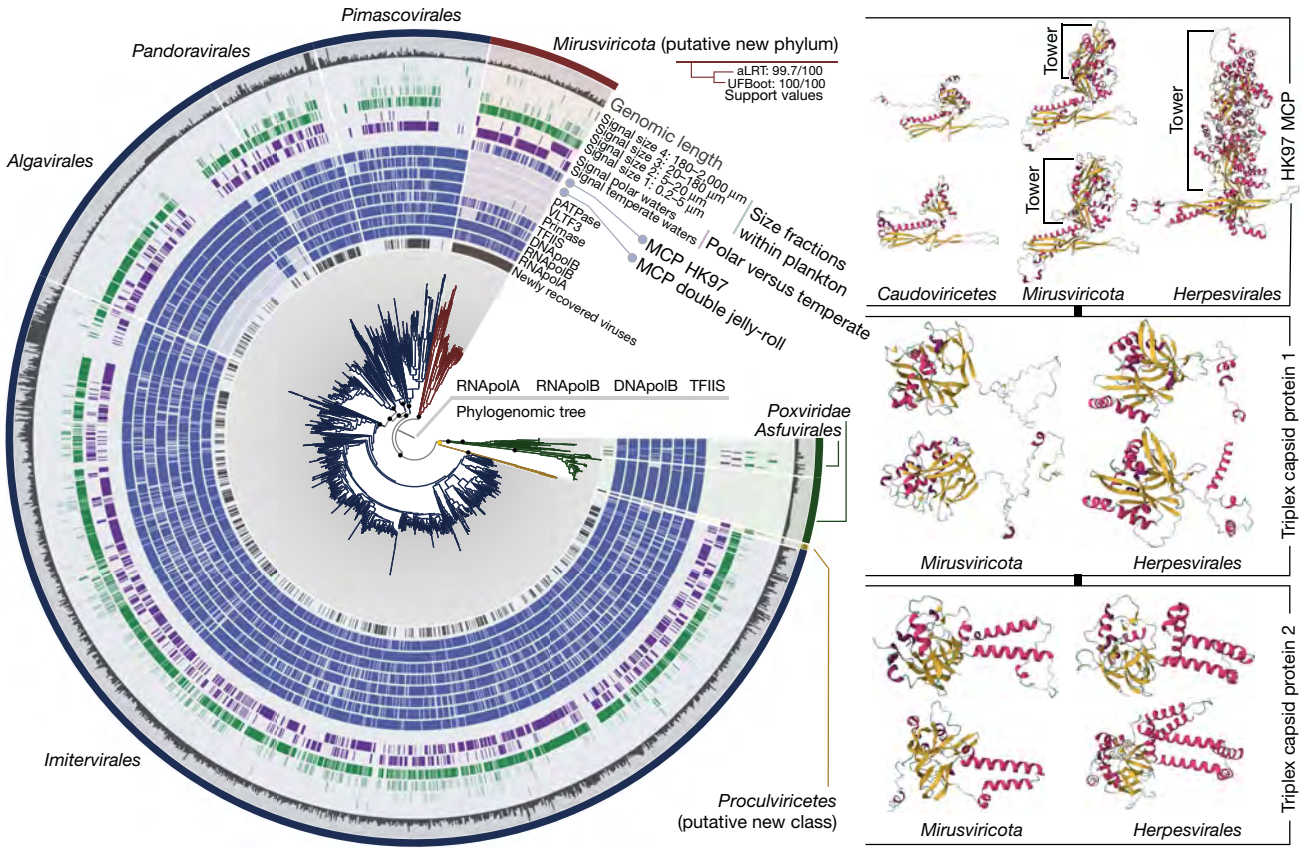

Fig. 1 | Evolutionary relationships between *Nucleocytoviricota*, *Herpesvirales* and mirusviruses. Left: a maximum-likelihood phylogenetic tree built from the GOEV database (1,722 genomes) on the basis of a concatenation of manually curated RNApolA, RNApolB, DNApolB and TFIIS genes (3,715 amino acid positions) using the posterior mean site frequency mixture model (LG + C30 + F + R10) and rooted between mirusviruses and the rest. Highlighted phylogenetic supports (dots in the tree) were considered high (approximation likelihood ratio (aLRT) ≥ 80 and ultrafast bootstrap approximation (UFBoot) ≥ 95, in black) or medium (aLRT ≥ 80 or UFBoot ≥ 95, in yellow; see Methods). The tree was decorated with rings of complementary information and visualized with anvi'o. Right: predicted 3D structures for the HK97 MCP of *Caudoviricetes*, mirusvirus and herpesvirus representatives obtained using AlphaFold2. Proteins are coloured on the basis of secondary structure properties. The panel also shows predicted 3D structures for the triplex capsid proteins of mirusvirus and herpesvirus representatives using the same methodology.

Mirusviruses are functionally complex

The 111 *Mirusviricota* MAGs contain a total of 22,242 genes organized into 35 core gene clusters present in at least 50% of MAGs, 1,825 non-core gene clusters and finally 9,018 singletons with no close relatives within the GOEV database (Supplementary Tables 6 and 7). Core gene clusters provided a window into critical functional capabilities shared across subclades of mirusviruses (Supplementary Table 8). Aside from the aforementioned core components of the virion and informational modules, they correspond to functions related to DNA stability (H3 histone), DNA replication (DNA replication licensing factor, glutaredoxin/ribonucleotide reductase, Holliday junction resolvase and 3′ repair exonuclease 1), transcription (TATA-binding protein), gene expression regulation (lysine specific histone demethylase 1A), post-transcriptional modification of RNA (RtcB-like RNA-splicing ligase) and proteins (putative ubiquitin protein ligase), protein degradation (trypsin-like, C1 and M16-family peptidases), cell growth control (Ras-related protein), detection of external signals (sensor histidine kinase) and light-sensitive receptor proteins (heliorhodopsins). Thus, mirusviruses encode an elaborate toolkit that could enable fine-tuning the cell biology and energetic potential of their hosts for optimal virus replication. Finally, ten core gene clusters could not be assigned any function on the basis of sequence or structural comparisons to proteins in reference databases and await experimental functional characterization.

Clustering of *Mirusviricota* MAGs and reference viral genomes from culture (including *Nucleocytoviricota*, *Herpesvirales* and *Caudoviricetes*) based on quantitative occurrence of gene clusters highlighted the strong functional differentiation between mirusviruses and herpesviruses and, conversely, a strong functional similarity between mirusviruses and *Nucleocytoviricota* (Extended Data Fig. 6 and Supplementary Table 9). Thus, function-wise, mirusviruses more closely resemble the *Nucleocytoviricota* viruses (many of which are also widespread at the surface of the oceans; see Fig. 1) as compared to *Herpesvirales*. To further explore the functional landscape of eukaryote-infecting marine viruses, we clustered their genomes on the basis of quantitative occurrence of gene clusters using the entire GOEV database (Supplementary Tables 6 and 7). The mirusviruses clustered together and were further organized into subclades in line with phylogenomic signals (Extended Data Fig. 7). By contrast, this analysis emphasized the complex functional makeup of *Nucleocytoviricota* lineages, with some clades (for example, the *Imitervirales* and *Algavirales*) split into multiple groups. Aside from the core components of the informational module, gene clusters connecting a substantial portion of *Mirusviricota* and *Nucleocytoviricota* genomes were dominated by functions involved in DNA replication: the glutaredoxin/ribonucleotide reductase, Holliday junction resolvase, proliferating cell nuclear antigen, dUTPase and DNA topoisomerase II. Commonly shared functions also included the Ras protein, patatin-like phospholipase (lipid degradation), peptidase C1,

a

Clade	Number of MAGs	Av. length (kb)	Av. number of contigs	Av. N50 (kb)	Av. GG content	Av. number of genes	Av. gene length (aa)	Av. number of KEGG functions	Av. number of gene clusters	Total coverage (939 metagenomes)	Oceanic regions: Polar: Arctic Ocean	Polar: Southern Ocean	Temperate: Indian Ocean	Temperate: Atlantic Ocean	Temperate: Pacific Ocean	Temperate: Med. Sea	Temperate: Red Sea	Size fractions: Size 1 0.2–5 µm	Size 2 3–20 µm	Size 3 20–180 µm	Size 4 180–2,000 µm
M1	42	169	18	24	43%	183	282	31	103	2,332×	7%	5%	11%	12%	42%	22%	1%	80%	13%	4%	3%
M2	40	253	29	16	41%	264	292	43	160	2,484×	41%	10%	5%	9%	13%	19%	3%	72%	19%	3%	6%
M3	17	174	17	20	40%	172	306	16	95	1,106×	0.3%	6%	6%	29%	40%	18%	1%	83%	15%	1%	0.4%
M4	6	159	18	17	53%	135	349	12	55	187×	0%	0%	17%	5%	48%	29%	0%	83%	0%	0.4%	17%
M5	2	158	18	12	44%	159	282	24	44	134×	100%	0%	0%	0%	0%	0%	0%	80%	20%	0.5%	0%
M6	2	92	9	23	48%	102	260	8	14	124×	100%	0%	0%	0%	0%	0%	0%	41%	53%	4%	2%
M7	1	171	14	17	58%	194	272	26	20	41×	100%	0%	0%	0%	0%	0%	0%	59%	41%	0%	0%

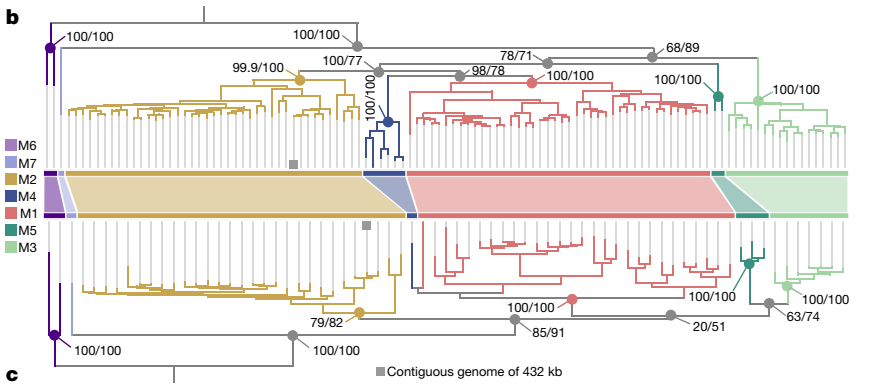

Fig. 2 | Genomic statistics and evolution of mirusviruses. a, Genomic and environmental statistics for the seven *Mirusviricota* subclades. Av., average; aa, amino acids; KEGG, Kyoto Encyclopedia of Genes and Genome; N50, the shortest contig length needed to capture 50% of the total assembly size; Med., Mediterranean. **b**, A maximum-likelihood phylogenetic tree built from the *Mirusviricota* MAGs on the basis of a concatenation of four hallmark informational genes (those encoding RNApolA, RNApolB, DNApolB and TFIIS; 3,715 amino acid positions) using the LG + F + R7 model. **c**, A maximum-likelihood phylogenetic tree built from the *Mirusviricota* MAGs on the basis of the MCP (701 amino acid positions) using the LG + R6 model. Both trees were rooted between clade M6 and other clades. Values at nodes represent branch supports (out of 100) calculated by the Shimodaira–Hasegawa-like aLRT (1,000 replicates; left score) and UFBoot (1,000 replicates; right score).

ubiquitin carboxy-terminal hydrolase (protein activity regulation) and the Evr1/Alr family (maturation of cytosolic Fe/S protein). Thus, the functional connectivity between the two phyla goes well beyond the informational module. On the other hand, hundreds of gene clusters and functions were significantly enriched in either mirusviruses or *Nucleocytoviricota* (Supplementary Tables 6–8), exposing distinct lifestyles for the two clades. Core gene clusters among the mirusviruses that were significantly less represented among *Nucleocytoviricota* genomes included the trypsin-like (73% of genomes in mirusviruses versus 9% in *Nucleocytoviricota*) and M16-family (60% versus 2%) peptidases, TATA-binding protein (59% versus 0%), heliorhodopsin (64% versus 5%) and histone (54% versus 2%). Phylogenetic inferences of the histones and rhodopsins point to a complex evolutionary history of these genes in both *Mirusviricota* and *Nucleocytoviricota*, with multiple horizontal transfer events between the virus clades and marine planktonic eukaryotes (Extended Data Fig. 8). In addition, a *Micromonas* heliorhodopsin may have originated from a mirusvirus (Extended Data Fig. 8), suggesting that *Mirusviricota* contributes, alongside *Nucleocytoviricota*[3,4], to the evolution of planktonic eukaryotes by means of gene flow.

Mirusviruses are abundant and active

To our knowledge, *Mirusviricota* represents the first eukaryote-infecting lineage of *Duplodnaviria* found to be widespread and abundant within plankton in the sunlit oceans. Indeed, mirusviruses were detected in 131 out of the 143 *Tara* Oceans stations, from pole to pole. They occurred mostly in the 0.2–5 µm (76.3% of the entire mirusvirus metagenomic signal) and 3–20 µm (15.4%) size fractions that cover a high diversity of unicellular planktonic eukaryotes[22] (Figs. 1 and 2 and Supplementary Table 10). Among the *Tara* Oceans metagenomes considered in our study, the total mean coverage of marine *Nucleocytoviricota* MAGs and culture genomes in GOEV was 15 times higher compared to that of the mirusvirus MAGs, reflecting the current imbalance in genomic units between these two phyla (1,706 versus 111). Yet, median cumulative mean coverage for the mirusviruses was higher compared to that for viruses in all *Nucleocytoviricota* orders, with the noticeable exception of *Algavirales* (Extended Data Fig. 9 and Supplementary Table 10). Thus, the mirusviruses are among the most abundant eukaryotic viruses characterized so far in the sunlit oceans.

The mirusviruses are not only abundant but also highly active within plankton. In fact, the mirusvirus MAGs, which contain just 3.8% of genes in GOEV, represent 13% of the *Tara* Oceans metatranscriptomic signal for this genomic database (Supplementary Table 11). This substantial in situ transcriptomic signal stresses the relevance of *Mirusviricota* to eukaryotic virus–host dynamics in marine systems. Mirusviruses were most active in the sunlit ocean (and especially in the euphotic subsurface layer enriched in chlorophyll) as compared to the mesopelagic zone (>200 m in depth), and within the cellular range of 0.2–20 µm (Fig. 3), in line with the metagenomic signal. The 35 core gene clusters for *Mirusviricota* represented 20% of the metatranscriptomic signal (including 12% for just seven capsid proteins), with remaining signal linked to non-core gene clusters (43%) and singletons (37%). Thus, highly diversified genes (nearly 10,000 singletons were identified) seem to play a critical role in the functional activity of *Mirusviricota* during infection of marine microbial eukaryotes.

Mirusviruses have different biogeographic distributions (for example, some are found only in the Arctic Ocean), yet their 35 core genes were expressed with similar levels in samples with metatranscriptomic signal, indicating a relatively homogeneous functional lifestyle regardless of latitude or subclade (Fig. 3 and Supplementary Table 11). The highest levels of expression were in genes coding for the capsid proteins, with ratios recapitulating the proportion of corresponding proteins in the capsid of herpesviruses (for example, more HK97 MCPs as compared

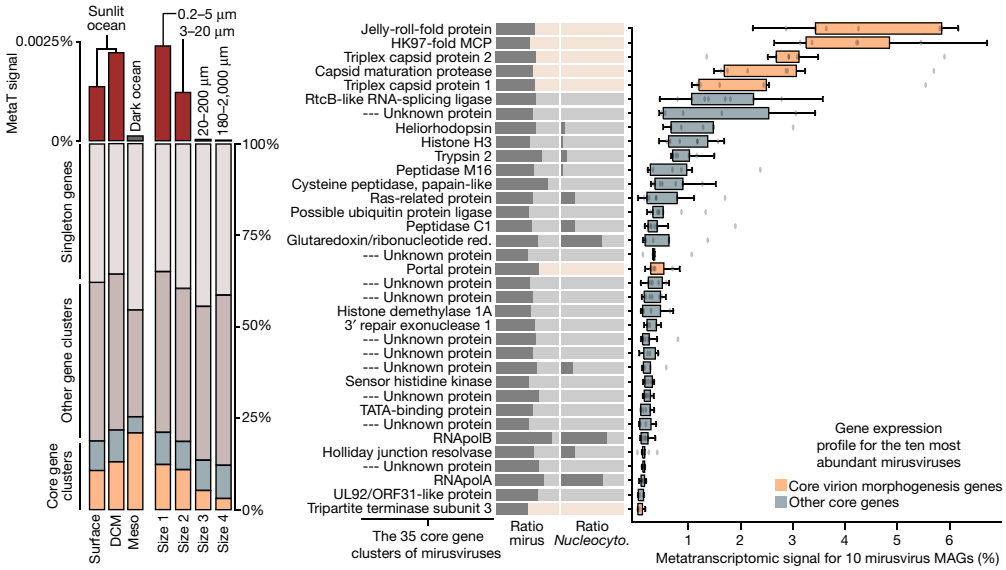

Fig. 3 | In situ expression profile of mirusviruses during infection. Left: summary of the overall metatranscriptomic signal of different gene categories for the mirusvirus MAGs among the *Tara* Oceans metatranscriptomes. DCM, deep chlorophyll maximum layer; Meso, mesopelagic (top dark ocean layer below 200 m). Right, summary of the occurrence of 35 *Mirusviricota* core gene clusters as a ratio for the mirusvirus MAGs (mirus) and *Nucleocytoviricota* (*Nucleocyto.*). The panel also shows box plots corresponding to the overall metatranscriptomic signal for genes corresponding to the 35 core gene clusters and occurring in the 10 most abundant mirusviruses among the *Tara* Oceans metagenomes. Percentage values are genome-centric and correspond to the percentage of mean coverage (sum across all the metatranscriptomes) of one gene when considering the cumulated mean coverage of all genes (sum across all the metatranscriptomes) found in the corresponding genome. Centre lines in box plots show the medians; box limits indicate the 25th and 75th percentiles; whiskers extend 1.5 times the interquartile range from the 25th and 75th percentiles; outliers are represented by dots ($n = 10$ points). Red., reductase.

to triplex or portal proteins). Genes coding for the new types of heliorhodopsin and histone were also expressed at high levels, pointing to an important functional role during infection. Collectively, the biogeographic and in situ transcriptomic patterns of mirusviruses suggest that they actively infect abundant marine unicellular eukaryotes in both temperate and polar waters.

Mirusviruses connect two viral realms

To further validate the genomic content of mirusviruses and to exclude the possibility of artificial chimaerism, we created an HMM for the newly identified *Mirusviricota* MCP and used it as bait to search for complete genomes in additional databases. First, we found only two *Mirusviricota* MCPs in a comprehensive viral genomic resource from the <0.2 µm size fraction of the surface oceans (Global Ocean Virome 2)[16], suggesting that most virions in this clade are larger than 0.2 µm in size. We subsequently screened for the *Mirusviricota* MCP in a database containing hundreds of metagenomic assemblies from the 0.2–3 µm size fraction of the surface oceans[30]. We found a contiguous *Mirusviricota* genome (355 genes) in the Mediterranean Sea affiliated to the clade M2 with a length of 431.5 kb, just 6 kb shorter than the longest *Mirusviricota* MAG (Fig. 2b,c). Its genes recapitulate the core functionalities of mirusviruses (for example, topoisomerase II, TATA-binding protein, histone, multiple heliorhodopsins, Ras-related GTPases, cell surface receptor, ubiquitin and trypsin), and 80 of these genes have a clear hit when compared to *Nucleocytoviricota* HMMs (see Methods and Extended Data Fig. 10). Most critically, not only are all hallmark genes for the informational (DNApolB, RNApolA, RNApolB and TFIIS) and virion (HK97-fold MCP, terminase, portal protein, capsid maturation protease and the two triplex capsid proteins) modules of *Mirusviricota* present but they also occur relatively homogeneously across the genome (Extended Data Fig. 10). Thus, this near-complete contiguous genome perfectly recapitulates the hallmark virion module traits shared only between mirusviruses and herpesviruses, as well as the informational module shared between *Mirusviricota* and *Nucleocytoviricota* (Fig. 4).

On the one hand, mirusviruses belong to the realm *Duplodnaviria* on the basis of their virion module. On the other hand, their hallmark informational genes have homologues prevalent in the phylum *Nucleocytoviricota* with unexpectedly high levels of sequence similarity. These results strongly indicate that this informational module originated in either giant viruses (giant virus origin hypothesis; Fig. 4b) or mirusviruses (mirusvirus origin hypothesis; Fig. 4c) and was then transferred between their two realms, most likely after the long-lasting coevolution of the corresponding genes between viruses and proto-eukaryotic hosts[9]. Thus, the mirusviruses are not only integral components of the ecology of eukaryotic plankton, but they also fill critical gaps in our understanding of the evolutionary trajectories of two major realms of double-stranded DNA viruses.

Discussion

Our phylogeny-guided genome-resolved metagenomic survey of plankton at the surface of five oceans and two seas exposed a major clade of large eukaryotic DNA viruses, with genomes that can reach more than 400 kb in length, which are diverse, prevalent and active in the sunlit oceans. This clade, dubbed *Mirusviricota*, corresponds to a putative new phylum within the realm *Duplodnaviria* that until now included only the bacteria- and archaea-infecting *Caudoviricetes* and animal-infecting *Herpesvirales*. The *Mirusviricota* phylum is organized into at least seven subclades that might correspond to distinct families. Although both mirusviruses and *Herpesvirales* are eukaryote-infecting duplodnaviruses, they exhibit very different genomic features. Most notably, mirusviruses substantially deviate from all other previously characterized groups of DNA viruses, with the virion morphogenesis module (the defining trait for highest-rank double-stranded DNA virus taxonomy) affiliated to the realm *Duplodnaviria* and the informational

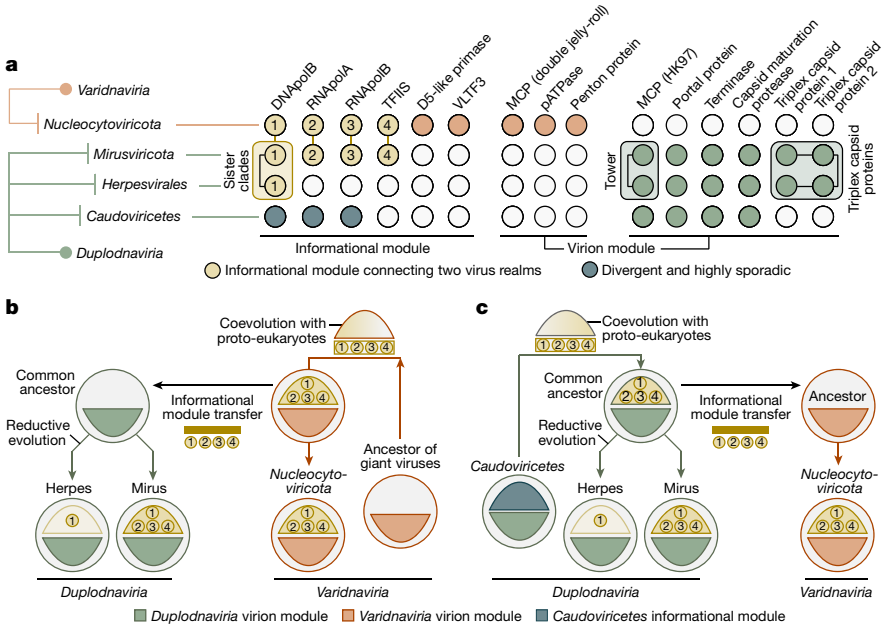

Fig. 4 | Evolutionary trajectories of the eukaryotic informational module. **a**, Summary of the occurrence of hallmark genes for the informational and virion modules in *Nucleocytoviricota*, mirusviruses, herpesviruses and *Caudoviricetes*. Informational module genes with a strong evolutionary relationship are connected with a line. Genes containing information pointing to a common eukaryotic viral ancestry between mirusviruses and herpesviruses are framed. VLTF3, viral late transcription factor 3. **b**,**c**, Descriptions of two evolutionary scenarios in which the informational module of eukaryote-infecting viruses within the realms *Duplodnaviria* and *Varidnaviria* first emerged in the ancestor of either *Nucleocytoviricota* (giant virus hypothesis) or mirusviruses (mirusvirus hypothesis).

module closely related to that of large and giant viruses within the realm *Varidnaviria*. These apparent chimaeric attributes were recapitulated in a near-complete contiguous genome of 431.5 kb. The discovery of *Mirusviricota* is a reminder that we have not yet grasped the full ecological and evolutionary complexity of even the most abundant double-stranded DNA viruses in key ecosystems such as the surface of our oceans and seas.

Mirusviruses are relatively abundant in various regions of the sunlit oceans where they actively infect eukaryotic plankton smaller than 20 µm in size and express a variety of functions. *Mirusviricota* has a cohesive and complex inferred lifestyle that includes unique features (many core genes are found only in this phylum) but also substantially overlaps with those of large and giant eukaryotic varidnaviruses[11,12]. These shared functionalities go well beyond the informational module and include ecosystem- and host-specific genes, which could have been horizontally transferred between the two groups of viruses or convergently acquired from the shared hosts at different time points during evolution. For instance, the patatin-like phospholipase shared between the two phyla had already been suggested to promote the transport of *Nucleocytoviricota* genomes to the cytoplasm and nucleus[31]. Functions enriched in mirusviruses as compared to the *Nucleocytoviricota* include phylogenetically distinct H3 histones (proteins involved in chromatin formation within the eukaryotic cells[32]) and heliorhodopsins (light-sensitive receptor proteins that can be used as proton channels by giant viruses during infection[33]). Together, biogeographic patterns, functional gene repertoires and metatranscriptomic signal indicate that mirusviruses influence the ecology of key marine eukaryotes using a previously overlooked lifestyle.

Viruses of the *Herpesvirales* and *Nucleocytoviricota* belong to two ancient virus lineages, *Duplodnaviria* and *Varidnaviria*, respectively, with their corresponding ancestors possibly antedating the last universal cellular ancestor[6,7]. Nevertheless, the exact evolutionary trajectories and the identity of the respective most recent common ancestors of these prominent eukaryote-infecting double-stranded DNA viral clades remain elusive, in part owing to the lack of known intermediate states. Particularly puzzling is the gap between the ubiquitous *Caudoviricetes*, some of which rival *Nucleocytoviricota* in terms of functional complexity and richness of their gene repertoires[34–36], and *Herpesvirales*, which are restricted to animal hosts and uniformly lack the transcription machinery and practice nuclear replication. The identification of *Mirusviricota* expands the presence of duplodnaviruses beyond animals to eukaryotic plankton hosts, strongly suggesting their ancient association with eukaryotes. The presence and location of the tower domain combined with the conservation of the two triplex capsid proteins (none of these is present in known *Caudoviricetes*) in both *Mirusviricota* and *Herpesvirales* (see Fig. 1) strongly suggests a common ancestry of these eukaryotic viruses, rather than independent evolution from distinct *Caudoviricetes* clades. The deep-branching positioning of mirusvirus informational genes attesting to one or multiple ancient transfers (Fig. 1 and Extended Data Fig. 2) and close similarity of the DNApolB between the two eukaryotic *Duplodnaviria* clades compared to other DNA virus clades (Extended Data Fig. 5) provide complementary information. With the shorter size of the tower domain and considering the later emergence of animals compared to unicellular eukaryotes, *Mirusviricota* viruses might more closely resemble the ancestral state of eukaryotic duplodnaviruses. Thus, mirusviruses point to a planktonic ancestry for herpesviruses, which would have undergone reductive evolution, most notably losing the transcription machinery, and specialized to the infection of animal cells[37].

Similarly enigmatic is the evolutionary trench between large and giant *Nucleocytoviricota* genomes and relatively simple varidnaviruses with modest gene repertoires for virion formation and genome replication (those infecting Bacteria and Archaea, as well as virophages, *Adenoviridae*, or else yaraviruses and polintoviruses[38,39]). It has been speculated that some of these simple varidnaviruses might represent evolutionary intermediates between bacteriophages and eukaryotic giant viruses from the phylum *Nucleocytoviricota*[5]. The genomic

complexity of mirusviruses within plankton, and their core functions shared with *Nucleocytoviricota* provide further insights. The informational module, and possibly other functions, may have been transferred from *Nucleocytoviricota* to the ancestor of mirusviruses (giant virus origin hypothesis), contributing to the complexification of eukaryotic duplodnaviruses. Under this scenario, a *Nucleocytoviricota* virus may have swapped its virion module with that of an uncharacterized duplodnavirus that co-infected the same host, while retaining the elaborate informational module. Yet, our data do not exclude the equally thought-provoking possibility of a transfer of the informational module from a mirusvirus to more simple ancestors of *Nucleocytoviricota* (mirusvirus origin hypothesis). This scenario could help explain the evolutionary leap from 'small' varidnaviruses to the overwhelmingly complex *Nucleocytoviricota*. Regardless of the hypothesis under consideration, mirusviruses clarify the evolutionary trajectory of eukaryotic double-stranded DNA viruses from both realms.

Overall, the prevalence, functional complexity and verified transcriptional activity of *Mirusviricota* point to a prominent role of the mirusviruses in the ecology of marine ecosystems. This putative phylum not only expands our understanding of plankton ecology, but it also provides new insights into virus evolution. Although the mirusviruses probably predated the emergence of herpesviruses, the timeline for *Mirusviricota* origins within plankton (before or after that of giant eukaryotic viruses) has yet to be elucidated. Moving forward, additional functional and genomic characterizations coupled with cultivation and environmental cell sorting for host identification will further contribute to our assessment of the lifestyle and prominence of mirusviruses within the oceans and beyond.

Online content

Any methods, additional references, Nature Portfolio reporting summaries, source data, extended data, supplementary information, acknowledgements, peer review information; details of author contributions and competing interests; and statements of data and code availability are available at https://doi.org/10.1038/s41586-023-05962-4.

1. Vincent, F., Sheyn, U., Porat, Z., Schatz, D. & Vardi, A. Visualizing active viral infection reveals diverse cell fates in synchronized algal bloom demise. *Proc. Natl Acad. Sci. USA* **118**, e2021586118 (2021).
2. Suttle, C. A. Marine viruses — major players in the global ecosystem. *Nat. Rev. Microbiol.* https://doi.org/10.1038/nrmicro1750 (2007).
3. Irwin, N. A. T., Pittis, A. A., Richards, T. A. & Keeling, P. J. Systematic evaluation of horizontal gene transfer between eukaryotes and viruses. *Nat. Microbiol.* **7**, 327–336 (2022).
4. Moniruzzaman, M., Weinheimer, A. R., Martinez-Gutierrez, C. A. & Aylward, F. O. Widespread endogenization of giant viruses shapes genomes of green algae. *Nature* https://doi.org/10.1038/s41586-020-2924-2 (2020).
5. Koonin, E. V., Dolja, V. V. & Krupovic, M. Origins and evolution of viruses of eukaryotes: the ultimate modularity. *Virology* **479–480**, 2–25 (2015).
6. Koonin, E. V. et al. Global organization and proposed megataxonomy of the virus world. *Microbiol. Mol. Biol. Rev.* **84**, e00061-19 (2020).
7. Krupovic, M., Dolja, V. V. & Koonin, E. V. The LUCA and its complex virome. *Nat. Rev. Microbiol.* **18**, 661–670 (2020).
8. Krupovic, M. & Koonin, E. V. Polintons: a hotbed of eukaryotic virus, transposon and plasmid evolution. *Nat. Rev. Microbiol.* **13**, 105–115 (2015).
9. Guglielmini, J., Woo, A. C., Krupovic, M., Forterre, P. & Gaia, M. Diversification of giant and large eukaryotic dsDNA viruses predated the origin of modern eukaryotes. *Proc. Natl Acad. Sci. USA* **116**, 19585–19592 (2019).
10. Woo, A. C., Gaia, M., Guglielmini, J., da Cunha, V. & Forterre, P. Phylogeny of the *Varidnaviria* morphogenesis module: congruence and incongruence with the tree of life and viral taxonomy. *Front. Microbiol.* **12**, 1708 (2021).
11. Schulz, F. et al. Giant virus diversity and host interactions through global metagenomics. *Nature* https://doi.org/10.1038/s41586-020-1957-x (2020).
12. Moniruzzaman, M., Martinez-Gutierrez, C. A., Weinheimer, A. R. & Aylward, F. O. Dynamic genome evolution and complex virocell metabolism of globally-distributed giant viruses. *Nat. Commun.* **11**, 1710 (2020).
13. Endo, H. et al. Biogeography of marine giant viruses reveals their interplay with eukaryotes and ecological functions. *Nat. Ecol. Evol.* **4**, 1639–1649 (2020).
14. Mann, N. H. Phages of the marine cyanobacterial picophytoplankton. *FEMS Microbiol. Rev.* **27**, 17–34 (2003).
15. Kaneko, H. et al. Eukaryotic virus composition can predict the efficiency of carbon export in the global ocean. *iScience* **24**, 102002 (2021).
16. Gregory, A. C. et al. Marine DNA viral macro- and microdiversity from pole to pole. *Cell* **177**, 1109–1123 (2019).
17. Laber, C. P. et al. Coccolithovirus facilitation of carbon export in the North Atlantic. *Nat. Microbiol.* **3**, 537–547 (2018).
18. Sunagawa, S. et al. *Tara* Oceans: towards global ocean ecosystems biology. *Nat. Rev. Microbiol.* https://doi.org/10.1038/s41579-020-0364-5 (2020).
19. Delmont, T. O. et al. Heterotrophic bacterial diazotrophs are more abundant than their cyanobacterial counterparts in metagenomes covering most of the sunlit ocean. *ISME J.* https://doi.org/10.1038/s41396-021-01135-1 (2021).
20. Delmont, T. O. et al. Functional repertoire convergence of distantly related eukaryotic plankton lineages abundant in the sunlit ocean. *Cell Genomics* https://doi.org/10.1016/J.XGEN.2022.100123 (2022).
21. Aylward, F. O., Moniruzzaman, M., Ha, A. D. & Koonin, E. V. A phylogenomic framework for charting the diversity and evolution of giant viruses. *PLoS Biol.* **19**, e3001430 (2021).
22. de Vargas, C. et al. Eukaryotic plankton diversity in the sunlit ocean. *Science* **348**, 1261605 (2015).
23. Carradec, Q. et al. A global ocean atlas of eukaryotic genes. *Nat. Commun.* **9**, 373 (2018).
24. Mihara, T. et al. Taxon richness of 'Megaviridae' exceeds those of Bacteria and Archaea in the ocean. *Microbes Environ.* **33**, 162–171 (2018).
25. Okoye, M. E., Sexton, G. L., Huang, E., McCaffery, J. M. & Desai, P. Functional analysis of the triplex proteins (VP19C and VP23) of herpes simplex virus type 1. *J. Virol.* **80**, 929–940 (2006).
26. Zhang, Y. et al. Atomic structure of the human herpesvirus 6B capsid and capsid-associated tegument complexes. *Nat. Commun.* **10**, 5346 (2019).
27. Duda, R. L. & Teschke, C. M. The amazing HK97 fold: versatile results of modest differences. *Curr. Opin. Virol.* **36**, 9–16 (2019).
28. Hua, J. et al. Capsids and genomes of jumbo-sized bacteriophages reveal the evolutionary reach of the HK97 fold. *mBio* **8**, e01579-17 (2017).
29. Kazlauskas, D., Krupovic, M., Guglielmini, J., Forterre, P. & Venclovas, C. S. Diversity and evolution of B-family DNA polymerases. *Nucleic Acids Res.* **48**, 10142 (2020).
30. Paoli, L. et al. Biosynthetic potential of the global ocean microbiome. *Nature* https://doi.org/10.1038/s41586-022-04862-3 (2022).
31. Legendre, M. et al. Diversity and evolution of the emerging Pandoraviridae family. *Nat. Commun.* **9**, 2285 (2018).
32. Talbert, P. B., Armache, K. J. & Henikoff, S. Viral histones: pickpocket's prize or primordial progenitor? *Epigenetics Chromatin* **15**, 21 (2022).
33. Hososhima, S. et al. Proton-transporting heliorhodopsins from marine giant viruses. *Elife* **11**, e78416 (2022).
34. Weinheimer, A. R. & Aylward, F. O. Infection strategy and biogeography distinguish cosmopolitan groups of marine jumbo bacteriophages. *ISME J.* https://doi.org/10.1038/s41396-022-01214-x (2022).
35. Al-Shayeb, B. et al. Clades of huge phages from across Earth's ecosystems. *Nature* **578**, 425–431 (2020).
36. Weinheimer, A. R. & Aylward, F. O. A distinct lineage of Caudovirales that encodes a deeply branching multi-subunit RNA polymerase. *Nat. Commun.* **11**, 4506 (2020).
37. Adler, B., Sattler, C. & Adler, H. Herpesviruses and their host cells: a successful liaison. *Trends Microbiol.* **25**, 229–241 (2017).
38. Yutin, N., Shevchenko, S., Kapitonov, V., Krupovic, M. & Koonin, E. V. A novel group of diverse Polinton-like viruses discovered by metagenome analysis. *BMC Biol.* **13**, 95 (2015).
39. Boratto, P. V. M. et al. Yaravirus: a novel 80-nm virus infecting Acanthamoeba castellanii. *Proc. Natl Acad. Sci. USA* **117**, 16579–16586 (2020).

Methods

Tara Oceans metagenomes and metatranscriptomes

We analysed 937 metagenomes and 1,149 metatranscriptomes from *Tara* Oceans available at the EBI under project PRJEB402. Supplementary Tables 1 and 11 report general information (including the number of reads and environmental metadata) for each metagenome and metatranscriptome.

Constrained automatic binning with CONCOCT

The 798 metagenomes corresponding to size fractions ranging from 0.8 µm to 2 mm were previously organized into 11 'metagenomic sets' on the basis of their geographic coordinates[19,20]. Those 0.28 trillion reads were used as inputs for 11 metagenomic co-assemblies using MEGAHIT[40] v1.1.1, and the contig header names were simplified in the resulting assembly outputs using anvi'o[41,42] v6.1. Co-assemblies yielded 78 million contigs longer than 1,000 nucleotides for a total volume of 150.7 Gb (refs. 19,20). Constrained automatic binning was carried out on each co-assembly output, focusing only on the 11.9 million contigs longer than 2,500 nucleotides. Briefly: anvi'o profiled contigs using Prodigal[43] v2.6.3 with default parameters to identify an initial set of genes; we mapped short reads from the metagenomic set to the contig using BWA v0.7.15 (ref. 44; minimum identity of 95%) and stored the recruited reads as BAM files using samtools[45]; anvi'o profiled each BAM file to estimate the coverage and detection statistics of each contig, and combined mapping profiles into a merged profile database for each metagenomic set. We then clustered contigs with the automatic binning algorithm CONCOCT[46] by constraining the number of clusters per metagenomic set to a number ranging from 50 to 400 depending on the set (total of 2,550 metagenomic blocks from about 12 million contigs)[19,20].

Diversity of DNA-dependent RNApolB genes

We used HMMER[47] v3.1b2 to detect genes matching to the DNA-dependent RNApolB among all 2,550 metagenomic blocks on the basis of a single HMM model. We used CD-HIT[48] v4.8.1 to create a non-redundant database of RNApolB genes at the amino acid level with sequence similarity <90% (longest hit was selected for each cluster). Short sequences were excluded. Finally, we included reference RNApolB amino acid sequences from Bacteria, Archaea, Eukarya and giant viruses[9]: the sequences were aligned with MAFFT[49] v7.464 and the FFT-NS-i algorithm with default parameters and trimmed at >50% gaps with Goalign v0.3.5 (https://www.github.com/evolbioinfo/goalign). We carried out a phylogenetic reconstruction using the best-fitting model according to the Bayesian information criterion from the ModelFinder[50] Plus option with IQ-TREE[51] v1.6.2. We visualized and rooted the phylogeny using anvi'o. This tree allowed us to identify RNApolB corresponding to the known classes of *Nucleocytoviricota*, as well as new RNApolB clades.

Phylogeny-guided genome-resolved metagenomics

Each metagenomic block containing at least one of the RNApolB genes of interest (see previous section) was manually binned using the anvi'o interactive interface to specifically search for *Nucleocytoviricota* and mirusvirus MAGs. First, we used HMMER[47] v3.1b2 to identify 8 hallmark genes (8 distinct HMM runs within anvi'o) as well as 149 additional orthologous groups often found in reference *Nucleocytoviricota* viruses[9] (a single HMM run within anvi'o). The interface considers the sequence composition, differential coverage, GC content and taxonomic signal of each contig, and displayed the eight hallmark genes as individual layers as well 149 additional orthologous groups often found in reference *Nucleocytoviricota* viruses[9] as a single extra layer for guidance. During binning, no restriction was applied in term of number of *Nucleocytoviricota* core gene markers present, as long as the signal suggested the occurrence of a putative MAG. Note that whereas some metagenomic blocks contained a limited number of MAGs, others contained dozens. Finally, we individually refined all of the *Nucleocytoviricota* and mirusvirus MAGs >50 kb in length as outlined in ref. 52, and renamed contigs they contained according to their MAG ID.

Creation of the GOEV database

In addition to the *Nucleocytoviricota* and mirusvirus MAGs characterized in our study, we included marine *Nucleocytoviricota* MAGs characterized using automatic binning in ref. 11 (n = 743) and ref. 12 (n = 444), in part using *Tara* Oceans metagenomes. We also incorporated 235 reference *Nucleocytoviricota* genomes mostly characterized by means of cultivation but also cell sorting within plankton[53]. We determined the average nucleotide identity of each pair of *Nucleocytoviricota* or mirusvirus MAGs using the dnadiff tool from the MUMmer package[54] v4.0b2. MAGs were considered redundant when their average nucleotide identity was >98% (minimum alignment of >25% of the smaller MAG in each comparison). Manually curated MAGs were selected to represent a group of redundant MAGs. For groups lacking manually curated MAGs, the longest MAG was selected. This analysis provided a non-redundant genomic database of 1,593 marine MAGs plus 224 reference genomes, named the GOEV database. We created a single contigs database for the GOEV database using anvi'o. Prodigal[43] was used to identify genes.

Curation of hallmark genes

The amino acid sequence datasets for RNApolA, RNApolB, DNApolB and TFIIS were manually curated through BLASTp alignments (BLAST[55] v2.10.1) and phylogenetic reconstructions, as previously described for eukaryotic hallmark genes[20]. Briefly, multiple sequences for a single hallmark gene within the same MAG were inspected on the basis of their position in a corresponding single-protein phylogenetic tree generated using the same protocol as described above (section entitled Diversity of DNA-dependent RNApolB genes). The genome's multiple sequences were then aligned with BLASTp to their closest reference sequence, and to each other. In case of important overlap with >95% identity (probably corresponding to a recent duplication event), only the longest sequence was conserved; in case of clear split, the sequences were fused and accordingly labelled for further inspection. Finally, RNApolA and RNApolB sequences shorter than 200 amino acids were also removed, as well as DNApolB sequences shorter than 100 amino acids, and TFIIS sequences shorter than 25 amino acids. This step created a set of curated hallmark genes.

Alignments, trimming and single-protein phylogenetic analyses

For each of the four curated hallmark genes, the sequences were aligned with MAFFT[49] v7.464 and the FFT-NS-i algorithm with default parameters. Sites with more than 50% gaps were trimmed using Goalign v0.3.5 (https://www.github.com/evolbioinfo/goalign). The L-INS-i algorithm of MAFFT and a 70% threshold for trimming gappy sites were used for the MCP sequences of mirusviruses, the heliorhodopsin and the histone sequences (for the heliorhodopsin and histone, sequences from ref. 20 and additional histone reference sequences from ref. 56 were added). IQ-TREE[51] v1.6.2 was used for the phylogenetic reconstructions, with the ModelFinder[50] Plus option to determine the best-fitting model according to the Bayesian information criterion. Supports were computed from 1,000 replicates for the Shimodaira–Hasegawa (SH)-like aLRT[57] and UFBoot[58]. As per the IQ-TREE manual, supports were deemed good when SH-like aLRT ≥ 80% and UFBoot ≥ 95%. Anvi'o v7.1 was used to visualize and root the phylogenetic trees. The trees in Extended Data Fig. 2 do not include ambiguous genomes identified iteratively with the single and concatenated proteins phylogenies (see the section describing the supermatrix phylogenetic analysis). For the large DNApolB analysis, *Duplodnaviria* and *Baculoviridae* sequences from the National Center for Biotechnology Information (NCBI) viral genomic database (https://www.ncbi.nlm.nih.gov/labs/virus/vssi/#/; accessed

April 2022), as well as eukaryotic and viral sequences from ref. 29, were collected, aligned and trimmed, and the tree was reconstructed, with the same approaches as described, except for the FFT-NS-i algorithm used with MAFFT and the gap threshold set to 50% for Goalign. Very distant clades were iteratively removed, as well as long branches and phylogenetically uninformative sequences estimated with Treemmer[59], on the basis of a relative tree length of 0.95.

Resolving hallmark genes occurring multiple times

We manually inspected all of the duplicated sequences (hallmark genes detected multiple times in the same genome) that remained after the curation step, in the context of the individual phylogenetic trees (see previous section). First, duplicates were treated as putative contaminations on the basis of major individual (that is, not conserved within a clade) incongruences with the position of the corresponding genome in the other single-protein trees. The putative contaminants were easily identified and removed. Second, we identified hallmark gene paralogues encapsulating entire clades and/or subclades, suggesting that the duplication event occurred before the diversification of the concerned viral clades. This is notably the case for most *Imitervirales*, which have two paralogues of the RNApolB. These paralogues were conserved for initial single-protein phylogenetic inferences, but then only the paralogue clades with the shortest branch were conserved for subsequent analyses, from single-protein trees to congruence inspection and concatenation. Finally, we also detected a small clade of *Algavirales* viruses containing a homologue of TFIIS branching distantly from the ordinary TFIIS type, suggesting a gene acquisition. These sequences were not included in subsequent analyses. This step created a set of curated and duplicate-free hallmark genes.

Supermatrix phylogenetic analysis of the GOEV database

Concatenations of the four aligned and trimmed curated and duplicated-free hallmark genes (methods as described above) were carried out to increase the resolution of the phylogenetic tree. Genomes containing only TFIIS out of the four hallmark genes were excluded. For the remaining MAGs and reference genomes, missing sequences were replaced with gaps. Ambiguous genomes determined on the basis of the presence of major and isolated (that is, not a clade pattern) incongruences within single and concatenated protein trees, as well as on frequent long branches and unstable positions in taxon sampling inferences, were removed. The concatenated phylogenetic trees were reconstructed using IQ-TREE[51] v1.6.2 with the best-fitting model according to the Bayesian information criterion from the ModelFinder[50] Plus option. For the analysis including the entire GOEV database, the resulting tree was then used as a guide tree for a phylogenetic reconstruction based on the site-specific frequency posterior mean site frequency mixture model[60] (LG + C30 + F + R10). For the concatenated trees, supports were computed from 1,000 replicates for the SH-like aLRT[57] and UFBoot[58]. As per the IQ-TREE manual, supports were deemed good when SH-like aLRT ≥ 80% and UFBoot ≥ 95%. Anvi'o v7.1 was used to visualize and root the phylogenetic trees.

Taxonomic inference of GOEV database

We determined the taxonomy of *Nucleocytoviricota* MAGs on the basis of the phylogenetic analysis results, using guidance from the reference genomes within the GOEV database as well as previous taxonomical inferences made in refs. 11,12,21.

Biogeography of the GOEV database

We carried out a mapping of all metagenomes to calculate the mean coverage and detection of the GOEV database. Briefly, we used BWA v0.7.15 (minimum identity of 95%) and a FASTA file containing the 1,593 MAGs and 224 reference genomes to recruit short reads from all 937 metagenomes. We considered MAGs were detected in a given filter when >25% of their length was covered by reads to minimize non-specific read recruitments[61]. The number of recruited reads below this cutoff was set to 0 before determining vertical coverage and percentage of recruited reads.

Metatranscriptomics of the GOEV database

We carried out a mapping of all *Tara* Oceans metatranscriptomes to calculate the mean coverage and detection of genes found in the GOEV database. Briefly, we used BWA v0.7.15 (minimum identity of 95%) and a FASTA file containing the 0.6 million genes to recruit short reads from all 937 metagenomes.

Orthologous groups from Orthofinder

Orthologous groups (OGs) in mirusvirus MAGs (n = 111), a mirusvirus near-complete contiguous genome and reference genomes from the Virus-Host Database (VHDB; including 1,754 *Duplodnaviria*, 184 *Varidnaviria* and 11 unclassified genomes) were generated. We used Orthofinder[62] v2.5.2 (-S diamond_ultra_sens) to generate OGs. A total of 26,045 OGs were generated and OGs (n = 9,631) with at least five genome observations were used to cluster genomes.

AGNOSTOS functional aggregation inference

AGNOSTOS v.1 partitioned protein-coding genes from the GOEV database in groups connected by remote homologies and categorized those groups as members of the known or unknown coding sequence space on the basis of the workflow described previously[63]. AGNOSTOS produces groups of genes with low functional entropy as shown in refs. 20,63 allowing us to provide functional annotation (Pfam domain architectures) for some of the gene clusters using remote homology methods.

Identification and modelling of the mirusvirus MCP

The putative MCP of mirusvirus and the other morphogenetic module proteins were identified with the guidance of AGNOSTOS results, using HHsearch against the publicly available Pfam v35, PDB70 and UniProt/Swiss-Prot viral protein databases[64,65]. The candidate MCP was then modelled using AlphaFold2 (refs. 66,67) (using Cobafold v1.4) and RoseTTAFold[68] v.1.1.0. The resulting 3D models were then compared to the MCP structures of phage HK97 and human cytomegalovirus and visualized using ChimeraX[69] v.1.4.

Functional inferences of *Nucleocytoviricota* genomes

Genes from the GOEV database were BLASTp-searched against VHDB[70], RefSeq[71], UniRef90 (ref. 72), NCVOGs[73] (all databases were updated to the November 2021 version) and NCBI nr database (August 2020) using Diamond[74] v2.0.6 with a cutoff E value 1×10^{-5}. A recently published GVOG database[21] was also used in annotation using hmmer[47] v3.2.1 search with an E value of 1×10^{-3} as a significant threshold. In addition, KEGG Orthology and functional categories were assigned with Eggnog-Mapper[75] v2.1.5. Finally, tRNAscan-SE[76] v2.0.7 predicted 7,734 tRNAs.

3D structure prediction of *Mirusviricota* core genes

Proteins corresponding to *Mirusviricota* core gene clusters and lacking functional annotation based on sequence similarities were modelled using AlphaFold2 v2.3.0 (refs. 66,67; -c full_dbs -t 2022-03-12). DALI server[77] was used to predict their functionality on the basis of protein structure comparisons.

3D structure prediction of *Duplodnaviria* hallmark virion module genes

Virion module genes of *Duplodnaviria* were collected from the NCBI protein database on the basis of the annotation in their initial submission. The genomes of virion module genes represent the viral families *Herpesviridiae*, *Alloherpesviridae*, *Ackermannviridae*, *Autographiviridae*, *Chaseviridae*, *Demerecviridae*, *Drexlerviridae*, *Herelleviridae*, *Myoviridae*, *Podoviridae*, *Schitoviridae*, *Siphoviridae*, *Zobellviridae*, *Guelinviridae*, *Rountreeviridae*, *Salasmaviridae* and an unclassified

caudovirus, lilyvirus. The gene clusters of *Mirusviricota* corresponding to those virion modules were collected in seven mirusvirus subclades. The 3D models were predicted using AlphaFold2 v2.3.0 (refs. 66,67) (-c full_dbs -t 2022-03-12), and the first ranked structure model was used for the following analyses.

3D structure comparisons

Foldseek v4.645 (ref. 78) was used to align multiple predicted protein structures with the program easy-search. The TM score of the alignment was calculated and normalized by alignment length. The clustering of 3D structures for the *Duplodnaviria* MCP was carried out using the anvi'o programs anvi-matrix-to-newick and anvi-interactive with manual mode.

Realm assignation of genes from a near-complete genome

Two in-house HMM databases were created as follows. First, all coding sequences (CDSs) labelled as *Nucleocytoviricota* were removed from the *Varidnaviria* CDS dataset (n = 53,776) in the VHDB[70] (May 2022). To this dataset, *Tara* Ocean *Nucleocytoviricota* MAGs (all were manually curated) and 235 reference *Nucleocytoviricota* genomes were integrated. The final *Nucleocytoviricota* protein database contained 269,523 CDSs. Similarly, we replaced all *Herpesvirales* CDSs in the VHDB *Duplodnaviria* CDS dataset with *Herpesvirales* protein sequences downloaded from NCBI in April 2022. Additionally, a marine *Caudovirales* database including jumbo phage environmental genomes[34,35] was integrated into the *Duplodnaviria* proteins. The final *Duplodnaviria* protein database contained 748,546 proteins. Proteins in the two databases were independently clustered at 30% sequence identity (-c 0.4 --cov-mode 5), using Linclust in MMseqs[79] v13-45111. Gene clusters with fewer than three genes were removed, and the remaining gene clusters were aligned using MAFFT[49] v7.487. HMM files (n = 16,689 and 57,259 for *Varidnaviria* and *Duplodnaviria*, respectively) were created using hmmbuild in HMMER3 (ref. 80) v3.2.1. All proteins in the near-complete *Mirusviricota* genome were searched against the two custom HMM databases using the hmmsearch with a cutoff E value of 1×10^{-6}.

Statistical analyses

One-sided Fisher's exact test (greater) was used to identify KEGG Orthology functions as well as gene clusters with remote homologies that are significantly enriched in 111 *Mirusviricota* MAGs compared to all other *Nucleocytoviricota* in the GOEV database, on the basis of the occurrence of those functions and gene clusters. P values were corrected using the Benjamini–Hochberg procedure in R, and values <0.05 were considered significant.

Naming of *mirus* and *procul*

The Latin adjective *mirus* (surprising, strange) was selected to describe the putative new *Duplodnaviria* phylum: the *Mirusviricota*. The Latin adverb *procul* (away, at distance, far off) was selected to describe the putative new class of *Nucleocytoviricota* discovered from the Arctic and Southern Oceans: the *Proculviricetes*.

Reporting summary

Further information on research design is available in the Nature Portfolio Reporting Summary linked to this article.

Data availability

Databases our study used include: *Tara* Oceans metagenomes and metatranscriptomes (https://www.ebi.ac.uk/ena/browser/view/PRJEB402); publicly available marine MAGs from the phylum *Nucleocytoviricota*[11,12]; the VHDB (https://www.genome.jp/virushostdb/); RefSeq (https://ftp.ncbi.nlm.nih.gov/refseq/); UniRef90 (https://ftp.ebi.ac.uk/pub/databases/uniprot/uniref/uniref90/); NCVOG (https://ftp.ncbi.nih.gov/pub/wolf/COGs/NCVOG/); and NCBI nr database (https://ftp.ncbi.nih.gov/blast/db/). Data generated in our study has been made publicly available at https://doi.org/10.6084/m9.figshare.20284713—this link provides access to: the RNApolB genes reconstructed from the *Tara* Oceans assemblies (along with references); individual FASTA files for the 1,593 non-redundant marine *Nucleocytoviricota* and mirusvirus MAGs (including the 697 manually curated MAGs from our survey) and 224 reference *Nucleocytoviricota* genomes contained in the GOEV database; the GOEV anvi'o contigs database; genes and proteins found in the GOEV database; manually curated hallmark genes; predicted 3D structures of the *Duplodnaviria* virion module (includes proteins and their alignments); phylogenies and associated anvi'o PROFILE databases with metadata; HMMs for hallmark genes; a FASTA file for the near-complete contiguous genome (SAMEA2619782_METAG_scaffold_2); and Supplementary Tables 1–11. Source data are provided with this paper.

40. Li, D., Liu, C. M., Luo, R., Sadakane, K. & Lam, T. W. MEGAHIT: an ultra-fast single-node solution for large and complex metagenomics assembly via succinct de Bruijn graph. *Bioinformatics* **31**, 1674–1676 (2014).
41. Eren, A. M. et al. Anvi'o: an advanced analysis and visualization platform for 'omics data. *PeerJ* **3**, e1319 (2015).
42. Eren, A. M. et al. Community-led, integrated, reproducible multi-omics with anvi'o. *Nat. Microbiol.* **6**, 3–6 (2021).
43. Hyatt, D. et al. Prodigal: prokaryotic gene recognition and translation initiation site identification. *BMC Bioinform.* **11**, 119 (2010).
44. Li, H. & Durbin, R. Fast and accurate short read alignment with Burrows-Wheeler transform. *Bioinformatics* **25**, 1754–1760 (2009).
45. Li, H. et al. The Sequence Alignment/Map format and SAMtools. *Bioinformatics* **25**, 2078–2079 (2009).
46. Alneberg, J. et al. Binning metagenomic contigs by coverage and composition. *Nat. Methods* **11**, 1144–1146 (2014).
47. Eddy, S. R. Accelerated profile HMM searches. *PLoS Comput. Biol.* **7**, e1002195 (2011).
48. Li, W. & Godzik, A. Cd-hit: a fast program for clustering and comparing large sets of protein or nucleotide sequences. *Bioinformatics* **22**, 1658–1659 (2006).
49. Katoh, K. & Standley, D. M. MAFFT multiple sequence alignment software version 7: improvements in performance and usability. *Mol. Biol. Evol.* **30**, 772–780 (2013).
50. Kalyaanamoorthy, S., Minh, B. Q., Wong, T. K. F., von Haeseler, A. & Jermiin, L. S. ModelFinder: fast model selection for accurate phylogenetic estimates. *Nat. Methods* **14**, 587–589 (2017).
51. Nguyen, L. T., Schmidt, H. A., von Haeseler, A. & Minh, B. Q. IQ-TREE: a fast and effective stochastic algorithm for estimating maximum-likelihood phylogenies. *Mol. Biol. Evol.* **32**, 268–274 (2015).
52. Delmont, T. O. & Eren, A. M. Identifying contamination with advanced visualization and analysis practices: metagenomic approaches for eukaryotic genome assemblies. *PeerJ* **4**, e1839 (2016).
53. Needham, D. M. et al. Targeted metagenomic recovery of four divergent viruses reveals shared and distinctive characteristics of giant viruses of marine eukaryotes. *Philos. Trans. R. Soc. B* **374**, 20190086 (2019).
54. Delcher, A. L., Phillippy, A., Carlton, J. & Salzberg, S. L. Fast algorithms for large-scale genome alignment and comparison. *Nucleic Acids Res.* **30**, 2478–2483 (2002).
55. Altschul, S. F., Gish, W., Miller, W., Myers, E. W. & Lipman, D. J. Basic local alignment search tool. *J. Mol. Biol.* **215**, 403–410 (1990).
56. Yoshikawa, G. et al. Medusavirus, a novel large DNA virus discovered from hot spring water. *J. Virol.* **93**, e02130-18 (2019).
57. Guindon, S. et al. New algorithms and methods to estimate maximum-likelihood phylogenies: assessing the performance of PhyML 3.0. *Syst. Biol.* **59**, 307–321 (2010).
58. Hoang, D. T., Chernomor, O., von Haeseler, A., Minh, B. Q. & Vinh, L. S. UFBoot2: improving the ultrafast bootstrap approximation. *Mol. Biol. Evol.* **35**, 518–522 (2018).
59. Menardo, F. et al. Treemmer: a tool to reduce large phylogenetic datasets with minimal loss of diversity. *BMC Bioinform.* **19**, 164 (2018).
60. Wang, H. C., Minh, B. Q., Susko, E. & Roger, A. J. Modeling site heterogeneity with posterior mean site frequency profiles accelerates accurate phylogenomic estimation. *Syst. Biol.* **67**, 216–235 (2018).
61. Delmont, T. O. et al. Nitrogen-fixing populations of Planctomycetes and Proteobacteria are abundant in surface ocean metagenomes. *Nat. Microbiol.* **3**, 804–813 (2018).
62. Emms, D. M. & Kelly, S. OrthoFinder: solving fundamental biases in whole genome comparisons dramatically improves orthogroup inference accuracy. *Genome Biol.* **16**, 157 (2015).
63. Vanni, C. et al. Unifying the known and unknown microbial coding sequence space. *Elife* **11**, e67667 (2022).
64. Gabler, F. et al. Protein sequence analysis using the MPI Bioinformatics Toolkit. *Curr. Protoc. Bioinform.* **72**, e108 (2020).
65. Steinegger, M. et al. HH-suite3 for fast remote homology detection and deep protein annotation. *BMC Bioinform.* **20**, 473 (2019).
66. Jumper, J. et al. Highly accurate protein structure prediction with AlphaFold. *Nature* **596**, 583–589 (2021).
67. Mirdita, M. et al. ColabFold: making protein folding accessible to all. *Nat. Methods* **19**, 679–682 (2022).
68. Baek, M. et al. Accurate prediction of protein structures and interactions using a three-track neural network. *Science* **373**, 871–876 (2021).
69. Pettersen, E. F. et al. UCSF ChimeraX: structure visualization for researchers, educators, and developers. *Protein Sci.* **30**, 70–82 (2021).

70. Mihara, T. et al. Linking virus genomes with host taxonomy. *Viruses* **8**, 66 (2016).
71. Pruitt, K. D., Tatusova, T. & Maglott, D. R. NCBI reference sequences (RefSeq): a curated non-redundant sequence database of genomes, transcripts and proteins. *Nucleic Acids Res.* **35**, D61–D65 (2007).
72. Suzek, B. E., Wang, Y., Huang, H., McGarvey, P. B. & Wu, C. H. UniRef clusters: a comprehensive and scalable alternative for improving sequence similarity searches. *Bioinformatics* **31**, 926–932 (2015).
73. Yutin, N., Wolf, Y. I., Raoult, D. & Koonin, E. V. Eukaryotic large nucleo-cytoplasmic DNA viruses: clusters of orthologous genes and reconstruction of viral genome evolution. *Virol. J.* **6**, 223 (2009).
74. Buchfink, B., Xie, C. & Huson, D. H. Fast and sensitive protein alignment using DIAMOND. *Nat. Methods* **12**, 59–60 (2015).
75. Huerta-Cepas, J. et al. eggNOG 5.0: a hierarchical, functionally and phylogenetically annotated orthology resource based on 5090 organisms and 2502 viruses. *Nucleic Acids Res.* **47**, D309–D314 (2019).
76. Lowe, T. M. & Eddy, S. R. tRNAscan-SE: a program for improved detection of transfer RNA genes in genomic sequence. *Nucleic Acids Res.* **25**, 955–964 (1997).
77. Holm, L. & Rosenström, P. Dali server: conservation mapping in 3D. *Nucleic Acids Res.* **38**, W545 (2010).
78. van Kempen, M. et al. Fast and accurate protein structure search with Foldseek. Preprint at *bioRxiv* https://doi.org/10.1101/2022.02.07.479398 (2022).
79. Hauser, M., Steinegger, M. & Söding, J. MMseqs software suite for fast and deep clustering and searching of large protein sequence sets. *Bioinformatics* **32**, 1323–1330 (2016).
80. Finn, R. D., Clements, J. & Eddy, S. R. HMMER web server: interactive sequence similarity searching. *Nucleic Acids Res.* **39**, W29–W37 (2011).

Acknowledgements Our survey was made possible by two scientific endeavours: the sampling and sequencing efforts by the *Tara* Oceans Project, and the bioinformatics and visualization capabilities afforded by anvi'o (https://anvio.org/). We are indebted to all who contributed to these efforts, as well as other open-source bioinformatics tools for their commitment to transparency and openness. *Tara* Oceans (which includes the *Tara* Oceans and *Tara* Oceans Polar Circle expeditions) would not exist without the leadership of the *Tara* Oceans Foundation and the continuous support of 23 institutes (https://oceans.taraexpeditions.org/). We also acknowledge the commitment of the CNRS and Genoscope/CEA. Some of the computations were carried out using the platine, titane and curie high-performance computing machine provided through GENCI grants (t2011076389, t2012076389, t2013036389, t2014036389, t2015036389 and t2016036389). This study was supported in part by FRANCE GENOMIQUE (ANR-10-INBS-09), the Japan Society for the Promotion of Science KAKENHI (18H02279 and 22H00384), the Research Unit for Development of Global Sustainability, Kyoto University Research Coordination Alliance, and the International Collaborative Research Program of the Institute for Chemical Research, Kyoto University (2022-26, 2021-29 and 2020-28). M.K. was supported by grants from the l'Agence Nationale de la Recherche (ANR-20-CE20-0009-02 and ANR-21-CE11-0001-01), M.G. was supported by ANR ALGALVIRUS ANR-17-CE02-0012, and T.O.D. was supported by ANR HYDROGEN ANR-14-CE23-0001. Part of the computational work was carried out at the SuperComputer System, Institute for Chemical Research, Kyoto University. This article is contribution number 141 of *Tara* Oceans.

Author contributions T.O.D. conducted the study, which was initiated alongside M.G. and P.F. M.G., L.M., M.K., C.V., E.P. and T.O.D. carried out the primary data analysis. T.O.D. completed the genome-resolved metagenomic analysis. M.G. and T.O.D. curated the marker genes and identified the biological duplicates. M.G. carried out phylogenetic and phylogenomic analyses. L.M. carried out functional analyses, gene comparisons and protein structure predictions with the supervision of H.O. C.V. produced gene clusters with remote homologies with the supervision of A.F.-G. M.K. identified the MCP of *Mirusviricota* and other key genes of the virion module. E.P. carried out comparative genomic, biogeographic and metatranscriptomic analyses. All authors contributed to interpreting the data and writing the manuscript.

Competing interests The authors declare no competing interests.

Additional information

Supplementary information The online version contains supplementary material available at https://doi.org/10.1038/s41586-023-05962-4.

Correspondence and requests for materials should be addressed to Tom O. Delmont.

Peer review information *Nature* thanks Frank Aylward, K. Eric Wommack and the other, anonymous, reviewer(s) for their contribution to the peer review of this work. Peer reviewer reports are available.

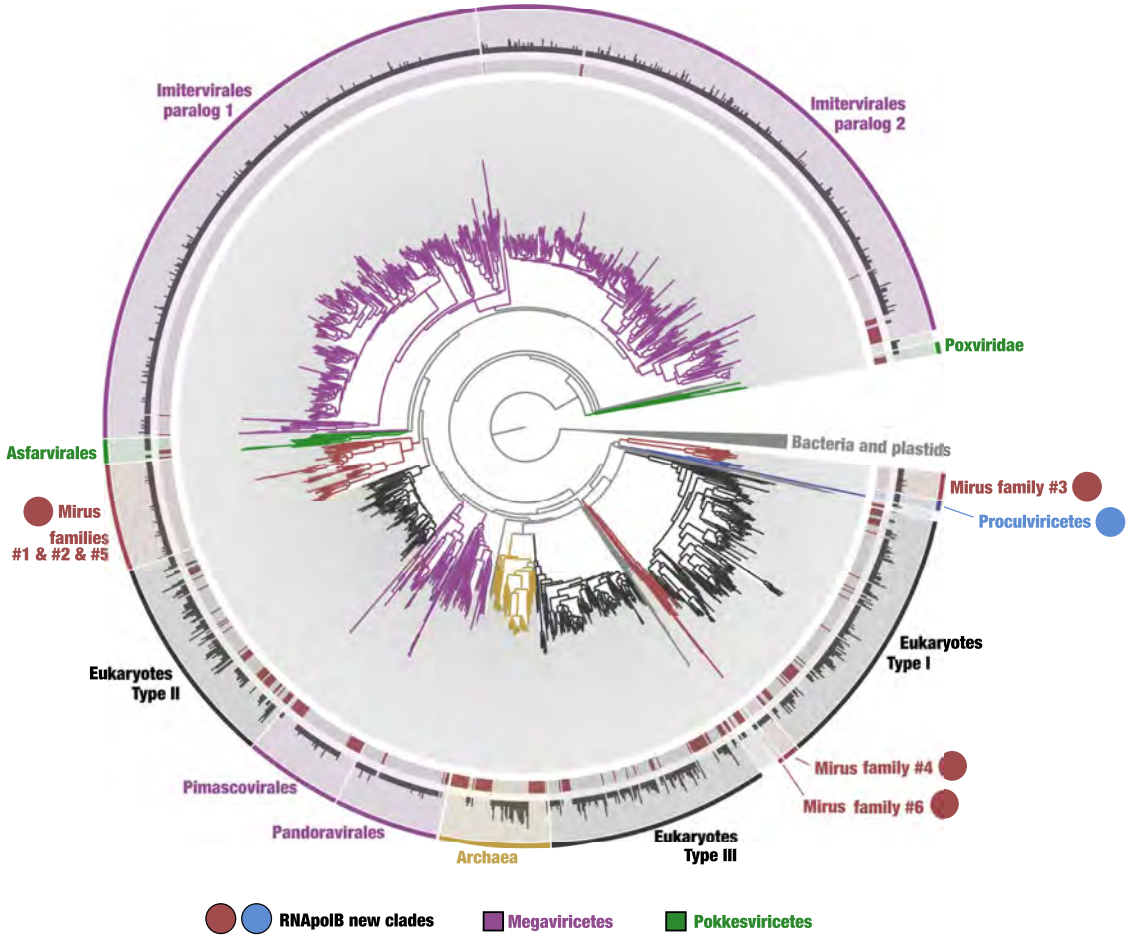

Extended Data Fig. 1 | Identification of novel DNA-dependent RNA polymerase B (RNApolB) clades in the sunlit ocean. The maximum-likelihood phylogenetic tree (LG+F+R10 model, 906 sites) is based on 2,728 RNApolB sequences more than 800 amino acids in length with similarity <90% (gray color in the inner ring) identified from 11 large marine metagenomic co-assemblies. This analysis also includes 262 reference RNApolB sequences (red color in the inner ring) corresponding to known archaeal, bacterial, eukaryotic and giant virus lineages for perspective. The middle ring shows the number of RNApolB sequences from the 11 metagenomic co-assemblies that match to the selected amino acid sequence with identity >90% (log10). The outer ring displays selections made for the different clades. Finally, RNApolB new lineages are labelled with a red dot for mirusviruses (subclades were characterized in subsequent analyses) and in blue for *Proculviricetes*.

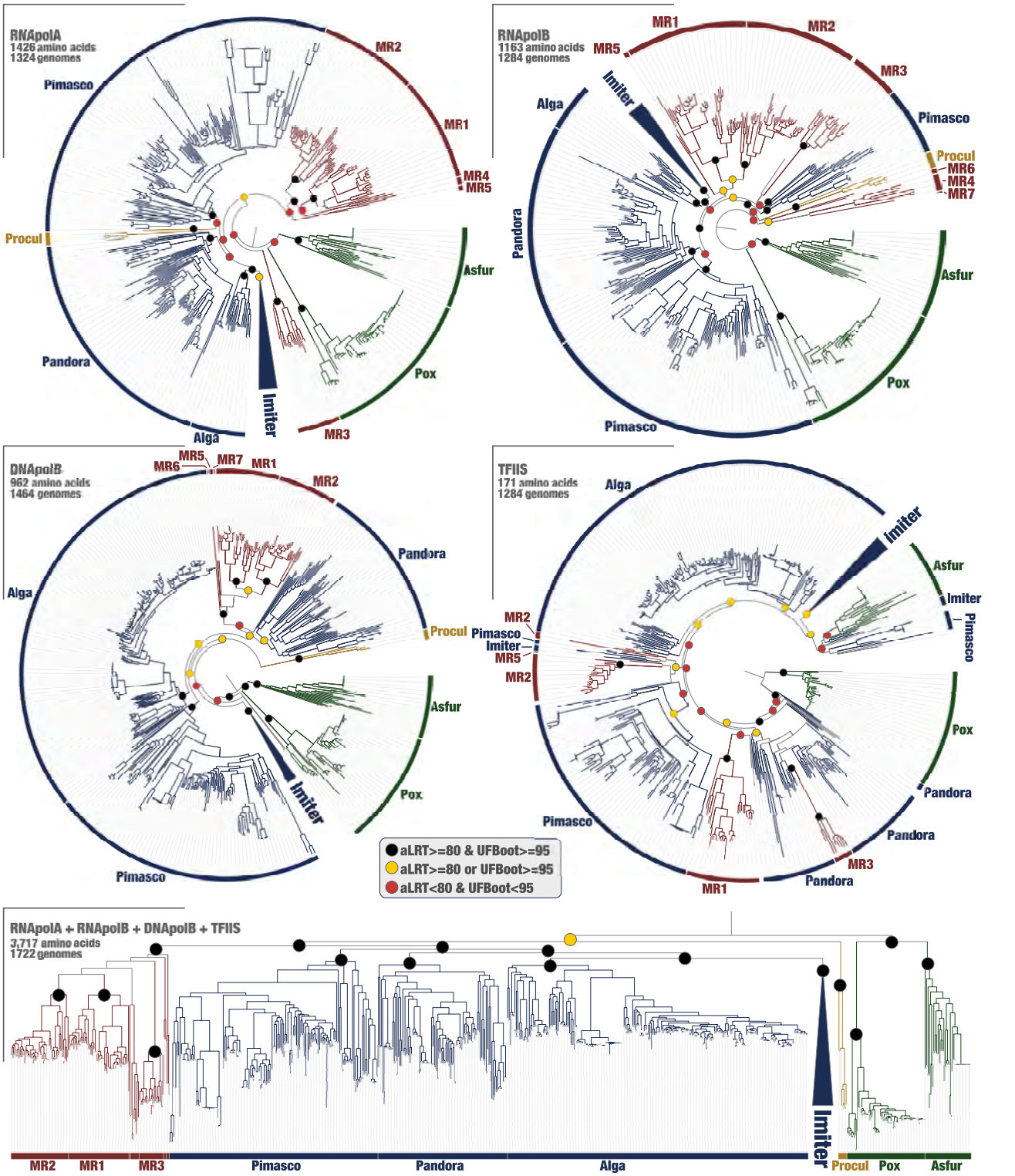

Extended Data Fig. 2 | Single-protein and concatenated phylogenies of the four informational hallmark genes in the GOEV database. Maximum-likelihood phylogenetic trees of the RNpolA, RNApolb, DNApolB and TFIIS were built from the GOEV database using the LG+F+R10 model (selected by ModelFinder Plus) and rooted between *Pokkesviricetes* and the rest. Phylogenetic supports were considered high (aLRT>=80 and UFBoot>=95, in black), medium (aLRT>=80 or UFBoot>=95, in yellow) or low (aLRT<80 and UFBoot<95, in red) (see Methods). Finally, the concatenated tree described in Fig. 1 is also presented at the bottom for perspective.

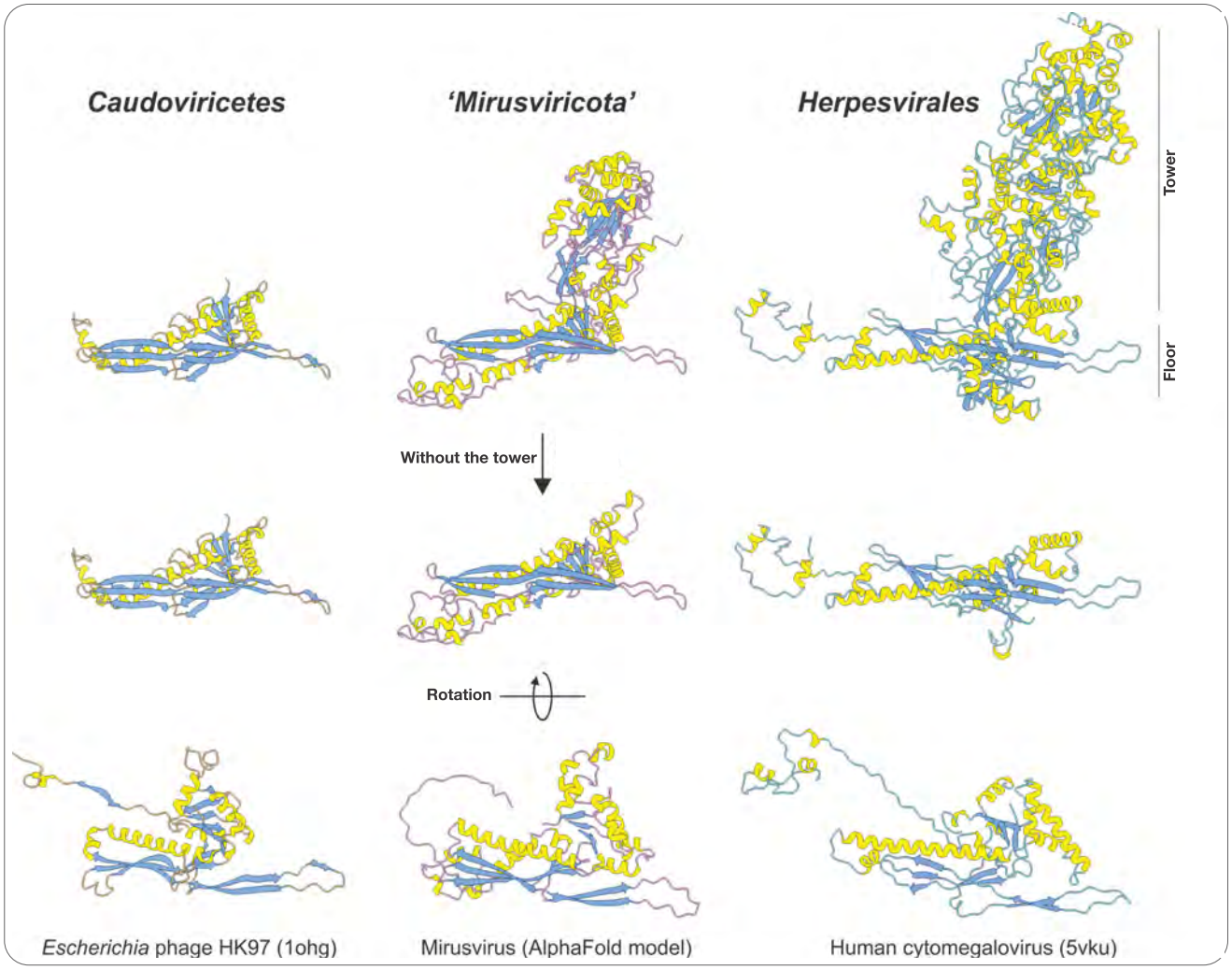

Extended Data Fig. 3 | 3D structure of the major capsid protein (MCP). The figure displays MCP 3D structures for *Escherichia* phage HK97 (*Caudoviricetes*), a representative genome for the mirusviruses (estimated using Alphafold), and the human cytomegalovirus (*Herpesvirales*). PDB accession numbers for the HK97 and cytomegalovirus MCPs are indicated in parentheses.

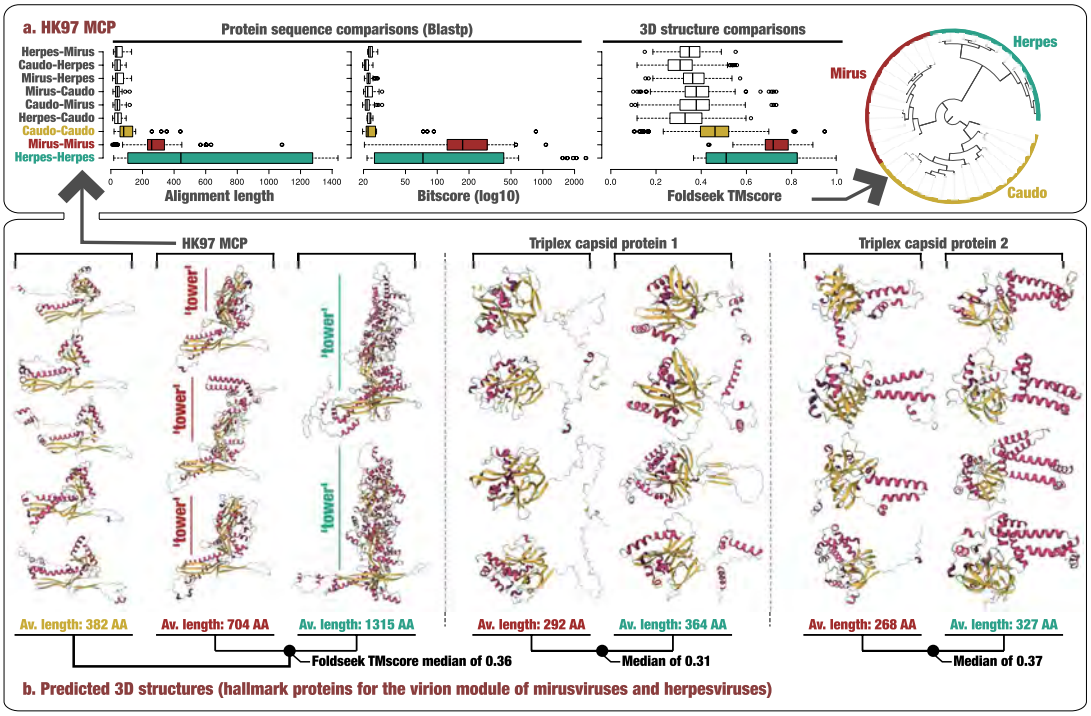

Extended Data Fig. 4 | Protein sequence and predicated 3D structures comparisons. Panel A displays protein sequence and 3D structure comparisons (Blastp and Foldseek) for the HK97 MCP of representatives covering various families from the three main *Duplodnaviria* clades. Center lines in boxplots show the medians; box limits indicate the 25th and 75th percentiles; whiskers extend 1.5 times the interquartile range from the 25th and 75th percentiles; outliers are represented by dots (from top to bottom, n = 22, 50, 38, 25, 35, 16, 40, 23 and 117 independent comparisons). The alignment values range from a minimum of 9 amino acids to a maximum of 1,437 amino acids. The bitscore values range from a minimum of 19.6 to a maximum of 2577. The Foldseek TMscore values range from a minimum of 0.09 to a maximum of 0.997. The dendrogram was generated using Euclidian distance and ward within anvi'o and is based on the Foldseek TMscore values. Panel B describes a selection of predicated 3D structures for the HK97 MCP and triplex proteins of representatives from the three main *Duplodnaviria* clades (*Caudoviricetes* viruses lack the triplex capsid proteins). Proteins are colored based on secondary structure properties.

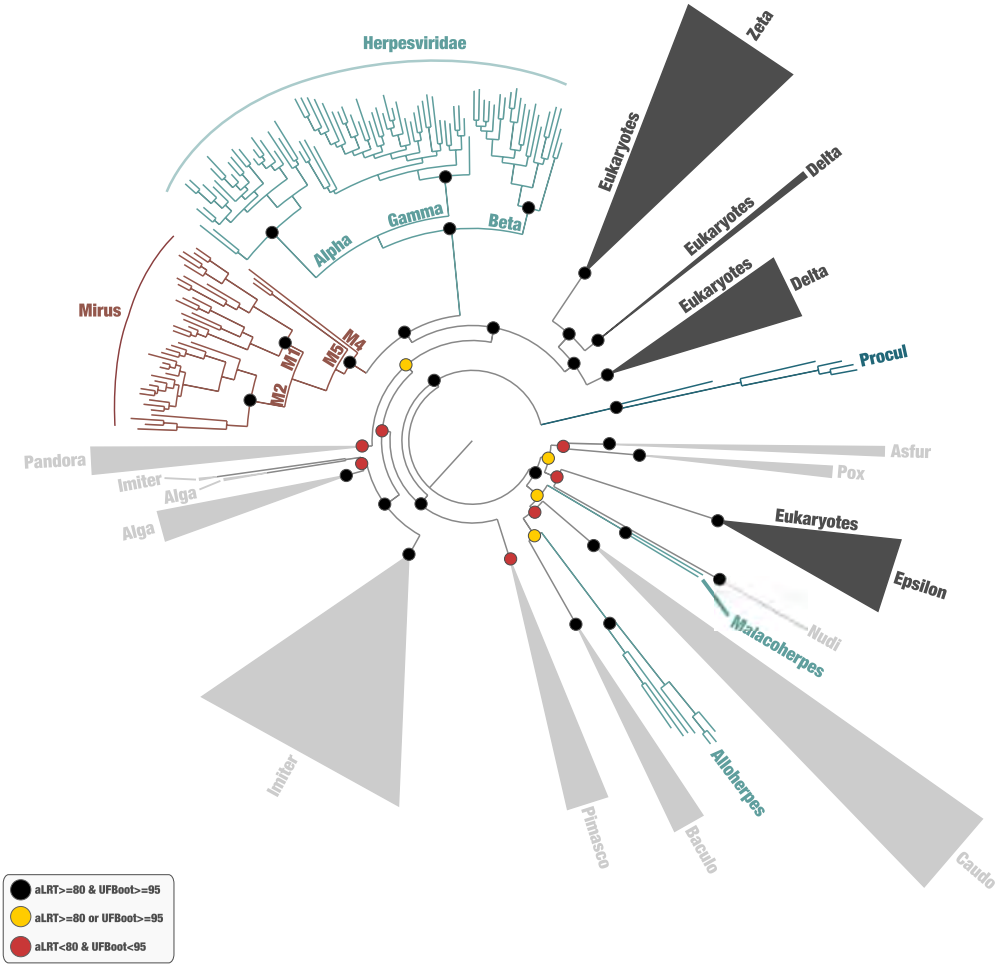

Extended Data Fig. 5 | Phylogeny of the DNApolB hallmark gene. The figure displays a maximum-likelihood phylogenetic tree (847 sites, 1,475 sequences) of DNA-polymerase B-family sequences using the LG+F+R10 model (selected by ModelFinder Plus) from the database described herein, *Duplodnaviria* and *Baculoviridae* sequences from the NCBI viral genomic database, and eukaryotic and viral sequences from Kazlauskas et al.[29] (see Methods). Eukaryotic Epsilon-type and related clades were used as outgroup. Phylogenetic supports were considered high (aLRT>=80 and UFBoot>=95, in black), medium (aLRT>=80 or UFBoot>=95, in yellow) or low (aLRT<80 and UFBoot<95, in red) (see Methods). Baculo: Baculoviridae; Caudo: Caudoviricetes; Nudi: Nudiviridae.

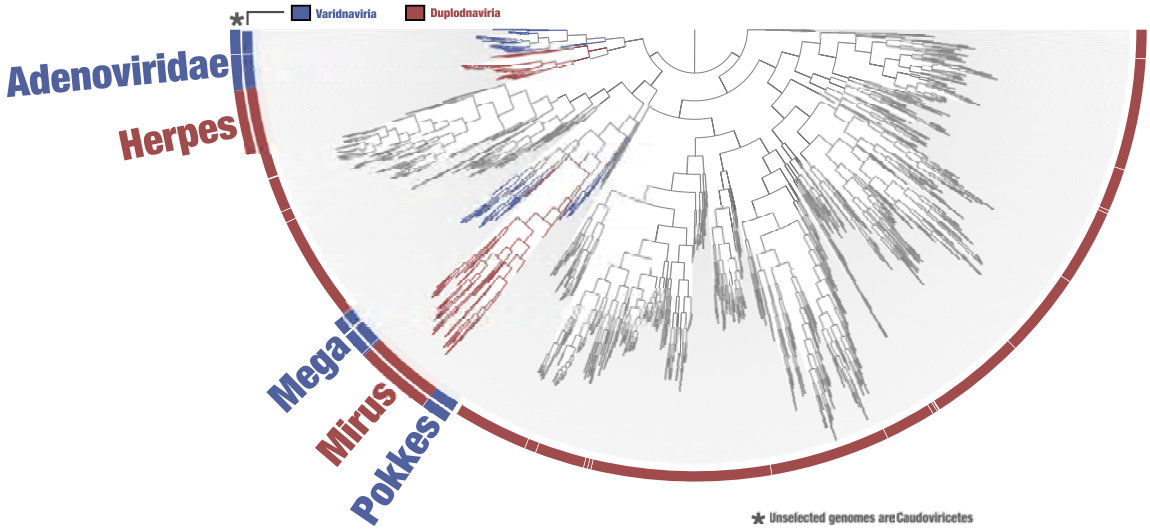

Extended Data Fig. 6 | Functional clustering of mirusviruses and reference viral genomes from culture. The inner tree is a clustering of *'Mirusviricota'* and other genomes based on the occurrence of all gene clusters (OrthoFinder method, Bray-Curtis distance).

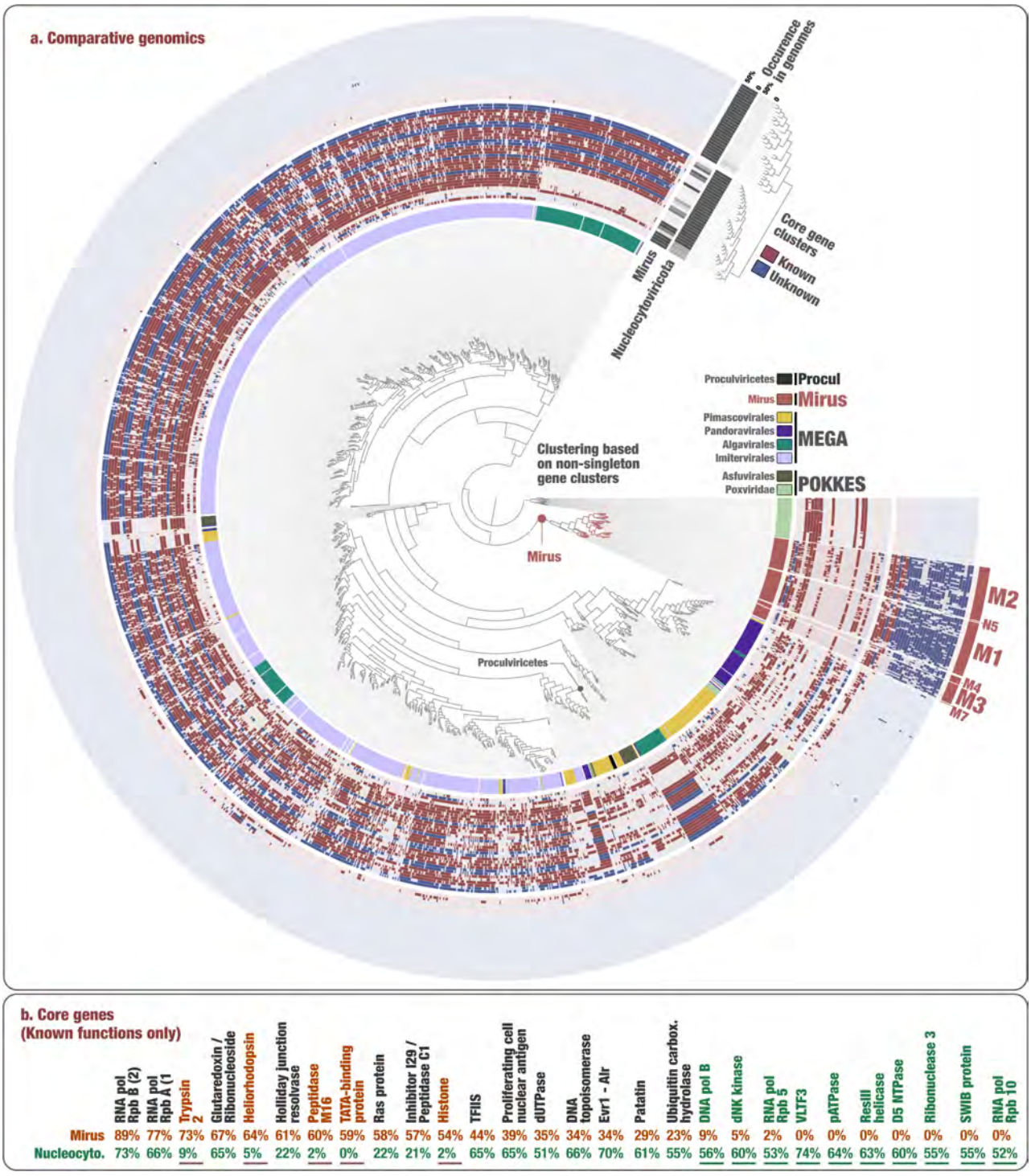

Extended Data Fig. 7 | Functional clustering of abundant and widespread marine viruses within mirusviruses and *Nucleocytoviricota*. In panel A, the inner tree is a clustering of 'Mirusviricota' and *Nucleocytoviricota* genomes >100 kbp in length based on the occurrence of all the non-singleton gene clusters (Euclidean distance), rooted with the *Chordopoxvirinae* subfamily of *Poxviridae* genomes. Rings of information display the main taxonomy of *Nucleocytoviricota* as well as the occurrence of 60 gene clusters detected in at least 50% of '*Mirusviricota*' or *Nucleocytoviricota*. The 60 gene clusters are clustered based on their occurrence (absence/presence) across the genomes. Panel B displays the occurrence of gene clusters of known Pfam functions detected in at least 50% of 'Mirusviricota' or *Nucleocytoviricota* genomes.

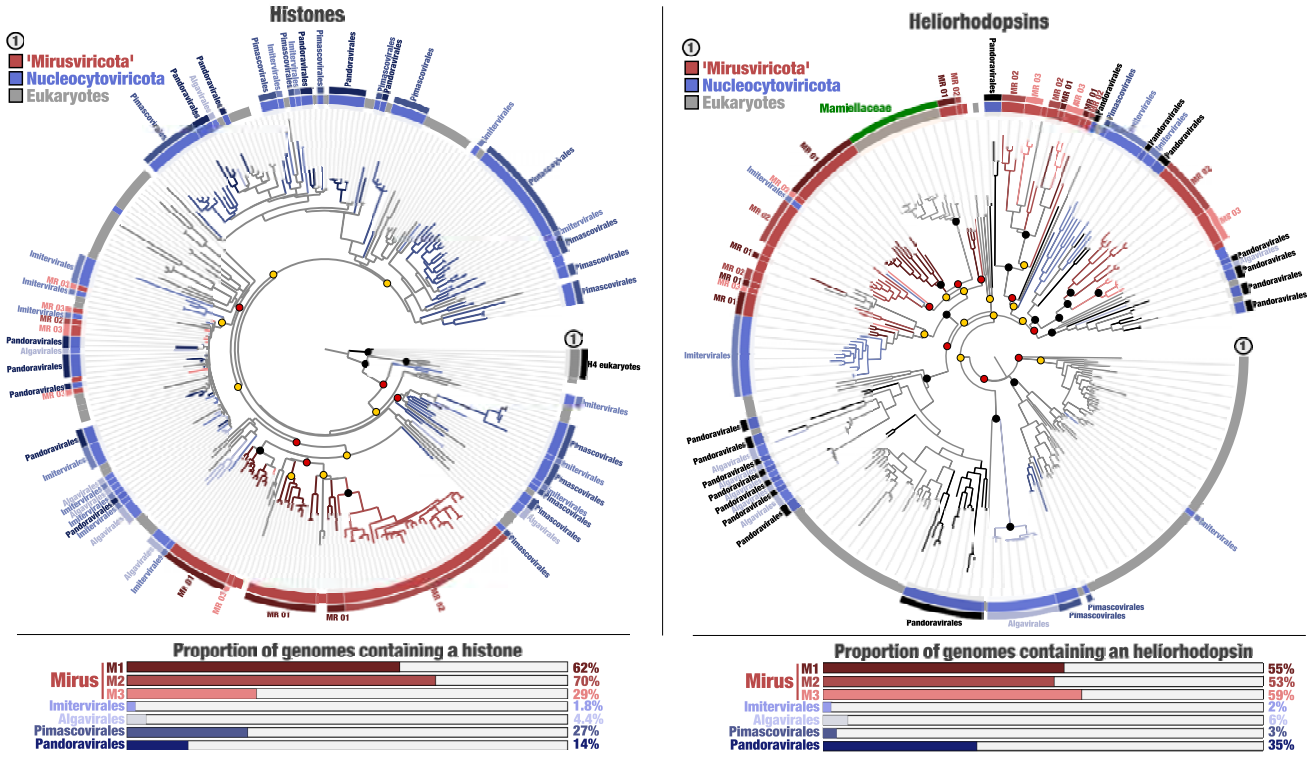

Extended Data Fig. 8 | Mirusviruses contain new phylogenetic clades of histones and heliorhodopsins. The figure displays two panels. Left panel displays a maximum-likelihood phylogenetic tree of histones occurring in the GOEV database and in eukaryotic MAGs, rooted with H4 (distant eukaryotic clade) (266 sequences; 180 sites) and based on the LG+R8 model. The various eukaryotic clades distant from H2-H3-H4 were excluded to focus on the more restrained viral signal. A ring provides additional taxonomic information. Bottom panel summarizes the proportion of genomes from different viral clades containing histones. Phylogenetic supports were considered high (aLRT>=80 and UFBoot>=95, in black), medium (aLRT>=80 or UFBoot>=95, in yellow) or low (aLRT<80 and UFBoot<95, in red) (see Methods). Right panel displays a maximum-likelihood phylogenetic tree of heliorhodopsins occurring in the GOEV database and in eukaryotic MAGs (280 sequences; 313 sites), rooted with a large clade enriched in eukaryotes and based on the VT+F+R8 model. A ring provides additional taxonomic information. Bottom panel summarizes the proportion of genomes from different viral clades containing heliorhodopsins. Phylogenetic supports were considered high (aLRT>=80 and UFBoot>=95, in black), medium (aLRT>=80 or UFBoot>=95, in yellow) or low (aLRT<80 and UFBoot<95, in red) (see Methods).

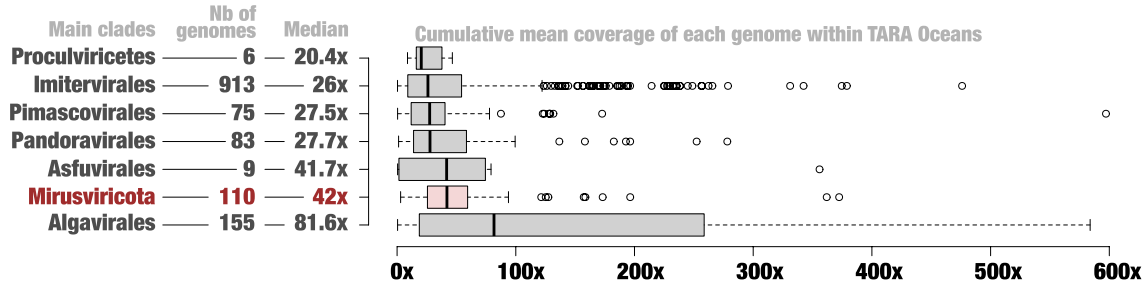

Extended Data Fig. 9 | Environmental signal of virus eukaryotic clades in the sunlit oceans. For each marine eukaryotic virus clades, the box plots display cumulative mean coverage of GOEV genomes among 937 *TARA* Oceans metagenomes. Only genome detected in at least one metagenome were considered. Center lines in boxplots show the medians; box limits indicate the 25th and 75th percentiles; whiskers extend 1.5 times the interquartile range from the 25th and 75th percentiles; outliers are represented by dots. The mean coverage values range from a minimum of 0.35x to a maximum of 6273.1x. The number of considered genomes per clade and their cumulative coverage median are also described.

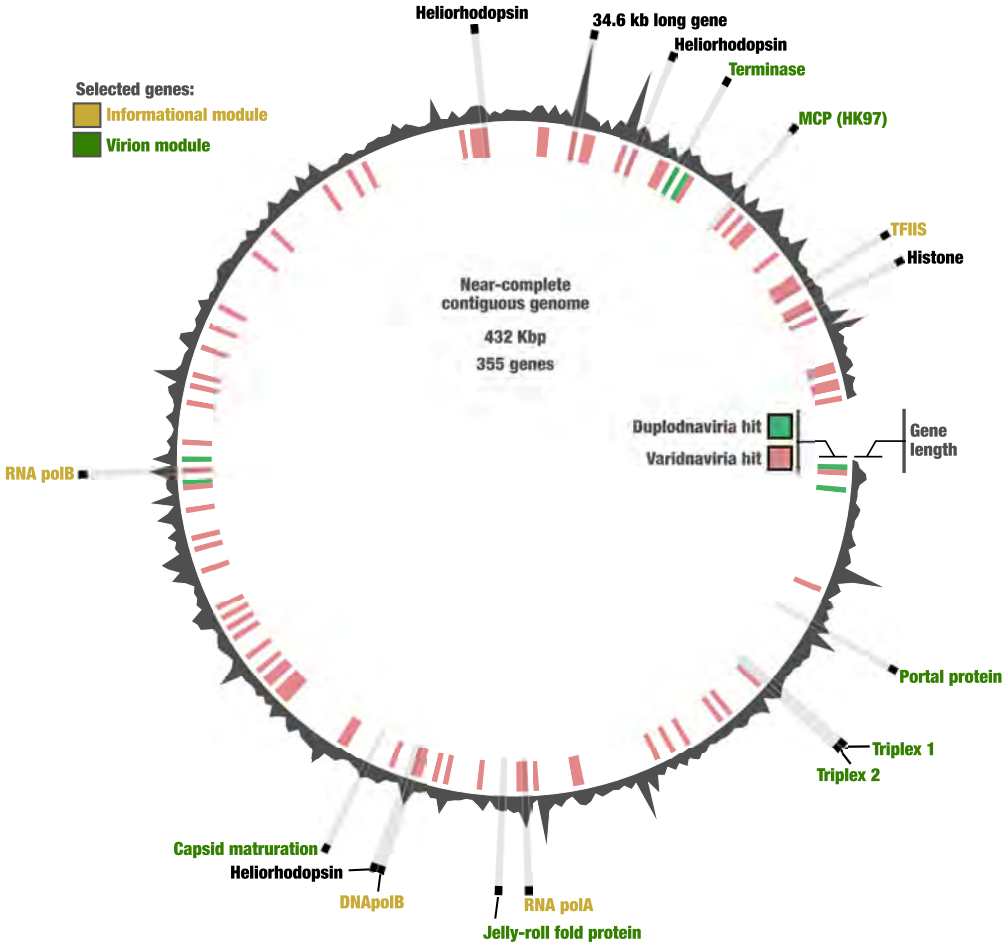

Extended Data Fig. 10 | A near-complete genome for *'Mirusviricota'*. Synteny of 355 genes in the mirusvirus near-complete contiguous genome highlighting the occurrence of hallmark genes for the informational and virion modules, as well as heliorhodopsins and histone. Genes with a hit to HMMs from either *Duplodnaviria* or *Varidnaviria* are labelled in green and red, respectively (inner tree).

nature communications

Article

https://doi.org/10.1038/s41467-023-40188-y

Unusual nuclear exchange within a germanium-containing aromatic ring that results in germanium atom transfer

Received: 22 March 2023

Accepted: 17 July 2023

Published online: 28 July 2023

Check for updates

Ryohei Nishino[1], Norihiro Tokitoh[1,2] ✉, Ryuto Sasayama[1], Rory Waterman[3] & Yoshiyuki Mizuhata[1,2] ✉

The delivery of single atoms is highly desirable for the straightforward synthesis of complex molecules, however this approach is limited by a lack of suitable atomic transfer reagents. Here, we report a germanium atom transfer reaction employing a germanium analogue of the phenyl anion. The reaction yields a germanium-substituted benzene, along with a germanium atom which can be transferred to other chemical species. The transfer of atomic germanium is demonstrated by the formation of well-defined germanium doped molecules. Furthermore, computational studies reveal that the reaction mechanism proceeds via the first example of an aromatic-to-aromatic nuclear germanium replacement reaction on the germabenzene ring. This unusual reaction pathway was further probed by the reaction of our aromatic germanium anion with a molecular silicon species, which selectively yielded the corresponding silicon-substituted benzene derivative.

In organic synthesis, the development of synthetic strategies relies on dividing the target molecule into simpler fragments (i.e., retrosynthetic analysis). The difficulty of a synthesis is often correlated to the number of the steps, and the accessibility of the compounds depends on the availability of requisite building blocks. Single atoms are the simplest building block of all molecules, however for most elements access to individual atoms for synthesis is impractical. This drives increased complexity, lower overall yield and poor atom economy in chemical synthesis. For compounds containing group 14 elements, the lack of available atomic synthons hampers synthesis. In recent years, progress has been made in understanding and utilizing molecular sources of elemental forms of these elements. A significant advance was the isolation of formally E(0) (E = Si, Ge, Sn, and Pb) compounds, termed metallylones, in which the central E(0) atom is coordinated by Lewis bases[1–7]. There are also reports of the related dinuclear compounds such as disilicon and digermanium[6,8–11]. While the nature of the bonding in these compounds is still being investigated[12–14], some such species exhibit reactivity which demonstrates their use as single Si, Ge, and Pb atom sources (Fig. 1a)[15–19]. For example, Wesemann and co-workers reported the synthesis of phosphine-stabilized digermavinylidene[15] and germasilavinyidene[16]. The natural resonance theory (NRT) analysis of these compounds revealed minor resonance contributions of the ylidone structure which possesses dative bonds L → E ← L (L = ligand), highlighting their potential utility as monoatomic-Si or -Ge synthons. Indeed, the reaction of these compounds with diimines or azides resulted in the formation of *N*-heterocyclic silylenes (NHSi) or N_4Ge_4 cubane-type clusters, respectively. Novel molecular architectures and improved synthetic efficiency are expected to be realized from atomic synthons of the heavier group 14 elements.

We have been studying aromatic compounds containing one or more skeletal heavy group 14 element (Si, Ge, and Sn) in so-called heavy benzenoids. They are extremely reactive and easily undergo auto-oligomerization. By employing bulky protecting groups such as Tbt (2,4,6-tris[bis(trimethylsilyl)methyl]phenyl), we have succeeded in synthesizing and isolating these as thermally stable compounds[20]. Recently, we demonstrated that the treatment of Tbt-substituted germa- or stannabenzene with KC_8 or alkali metal naphthalenides

[1]Institute for Chemical Research, Kyoto University, Gokasho, Uji, Kyoto 611-0011, Japan. [2]Integrated Research Consortium on Chemical Sciences, Gokasho, Uji, Kyoto 611-0011, Japan. [3]Department of Chemistry, University of Vermont, Burlington, VT 05405-0125, USA. ✉e-mail: tokitoh@boc.kuicr.kyoto-u.ac.jp; mizu@boc.kuicr.kyoto-u.ac.jp

https://doi.org/10.1038/s41467-023-40188-y

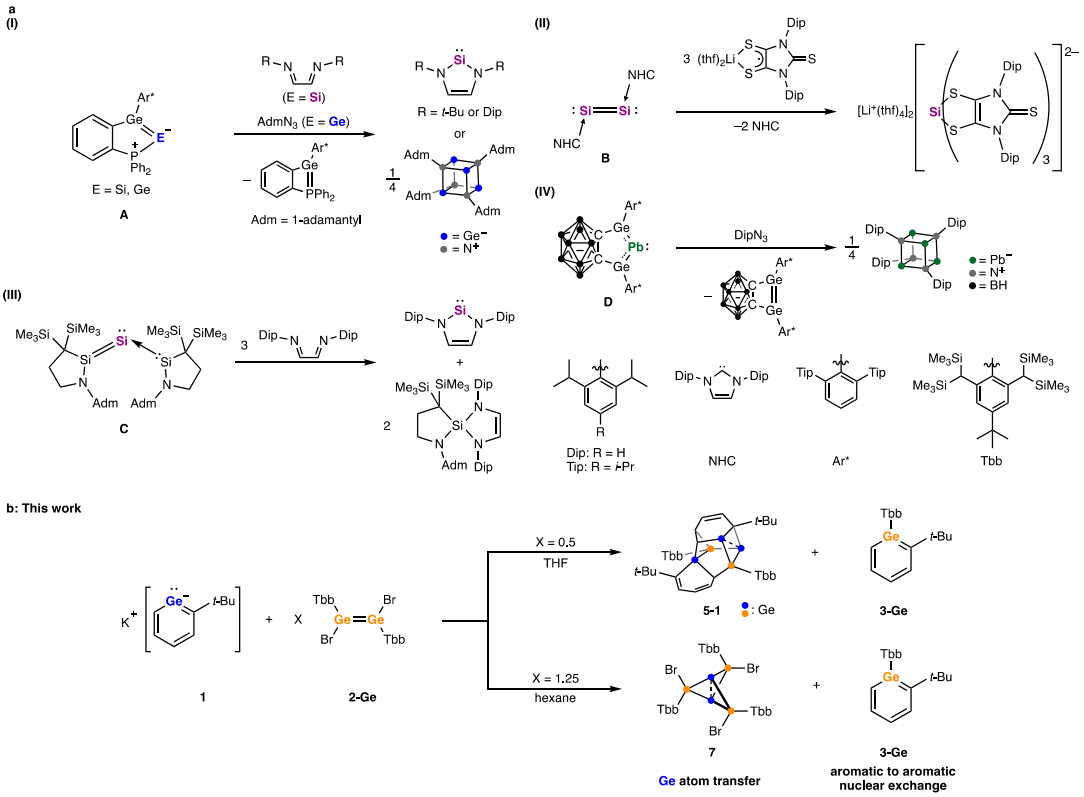

Fig. 1 | Atomic synthons of group 14 elements. a Low-valent compounds exhibiting single-atom transfer reactions. **b** Reaction of potassium germabenzenide **1** with dibromodigermene **2-Ge** which affords germabenzene **3-Ge** and molecular germanium clusters via Ge atom transfer.

resulted in the elimination of Tbt group to give heavy analogs of phenyl anion, i.e., germa[21,22] and stannabenzenyl anions[23]. It is notable that these heavy phenyl anion analogs are thermally stable despite a lack of steric protection. As demonstrated by their reactions with Cp*RuCl[24] and chlorosilanes[25], these heavy phenyl anion analogs have found utility as nucleophiles leading to new syntheses. During the investigation of the reaction of germabenzenyl anion **1** with 1,2-dibromodimetallenes, Tbb(Br)Ge=Ge(Br)Tbb (**2-Ge**) and Tbb(Br)Si=Si(Br)Tbb (**2-Si**, Tbb = 4-*tert*-butyl-2,6-bis[bis(trimethylsilyl)methyl]phenyl), we uncovered an unusual germanium atom transfer reaction (Fig. 1b). The observed reactivity is ascribed to an unusual Ge atom replacement on the aromatic germabenzenyl ring to the dimetallene-derived Ge or Si atom, giving the corresponding germa- (**3-Ge**) or silabenzene (**3-Si**), which provides insight into the atom transfer process. Such heteroatom substitution chemistry is reminiscent of pyrylium salts ($C_5R_5O^+$), which are isoelectronic to phenyl anions and undergo a variety of oxygen atom replacement reactions, allowing for the synthesis of various aromatic heterocycles[26].

Results and discussion

Reactions of potassium germabenzenide 1 with 1,2-dibromodigermene 2-Ge

In continuation of our studies examining the use of the potassium germabenzenide **1** as a nucleophile, **1** was combined with the 1,2-dibromodigermene **2-Ge** bearing Tbb groups[27] in THF solution (Fig. 2a). This initial reaction yielded several compounds, but upon solvent exchange to benzene-d_6 followed by heating and exposure to ambient light, a mixture of germabenzene **3-Ge** and the Ge/C cluster **5-2** was ultimately obtained. The observation of the germabenzene **3-Ge** bearing a Tbb group was quite unexpected as it suggests the germanium atom in the aromatic ring is derived from **2-Ge** rather than **1**. Crystallization of the reaction mixture from hexane afforded **5-2** as blue-green crystals in 19% yield which were fully characterized. The reaction initially afforded three compounds: germabenzene **3-Ge**, digermabenzenylgermyl anion **4**, and **5-1**. Subsequent heating of the mixture resulted in the conversion of **4** to **3-Ge** and **5-1**. The conversion of **5-1** to **5-2** was observed upon exposure to ambient light (Supplementary Figs. 26–28). Each **3-Ge, 4**, and **5-1** could be prepared independently to unambiguously confirm their identity. The isolated compound **5-1** is completely unchanged under thermal conditions in the dark (75 °C in C_6D_6) and isomerizes to **5-2** only when exposed to ambient light.

Although the formation mechanism of **5-1** is not clear, both Ge/C clusters **5-1** and **5-2** consist of two molecules of germabenzenylgermylene **6** and a single additional Ge atom (Fig. 2b). Because it is known that a dibromodigermene ([R(Br)Ge]$_2$) is in equilibrium with a bromogermylene [R(Br)Ge:] in solution[28–30], the initial formation of **6** is possible although it is likely a transient species and was not detected by ^{1}H NMR spectroscopy during the course of the reaction. The structures of **5-1** and **5-2** are similar to each other except for the connecting positions between the Ge2 atom and the GeC_5 ring. The transformation of **5-1** to **5-2** can be explained by a [1,3]-sigmatropic rearrangement (on C3-C4-C5-Ge2 moiety, see Fig. 2b), consistent with the observation that exposure to ambient light is required to induce isomerization.

To gain further insight into this unexpected reactivity, the chemistry of germyl anion **4** was investigated (Fig. 3, eq. i). Compound **4** itself is thermally stable based on heating experiments in toluene-d_8 solution. On the other hand, the addition of [Tbb(Br)Ge]$_2$ (**2-Ge**) to isolated **4** in C_6D_6 at room temperature afforded **3-Ge**. However, it should be noted that the conversion of **4** was incomplete at this stage. Analogous to the reaction of **1** with **2-Ge**, heating was necessary for the reaction of **4** with **2-Ge** to achieve full conversion to **3-Ge** and Ge/C cluster **5-1**. As noted above, exposure to ambient light for 3 h gave

https://doi.org/10.1038/s41467-023-40188-y

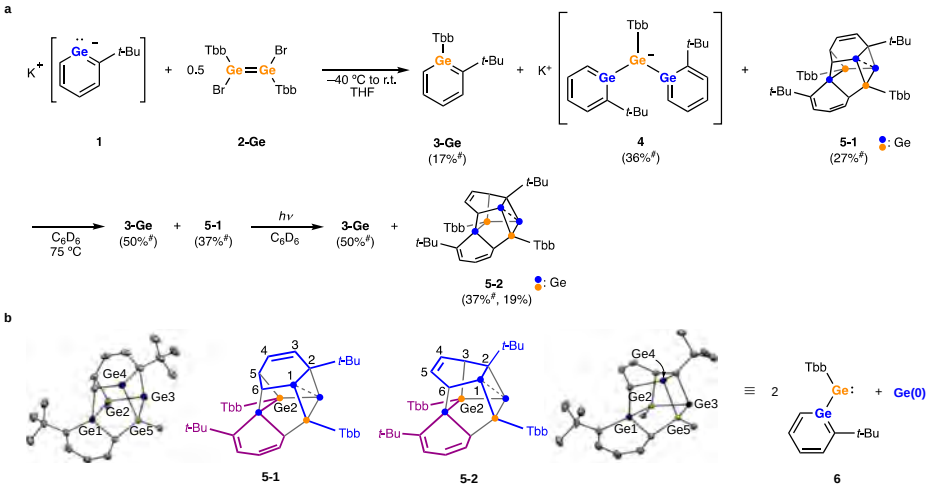

Fig. 2 | Reaction of potassium germabenzenide 1 **with 1,2-dibromodigermene** 2-Ge**. a** Products and the yields. Yields marked with # were determined by ^{1}H NMR spectroscopy. **b** Structures of Ge/C cluster **5-1** and **5-2**. Thermal ellipsoids were plotted at 50% probability. Hydrogen atoms and Tbb groups were omitted for clarity.

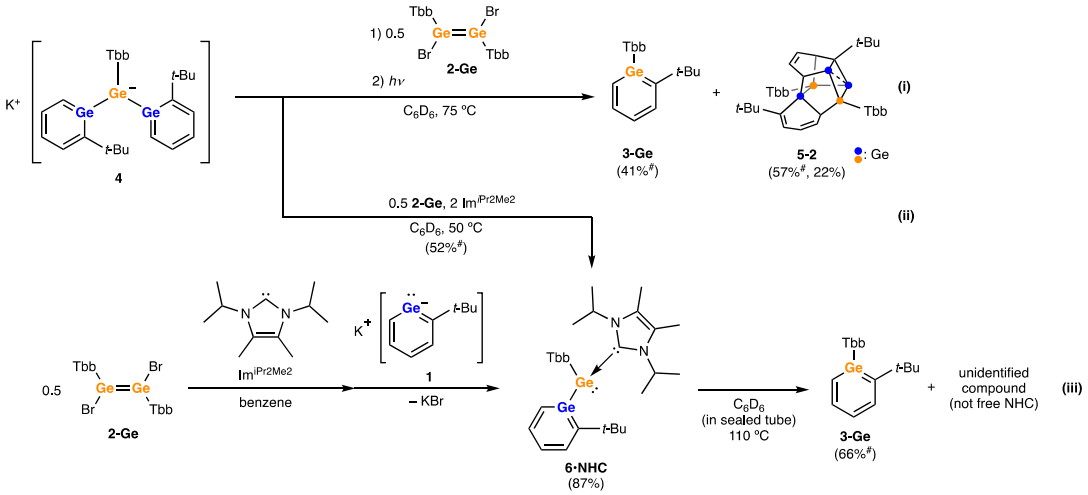

Fig. 3 | Reactivity of germyl anion 4 **and germabenzenylgermylene NHC complex** 6·NHC**.** NMR yields are marked with #. Reaction of **4** with **2-Ge** gave germabenzene **3-Ge** and cluster **5-1** which isomerized to **5-2** by ambient light (eq. **i**) while the reaction in the presence of NHC afforded **6·NHC** (eq. **ii**). Thermolysis of **6·NHC** forms corresponding germabenzene **3-Ge** (eq. **iii**).

5-2. When the reaction was conducted in the presence of 1,3-diisopropyl-4,5-dimethylimidazol-2-ylidene ($Im^{iPr2Me2}$), germabenzenylgermylene NHC adduct **6·NHC** was formed (Fig. 3, eq. ii). This result strongly suggests the formation of an intermediary germabenzenylgermylene **6** in this chemistry.

The independent preparation of **6·NHC** was accomplished by the reaction of the NHC complex of [Tbb(Br)Ge:] with **1** to give a yellow-orange solid in 87% yield (Fig. 3, eq. iii). Single crystals were obtained from a benzene/hexane solution, and the molecular structure of **6·NHC** was determined by X-ray crystallographic analysis. Heating a C_6D_6 solution of **6·NHC** at 110 °C for 12 h resulted in the complete consumption of **6·NHC** and the formation of germabenzene **3-Ge** (Fig. 3, eq. iii). The chemical shifts assigned to the $Im^{iPr2Me2}$ unit were also changed from those of **6·NHC** but were different from those of the free carbene $Im^{iPr2Me2}$, suggesting the formation of an NHC complex of zero-valent germanium atom(s). However, the structure of NHC-related compound has not yet been determined. Overall, all experimental results strongly suggest that **3-Ge** is not formed from **4** but from **6**.

Mechanistic investigation of the formation of germabenzene 3-Ge

The potential energy surface of the model compound of **6**, Gebzl(H)Ge: (**6a**, Gebzl = 1-germabenzenyl), was explored using GRRM[31] calculations to shed light on the formation mechanism of germabenzene **3-Ge**. It gave 341 local minima and 303 transition states including only one chemically and energetically allowed isomerization pathway of **6a** via **TS1a-TS4a** (maximum ΔE: + 16.5 kcal mol^{-1} relative to **6a**, see Supplementary Fig. 39). It was determined that the Ge atom of the germabenzenyl ring was exchanged for that of the germylene in four steps to form the germabenzene-bridged germylene **INT4a**. It should be noted that the single step pathway from **6a** to **INT4a** via **TS5a** with retaining the original germabenzenyl ring (hydrogen transfer to germabenzene moiety) was also located in GRRM calculations, but this path is unfavorable due to its high energy barrier (+41.4 kcal mol^{-1} relative to **6a**). Similarly, the barrier for the aryl transfer reaction in the phenyl-substituted model, Gebzl(Ph)Ge: (**6b**), was calculated to be +37.1 kcal mol^{-1} (Supplementary Fig. 40), and thus Tbb transfer can be ruled out in this system.

https://doi.org/10.1038/s41467-023-40188-y

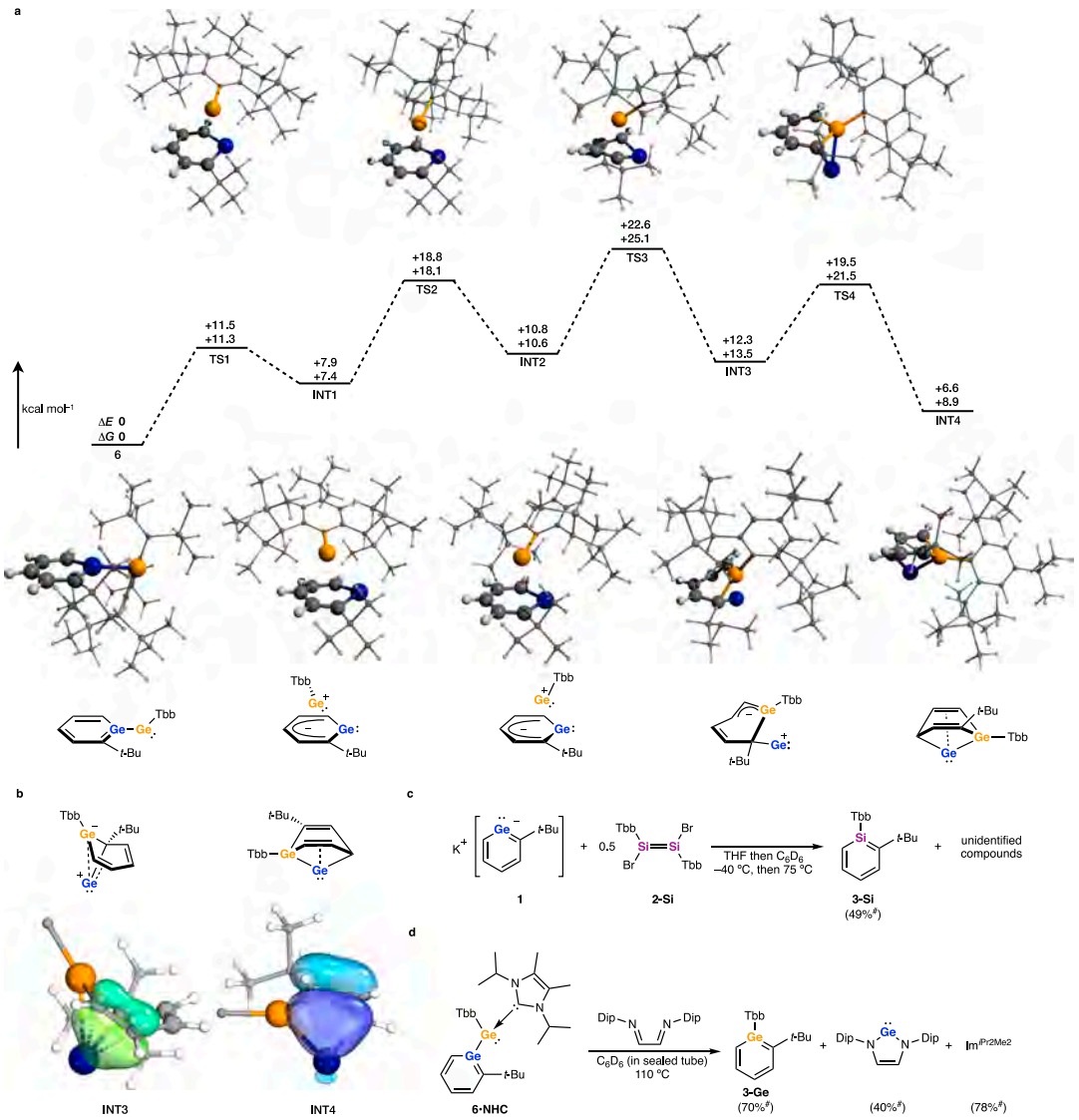

Fig. 4 | Validation of isomerization pathway of germabenzenylgermylene 6. NMR yields are marked with #. **a** Energy diagrams of the isomerization pathway of **6** at the B3LYP-D3/6-31 + G(2df,p) level of theory. **b** Intrinsic bonding orbitals of **INT3** and **INT4**. Electron delocalization among C–C–Ge is indicated. **c** Reaction of potassium germabenzenide **1** with dibromodisilene **2-Si** affording silabenzene **3-Si**. **d** Thermolysis of **6·NHC** in the presence of diimine.

The isomerization path optimization of non-truncated molecule **6** based on the results of GRRM calculations was also successfully found (Fig. 4a). The maximum energy barrier computed (ΔG = 25.1 kcal mol^{-1} relative to **6**) appears to be too high for isomerization to progress at room temperature. Experimentally, the formation of **3-Ge** is in competition with the formation of **4**, and the isomerization path of **6** is not necessarily favorable. However, concomitant KBr elimination during the formation of **6** and aromatization by Ge atom extrusion from **INT4** are considered to be exothermic. We presume that these steps supply the driving force necessary for this isomerization pathway. It should also be considered that Ge atom transfer from **INT4** is reasonable because it can restore aromaticity through Ge atom extrusion. The Ge/C cluster **5** appears to be formed from this Ge atom with two molecules of germabenzenylgermylene **6**.

It is notable that strong homoconjugative interactions between the outer Ge atom and a C = C bond are present in **INT3** and **INT4**. Natural bonding orbital (NBO) analysis revealed large second order perturbation energies of the $\pi_{C=C} \rightarrow$ Ge interactions in **INT3** (87.6 kcal mol^{-1}) and **INT4** (59.2 kcal mol^{-1}), respectively. Furthermore, delocalization of two electrons among the Ge–C–C moiety were observed within the HOMO−1 of **INT3** and HOMO−4 of **INT4** (Supplementary Figs. 54 and 55) as well as in the intrinsic bonding orbitals (IBO)[32,33] of each compound (Fig. 4b). These types of interactions inducing homoaromaticity are widely accepted in general organic chemistry[34] and have also been observed in silyl- or germyl cations[35,36] and metallylenes[37–39].

To confirm that the Ge atom on the germabenzenyl ring is indeed exchanged, the reaction of **1** with the 1,2-dibromodisilene **2-Si** was investigated (Fig. 4c). While it was not possible to isolate the intermediates of this reaction due to a lack of crystallinity of the products, the formation of silabenzene **3-Si** was confirmed spectroscopically in 49% yield under the same experimental conditions as the reaction of **1** with **2-Ge**. Importantly, no germabenzene **3-Ge** was observed. The formation of silabenzene **3-Si** was confirmed on the observation of a characteristic pattern corresponding to the silabenzene ring in the ^{1}H NMR spectrum as well as the characteristic chemical shift in the ^{29}Si NMR spectrum (81.1 ppm)[40].

This reaction clearly demonstrates a Ge atom replacement on the germabenzenyl ring with a Si atom, a net Ge atom transfer reaction. Although it is difficult to experimentally confirm the exchange in the aforementioned reaction with a digermene, a similar exchange of germanium atoms between germabenzenyl and germylene moieties is likely as proposed by the DFT calculations. Related heteroatom exchange reactions between aromatic compounds have been observed previously. For example, the synthesis of phosphabenzene from pyrylium by using $P(SiMe_3)_3$ or $P(CH_2OH)_3$ is proposed to proceed in this way[41,42]. However, there is almost no example of equivalent reactivity for group 14 elements. Müller and co-workers reported the Ge to Si exchange reaction of a germoldiide giving a silole[39], but this reaction proceeds with dearomatization. To the best of our knowledge, the reactions reported here are the first examples of an aromatic-to-aromatic nuclear exchange reaction on a benzene ring consisting only of group 14 elements.

The capacity of **6·NHC** to act as a source of Ge atoms was further demonstrated by the thermolysis of **6·NHC** in the presence of diimine [(DipN=CH−)$_2$, Dip = 2,6-diisopropylphenyl] (Fig. 4d). Heating a C_6D_6 solution in a sealed tube at 110 °C for 5 days gave the corresponding *N*-heterocyclic germylene (NHGe)[43] and the free carbene, $Im^{iPr2Me2}$. The research groups of Wesemann[17] and Iwamoto[18] have reported the silicon atom transfer reactions of **A** or **C** to diimines, resulting in the formation of an *N*-heterocyclic silylene (Fig. 1a). The formation of NHGe clearly indicates a Ge atom transfer from **6·NHC** to the diimine, consistent with the mechanism proposed herein.

To summarize these results, a possible reaction mechanism can be proposed in which the first step is the formation of germabenzenylgermylene **6** from potassium germabenzenide **1** and bromogermylene [Tbb(Br)Ge:]. While the additional equivalent of **1** to **6** gives germyl anion **4**, the reverse pathway from **4** to **6** also is possible. Compound **6** can isomerize to **INT4** with the driving force of strong homoconjugative interaction between the outer Ge atom and the C = C bond via four steps. Finally, **INT4** releases the Ge atom to form germabenzene **3-Ge**, and the extruded Ge atom is captured by two molecules of germabenzenylgermylene **6** to give **5-1** (Fig. 5).

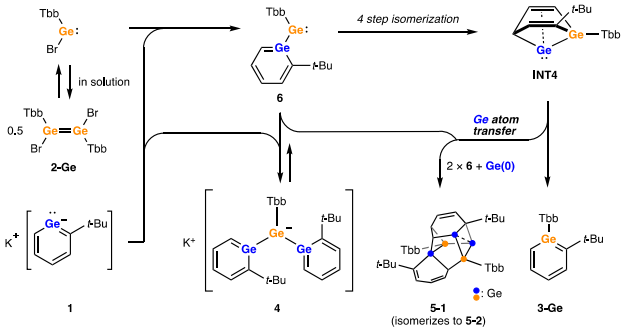

Fig. 5 | Formation mechanism of germabenzene **3-Ge** and cluster **5-1** in the reaction of potassium germabenzenide **1** with dibromodigermene **2-Ge**.

Germanium transfer to bromogermylene: formation of [1.1.1] propellane skeleton

We also carried out the reaction of potassium germabenzenide **1** with 1,2-dibromodigermene **2-Ge** in hexane rather than THF, which resulted in the formation of another germanium cluster compound, 2,4,5-tribromopentagerma[1.1.1]propellane **7** (Fig. 6a). The propellane skeleton has long been studied due, in part to interest in the interactions between the bridgehead positions and relevant [1.1.1]propellane skeletons composed solely of Ge atoms have been reported in ref. 44 and ref. 45. To a hexane solution of 1.25 eq. (2.50 eq. as bromogermylene) of **2-Ge, 1** was added at room temperature. Due to the insolubility of **1** in hexane, the complete consumption of **1** was observed visually after a few minutes. The ^{1}H NMR spectrum of the reaction mixture indicated the formation of **3-Ge** along with multiple unidentified compounds that are considered to be reaction products of Ge atom(s) and bromogermylene(s) [Tbb(Br)Ge:]. The reaction mixture converged to **3-Ge** and **7** after heating to 60 °C for 12 h. The structure of **7** was determined by the X-ray crystallographic analysis (Fig. 6b). The formation of **7** can be explained by the slow consumption of **1** due to the poor solubility in hexane. The slow formation of germabenzenylgermylene **6** causes the capture of the Ge atom of **INT4** by [Tbb(Br)Ge:], rather than by **6** as observed in THF.

The formation of **7** clearly indicates that the Ge atom is not always transferred to **6**. In addition, the products containing naked Ge atoms such as **5** and **7** are attracting increased interest due to their similarity with the elemental germanium. These experimental results suggest the potential availability of this reactivity as a unique synthetic method for the controllable formation of molecular germanium clusters bearing naked Ge atoms, the germanium analog of siliconoids[46].

We have demonstrated a germanium atom transfer reaction involving potassium germabenzenide **1** and 1,2-dibromodigermene **2-Ge**. This methodology has already been applied to yield two germanium clusters, **5** and **7**, which contain naked Ge atoms. The first step of the reaction is the formation of germabenzenylgermylene **6**, which isomerizes into germabenzenyl ring bridged germylene **INT4**. It is proposed that Ge atom extrusion occurs from **INT4** to also give germabenzene **3-Ge**. Compound **6** was isolable as an NHC derivative **6·NHC** and indeed demonstrated to act as a Ge(0) source in the reaction with a diimine. It was also found that the Ge atom of the germabenzenyl ring of **1** was replaced by the Ge or Si atom of **2**. This unprecedented aromatic-to-aromatic nuclear exchange reaction is expected to be utilized as a novel synthetic method for heavy benzene derivatives and may also provide access to new, unsaturated molecular germanium clusters as well as heavy benzenes.

Methods

Reaction of potassium 2-*tert*-butylgermabenzenide 1 with 0.5 eq of [Tbb(Br)Ge]$_2$ (2-Ge) in THF

To a THF (3 mL) solution of [Tbb(Br)Ge]$_2$ (**2-Ge**, 30.1 mg, 0.0250 mmol) was added a THF (3 mL) solution of **1** (11.6 mg, 0.0498 mmol) at −40 °C and stirred for 1 h at room temperature. After all solvents were removed in vacuo, the resultant brown solid was dissolved in C_6D_6 and then transferred to J. Young NMR tube. To this solution, 5.0 µL of 1,4-dioxane was added as an internal standard. ^{1}H NMR spectrum indicated the formation of germabenzene **3-Ge**

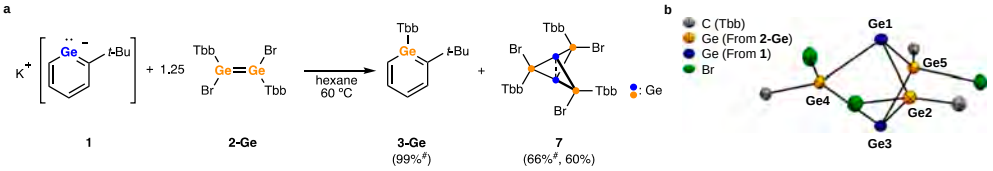

Fig. 6 | **Reaction of** 1 **with 1.25 eq. of** 2-Ge **in hexane. a** Products and the yields. NMR yields are marked with #. **b** Thermal ellipsoid plots of **7** at the 50% probability level. Tbb groups were omitted for clarity.

(17%), germyl anion **4** (36%), Ge/C cluster **5-1** (27%), and unidentified compounds. The yields were calculated as the conversion ratio based on **1**. Heating the mixture at 75 °C for 12 h increased the yields of **3-Ge** (50%) and **5-1** (37%) with the full consumption of **4**. Subsequent exposure to the ambient light for 5 h gave the mixture of **3-Ge** (50%) and **5-2** (37%). After filtration and removal of solvents in vacuo, crystallization from hexane afforded **5-2** (7.3 mg, 0.0048 mmol, 19% based on **1**) as blue-green crystals; m.p. 207–209 °C; Anal. Calcd. for $C_{66}H_{124}Ge_5Si_8$: C, 52.65; H, 8.30. Found: C, 52.42, H, 8.44; HRMS (DART): Calcd. for $C_{66}H_{125}Ge_5Si_8$ $[M+H]^+$: 1505.4055; found: 1505.3957 $[M+H]^+$; ^{1}H NMR (600 MHz, C_6D_6, 348 K): δ 0.22–0.36 (s + s + s + s, 72H), 1.15 (s, 9H), 1.21 (s, 9H), 1.31 (s, 9H), 1.34 (s, 9H), 2.15 (br s, 2H), 2.67 (br s, 2H), 3.07 (dd, 1H, J = 8.4, 1.2 Hz), 3.10 (dd, 1H, J = 3.6, 3.6 Hz), 4.97 (d, 1H, J = 9.0 Hz), 5.69 (ddd, 1H, J = 10.2, 7.2, 3.6 Hz), 5.96 (dd, 1H, J = 10.2, 3.6 Hz), 6.20 (ddd, 1H, J = 9.0, 8.4, 1.2 Hz), 6.49 (d, 1H, J = 7.2 Hz), 6.87 (s, 2H), 6.88 (t, 1H, J = 8.4 Hz), 7.00 (s, 2H); ^{13}C NMR (150 MHz, C_6D_6, 348 K): δ 1.8 (q), 1.9 (q), 2.2 (q), 3.0 (q), 30–32 (br), 31.27 (q), 31.30 (q), 33–34 (br), 33.1 (q), 34.3 (s), 34.5 (s), 36.9 (q), 37.5 (s), 38.2 (d), 40.7 (d), 44.6 (s), 62.2 (d), 122.8 (two signals are overlapped, d + d), 126.7 (d), 128.0 (d), 128.3 (d), 130.2 (d), 132.6 (d), 136.0 (s), 138.4 (s), 149.4 (s), 149.9 (two signals are overlapped, s + s), 151.4 (s), 159.5 (s), 183.6 (s). All signals were assigned by 2D-NMR (COSY, HSQC, HMBC, NOESY) techniques. The signals at 128.0 and 128.3 are undetectable in the ^{13}C{^{1}H} NMR spectrum due to overlapping with the signals of C_6D_6. These signals were observed and assigned by ^{13}C DEPT 135 and various hetero nuclear 2D-NMR techniques.

Reaction of potassium 2-*tert*-butylgermabenzenide 1 with 0.5 eq of [Tbb(Br)Si]$_2$ (2-Si) in THF

To a THF (3 mL) solution of [Tbb(Br)Si]$_2$ (**2-Si**, 20.0 mg, 0.0179 mmol) was added a THF (3 mL) solution of **1** (8.3 mg, 0.036 mmol) at −40 °C, and the combined solution was stirred for 1 h at room temperature. After all solvents were removed in vacuo, the resultant brown solid was dissolved in C_6D_6, then transferred to J. Young NMR tube with the addition of 5.0 μL of 1,4-dioxane as an internal standard. The ^{1}H NMR spectrum showed the formation of silabenzene **3-Si** and unidentified compounds. Heating the mixture at 75 °C for 12 h resulted in the color changing to deep purple and the formation of 49% silabenzene **3-Si**. Attempts to isolate **3-Si** by recrystallization and sublimation were unsuccessful, and the structure of **3-Si** was confirmed by the following NMR signals (Supplementary Figs. 30–33). ^{1}H NMR (400 MHz, C_6D_6, 298 K): δ 0.10 (s, 18H), 0.17 (s, 18H), 1.30 (s, 9H), 1.46 (s, 9H), 2.52 (s, 2H), 6.77 (dd, 1H, J = 9.2, 7.6 Hz), 6.95 (s, 2H), 7.23 (d, 1H, J = 12.0 Hz), 7.87 (dd, 1H, J = 12.0 Hz, 7.6 Hz), 7.96 (d, 1H, J = 9.2 Hz); ^{29}Si NMR (79 MHz, C_6D_6, 298 K): δ 81.1.

Data availability

All data generated or analyzed during this study are included in this Article and its Supplementary Information files. The X-ray crystallographic coordinates for structures reported in this study have been deposited at the Cambridge Crystallographic Data Centre (CCDC), under deposition numbers 2246032 (**3**), 2246033 (**4·18c6**), 2268057 (**5-1**), 2246034 (**5-2**), 2246035 (**6·NHC**), and 2246036 (**7**). These data can be obtained free of charge from The Cambridge Crystallographic Data Centre via www.ccdc.cam.ac.uk/data_request/cif. The coordinates of the optimized structures are present in the source file. Source data are provided with this paper.

References

1. Frenking, G. et al. New bonding modes of carbon and heavier group 14 atoms Si-Pb. *Chem. Soc. Rev.* **43**, 5106–5139 (2014).
2. Frenking, G., Hermann, M., Andrada, D. M. & Holzmann, N. Donor-acceptor bonding in novel low-coordinated compounds of boron and group-14 atoms C-Sn. *Chem. Soc. Rev.* **45**, 1129–1144 (2016).
3. Yao, S., Xiong, Y. & Driess, M. A new area in main-group chemistry: zerovalent monoatomic silicon compounds and their analogues. *Acc. Chem. Res.* **50**, 2026–2037 (2017).
4. Zhao, L. L., Hermann, M., Holzmann, N. & Frenking, G. Dative bonding in main group compounds. *Coord. Chem. Rev.* **344**, 163–204 (2017).
5. Majhi, P. K. & Sasamori, T. Tetrylones: an intriguing class of monoatomic zero-valent group 14 compounds. *Chem. Eur. J.* **24**, 9441–9455 (2018).
6. Nesterov, V. et al. NHCs in main group chemistry. *Chem. Rev.* **118**, 9678–9842 (2018).
7. Yao, S., Xiong, Y., Saddington, A. & Driess, M. Entering new chemical space with isolable complexes of single, zero-valent silicon and germanium atoms. *Chem. Commun.* **57**, 10139–10153 (2021).
8. Wang, Y. et al. A stable silicon(0) compound with a Si=Si double bond. *Science* **321**, 1069–1071 (2008).
9. Wang, Y. & Robinson, G. H. Carbene-stabilized main group diatomic allotropes. *Dalton Trans.* **41**, 337–345 (2012).
10. Wang, Y. & Robinson, G. H. *N*-Heterocyclic carbene-main-group chemistry: a rapidly evolving field. *Inorg. Chem.* **53**, 11815–11832 (2014).
11. Doddi, A., Peters, M. & Tamm, M. *N*-Heterocyclic carbene adducts of main group elements and their use as ligands in transition metal chemistry. *Chem. Rev.* **119**, 6994–7112 (2019).
12. Frenking, G. Dative bonds in main-group compounds: a case for more arrows! *Angew. Chem. Int. Ed.* **53**, 6040–6046 (2014).
13. Himmel, D., Krossing, I. & Schnepf, A. Dative bonds in main-group compounds: a case for fewer arrows! *Angew. Chem. Int. Ed.* **53**, 370–374 (2014).
14. Himmel, D., Krossing, I. & Schnepf, A. Dative or not dative? *Angew. Chem. Int. Ed.* **53**, 6047–6048 (2014).
15. Krebs, K. M. et al. Phosphine-stabilized digermavinylidene. *J. Am. Chem. Soc.* **141**, 3424–3429 (2019).
16. Wilhelm, C., Raiser, D., Schubert, H., Sindlinger, C. P. & Wesemann, L. Phosphine-stabilized germasilenylidene: source for a silicon-atom transfer. *Inorg. Chem.* **60**, 9268–9272 (2021).
17. Wang, Y. et al. Carbene-stabilized disilicon as a silicon-transfer agent: synthesis of a dianionic silicon tris(dithiolene) complex. *Angew. Chem. Int. Ed.* **59**, 8864–8867 (2020).
18. Koike, T., Nukazawa, T. & Iwamoto, T. Conformationally switchable silylone: electron redistribution accompanied by ligand reorientation around a monatomic silicon. *J. Am. Chem. Soc.* **143**, 14332–14341 (2021).
19. Chen, M., Zhang, Z., Qiao, Z., Zhao, L. & Mo, Z. An isolable bis(-germylene)-stabilized plumbylone. *Angew. Chem. Int. Ed.* **62**, e202215146 (2023).
20. Tokitoh, N. Synthesis of aromatic species containing a heavier group 14 element by taking advantage of kinetic stabilization. *Bull. Chem. Soc. Jpn.* **77**, 429–441 (2004).
21. Mizuhata, Y., Fujimori, S., Sasamori, T. & Tokitoh, N. Germabenzenylpotassium: a germanium analogue of a phenyl anion. *Angew. Chem. Int. Ed.* **56**, 4588–4592 (2017).
22. Fujimori, S., Mizuhata, Y. & Tokitoh, N. Heavy phenyllithium and -sodium: synthesis and characterization of germanium analogues of phenyl anion ('germabenzenyl anions'). *Chem. Lett.* **47**, 708–710 (2018).
23. Fujimori, S., Mizuhata, Y. & Tokitoh, N. Stannabenzenylpotassium: the first isolable tin-containing benzene derivative. *Chem. Eur. J.* **24**, 17039–17045 (2018).
24. Fujimori, S., Mizuhata, Y. & Tokitoh, N. Ru-complexes of an anionic germabenzenyl ligand. *Chem. Commun.* **54**, 8044–8047 (2018).
25. Mizuhata, Y., Fujimori, S. & Tokitoh, N. Reaction of germabenzenylpotassium with TBDMSCl: unusual trimerization of germabenzene skeletons. *Phosphorus, Sulfur Silicon Relat. Elem.* **195**, 936–939 (2020).

26. Li, Y., Wang, H. & Li, X. Over one century after discovery: pyrylium salt chemistry emerging as a powerful approach for the construction of complex macrocycles and metallo-supramolecules. *Chem. Sci.* **11**, 12249–12268 (2020).
27. Sasamori, T. et al. Synthesis and characterization of a 1,2-digermabenzene. *Organometallics* **34**, 2106–2109 (2015).
28. Simons, R. S., Pu, L., Olmstead, M. M. & Power, P. P. Synthesis and characterization of the monomeric diaryls M{C_6H_3-2,6-Mes_2}$_2$ (M = Ge, Sn, or Pb; Mes = 2,4,6-$Me_3C_6H_2$–) and dimeric aryl–metal chlorides [M(Cl){C_6H_3-2,6-Mes_2}]$_2$ (M = Ge or Sn). *Organometallics* **16**, 1920–1925 (1997).
29. Sasamori, T., Sugiyama, Y., Takeda, N. & Tokitoh, N. Structure and properties of an overcrowded 1,2-dibromodigermene. *Organometallics* **24**, 3309–3314 (2005).
30. Hayakawa, N. et al. 1,2-Dihalodigermenes bearing bulky Eind groups: synthesis, characterization, and conversion to halogermylenoids. *Dalton Trans.* **47**, 814–822 (2018).
31. Maeda, S., Ohno, K. & Morokuma, K. Systematic exploration of the mechanism of chemical reactions: the global reaction route mapping (GRRM) strategy using the ADDF and AFIR methods. *Phys. Chem. Chem. Phys.* **15**, 3683–3701 (2013).
32. Knizia, G. Intrinsic atomic orbitals: an unbiased bridge between quantum theory and chemical concepts. *J. Chem. Theory Comput.* **9**, 4834–4843 (2013).
33. Knizia, G. & Klein, J. E. Electron flow in reaction mechanisms–revealed from first principles. *Angew. Chem. Int Ed.* **54**, 5518–5522 (2015).
34. Gleiter, R. & Haberhauer, G. *Aromaticity and Other Conjugation Effects* (Wiley-VCH, 2012).
35. Ishida, Y., Sekiguchi, A. & Kabe, Y. 1,4,5-Trigermabicyclo[2.1.0]pent-2-en-5-ylium: the isolable bishomocyclopropenylium ion containing a heavier group 14 element. *J. Am. Chem. Soc.* **125**, 11468–11469 (2003).
36. Gerdes, C., Saak, W., Haase, D. & Müller, T. Dibenzosilanorbornadienyl cations and their fragmentation into silyliumylidenes. *J. Am. Chem. Soc.* **135**, 10353–10361 (2013).
37. Dong, Z., Reinhold, C. R., Schmidtmann, M. & Müller, T. A germylene stabilized by homoconjugation. *Angew. Chem. Int. Ed.* **55**, 15899–15904 (2016).
38. Dong, Z., Reinhold, C. R. W., Schmidtmann, M. & Müller, T. A stable silylene with a σ^2, π- butadiene ligand. *J. Am. Chem. Soc.* **139**, 7117–7123 (2017).
39. Reinhold, C. R. W. et al. A one-step germole to silole transformation and a stable isomer of a disilabenzene. *Chem. Eur. J.* **24**, 848–854 (2018).
40. Wakita, K., Tokitoh, N., Okazaki, R. & Nagase, S. Synthesis and properties of an overcrowded silabenzene stable at ambient temperature. *Angew. Chem. Int. Ed.* **39**, 634–636 (2000).
41. Märkl, G., Lieb, F. & Merz, A. A new synthesis of phosphabenzene derivatives. *Angew. Chem. Int. Ed. Engl.* **6**, 458–459 (1967).
42. Märkl, G. 2,4,6-Triphenylphosphabenzene. *Angew. Chem. Int. Ed. Engl.* **5**, 846–847 (1966).
43. Baker, R. J., Jones, C., Mills, D. P., Pierce, G. A. & Waugh, M. Investigations into the preparation of groups 13–15 *N*-Heterocyclic carbene analogues. *Inorg. Chim. Acta* **361**, 427–435 (2008).
44. Nied, D., Klopper, W. & Breher, F. Pentagerma[1.1.1]propellane: a combined experimental and quantum chemical study on the nature of the interactions between the bridgehead atoms. *Angew. Chem. Int. Ed.* **48**, 1411–1416 (2009).
45. Ito, Y. et al. Spirobis(pentagerma[1.1.1]propellane): a stable tetraradicaloid. *J. Am. Chem. Soc.* **135**, 6770–6773 (2013).
46. Heider, Y. & Scheschkewitz, D. Stable unsaturated silicon clusters (siliconoids). *Dalton Trans.* **47**, 7104–7112 (2018).

Acknowledgements

This work was supported by JSPS KAKENHI Grant Numbers JP19H05635 (N.T. and Y.M.), JP20K20447 (N.T.), JP19H05528 (N.T.), JP18H01963 (Y.M.), and JP16H04110 (N.T.) and Integrated Research Consortium on Chemical Science (IRCCS). Y.M. gratefully acknowledges ISHIZUE 2022 of Kyoto University. This study was supported by the Joint Usage/Research Center [JURC, Institute for Chemical Research (ICR), Kyoto University] by providing access to a Bruker Avance III 600 NMR spectrometer. We are furthermore grateful for the computation time, which was provided by the Super Computer Laboratory (ICR, Kyoto University). Elemental analyses were carried out at the Microanalytical Laboratory of the ICR (Kyoto University). The authors thank Prof. Masahiro Yamanaka (Rikkyo Univ.) for the helpful discussion about computational studies. Preliminary X-ray diffraction data of **5-2** and **6·NHC** were collected at the BL02B1 beamline of SPring-8 (JASRI, 2022A1621 and 2022A1200).

Author contributions

Y.M., R.N., and N.T. determined the research strategy, and R.N. and R.S. performed the synthetic experiments. R.N. collected the physical properties and spectral data of all compounds appearing in this paper. R.N. and Y.M. performed the X-ray crystallographic analyses and theoretical calculations. Y.M., N.T., and R.W. supervised the work. All authors co-wrote the paper.

Competing interests

The authors declare no competing interests.

Additional information

Supplementary information The online version contains supplementary material available at https://doi.org/10.1038/s41467-023-40188-y.

Correspondence and requests for materials should be addressed to Norihiro Tokitoh or Yoshiyuki Mizuhata.

Peer review information *Nature Communications* thanks the anonymous reviewers for their contribution to the peer review of this work. A peer review file is available.

4. 参考資料

京都大学化学研究所
化学関連分野の深化・連携を基軸とする先端・学際グローバル研究拠点
令和５年度国際共同利用・共同研究公募要領

京都大学化学研究所は、「化学に関する特殊事項の学理及び応用の研究を掌る」ために、化学を中心とする分野で基礎研究に重点を置いた先端研究に邁進して参りました。平成 22 年度より国立大学共同利用・共同研究拠点としての活動を始め、平成３０年にはそのグローバルな事業展開が評価され、文部科学大臣から国際共同利用・共同研究拠点として認定されました。これを受けて平成３１年度からは第１期、さらに令和３年の再認定を受けて同４年度からは第２期の国際共同利用・共同研究拠点活動を実施し、多様でグローバルな化学分野の共同研究を一層強力に推進すべく、さらなる事業展開を図っております。

つきましては、化学が関わる分野でご活躍の皆様のご意見・ご要望を尊重しつつ、世界の化学の基礎・応用研究を皆様とともに一層推進することを念頭に置き、下記の要領で令和５年度の拠点共同利用・共同研究の課題公募をさせて頂きたく存じます。

この公募に当たりましては、分野選択型（計画研究型）、課題提案型、連携・融合促進型および施設・機器利用型の四つに分けて研究課題を募集いたします。令和４年度から、分野選択型には従来の【基幹分野】の他に、化学研究所が重要分野と考える【特定分野】を設けました。これらの課題の実施に際しては当研究所の専任教員または客員教員との共同研究を基調といたしますが、いずれの課題でも後述の共通設備・機器・資料等のご利用が可能です。なお、各課題とも、海外研究者を研究代表者あるいは研究協力者とする国際共同研究（この場合、英語フォームで申請下さい）と、国内研究者を研究代表者とする国内共同研究を実施致します。これらの点も勘案いただき、本公募要領の詳細について十分ご確認の上、期日までにご申請下さいますようお願いいたします。

京都大学化学研究所長　　青山卓史
共同研究ステーション長　小野輝男

1. 研究期間

１年間（令和５年４月１日から令和６年３月３１日まで）。

2. 研究課題分類

下記のような分類（型）ごとに研究課題を募集いたします。いずれの課題についても、分類ないし分野の担当者もしくは当研究所で対応する共同研究者にご一報の上、ご申請下さい。

2-1. 分野選択型（計画研究型）研究課題

分野選択型（計画研究型）研究課題は、あらかじめ設定された分野に関して化学研究所内の研究者と共同で遂行する課題です。令和５年度は下記の基幹５分野および特定１分野について課題を公募いたします。６分野を合わせて、萌芽的な課題と発展的な課題をそれぞれ２５件程度、採択の予定です。

2-1-1. 分野選択型【基幹分野】研究課題

ビーム科学分野（担当者：若杉 昌徳；wakasugi.masanori.8z@kyoto-u.ac.jp）
基本テーマ：先進量子ビームの開発と新奇診断分析手法の創出
趣旨：レーザー、X 線、電子線、イオンビームなどの量子ビームの高度化とその先端的診断分析法への応用を進めます。また、これらの量子ビームを複合的に用いて、極微細領域での超高速化学・物理現象の解明を目指します。

元素科学分野（担当者：大木 靖弘; ohki@scl.kyoto-u.ac.jp）
基本テーマ：元素科学に基づく物質創製・機能創出
趣旨：元素の新たな特性を引き出し、この特性をもとに優れた機能を有する新物質を創製します。元素と社会との関わりを俯瞰した元素戦略研究も推進します。物質の機能は、構成元素の特性を相乗的に反映

して発現します。この発現機構を明らかとし、望みの機能を意のままに創出することを目指します。

バイオ情報学分野（担当者：阿久津 達也; takutsu@kuicr.kyoto-u.ac.jp）
基本テーマ：バイオ情報を含む複合情報の融合解析
趣旨：ゲノムやメタゲノムに代表される最新バイオ情報に立脚して、バイオ情報がいかに生体内や自然環境における化学現象と関わっているかを明らかにし、生命システムについての化学的理解の深化を図ります。さらに、その成果を応用して、ゲノム創薬やパーソナライズド医療などへの展開も目指します。

物質合成分野（担当者：村田 靖次郎; yasujiro@scl.kyoto-u.ac.jp）
基本テーマ：複合機能材料の戦略的創製
趣旨：異種材料のハイブリッド化・複合化ならびにナノサイズ化に重点を置き、新規な機能をもつ新世代材料や分子システムの創製を目指すとともに、生体の認識、応答、反応などの諸機能を担う例えば生体膜等も複合機能材料と捉え、機能物質と生命現象の化学的相関の解明も目指します。

現象解析分野（担当者：長谷川 健; htakeshi@scl.kyoto-u.ac.jp）
基本テーマ：複合測定に基づく物質解析
趣旨：化学を基盤とする多種の分光学的手法・解析的手法を複合的に駆使して、天然および人工物質の構造・性質を分子レベルから巨視的レベルまで階層的に理解・記述することを目指し、一方、その結果を還元することによって新たな物質科学の枠組みを構築する取組みも目指します。

2-1-2. 分野選択型【特定分野】研究課題

量子情報・スピントロニクス分野（担当者：小野 輝男; ono@scl.kyoto-u.ac.jp）
基本テーマ： 量子情報・スピントロニクス分野
趣旨：物理学、応用物理学、電子工学、磁気工学、材料科学、化学、情報科学および境界領域の新しい科学技術の創造により、古典情報と量子情報技術を融合・発展させ、Society 5.0 とポストコロナ社会で必要とされる将来情報技術の基盤構築を目指します。

2-2. 課題提案型研究課題（担当者：寺西 利治; teranisi@scl.kyoto-u.ac.jp）
課題提案型研究課題は、前項１で設定した一つの分野に留まらない分野、あるいはそれ以外の分野について、化学関連分野の研究者から自由にご提案いただく課題です。萌芽的な課題と発展的な課題を、それぞれ２０件程度、採択の予定です。新分野の開拓につながるような課題を特に歓迎いたします。なお、緊急性・重要性が極めて高いと判断した課題については、前記の応募期日にかかわらず、直ちに採択することもあります。

2-3. 連携・融合促進型研究課題（担当者：栗原 達夫; kurihara@scl.kyoto-u.ac.jp）
連携・融合促進型研究課題は、化学関連分野における国内外の研究連携の強化を主目的とする共同研究課題です。国外も念頭に置く場合は、化学研究所の部局間国際学術交流締結先 (http://www.kuicr.kyoto-u.ac.jp/sites/international_exchange/agreement/ 参照)との共同研究を開始する場を求めていただくことも可能です。また、この目的に沿った研究集会の開催も本課題として応募いただけます。５件程度を採択する予定です。

2-4. 施設・機器利用型研究課題（担当者：二木 史朗; futaki@scl.kyoto-u.ac.jp）
施設・機器利用型研究課題は、拠点ホームページに記載の共通設備・機器・資料等（https://www.icr-ijurc.jp/equipment/）の利用を主とする共同研究課題です。１５件程度を採択する予定です。

令和５年度国際共同利用・共同研究経費概算値

	経費上限／件*（千円）	
	国際共同研究	国内共同研究
分野選択型萌芽的研究	1,000	800
分野選択型発展的研究	2,000	1,500
課題提案型萌芽的研究	1,000	800
課題提案型発展的研究	2,000	1,500
連携・融合促進型研究	1,000	800
施設・機器利用型研究	1,000	800

*表中の金額は目安です。予算の状況に応じた減額もありえますことをご了解下さい。
経費内での備品費、消耗品費、旅費の配分は、申請者と化学研究所の共同研究者
が協議して決定下さい。特に、旅費については、地域性を勘案してご決定下さい。

3. 共同研究応募方法

3-1. 申請資格

国公私立大学、国公私立研究機関、独立行政法人等の専任研究者、または、これに準ずる者。

3-2. 申請書記入要領

申請に当たっては、該当する募集分類・分野の担当者もしくは当研究所で対応する共同研究者と、事前に研究課題、研究内容、研究経費に関して、必ずご協議下さい。対応する共同研究者は、当研究所の専任教員または令和 5 年度客員教員からお選び下さい。なお、教員のリストは下記の化学研究所ホームページをご参照下さい。

教員リスト　http://www.kuicr.kyoto-u.ac.jp/sites/research_activities/chemist/

また、対応する共同研究者をお決めになれない場合は、各分類・分野の担当者に、まず、ご相談ください。
上記の表の経費上限は目安です。特に、経費内での備品費、消耗品費、旅費の配分については、当研究所で対応する共同研究者と十分にご協議の上で申請下さい。特に、旅費については、地域性を勘案してご申請下さい。

課題申請は、本要領に添付の分野選択型共同利用・共同研究申請書（様式１）、課題提案型共同利用・共同研究申請書（様式２）、連携・融合促進型共同利用・共同研究申請書（様式３）、施設・機器利用型共同利用・共同研究申請書（様式４）に必要事項を記入し、下記の要領で、化学研究所共同研究推進室にご提出下さい。

なお、各課題とも、海外研究者を研究代表者あるいは研究協力者とする国際共同研究も実施可能です。この場合、英語フォーム（Forms 1~4）の左肩の欄にチェックを入れて、当研究所の共同研究者に提出をご依頼下さい。

<記入上の注意事項>

1. ※を付した事項は当研究所で記入します。
2. 当研究所で対応する共同研究者は必ずご記入下さい。
3. 申請者（研究代表者）と共同研究者の役割分担を明記して下さい。事前に共同研究者の承諾を得ていただくことが必要です。
4. 申請書は 3 頁以内にまとめて下さい。

3-3. 提出期限および提出先

応募に当たっては、前記の申請書にご記入の上、令和５年１月２０（金）までに、下記宛に電子メール添付書類（Word 書類）としてお送り下さい。

問い合わせ先
京都大学化学研究所 共同研究推進室
E-mail: icr-hub@scl.kyoto-u.ac.jp，電話: (0774)38-3107

4. 課題選考と採択通知

応募課題の採否は、当研究所の共同研究委員会で審査し、運営評議会の承認を経て決定されます。審査に際しては、共同研究の申請内容だけでなく、予算枠や、共通設備・機器・資料の使用時間等も考慮いたします。採否の結果（内定）については、令和５年３月に当研究所の所長から研究代表者に通知いたします。

5. 研究の実施および研究成果報告

5-1. 研究経費等

研究代表者と当研究所で対応する共同研究者には、予算の範囲内で、研究経費（備品費および消耗品費）と旅費が支給されます。また、研究協力者（学生も含めることが可能です*）にも予算の範囲内で旅費が支給されます。共同研究の実施に当たっては、まず対応する共同研究者にご連絡下さい。なお、当研究所には、共同研究者のための宿泊施設はありません。

＊研究協力者について、学生の場合は原則として大学院生といたします。なお、傷害保険等に加入していることが必要です。

5-2. 研究成果報告

採択された研究課題については、研究成果報告書を次に記す作成要領に従って記載・提出していただきます。その報告書は、まとめて当研究所の国際共同利用・共同研究報告書集として公開させていただく予定です。また、その内容を研究成果報告会でご報告いただくことがあります。なお、報告会についての詳細は、採択課題の研究代表者に後日お知らせいたします。

5-3. 研究成果報告書の作成要領

分野選択型研究、課題提案型研究、施設・機器利用型研究については１頁、連携・融合促進型研究については２頁の報告書を（様式５）を用いて作成下さい。Ａ４版の用紙には１頁あたり１，２００字程度が記載できます。図表などカラーを用いても構いませんが、報告書集刊行の際はモノクロ印刷になることもありますので、その点をお含み置き下さい。

１頁の１行目の中央に研究課題名、３行目に右詰めで研究代表者の氏名と所属、５行目から本文を記載して下さい。なお、当研究所で対応した共同研究者は報告書の共著者とはせず、必要に応じて本文中に明記して下さい。また、国際共同研究の場合、報告書は英文でご作成ください。

5-4. 報告書の内容

形式は自由ですが、例えば、実験的研究では、目的、実験方法、実験結果、考察、成果報告（論文、学会発表等）をお書き下さい。なお、連携・融合促進型研究で研究集会を開催した場合には、研究集会のプログラム、参加者名簿（所属機関・部局・職名を明記）、および、作成された場合は要旨集またはプロシーディングスを添付して下さい。

5-5. 報告書の提出

提出締切日は、令和 6 年２月末日とします。電子ファイル（Word ファイルと PDF ファイル）を、下記宛にお送り下さい。なお、ファイル名は「課題番号＋代表者名（姓）」として下さい（例：2023-1 田中.doc、2023-1 田中.pdf）。

問い合わせ先
京都大学化学研究所 共同研究推進室
E-mail: icr-hub@scl.kyoto-u.ac.jp，電話: (0774)38-3107

5-6. 研究成果の公開

学術論文などによる研究成果の公開に際しては、京都大学化学研究所の国際共同利用・共同研究として行われたことを明記して下さい。英文での謝辞例を次に示します。

謝辞例: This work was supported by the International Collaborative Research Program of Institute for Chemical Research, Kyoto University (grant # XXXX).
日本語での謝辞は、この英文表記に準ずるものとして下さい。

化学研究所　国際共共拠点 R5年度採択課題（応募223件，採択 147件，採択率 65.9 %，国際共同研究割合48.2%）

課題番号	研究代表者	研究代表者所属	化研内 研究協力者	型	選択 分野	実施 状況	国際	課題名（和文・英文）
2023-1	RAFFY Quentin	Institut Plurisdisciplinaire Hubert Curien (IPHC)	小川原 亮	分野選択型	1	萌芽的	国際	高線量率電子線照射によるタンパク質の放射線分解の研究
								Radiolysis of concentrated native proteins by accelerated electrons
2023-2	Ma, Yue	RIKEN, Meson Science Laboratory, Senior Research Scientist	塚田 暁	分野選択型	1	発展的		エネルギー敏感型ミュオンスピン回転(muSR)分光計の開発
								Development of energy sensitive muon spin rotation (muSR) spectrometer
2023-3	大西 哲哉	理化学研究所・仁科加速器科学研究センター	若杉　昌徳	分野選択型	1	萌芽的		ナノ構造を持つ ISOL 用標的の開発
								Development of new nano-structure target for ISOL
2023-4	W. M. C. Sameera	University of Colombo, Department of Chemistry	大木 靖弘	分野選択型	2	発展的	国際	立方体型[Mo3S4Pd]クラスター錯体を触媒とするCO2還元反応の理論解析
								On the mechanism of the CO2 reduction catalyzed by cubic [Mo3S4Pd] clusters: a computational study
2023-5	Todd B. Marder	Julius-Maximilians-Universität Würzburg, Institut für Anorganische Chemie	梶 弘典	分野選択型	2	発展的	国際	剛直な平面三配位ホウ素骨格をアクセプターとする新規発光材料の開発とデバイス評価
								Development and device evaluation of new D-A emitters based on rigidified planar triarylborone acceptors
2023-6	Wei-Tin Chen	National Taiwan University, Center for Condensed Matter Sciences	島川 祐一	分野選択型	2	発展的	国際	
								Design and Tailoring Advanced Functional Materials: Symmetry Operation and High Pressure Synthesis
2023-7	García Martín	Departamento de Química Inorgánica, Facultad de Ciencias Químicas, Universidad Complutense	島川 祐一	分野選択型	2	発展的	国際	
								High-performance materials for energy storage electrochemical devices
2023-8	KOEDTRUAD Anucha	Chinese Academy of Science (CAS), Institute of High Energy Physics (IHEP), Chinese Spallation Neutron Source (CSNS)	島川 祐一	分野選択型	2	萌芽的	国際	固体電解質材料Li—Al—Clの高圧合成とLiイオン伝導度の研究
								High-pressure synthesis and Li conducting study of Li-Al-Cl compounds as solid electrolytes in batteries
2023-9	Haichuan Guo	China Spallation Neutron Source Science Center (CSNS), Institute of High Energy Physics, Chinese Academy of Sciences	島川 祐一	分野選択型	2	萌芽的	国際	金属酸化物における高温結晶構造及び酸素伝導特性研究
								Crystal structures and oxygen conduction properties research of metal oxides at high temperature
2023-10	ALAKANANDA HAJRA	DEPARTMENT OF CHEMISTRY, VISVA-BHARATI UNIVERSITY	中村 正治	分野選択型	2	発展的	国際	
								Photocatalytic C-H Bond Functionalization
2023-11	Toru Hashimoto	Sanyo-Onoda City University Department of Applied Chemistry, Faculty of Engineering, Assistant Professor	中村 正治	分野選択型	2	萌芽的	国際	有機分子触媒を用いたリグニン由来芳香族化合物の分子変換法の開発
								Development of Transformation of Lignin-based Aromatic Building Blocks Using Organocatalyst
2023-12	Takeaki Iwamoto	Tohoku University, Department of Chemistry, Professor	水畑 吉行	分野選択型	2	発展的	国際	非対称型高周期典型元素π電子系の開拓と物性解明
								Development of Unsymmetrical π-Electron Systems of Heavier Main Group Elements and Elucidation of Their Property
2023-13	Takahiro Sasamori	University of Tsukuba, Department of Chemistry, Faculty of Pure and Applied Sciences	若宮 淳志	分野選択型	2	発展的	国際	高性能ペロブスカイト太陽電池作成に有効な高活性酸化スカベンジャーの開発
								Creation of Effective Oxidation Scavenger for Efficient Perovskite-based Solar Cells
2023-14	志賀 拓也	筑波大学・数理物質系化学域	檜垣 達也	分野選択型	2	萌芽的		ホスフィンで保護された鉄クラスター群の合成と磁性の評価
								Synthesis of Phosphine-Protected Iron Clusters to Study their Magnetic Properties
2023-15	亀尾 肇	大阪公立大学・大学院理学研究科・准教授	大木 靖弘	分野選択型	2	萌芽的		シランの求核的活性化を鍵要素とするケイ素-酸素変換反応の開発
								Catalytic Activation of Silicon-Oxygen Bond via Nucleophilic Activation of Silane
2023-16	小笠原 正道	徳島大学・大学院社会産業理工学研究部	大木 靖弘	分野選択型	2	萌芽的		「面不斉から面不斉への不斉転写」を基軸とする面不斉メタロセンの不斉合成
								Asymmetric synthesis of planar-chiral metallocenes by plane-to-plane chirality transfer
2023-17	中島 隆行	奈良女子大学・研究院自然科学系化学領域	大木 靖弘	分野選択型	2	萌芽的		Cuヒドリド錯体と官能基化シリカの組み合わせによるCO2還元触媒の開発
								Carbon fixation catalysts composed of well-defined Cu-hydride complexes and functionalized organosilica

2023-18	近藤 美欧	大阪大学・大学院工学研究科	谷藤 一樹	分野選択型	2	萌芽的		電子移動制御を利用したナノ金属クラスター触媒の高活性化 Development of highly active metal cluster catalysts by using electron Transfer network
2023-19	新井 敏	金沢大学・ナノ生命科学研究所	大宮 寛久	分野選択型	2	発展的		コリン作動薬の光機能制御に資するケージド分子技術 A Caging Strategy for Cholinergic Optopharmacology
2023-20	平井 健二	北海道大学・電子科学研究所	金光 義彦	分野選択型	2	萌芽的		振動強結合を用いた発光特性の制御 Modulated Luminescence of Coordination Complex under Vibrational Strong Coupling
2023-21	山田 泰裕	千葉大学・大学院理学研究院	金光 義彦	分野選択型	2	萌芽的		半導体光学冷却に向けたドットインクリスタル型ペロブスカイトの光物性の解明 Spectroscopic study of dot-in-crystal perovskites toward semiconductor optical refrigeration
2023-22	小川 佳宏	上越教育大学・学校教育研究科	金光 義彦	分野選択型	2	萌芽的		二次元光学フーリエ分光法による鉛ペロブスカイト太陽電池の量子物性の探求 Quantum properties of lead perovskite solar cells by two-dimensional optical Fourier transform spectroscopy
2023-23	立崎 武弘	東海大学・情報理工学部コンピュータ応用工学科	金光 義彦	分野選択型	2	発展的		低温強磁場対応THz-STMの開発と評価 Development and evaluation of THz-STM for low-temperature and high magnetic field
2023-24	小布施 秀明	北海道大学・工学研究院	廣理 英基	分野選択型	2	萌芽的		非エルミート・トポロジカルエッジ状態によるテラヘルツレーザー Terahertz Laser by Topological Edge States in Non-Hermitian Systems
2023-25	細川 三郎	京都工芸繊維大学・材料化学	菅 大介	分野選択型	2	萌芽的		酸化物における水素スピルオーバー制御 Controlling hydrogen spillover on oxides
2023-26	ILIES Laurean	理化学研究所・環境資源科学研究センター	中村 正治	分野選択型	2	発展的		基質認識による位置選択的C-H活性化反応の開発 Regioselective C-H Activation Enabled by Substrate Recognition
2023-27	山口 佳隆	横浜国立大学・大学院工学研究院	中村 正治	分野選択型	2	発展的		コフェイシャル型複核錯体の開発 Development of co-facial-type dinuclear complexes
2023-28	竹歳　絢子	横浜国立大学・大学院工学研究院	中村 正治	分野選択型	2	萌芽的		高選択的官能基変換のための格子欠陥型酸化ニッケル触媒の開発 Development of defective nickel oxide catalysts for highly selective functionalization
2023-29	光藤 耕一	岡山大学・学術研究院自然科学学域	若宮 淳志	分野選択型	2	萌芽的		ジフルオロボリル基またはスルホニル基を有するπ共役系分子の効率合成とその物性 Efficient synthesis and physical properties of π-extended molecules bearing difluoroboryl or sulfonyl groups
2023-30	Jiangning Song	Monash University, Biomedicine Discovery Institute,	阿久津 達也	分野選択型	3	発展的	国際	タンパク質のミスセンス突然変異による安定性の変化予測のための機械学習方式の開発 Developing machine learning approaches for prediction of protein stability changes upon missense mutations
2023-31	Jinn-Moon Yang	National Yang Ming Chiao Tung University, Department of Biological Science and Technology/Institute of Bioinformatics & Systems Biology	阿久津 達也	分野選択型	3	発展的	国際	深層学習を用いたオミクスデータとモジュールに基づくネットワークデータの統合解析による腫瘍細胞分類 Integrating omics data and module-based network with deep learning to develop cancer type predictive models
2023-32	Tom O. Delmont	CNRS, Genoscope, UMR8030	緒方 博之	分野選択型	3	発展的	国際	大型DNAウイルスの生態と進化 Ecology and evolution of large and giant DNA viruses
2023-33	David Demory	CNRS, UMR7231	遠藤 寿	分野選択型	3	発展的	国際	メタゲノミクスと温度依存型ウイルス感染モデルを用いたMicromonasウイルスの全球海洋分布に関する研究 Application of metagenomics and a temperature-driven mathematical model to estimate the global distribution of Micromonas viruses
2023-34	Masayuki Karasuyama	Nagoya Institute of Technology, Department of Computer Science	馬見塚 拓	分野選択型	3	萌芽的	国際	統計的機械学習による効率的なグラフ構造データ解析法の開発 A Study on Statistical Machine Learning for Efficient Graph Structured Data Analysis
2023-35	田口 善弘	中央大学・理工学部	田村 武幸	分野選択型	3	萌芽的		テンソル分解を用いた教師なし学習による変数選択法を用いたMetNetComp Databaseの予測評価 Evaluation of prediction with MetNetComp using tensor decomposition based unsupervised feature extraction
2023-36	ホセ ナチェル	東邦大学・理学部情報科学科	阿久津 達也	分野選択型	3	萌芽的		確率的最小支配集合による複雑ネットワークの制御と解析 Control and Analysis of Complex Networks via Probabilistic Minimum Dominating Sets

2023-37	武村 政春	東京理科大学・教養教育研究院	緒方 博之	分野選択型	3	萌芽的		巨大ウイルス感染アメーバのトランスクリプトーム解析による宿主・巨大ウイルス相互作用の解明 Elucidation of host-giant virus interaction using transcriptomics of giant virus-infected acanthamoeba cells
2023-38	西村 陽介	国立研究開発法人海洋研究開発機構・生命理工学センター	緒方 博之	分野選択型	3	萌芽的		ウイルスダークマターの解明に向けたウイルスゲノム情報基盤の構築 Development of a viral genome information infrastructure for elucidation of viral dark matter
2023-39	茅野 光範	帯広畜産大学・グローバルアグロメディシン研究センター	馬見塚 拓	分野選択型	3	発展的		効果的な生体分子解析方法の開発と医学・農学への応用 Effective biomolecular analysis and application to medical and agricultural research
2023-40	Markus W. Ribbe	Department of Molecular Biology and Biochemistry, Department of Chemistry, University of California, Irvine	谷藤 一樹	分野選択型	4	発展的	国際	合成化学を利用した窒素還元酵素の活性中心生合成機構の解明 Investigations into cofactor biosynthesis of N2-reducing enzyme via semi-synthetic approach
2023-41	Sunkyu Han	KAIST, Department of Chemistry	大宮 寛久	分野選択型	4	発展的	国際	 Radical-polar crossover catalysis for synthesis of complex natural products
2023-42	Eli Zysman-Colman	University of St Andrews, Organic Semiconductor Centre, EaStCHEM School of Chemistry	梶 弘典	分野選択型	4	発展的	国際	長寿命素子を志向した短い励起子寿命を示す多重共鳴型熱活性遅延蛍光材料の開発 Development of multi-resonant TADF emitters with short delayed lifetimes and their use in long lifetime OLEDs.
2023-43	P. Rajamalli	Materials Research Centre, Indian Institute of Science, Bangalore.	梶 弘典	分野選択型	4	発展的	国際	塗布型有機ELにおける光取り出し効率向上を目指した直線型熱活性遅延蛍光材料の設計と合成 Design and synthesis of linear molecules for improving outcoupling efficiency of solution-possessed OLEDs
2023-44	Atsushi GOTO	School of Physical & Mathematical Sciences – Division of Chemistry & Biological Chemistry Nanyang Technological University	黄瀬 雄司	分野選択型	4	発展的	国際	おたまじゃくし状ヤヌス型セルロースナノクリスタルの精密合成と高次構制御 Precise synthesis and controlling higher order structure of tadpole-like Janus cellulose nanocrystal
2023-45	Yasuhiro Tachibana	RMIT University, School of Engineering	寺西 利治	分野選択型	4	発展的	国際	鉛フリーハロゲン化金属ペロブスカイトの開発 Development of lead free metal halide perovskite
2023-46	CHAOLUMEN	Inner Mongolia University (IMU), College of Chemistry and Chemical Engineering	橋川 祥史	分野選択型	4	発展的	国際	非6員環をもつグラフェンナノリボンの合成 Synthesis of Graphene Nanoribbons Containing Non-Hexagonal Rings
2023-47	Sheng ZHANG	Engineering Research Center for Nanomaterials (ERCN), Henan University	村田 靖次郎	分野選択型	4	発展的	国際	開口フラーレンをビルディングブロックとする光電子材料 Optoelectronic Materials with Open-cage C60 Derivatives as Building Blocks
2023-48	MARGETIC, Davor	Rudjer Boskovic Institute, Division of organic chemistry and biochemistry	村田 靖次郎	分野選択型	4	発展的	国際	グアニジン修飾イサチンのプラトー付加環化における反応性に関する研究 The Reactivity of Guanidino-Isatins in Prato Cycloaddition Reaction
2023-49	DEBUIGNE Antoine	University of Liege, Belgium, Chemistry Department, Center for Education and Research on Macromolecules	山子 茂	分野選択型	4	萌芽的	国際	テルル媒介ラジカル重合と多成分重合法の融合による刺激応答性ポリペプトイド／ポリビニルアミド共重合体の創製 Combining Tellurium Mediated Radical Polymerization and Multicomponent Polymerization towards Unique Stimuli Responsive polypeptoids/ poly(N-vinyl amide)s Copolymers
2023-50	Akinori Saeki	Department of Applied Chemistry, Graduate School of Engineering, Osaka University	若宮 淳志	分野選択型	4	発展的	国際	ペロブスカイト太陽電池性能向上に向けた機能分子開発 Development of functional molecule for efficient perovskite solar cells
2023-51	太田 雄大	山口東京理科大学・工学部応用化学科	大木 靖弘	分野選択型	4	萌芽的		ポルフィリン二量体分子触媒の構造反応性相関に関する研究 Studies of geometric and electronic structure/reactivity correlation in cofacial metalloporphyrin dimers.
2023-52	若林 成知	鈴鹿医療科学大学・保健衛生学部医療栄養学科	大木 靖弘	分野選択型	4	萌芽的		ホウ素の特性を活かした自己集合性アズレン類の合成ならびに反応・機能開拓 Synthesis of Self-Assembled Azulene Derivatives Utilizing Boron, and Creation of New Reactions and Functions
2023-53	稲木 信介	東京工業大学・物質理工学院	大宮 寛久	分野選択型	4	発展的		電気化学的・光化学的手法を用いた分解型有機合成 Electrochemical and Photochemical Degradation Reaction
2023-54	平井 剛	九州大学・大学院薬学研究院	大宮 寛久	分野選択型	4	発展的		光駆動型有機硫黄触媒による糖修飾 Light-driven Organosulfur Catalysis for Sugar Modification
2023-55	平井 智康	大阪工業大学・工学部応用化学科	竹中 幹人	分野選択型	4	萌芽的		シロキサン主鎖骨格の二次構造制御とキラルシリカへの展開 Controlling of Secondary Structure in Polysiloxane Main Chain and Application for Chiral Silica

2023-56	谷 敬太	大阪教育大学・教育学部	辻井 敬亘	分野選択型	4	発展的		カルバゾロファンを側鎖に持つポリマーの合成とホール輸送及びCPL材料への応用 Synthesis of Polymers Having Carbazolophane Moiety and Their Application of Hole Transport and CPL Materials
2023-57	鈴木 充朗	大阪大学・大学院工学研究科	村田 靖次郎	分野選択型	4	発展的		共有結合性有機固溶体の設計に関する基盤的研究 Elucidation of design principles of covalent organic solid solutions
2023-58	清水 章弘	大阪大学・大学院基礎工学研究科物質創成専攻	廣瀬 崇至	分野選択型	4	発展的		発光性基底三重項ジラジカルの合成と物性 Synthesis and Properties of Emissive Triplet Diradicals
2023-59	永木 愛一郎	北海道大学・大学院理学研究科	山子 茂	分野選択型	4	発展的		フロー反応装置による官能性ビニルテルリド合成を鍵とする重合反応の開発 Polymerization of functional vinyltellurides prepared by flow reactors
2023-60	岸 亮平	大阪大学・大学院基礎工学研究科	茅原 栄一	分野選択型	4	発展的		大環状共役系における電子の非局在性の荷電・スピン・励起状態依存性の研究 Study on dependence of electron delocalization on charged, spin and excited states in conjugated macrocycles
2023-61	安倍 学	広島大学・大学院先進理工系科学研究科	茅原 栄一	分野選択型	4	発展的		マクロ環骨格内に導入したラジカルの化学: SOMO-HOMOエネルギー逆転 A Study on radicals in macrocyclic systems: SOMO-HOMO Energy Conversion
2023-62	土戸 良高	東京理科大学・理学部第一部化学科	茅原 栄一	分野選択型	4	発展的		動的金—炭素結合による大環状金錯体の再組織化を利用したドナー・アクセプター型新規シクロパラフェニレン類の合成と機能開拓 Synthesis and Functionally Development of Donor-Acceptor Cycloparaphenylene Derivatives through Reorganization of Macrocyclic Gold Complexes via Dynamic Gold-Carbon Bonds
2023-63	HO, Tung-Yuan	Academia Sinica, Research Center for Environmental Changes	宗林 由樹	分野選択型	5	発展的	国際	北太平洋における微量金属の元素・同位体組成：起源と内部循環 (4) Trace metal elemental and isotopic composition in the North Pacific Ocean: sources and internal cycling (4)
2023-64	Tadanori Koga	Stony Brook University, Department of Material Science and Chemical Engineering	竹中 幹人	分野選択型	5	発展的	国際	高分子ナノコンポジットの補強メカニズムの解明-III Resolving the structure-dynamics-property relationship in polymer nanocomposites under uniaxial stretching-III
2023-65	Sathish K. Sukumaran	Graduate School of Organic Materials Science, Yamagata University	佐藤 健	分野選択型	5	発展的	国際	高分子液体の高周波応答: レオロジーおよび誘電緩和 High Frequency Response of Polymeric Liquids: Rheology and Dielectric Relaxation
2023-66	五月女 光	大阪大学・大学院基礎工学研究科物質創成専攻	梶 弘典	分野選択型	5	発展的		不均一構造分布をもつ熱活性化遅延蛍光分子集合体における超高速励起子ダイナミクス Ultrafast Exciton Dynamics in Thermally Activated Delayed Fluorescence Molecular Aggregates with Heterogeneous Conformational Distribution
2023-67	小島 一信	大阪大学・大学院工学研究科	金光 義彦	分野選択型	5	萌芽的		高い発光効率を有する半導体中における新奇光現象の探索 Exploration of novel optical phenomena in semiconductors with high quantum efficiency of radiation
2023-68	中口 譲	近畿大学・理工学部	宗林 由樹	分野選択型	5	萌芽的		大阪湾およびその流入河川水中の生物活性微量金属の化学量論 Stoichiometry of bioactive trace metals in the Osaka Bay and its inflowing river waters
2023-69	向井 浩	京都教育大学・教育学部理学科	宗林 由樹	分野選択型	5	萌芽的		イオン液体の金属錯体担持型高分子包接膜による金属イオンの高選択的膜分離に関する研究 Study on high selective membrane separation of metal ions by use of polimer inclusion membranes of ionic liquid containing the metal complexes
2023-70	飯田 健二	北海道大学・触媒科学研究所	寺西 利治	分野選択型	5	発展的		プラズモニック合金ナノ粒子を設計するための理論的指針の構築 Construction of Theoretical Guidelines for Designing Plasmonic Nanoalloys
2023-71	三枝 栄子	大阪公立大学・大学院理学研究科化学専攻	長谷川 健	分野選択型	5	萌芽的		固体イオンセンサーを指向した発光性ランタノイド錯体の集積化と膜構造解析 Fabrication and characterization of luminescent thin films of lanthanide complexes for solid-state ion sensors
2023-72	園山 正史	群馬大学・大学院理工学府	長谷川 健	分野選択型	5	萌芽的		新規ハイブリッド型部分フッ素化リン脂質二分子膜の構造・物性の解析 Physicochemical characterization of novel hybrid partially fluorinated phospholipid bilayers
2023-73	粕谷 素洋	公立小松大学・生産システム科学部	長谷川 健	分野選択型	5	萌芽的		フッ素系樹脂の摩耗に伴う分子配向変化の観測 Characterization of molecular orientation during wear of fluoropolymer
2023-74	河内 孝之	京都大学・生命科学研究科	山口 信次郎	分野選択型	5	萌芽的		基部陸上植物苔類ゼニゴケにおける活性型ジベレリンの単離と同定 Identification of active gibberellins in the basal land plant Marchantia polymorpha

2023-75	土肥 侑也	名古屋大学・大学院工学研究科	佐藤 健	分野選択型	5	萌芽的		モデルニ次元シート状高分子の調製と精密キャラクタリゼーション Preparation and Precise Characterization of Model Two-Dimensional Sheet-Shaped Polymers
2023-76	Atsufumi Hirohata	University of York, Department of Electronic Engineering	小野 輝男	分野選択型	特定	萌芽的	国際	補償温度近傍でのフェリ磁性薄膜試料が示すスピンホール及びスピンネルンスト効果 Spin signals in a ferrimagnetic film near the compensation temperature
2023-77	Kab-Jin Kim	Korea Advanced Institute of Science and Technology, Department of Physics	小野 輝男	分野選択型	特定	発展的	国際	ハイブリッドマグノニック系での量子マグノン研究 Characterization of quantum magnon using hybrid magnonic systems
2023-78	Sanghoon Kim	University of Ulsan, Department of Physics	小野 輝男	分野選択型	特定	発展的	国際	 Non-reciprocity of spin wave propagation generated by orbital Hall effect in transition metal dichalcogenides
2023-79	Gopalakrishnan Balasubramanian	Helmholtz-Zentrum Dresden-Rossendorf (HZDR)	水落 憲和	分野選択型	特定	発展的	国際	表面近傍NV中心の安定化とスピンダイナミクスの研究 Research toward stable NV centers at shallow region and spin dynamics in diamond
2023-80	Takuya F. Segawa	Laboratory for Physical Chemistry, ETH Zürich	水落 憲和	分野選択型	特定	発展的	国際	ナノダイヤモンド中のNV中心作製効率化研究 Research on the efficiency enhancement of the NV centers creation in nanodiamond
2023-81	Jörg Wrachtrup	Stuttgart University	水落 憲和	分野選択型	特定	発展的	国際	ダイヤモンドにおける高感度NV量子センサーの研究 Research toward high sensitive NV quantum sensor in diamond
2023-82	田中 雅章	名古屋工業大学・大学院工学研究科	小野 輝男	分野選択型	特定	萌芽的		垂直磁化をもつ強磁性導電体薄膜を用いたスピン注入の研究 Study on the spin injection using perpendicularly magnetized ferromagnetic conductor film
2023-83	長浜 太郎	北海道大学工学研究院応用化学部門	小野 輝男	分野選択型	特定	発展的		新規Fe基$D0_3$型合金薄膜の開発と熱電効果の機構の解明 Development of Fe-based D03 type alloys and its Thermoelectric property
2023-84	諸田 美砂子	産業技術総合研究所・デバイス技術研究部門	小野 輝男	分野選択型	特定	萌芽的		カルコゲナイド系超格子のトポロジカル相制御の実証 Demonstration of topological phase control in chalcogenide superlattices
2023-85	徳田 規夫	金沢大学・ナノマテリアル研究所	水落 憲和	分野選択型	特定	発展的		ダイヤモンド量子センサのための表面状態研究 Research of surface state for diamond quantum sensor
2023-86	牧野 俊晴	産業技術総合研究所・先進パワーエレクトロニクス研究センター	水落 憲和	分野選択型	特定	発展的		量子センサの高感度化に向けたリンドープダイヤモンド合成と量子科学技術研究 Research of quantum technology and diamond synthesis for higher sensitivity of NV quantum sensor
2023-87	QU, Li-Jia	Peking University, School of Life Sciences	青山 卓史	課題提案型		発展的	国際	花粉管形成におけるPIP5K遺伝子の役割 Role of PIP5K Genes in Pollen Tube Development
2023-88	JARMOLOWSKI, Artur	Adam Mickiewicz University, Institute of Molecular Biology and Biotechnology, Department of Gene Expression	柘植 知彦	課題提案型		発展的	国際	植物をモデルに用いたmRNA 3'UTR制御機構の分子生物学的解析 Molecular mechanisms of mRNA processing governing 3'UTR ends by using plant as a model system
2023-89	GALBIATI, Massimo	National Council of Research (CNR), Institute of Agricultural Biology and Biotechnology (IBBA)	柘植 知彦	課題提案型		発展的	国際	乾燥耐性制御因子AtMYB60の多段階的遺伝子発現制御機構の理解と作物応用 Exploiting AtMYB60 regulation for water use efficiency and drought resistance in crops
2023-90	RUBIO, Vicente	National Center of Biotechnology (CNB-CSIC), Plant Molecular Genetics Department	柘植 知彦	課題提案型		発展的	国際	植物形態形成におけるRNAプロセシングを制御する遺伝子発現制御ネットワーク Chromatin, epigenetic and proteolytic regulation of RNA processing in plant morphogenesis
2023-91	Lu Zhou	Fudan University, School of Pharmacy	上杉 志成	課題提案型		発展的	国際	タンパク質相分離を選択的に阻害する自己集合化合物 Self-Assembling Compounds That Selectively Inhibit Protein Phase-Separation
2023-92	Yan-Mei Li	Tsinghua University, Department of Chemistry	上杉 志成	課題提案型		発展的	国際	安全性を最適化した癌ワクチンアジュバントの開発 Development of Cancer Vaccine Adjuvants with Optimized Safety Profiles
2023-93	Christin Bednarek	Karlsruhe Institute of Technology, Institut of Organic Chemistry	梶 弘典	課題提案型		発展的	国際	赤および近赤外多重共鳴熱活性化遅延蛍光材料の開発 Red and Near-Infrared Multi-Resonance Thermally Activated Delayed Fluorescence Emitters

2023-94	Xianzhu Dai	College of Resources and Environment, Southwest University	栗原 達夫	課題提案型		発展的	国際	低温適応微生物を用いた低温異種タンパク質分泌生産系の構築 Construction of heterologous protein secretion system at low temperatures by using cold-adapted microorganisms
2023-95	Maria Michela Corsaro	University of Naples Federico II, Department of Chemical Sciences	栗原 達夫	課題提案型		発展的	国際	細菌が放出する外膜小胞の表層多糖の構造機能解析 Structural and functional analysis of the surface polysaccharides of outer membrane vesicles released by bacteria
2023-96	Jikun Chen	University of Science and Technology Beijing, RP China, School of Materials Science and Engineering	島川 祐一	課題提案型		発展的	国際	 High pressure synthesis of the metastable rare-earth nickelates with Ni-site substitutions for synchronizing their electronic phase transition and potential magnetic transitions
2023-97	Pinghe Cai	Xiamen University, Department of Marine Chemistry and Geochemistry	宗林 由樹	課題提案型		発展的	国際	 Formation of authigenic $CaCO_3$ on the ocean floor below the compensation depth
2023-98	Maya Endoh	Stony Brook University, Department of Material Science and Chemical Engineering	竹中 幹人	課題提案型		発展的	国際	高分子ナノ表面構造による殺菌効果-V Fabrication of nanotopographical polymer surfaces for bactericidal properties-V
2023-99	Chiaki YOSHIKAWA	National Institute for Materials Science (NIMS), Research Center for Functional Materials	辻井 敬亘	課題提案型		萌芽的	国際	多孔質材料の高度構造制御による新規細胞培養基材の開発 Fabrication of novel cell culture substrates using well-defined porous materials
2023-100	Jean-Pierre Bucher	Université de Strasbourg, Institut de Physique et Chimie des Matériaux (IPCMS)	寺西 利治	課題提案型		発展的	国際	 Interdisciplinary Approach to Nanostructured Materials for Applications
2023-101	Kensuke Homma	Hiroshima University, Physics	時田 茂樹	課題提案型		発展的	国際	宇宙暗黒成分解明へ向けた真空内四光波混合の探索 Search for four-wave-mixing in the vacuum – Unveiling dark components in the Universe –
2023-102	Thomas Wirth	Cardiff University, School of Chemistry	中村 正治	課題提案型		発展的	国際	 Advanced Oxygen – mediated Flow Chemistry
2023-103	Ilaria BONADUCE	University of Pisa, Dept. of Chemistry and Industrial Chemistry	PINCELLA Francesca	課題提案型		萌芽的	国際	アジアの生漆・重合漆サンプルの合成と特性評価：材料科学・文化遺産保全学のための包括的漆ライブラリーの開発に向けて Synthesis and characterization of raw and polymerized Asian lacquer samples: towards the development of a comprehensive collection of lacquer reference samples for materials science and conservations studies
2023-104	Sílvia PUJALS	Institute for Advanced Chemistry of Catalonia (IQAC), Supramolecular chemistry group, Biological Chemistry department C	二木 史朗	課題提案型		発展的	国際	ナノ医薬の新規細胞内効率的送達法 Novel strategy for intracellular delivery of nanomedicines
2023-105	Anne S. Ulrich	Karlsruhe Institute of Technology (KIT), Institute of Organic Chemistry (IOC) and Institute of Biological Interfaces (IBG-2)	二木 史朗	課題提案型		発展的	国際	曲率誘導ペプチドの構造活性相関と応用 Structural and functional analysis of curvature-inducing peptides and application
2023-106	Zuhua He	Chinese Academy of Sciences, CAS Center for Excellence in Molecular Plant Sciences, Institute of Plant Physiology and Ecology	山口 信次郎	課題提案型		発展的	国際	イネの成長ホルモンの不活性化機構の解析 Molecular mechanisms for the inactivation of a growth hormone in rice
2023-107	Yunde Zhao	University of California San Diego, Division of Biological Sciences, Department of Cell and Developmental Biology	増口 潔	課題提案型		萌芽的	国際	新規ストリゴラクトン輸送体タンパク質の解析 Analysis of novel transporters for strigolactones or their biosynthetic intermediates
2023-108	Matthew J. Fuchter	Imperial College London (ICL), Chemistry	山子 茂	課題提案型		発展的	国際	シクロパラフェニレンとキラルフラーレンの超分子錯体形成とキラル光学材料への応用 Cycloparaphenylenes and Chiral Fullerenes for Supramolecular Architectures in Chiroptical Applications
2023-109	Stefan Bräse	Karlsruhe Institute of Technology, Institut of Biological and Chemical System, IBCS-FMS	山子 茂	課題提案型		発展的	国際	パラシクロファンコアを有するキラルシクロフェニレン Chiral cyclophenylene with an [2.2]paracyclophane core
2023-110	Hao-Wu Lin	Department of Materials Science and Engineering, National Tsing Hua University	若宮 淳志	課題提案型		発展的	国際	多次元ペロブスカイト発光と光応答材料の開発 Development of Multi-dimensional Perovskite Light-emission and Photo-response Materials
2023-111	Atsushi Takano	Nagoya University, Department of Molecular and Macromolecular Chemistry	松宮 由実	課題提案型		萌芽的	国際	高純度、高分子量環状高分子の精密合成と粘弾性 Precise synthesis and viscoelastic properties of ring polymers with high purity and high molecular weight

2023-112	Ryoko Shimada	Department of Mathematics, Physics and Computer Science, Japan Women's University	佐藤 健	課題提案型		発展的	国際	液晶/溶媒混合系の一相等方状態における濃度ゆらぎと配向ゆらぎの相関 Correlation of concentration and orientation fluctuations in mixture of liquid crystal/solvent isotropic one-phase state
2023-113	Osamu Urakawa	Osaka University, Department of Macromolecular Science	松宮 由実	課題提案型		萌芽的	国際	擬ロタキサン型架橋高分子エラストマーの力学物性評価 Evaluation of Mechanical Properties for Polymer Elastomers with Pseudo-Rotaxane Type Cross-Links
2023-114	上田 晴子	甲南大学・理工学部	青山 卓史	課題提案型		萌芽的		植物細胞の原形質流動におけるリン脂質の関わり Involvement of phospholipids in cytoplasmic streaming in plant cells
2023-115	菊地 和也	大阪大学・大学院工学研究科	上杉 志成	課題提案型		発展的		細胞内相分離タンパク質のリアルタイム可視化 Real-Time Visualization of Cellular Phase-Separating Proteins
2023-116	西川 元也	東京理科大学・薬学部	上杉 志成	課題提案型		発展的		合成小分子化合物による細胞の遠隔操作 Remote Control of Cells by Synthetic Small Molecules
2023-117	木村 謙介	理化学研究所・開拓研究本部	梶 弘典	課題提案型		発展的		量子化学計算と原子スケール分光によるドナー・アクセプター分子系の探求 Investigation of donor-acceptor molecular systems by quantum chemical calculations and atomic-scale spectroscopy
2023-118	豊竹 洋佑	立命館大学・生命科学部生物工学科	栗原 達夫	課題提案型		萌芽的		酢酸菌における膜脂質依存的な発酵ストレス応答の解析 Analysis of membrane lipid-dependent fermentation stress response in acetic acid bacteria
2023-119	大森 勇門	大阪工業大学・工学部 生命工学科	栗原 達夫	課題提案型		萌芽的		Geobacillus kaustophilusにおける2種類のアラニン脱水素酵素の構造・機能解析 Studies on the structures and functions of two alanine dehydrogenases in Geobacillus kaustophilus
2023-120	山崎 思乃	関西大学・化学生命工学部	栗原 達夫	課題提案型		発展的		腸内細菌が放出する細胞外膜小胞の機能解析とその応用 Functional analysis and applications of extracellular vesicles produced by intestinal bacteria
2023-121	土屋 敬志	物質・材料研究機構・国際ナノアーキテクトニクス研究拠点	菅 大介	課題提案型		発展的		金属酸化物の電気化学的制御と新奇物性探索 Electrochemical control of metal oxides and Exploration of their functional properties
2023-122	倉橋 健介	大阪公立大学工業高等専門学校・環境物質化学コース	宗林 由樹	課題提案型		萌芽的		界面活性剤を含浸させた溶媒含浸樹脂による希土類元素の分離 Separation of rare earth elements using solvent impregnated resin using surfactants
2023-123	大野 工司	大阪公立大学・工学研究科	辻井 敬亘	課題提案型		発展的		ポリマーブラシ付与複合微粒子系潤滑添加剤の開発 Polymer-brush-decorated hybrid particles as lubricant additives
2023-124	村瀬 浩貴	共立女子大学・家政学部被服学科	辻井 敬亘	課題提案型		発展的		3Dプリンタを用いたモノリスの3次元構造制御 Manipulation of Three Dimensional Structure of Polymer Monoliths by 3D Printer
2023-125	江目 宏樹	山形大学・大学院理工学研究科	猿山 雅亮	課題提案型		萌芽的		ポンププローブ過渡吸収分光法を駆使した三次元量子ドット超格子の超短時間光熱変換現象の解明 Observation of photothermal conversion in 3D quantum dot superlattices using pump-probe transient absorption spectroscopy
2023-126	真島 豊	東京工業大学・フロンティア材料研究所	寺西 利治	課題提案型		発展的		CdS/CdTeタイプII型二量体単一ナノ粒子を用いた世界最小ダイオードの室温動作 Room Temperature Operable CdS/CdTe Type Ⅱ Dimer-Quantum-dot Diode
2023-127	山添 誠司	東京都立大学・大学院理学研究科化学専攻	寺西 利治	課題提案型		萌芽的		担持金属－金属酸化物クラスター複合化による協奏的触媒機能の創出 Development of cooperative catalysis by hybridization of supported metal nanoparticles with metal oxide clusters
2023-128	松井 隆太郎	京都大学大学院・エネルギー科学研究科	時田 茂樹	課題提案型		萌芽的		積層CNTターゲットへの高強度レーザー照射による高エネルギー電子生成に関する実験研究 Study and experiment of the high-energy electron generation by the high-power laser-irradiation to the stacked CNT target
2023-129	岸本 泰明	京都大学大学院・エネルギー科学研究科	時田 茂樹	課題提案型		発展的		高強度レーザーと構造性媒質との相互作用による準定常強磁場の生成と検証 Measurement of quasi-stable strong magnetic field by the interaction between a high-power laser and structured medium
2023-130	江口 暁子	三重大学・大学院医学系研究科消化器内科学	二木 史朗	課題提案型		発展的		細胞外小胞の標的細胞への移行メカニズムの解明 Investigation of cellular uptake mechanism using extracellular vesicles

2023-131	中瀬 生彦	大阪公立大学・大学院理学研究科生物化学専攻	二木 史朗	課題提案型		発展的		エクソソームの細胞内への送達設計 Design of intracellular delivery systems for extracellular vesicles
2023-132	瀬戸 義哉	明治大学・農学部	山口 信次郎	課題提案型		発展的		「非典型的」ストリゴラクトン類の植物ホルモンおよび根圏シグナルとしての機能解析 Functional analysis of non-canonical strigolactones as plant hormones and root-derived signals
2023-133	灰野 岳晴	広島大学・大学院先進理工系科学研究科	山子 茂	課題提案型		発展的		超分子化学による分枝型合成ポリマーの精密配列制御 Development of structurally well-defined branched supramolecular polymers
2023-134	Chengshan Wang	Middle Tennessee State University, Chemistry	長谷川 健	連携・融合促進型			国際	 Determine the three-dimensional structure of 13C=18O labeled α-synuclein(61-95) in the Langmuir-Blodgett film and supported phospholipid bilayer by MAIRS2
2023-135	Hironobu HOJO	Osaka University, Institute for Protein Research	二木 史朗	連携・融合促進型			国際	高効率蛋白質化学合成 High-efficacy protein chemical synthesis
2023-136	Hirokazu Tamamura	Tokyo Medical and Dental University, Institute of Biomaterials and Bioengineering (IBB-TMDU)	二木 史朗	連携・融合促進型			国際	中分子ペプチドによる細胞内タンパク質ータンパク質相互作用の調節 Modulation of in-cell protein-protein interactions using mid-sized peptides
2023-137	Tadashi Inoue	Osaka University, Department of Macromolecular Science	松宮 由実	連携・融合促進型			国際	東アジア圏の若手レオロジストのための第17回ワークショップ The 17th International Workshop for East Asian Young Rheologists
2023-138	伊藤 貴浩	京都大学・医生物学研究所	梶 弘典	連携・融合促進型				固体核磁気共鳴分光法による新たな代謝解析法の開発とがん細胞生物学への応用 A novel interdisciplinary approach to cancer metabolism research by solid state nuclear magnetic resonance spectroscopy
2023-139	Natthaphol CHOMSAENG	Burapha University, Advanced Materials Engineering	治田 充貴	施設・機器利用型			国際	 Microstructural Investigation by Atomic Resolution Transmission Electron Microscopy of Novel Alloys
2023-140	Torranin CHAIRUANGSRI	Chiang Mai University, Industrial Chemistry	治田 充貴	施設・機器利用型			国際	 Electron Energy Loss Spectroscopy and High-Resolution Transmission Electron Microscopy of Novel Functional Materials
2023-141	Ming-Wen Chu	National Taiwan University, Center for Condensed Matter Sciences	治田 充貴	施設・機器利用型			国際	 Plasmon Excitations in Charge-Density-Wave Systems: A Momentum-Dependent Electron-Energy Loss Spectroscopy Investigation
2023-142	Kunlang Ji	Centre for Science at Extreme Conditions and School of Chemistry, University of Edinburgh	島川 祐一	施設・機器利用型			国際	 High-pressure synthesis of transition metal oxides with novel properties
2023-143	宮本 光貴	島根大学・総合理工学部	治田 充貴	施設・機器利用型				核融合炉材料中の水素・ヘリウム滞留挙動の解明 Elucidation of Hydrogen and Helium Retention Behavior in Fusion Materials
2023-144	斉藤 光	九州大学・先導物質化学研究所	治田 充貴	施設・機器利用型				高効率の高速電子線検出用シンチレータの開発に向けたCs4PbBr6/CsPbBr3コンポジット材料のナノ構造解析 Nano structural analysis of Cs4PbBr6/CsPbBr3 composite for the development of a scintillator for fast electron beam detection with high efficiency
2023-145	小島 完興	量子科学技術研究開発機構・光量子科学研究部	時田 茂樹	施設・機器利用型				レーザー駆動イオン加速機構による高品質なイオンビーム生成のためのレーザー照射条件の最適化 Optimization of laser irradiation conditions for high-quality ion beam generation by laser-driven ion acceleration
2023-146	秦野 修	奈良県立医科大学・医学部	中村 正治	施設・機器利用型				スギ木質組織構造の効率的化学分解過程から先端化学物質生産をめざした質量分析解析 Mass spectrometry analysis for the production of advanced chemical materials from the efficient chemical decomposition process of cedar wood tissue structure
2023-147	高橋 まさえ	東北大学・大学院理学研究科	水畑 吉行	施設・機器利用型				平面二次元シートに埋め込まれた低次元ケイ素材料の理論設計と動作原理の探求 Theoretical design of low-dimensional silicon material embedded in a flat two-dimensional sheet and exploration for operating principles